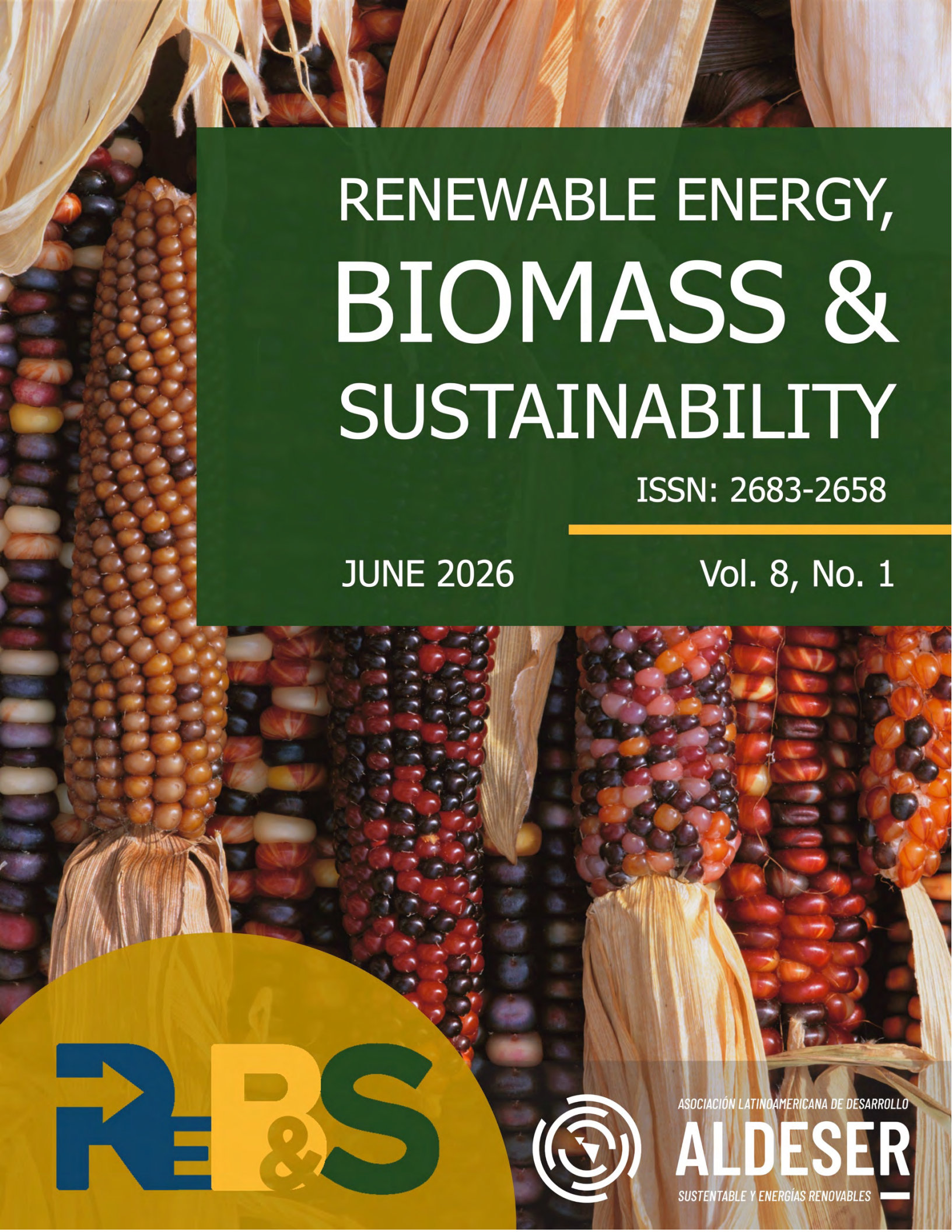

RENEWABLE ENERGY, BIOMASS & SUSTAINABILITY

ISSN: 2683-2658

JUNE 2026 Vol. 8, No. 1

RE&S

ASOCIACIÓN LATINOAMERICANA DE DESARROLLO

ALDESER

SUSTENTABLE Y ENERGÍAS RENOVABLES

Renewable Energy, Biomass & Sustainability
Vol. 8 No. 1 (2026)

Published: January 25, 2026

Renewable Energy, Biomass & Sustainability, Vol. 8, No. 1, June 2026, is a biannual publication, published and edited by Asociación Latinoamericana de Desarrollo Sustentable y Energías Renovables A.C. (ALDESER), Sur 4 No. 270, Colonia Centro, C.P. 94300, Orizaba, Veracruz, Mexico, Tel. 2722372285, Web Page: https://aldeser.org/revistas.html and email address: secretariat@aldeser.org.

The Reservation of Rights of Exclusive Use Certificate No.: 04-2025-060617423800-102, ISSN: 2683-2658, are both granted by the Instituto Nacional del Derecho de Autor (INDAUTOR, Mexico). Responsible for the last update of this issue: Andrea Alvarado Vallejo. Date of last modification, April 25, 2026.

Table of Contents

Impact of Photosynthetically Active Radiation (PAR) on the cultivation of marine microalgae in open systems under tropical climatic conditions

Valeria I. Barajas-Cardona, Juan C. Zavala-Reyes y Regina M. González-Balderas *

Escuela Nacional de Estudios Superiores Unidad Mérida, Universidad Nacional Autónoma de México, Tablaje Catastral N°6998, Carretera Mérida-Tetiz, km. 4.5, Municipio Ucú, Yucatán, México, C.P. 97357

* Corresponding author: regina.gonzalez@enesmerida.unam.mx; Tel.: (999 399 0901)

Received: March 31, 2025 Accepted: June 3, 2025 Published: January 26, 2026

DOI: https://doi.org/10.56845/rebs.v8i1.659

Abstract: Solar energy is the most cost-effective source for microalgae cultivation. Open-system biomass production enhances the sustainability of biofuel processes due to lower installation and operational costs. However, these systems are less efficient than closedsystems, as controlling light intensity and quality is challenging. This study evaluates the effect of photosynthetically active radiation (PAR) on marine microalgae cultivation in an open system under tropical climate conditions. The experiment was conducted in Mérida, Yucatán, using native microalgal strains to enhance adaptation. Throughout cultivation, PAR, nutrient concentrations, pH, and temperature were monitored to assess their interactions. Two trials were conducted in autumn (October–November) using three reactors exposed to different durations of solar radiation. Results indicate that the total daily PAR (30.6 mol/m²/day) exceeded the optimal growth range (20 mol/m²/day), leading to culture collapse within 14 days. Additionally, reactors exposed to longer sunlight exhibited greater temperature and pH fluctuations. No significant biomass accumulation or nutrient variation was observed. This study underscores the need for environmental monitoring in outdoor systems to optimize microalgae cultivation and better understand its applications and limitations.

Keywords: Photosynthetically active radiation, open pounds, microalgae

Introduction

Microalgae are photosynthetic autotrophs capable of utilizing solar or artificial light as an energy source to convert carbon dioxide (CO_2) and water into organic compounds, releasing oxygen (O_2) as a by-product. Their photosynthetic efficiency surpasses that of higher plants, as they can convert solar energy into biomass and other metabolites up to five times faster. This remarkable capacity for biomass production makes microalgae highly attractive for numerous biotechnological applications (Posten & Walter, 2012).

Among their most relevant applications, microalgae are widely used in bioremediation due to their ability to remove pollutants and toxic substances, often accumulating high concentrations of these compounds without impairing their physiological activity (Shao *et al*., 2022). They are also employed in the treatment of domestic, industrial, and livestock wastewater. Furthermore, microalgae represent a promising feedstock for biofuel production, offering a feasible alternative to the depletion of fossil fuel reserves (rChisti, 2016).

Microalgal biomass can be cultivated in open systems, exposed to outdoor environmental conditions, or in closed photobioreactors, where growth parameters can be tightly controlled. Although closed systems provide superior control, their large-scale implementation is limited by high operational costs, particularly those associated with artificial illumination and temperature regulation (Barceló-Villalobos *et al*., 2019). Consequently, assessing cultivation strategies that capitalize on natural solar radiation is essential, as is evaluating the influence of climatic and geographical factors on biomass productivity (González-Camejo *et al*., 2019). A key challenge in this context lies in identifying and selecting strains with high productivity under outdoor conditions. Additionally, tropical regions have been identified as optimal zones for microalgal biomass production, exhibiting the highest global productivity according to several studies (Dias *et al*., 2021).

Regardless of the cultivation system, region, or selected strain, parameters such as temperature, nutrient availability, and light intensity must be carefully managed, as they strongly influence growth kinetics and biochemical composition. Among these parameters, photosynthetically active radiation (PAR) plays a critical role, representing the fraction of the solar spectrum usable for photosynthesis. PAR spans wavelengths from 400 to 700 nm—approximately 50% of total solar radiation—with intensities typically ranging from 800 to 1000 W/m² (Dolganyuk *et al*., 2020). Although visible

light from blue to red wavelengths supports photosynthesis, radiation outside this range, such as ultraviolet or infrared, does not contribute to energy capture and may even damage photosynthetic cells.

Most microalgal species require between 5 and 20 mol/m²/day of PAR to achieve optimal growth. Lower doses restrict biomass accumulation, whereas higher doses increase the risk of photoinhibition, a light-induced reduction in photosynthetic efficiency. Therefore, quantifying PAR in outdoor cultures is essential for determining optimal solar exposure according to the physiological requirements of specific strains. This practice enhances photosynthetic efficiency, maximizes biomass productivity, and mitigates light-induced damage. Additionally, reliance on natural solar radiation significantly improves the economic and environmental sustainability of biomass production for biofuel applications. Nonetheless, open systems remain challenging due to the inherent difficulty of regulating solar radiation intensity and quality (Guedes *et al*., 2023).

In this context, the present study evaluates the influence of PAR on the cultivation of marine microalgae in an open system. The experiment was conducted under tropical climatic conditions in Mérida, Yucatán, Mexico, a region characterized by high solar irradiance, which is favorable for outdoor biomass production. Native microalgal strains from the Yucatán Peninsula were used, facilitating their adaptation to local environmental conditions. Throughout cultivation, biomass concentration, nutrient levels, pH, and temperature were monitored alongside PAR to determine its effect on these key variables.

Materials and Methods

Study Area

The study was conducted on the terrace of the Teaching Building at the National School of Higher Studies, Mérida Unit (Mexico). The region exhibits a bi-seasonal tropical climate consisting of a prolonged dry season and a summer rainy season. According to the Köppen classification modified by García *et al*. (2010), the climate is tropical with a mean annual temperature of 26 °C and maximum temperatures reaching 38 °C. Solar irradiance is consistently high; annual average radiation is 425.27 W/m², with monthly values exceeding 1000 W/m² between May and October (Morcillo Herrera, 2016).

Microalgae Cultivation

A marine microalgal consortium isolated from Sisal, Hunucmá, Yucatán, was cultivated in 4-L reactors. Each reactor included a volume indicator to detect evaporation losses. The culture medium consisted of a 50:50 mixture of seawater and distilled water supplemented with 47 ± 0.26 mg/L N-NO_3^- and 3.58 ± 0.25 mg/L P-PO_4^{3-}, with a pH of 7.32 and a salinity of 22.54 ± 0.41‰.

The experiment was performed during October and November, when the expected mean monthly solar radiation is approximately 425.27 W/m². Reactors were placed 2 meters apart near the environmental monitoring station and positioned to provide different daily sunlight exposures:

- Reactor I: sunrise–13:00 h
- Reactor II: sunrise–16:00 h
- Reactor III: sunrise–sunset (17:30–18:00 h)

Reactors were sealed with perforated lids to prevent insect intrusion while allowing adequate ventilation. Biomass concentration was determined as Total Suspended Solids (TSS) according to APHA (1992). Nutrient concentrations (P-PO_4^{3-} and N-NO_3^-) were measured using a dual-beam UV-visible spectrophotometer (Agilent Cary 60) following APHA (1992). Temperature and pH were monitored using an Extech EC500 multiparameter meter after calibration with standard solutions and homogenization of the cultures

PAR Monitoring

Photosynthetically Active Radiation (PAR) was measured using a monitoring station equipped with a pyranometer (S-LIB-M003) and a PAR sensor (S-LIA-M003), connected to a HOBO U30 datalogger. Instantaneous readings were collected every 30 seconds, and averaged values were logged every 1-minute internal. Data acquisition and retrieval were performed using HOBOware® software.

Results and Discussion

Two experimental assays were conducted. Figure 1 displays the growth curves and nutrient removal profiles obtained duringthe first assay. In all three reactors, microalgal cultures failed to survive beyond ten days. Nutrient concentrations ($P\text{-}PO_4^{3-}$ and $N\text{-}NO_3^-$) showed no significant decrease during the 14-day period, indicating minimal nutrient assimilation and absence of measurable biomass accumulation.

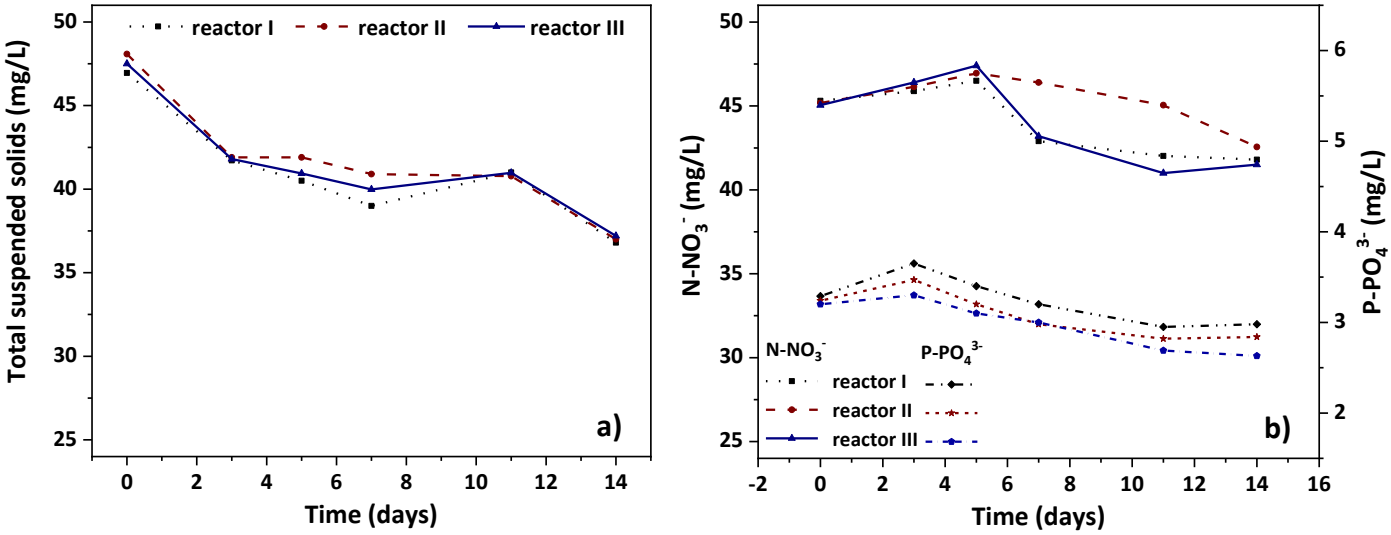

Figure 1. Growth dynamics (a) and nutrient removal profiles (b) of the marine microalgal consortium cultivated in an open system during the first experimental assay

These results suggest that the cultures experienced thermal stress caused by extended exposure to solar radiation. Reactors I, II, and III received approximately 8, 11, and 14 hours of direct sunlight per day, respectively. The presence of perforated lids and the placement of reactors on a concrete surface likely intensified heat retention, as concrete acts as a thermal mass and contributes to maintaining elevated temperatures within the reactors.

Temperature profiles shown in Figure 2a support this interpretation: reactor temperatures reached values as high as 35 °C, particularly in Reactors II and III, which were exposed to longer photoperiods. Correspondingly, Figure 2b shows notable pH fluctuations, primarily following periods of increased temperature, suggesting substantial physiological stress within the cultures.

Together, these findings indicate that excessive thermal load was the primary factor limiting culture survival, nutrient removal, and biomass production during the first experimental assay.

In the second experimental assay (Figure 3), reactor overheating was addressed by removing the plastic lids and covering the reactors with mosquito netting to maintain aeration while preventing contamination. Despite this modification, the cultures did not display measurable biomass accumulation; TSS values remained constant at approximately ~43 mg/L (Figure 3a). Consistent with the growth results, nutrient concentrations ($N\text{-}NO_3^-$ and $P\text{-}PO_4^{3-}$) showed no significant depletion over time, indicating a lack of measurable nutrient removal under these conditions.

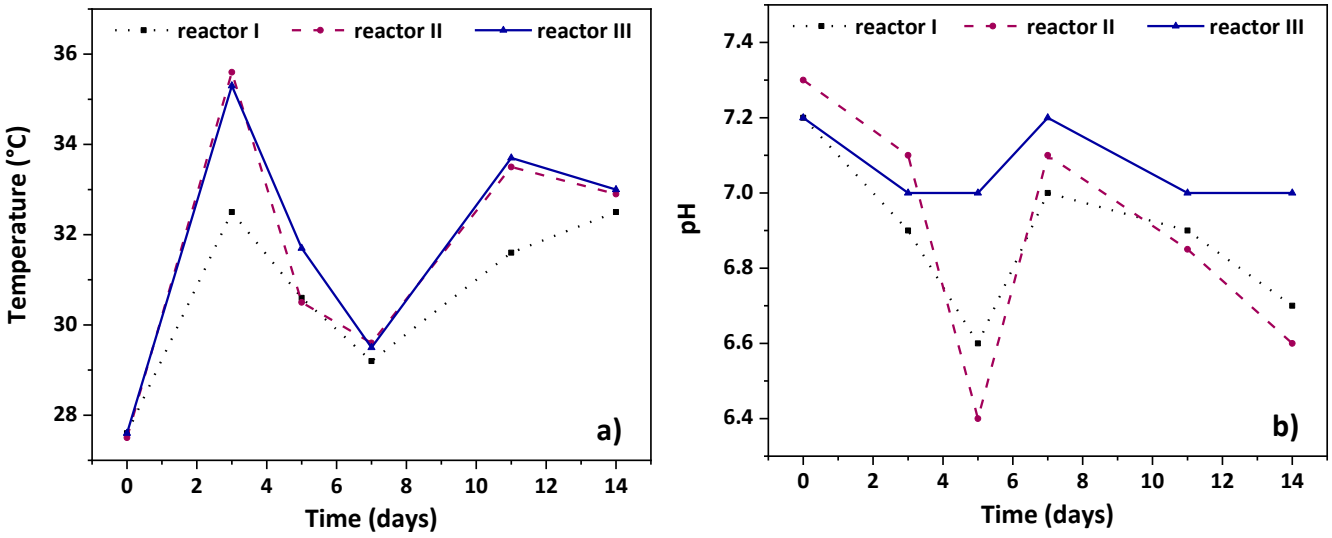

Figure 2. Solar exposure effects on (a) culture temperature and (b) pH in reactors I, II, and III during the first experimental assay

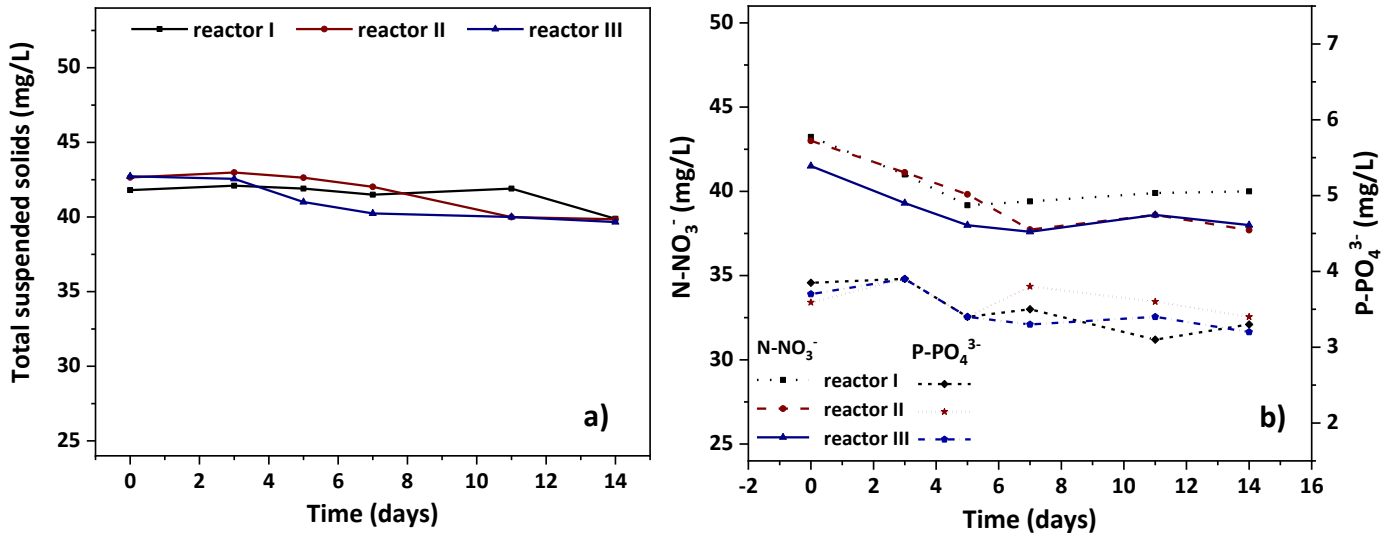

Figure 3. Growth dynamics (a) and nutrient removal profiles (b) of the microalgal consortium cultivated in an open system during the second experimental assay

Visual assessment of culture pigmentation revealed distinct responses among reactors, particularly after day 7. Reactor I, exposed to the least sunlight, displayed progressive pigment fading, suggesting insufficient irradiance to sustain optimal photosynthetic performance. Reactor II showed the most stable appearance, maintaining uniform dark green coloration throughout the first ten days, consistent with an intermediate and apparently favorable light regime. However, despite this stable pigmentation, no measurable biomass increases or exponential growth phase occurred. Following day 10, the culture in reactor II also collapsed, indicating that environmental stressors ultimately exceeded the consortium's tolerance threshold.

Reactor III exhibited marked pigment loss beginning on day 7, shifting from dark green to yellowish tones, indicative of chlorophyll degradation and photo stress. This response aligns with the extended solar exposure experienced by this reactor, the longest among the three. Despite this stress, the microalgal consortium—composed of native strains from the Yucatán Peninsula—survived more than ten days under high irradiance and elevated internal temperatures.

Routine inspection of reactor volume indicators revealed no detectable water loss, suggesting that temperatures did not reach levels sufficient to induce evaporation. Temperature dynamics (Figure 4a) showed a reduction immediately after replacing the plastic lids with mosquito netting. Temperature increases closely followed exposure duration:

reactor III reached values up to 2 °C above those in reactors I and II. pH remained comparatively stable, with smaller fluctuations than those observed in the first experimental assay.

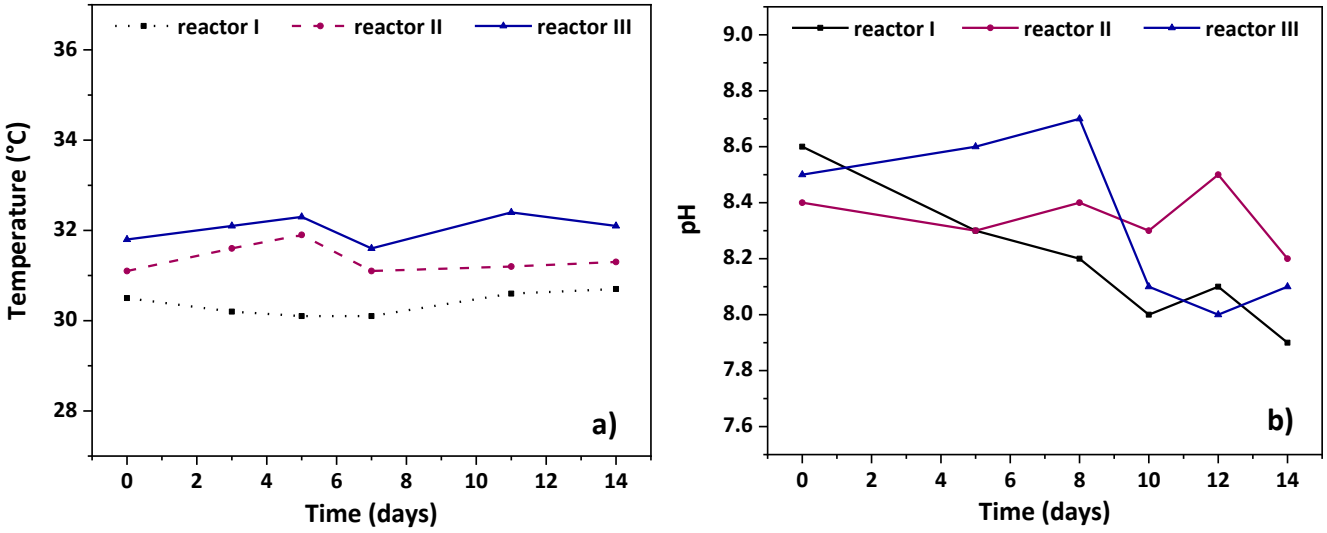

Figure 4. Influence of solar exposure on (a) culture temperature and (b) pH in reactors I, II, and III during the second experimental assay

PAR measurements (Figure 5) recorded between October 1 and November 15 revealed an average daily total of 30.6 mol/m²/day. This value substantially exceeded the optimal irradiance for microalgal growth (<20 mol/m²/day). The high radiation load is therefore identified as a major factor limiting culture persistence, as excessive irradiance can induce photoinhibition and severely compromise microalgal viability.

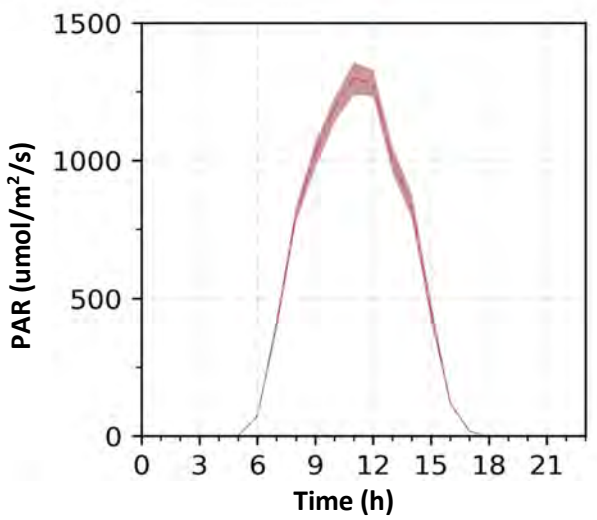

Figure 5. Diurnal PAR profile showing mean values (marron line) and the corresponding 95% confidence interval (shaded region)

The mean diurnal PAR pattern (Figure 5) is represented by a dotted line summarizing all measurements collected during the study period, along with a 95% confidence interval (shaded region). PAR values became positive shortly after 05:00 h and increased rapidly, surpassing 500 µmol/m²/s between 08:00 and 15:00 h. Peak irradiance exceeding 1000 µmol/m²/s occurred consistently from 09:00 to 14:00 h, a period of sustained high radiation that likely imposed substantial photo stress on reactor III due to its extended exposure duration.

The PAR time series (Figure 6) further illustrates pronounced diurnal variability, with instantaneous peaks occasionally exceeding 2000 µmol/m²/s near midday on several days. This pattern remained stable throughout the experiment, indicative of predominantly clear-sky conditions and limited atmospheric attenuation. These high-intensity events are

important when interpreting culture performance, as they represent acute irradiance levels capable of inducing photoinhibition.

Comparation of Figures 5 and 6 demonstrates the necessity of analyzing both averaged irradiance profiles and extreme events. While the mean diurnal curve in Figure 5 yields a smoothed pattern with a maximum near 1250 µmol/m²/s, the instantaneous measurements capture short-lived but intense spikes above 2000 µmol/m²/s, highlighting periods of potentially severe stress for the microalgae.

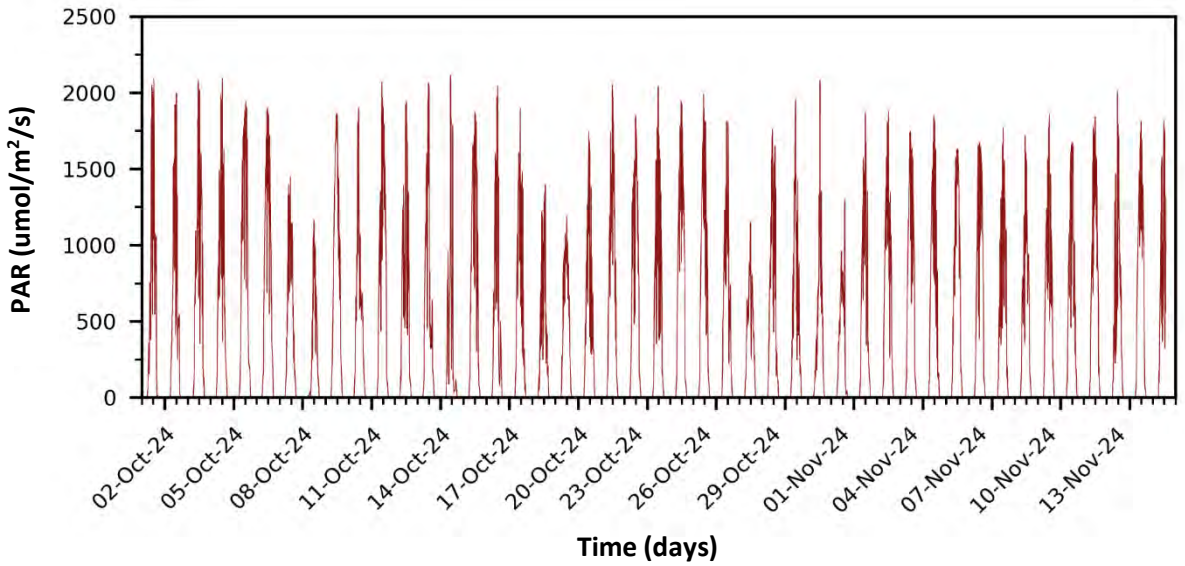

Figure 6. Time series of photosynthetically active radiation (PAR) measured in Mérida, Yucatán, between 1 October and 15 November 2024

Few studies have explicitly evaluated the role of PAR in outdoor microalgae cultivation systems. Consistent with findings by Guedes *et al*. (2023), our results reaffirm that solar irradiance is a viable and accessible energy source for microalgae production, particularly in regions with limited technological or economic resources.

Despite its advantages, reliance on natural sunlight introduces challenges due to the difficulty of controlling irradiance intensity and spectral quality—factors shown here to affect culture stability and performance. Nonetheless, these constraints can be partially addressed through system-level design interventions, including optimized reactor orientation, use of high-transmittance materials, PAR-triggered automated exposure control, and continuous monitoring of environmental parameters. Such measures could enhance biomass productivity while mitigating photo inhibitory stress. However, implementing these strategies requires careful management to ensure consistent operation and to avoid unintended environmental or physiological impacts on the cultures.

Conclusions

The findings of this study demonstrate that sunlight exposure time is a primary driver of the performance of the native microalgal consortium cultivated in open systems. The absence of detectable changes in nutrient concentration or biomass suggests that light availability—rather than nutrient limitation—was the dominant factor constraining growth. Both insufficient and excessive irradiance led to rapid culture decline, indicating a narrow operational window for maintaining stable biomass productivity. The combined effects of prolonged irradiance and temperature fluctuations appear to further influence culture viability, underscoring the strong coupling between light and thermal stress in outdoor environments.

Continuous PAR measurements provided critical insights into the relationship between environmental variability and culture dynamics. These data emphasize the value of sustained monitoring, which enables the identification of irradiance thresholds, informs system design, and strengthens reproducibility for future experiments.

Collectively, the results highlight the necessity of implementing robust environmental monitoring systems in outdoor cultivation platforms. Such systems not only support informed decision-making for process optimization but also clarify the practical limitations and potential of microalgal biomass production under natural irradiance regimes. This study therefore establishes an empirical basis for future research aimed at improving system resilience, optimizing light management strategies, and enhancing productivity in open microalgae cultivation systems.

Acknowledgments and Funding: The authors express their gratitude to the Programa de Apoyo a Proyectos de Investigación e Innovación Tecnológica (PAPIIT, UNAM), project IA104423, *"Interaction between vegetation, urban infrastructure, and the atmosphere: study of the urban climate and its surroundings through atmospheric models."* The authors also thank ENES–Mérida for providing the facilities necessary to carry out this work. Additionally, we acknowledge the support of the PAPIIT scholarship program, part of the Elisa Acuña scholarship program, for the scholarship awarded (folio 271924, scholarship ID B242109).

Author contributions: V.I.B.C.: data collection and analysis; J.C.Z.R.: funding acquisition, interpretation of data and editing; R.M.G.B.; conceptualization, writing and interpretation of data.

References

APHA, AWWA, & WPCF. (1992). *Standard methods for the examination of water and wastewater* (18 ed.). Washington, E.U.A.

Barceló-Villalobos, M., Fernandez-del Olmo, P., Guzmán, J. L., Fernández-Sevilla, J. M., & Acien Fernández, F. G. (2019). Evaluation of photosynthetic light integration by microalgae in a pilot-scale raceway reactor. *Bioresource Technology*, *280*, 404–411. https://doi.org/10.1016/j.biortech.2019.02.032

Chisti, Y. (2007). Biodiesel from microalgae. *Biotechnology Advances*, *25*(3), 294–306. https://doi.org/10.1016/j.biotechadv.2007.02.001

Dias, R. R., Lasta, P., Vendruscolo, R. G., Wagner, R., Zepka, L. Q., & Jacob-Lopes, E. (2021). Mapping the performance of photobioreactors for microalgae cultivation. Part II: Equatorial and tropical climate zone. *Journal of Chemical Technology and Biotechnology*, *96*, 613–621. https://doi.org/10.1002/jctb.6574

Dolganyuk, V., Shkrabets, F., Azarkina, A., Zayats, Y., Shevchuk, O., Pashtetskiy, V., & Nagurskaya, N. (2020). Microalgae: A review of the basics of cultivation, use, and prospects for development. *Energies*, *13*(19), 4927. https://doi.org/10.3390/en13194927

García, D., González, M., & Elena, M. (2010). *Biodiversidad y desarrollo humano en Yucatán*. CICY, PPD-FMAM, CONABIO, SEDUMA, 10–16, 125–129.

González-Camejo, J., Jiménez-Benítez, A., Ruano, M. V., Robles, R., Barat, A., & Ferrer, J. (2019). Optimising an outdoor membrane photobioreactor for tertiary sewage treatment. *Journal of Environmental Management*, *245*, 76–85. https://doi.org/10.1016/j.jenvman.2019.05.010

Guedes, V. C., Palma, G. M., & Horta, A. C. L. (2023). Una evaluación de las longitudes de onda, la intensidad y el control de la luz para la producción de microalgas en fotobiorreactores: una revisión. *Brazilian Journal of Chemical Engineering*. https://doi.org/10.1007/s43153-023-00388-x

Morcillo Herrera, C. M. (2016). *Seguidor del punto de máxima potencia de un sistema fotovoltaico con redes neuronales*. Centro de Investigación Científica de Yucatán.

Posten, C., & Walter, C. (2012). *Microalgal biotechnology: Integration and economy*. De Gruyter.

Shao, H., Sun, Y., Jiang, X., Hu, J., Guo, C., Lu, C., Guo, F., Sun, C., Wang, Y., & Dai, C. (2022). Towards biomass production and wastewater treatment by enhancing the microalgae-based nutrients recovery from liquid digestate in an innovative photobioreactor integrated with dialysis bag. *Journal of Environmental Management*, *317*, 115337. https://doi.org/10.1016/j.jenvman.2022.115337

Experimental and numerical study of a three-blade horizontal turbine in a wind tunnel

Luis César Delgado-Escobar [1], Valaur Ekbalam Márquez-Baños [2], Román Guadarrama-Pérez [3], Felipe González-Montañez [1], Victor M. Jimenez-Mondragón [1], Javier Valencia-López [4], Alejandra Manuela Vengoechea-Pimienta [1], y Jorge Ramírez-Muñoz [1,*]

[1] Departamento de Energía, DCBI, Universidad Autónoma Metropolitana unidad Azcapotzalco, Azcapotzalco, CDMX, México
[2] Área de Química, Departamento de Preparatoria Agrícola, Universidad Autónoma Chapingo, Texcoco, Estado de México, México
[3] Departamento de Ingeniería Química, TecNM/Instituto Tecnológico Superior de El Mante, Ciudad Mante, Tamaulipas, México
[4] Departamento de Procesos y Tecnología, DCNI, Universidad Autónoma Metropolitana unidad Cuajimalpa, Cuajimalpa, CDMX, México
* Autor de correspondencia: jrm@azc.uam.mx; Tel.: +52 55-53189000, ext. 2195

Received: June 26, 2025 Accepted: October 2, 2025 Published: January 26, 2026
DOI: https://doi.org/10.56845/rebs.v8i1.679

Abstract: Electricity generation from renewable sources is essential for sustainable development and is particularly critical in regions affected by energy poverty. In this context, micro-scale wind turbines offer a viable alternative for electrifying isolated rural communities. This study evaluates, experimentally and numerically, the performance of a three-bladed horizontal-axis wind turbine designed to operate under controlled conditions in a wind tunnel. The turbine was fabricated by 3D printing and tested in the wind tunnel of the Autonomous Metropolitan University–Azcapotzalco, Mexico. Steady-state numerical simulations were performed in ANSYS Fluent using the k-ω SST turbulence model. The computational domain was discretized with polyhedral and hexahedral elements under Multiple Reference Frame (MRF) rotational conditions. A mesh-independence analysis based on the numerical torque was conducted, resulting in an optimal mesh of 2,191,718 elements. The numerical model was subsequently validated against experimental data, showing an average torque deviation of 9.27%. Flow visualization through streamlines and velocity-magnitude contours revealed unwanted vortices in the tail-vane region, which induced flow instability and mechanical vibrations in the current design. These effects should be mitigated in future design improvements. The turbine efficiency curve was obtained from electrical power measurements under different resistive loads, adjusted via a light-bulb resistance board, at a wind-tunnel speed of 18.19 m/s. The maximum efficiency achieved was 24%, corresponding to a generated power of 15.2 W at a rotational turbine speed of 3224 RPM. The results validate the proposed CFD model and provide a solid basis for future design optimization of micro-scale wind power systems for rural applications.

Keywords: wind energy, small-scale wind turbine, CFD simulation, wind tunnel, wind turbine efficiency

Introduction

Access to electrical energy is fundamental to human development, as it enables essential services such as potable water, sanitation, healthcare, education, lighting and transportation (Sánchez-Santillán, 2021). At the domestic level, energy availability directly influences well-being and productivity by enabling cooking, ventilation, lighting, and the use of electronic devices (Espinosa-Dorado & Carrillo Núñez, 2021).

However, despite the growing recognition of the importance of energy access, millions of people worldwide still lack it, primarily due to high costs or insufficient electrical infrastructure (Espinosa-Dorado & Carrillo Núñez, 2021). This condition is known as energy poverty. To address this challenge, in 2015 the Member States of the United Nations (UN) established Sustainable Development Goal (SDG) No. 7, which aims to ensure universal access to affordable, reliable, and modern energy by 2030 (UN, 2015). Although significant progress has been made, reducing the share of the global population without electricity from 13% in 2021 to 9% in 2023, equivalent to 675 million people, there is still much work to be done (UN, 2023).

In Mexico, the National Institute of Statistics and Geography (INEGI) reported that around 1% of the population lacked adequate electricity access in 2020, representing about 1.2 million people living under energy poverty conditions (INEGI, 2020). This situation particularly affects rural and marginalized communities, where grid expansion is often economically unfeasible.

Renewable energy technologies, particularly micro-scale wind energy systems, offer a sustainable alternative for meeting the basic electricity demands of isolated communities. Micro-scale wind turbines, typically generating between 100 and 500 W, provide advantages such as compact size, low cost, and simple installation, making them suitable for rural electrification, community projects, or educational applications (Zemamou, Aggour & Toumi, 2017).

A conventional wind energy system consists of a turbine, an electric generator, a power electric converter, and an energy storage unit (Ramírez, Parra & González, 2012). The turbine converts wind kinetic energy into mechanical energy, which is then transformed into electrical power in the generator (Escobar-Díaz & Barrero-Páez, 2009). Because the generator performance depends on the aerodynamic torque produced by the turbine, optimizing the rotor design is crucial for efficient operation.

For this reason, various researchers have focused on turbine design, evaluating parameters such as the orientation of the rotation axis (horizontal or vertical), the number and spacing of blades, and the torsion angle, among others, to maximize the capture of kinetic energy. According to Betz's law, only about 60% of the wind's kinetic potential can theoretically be converted into usable energy (Betz, 1966). In the market, different turbine types are available, particularly Savonius type turbines, which are vertical-axis devices characterized by their ability to operate independently of wind direction and with relatively low wind speeds. These turbines can capture up to 37% of the wind's potential energy (Zemamou, Aggour & Toumi, 2017).

Although the technologies mentioned have produced excellent results, they also present certain disadvantages, such as visual and noise pollution generated by wind systems (Van der Zwaan & Rabl, 2003). Therefore, there is still a broad field of study aimed at optimizing the design of these energy generation systems. In the development of micro-scale wind turbines, Computational Fluid Dynamics (CFD) has become a key tool to optimize design and improve energy conversion efficiency (Arpino *et al*., 2017; Lanzafame *et al*., 2013). Through CFD, it is possible to analyze airflow behavior around the turbine, evaluate the impact of different design parameters, and predict aerodynamic performance before constructing a physical prototype (Kale *et al*, 2013; Wang & Zhan, 2013).

In this work, the efficiency of a three-blade turbine is analyzed under controlled conditions in a wind tunnel. In addition, a CFD model of the same turbine was developed and validated using experimental data, allowing for future improvements to this design.

Materials and Methods

The turbine radius, measured from the center of rotation to the blade tip, is 11.2 cm. Experimental tests were conducted at a wind speed of 18.2 m/s in the wind tunnel of the Autonomous Metropolitan University–Azcapotzalco, facility designed to generate a controlled and uniform airflow within a confined section. The experimental setup is shown in Figure 1. It should be noted that a wind speed of 18.2 m/s is relatively high for the continuous operation of a micro-scale wind turbine; however, this velocity was intentionally selected to evaluate the structural response and maximum performance of the rotor under high-load conditions, which is essential for defining its safe operational limits.

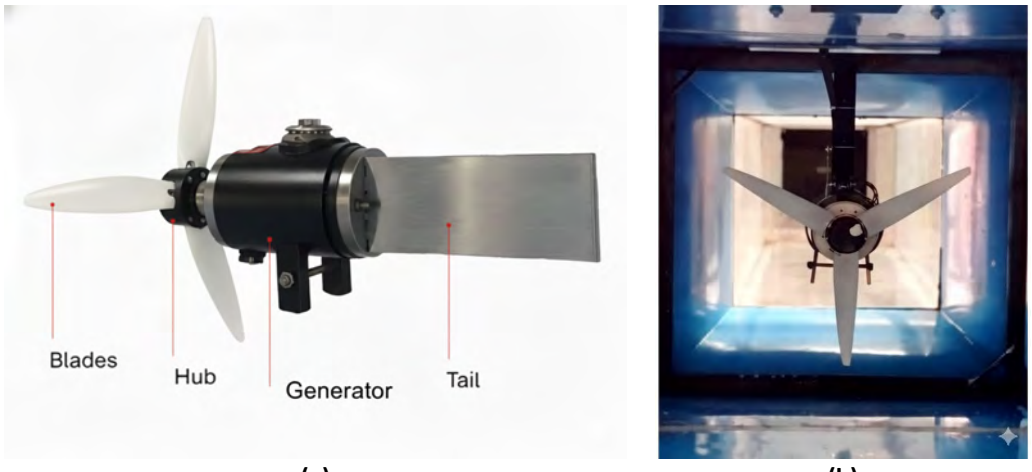

(a) **(b)**

Figure 1. (a) Three-blade wind turbine and (b) turbine mounted in the experimental wind tunnel

The efficiency of the wind turbine under steady wind conditions (18.2 m/s) was evaluated from electrical voltage and current measurements as a function of the applied resistive load. The load bank consisted of sixteen 7.5 W incandescent light bulbs connected in parallel, used as resistive elements to draw electrical power from the generator. The bulbs were mounted on a load board equipped with a digital multimeter for data acquisition, as shown in Figure 2.

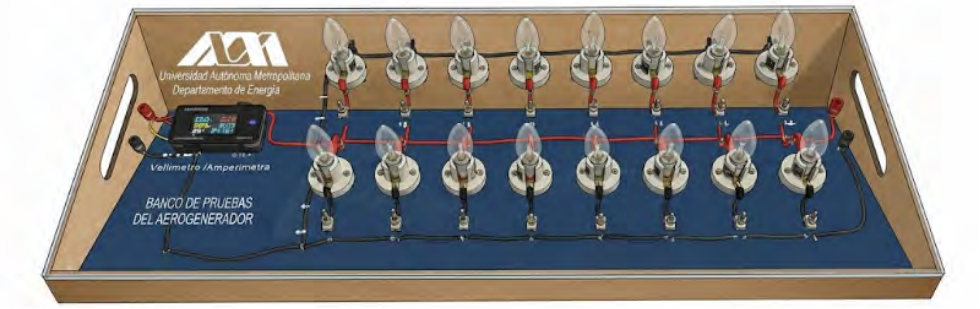

Figure 2. Board of 16 resistive loads (light bulbs) connected in parallel

Using this board, the turbine energy conversion efficiency (η) was calculated as the ratio of the electrical power generated by the DC turbine (P_{elec}) to the wind power (P_v), multiplied by the Betz limit, as expressed in Equation 1.

$$\eta = \frac{P_{elec}}{P_v} = \frac{V \cdot I}{0.593\left(\frac{1}{2}\rho A v^3\right)} \quad \textbf{(1)}$$

where ρ is the air density, A the projected area of the turbine, v the wind velocity, and V and I represent the generated voltage and current, respectively.

To validate the numerical simulations, in situ measurements were performed to quantify the electrical power consumed by the wind turbine installed in the wind tunnel under static conditions (without airflow) and with the rotor operating at the desired speeds. To accomplish this, the wind turbine was driven at specific rotational speeds by regulating the input voltage using a direct current (DC) power supply with an operating range of 0–120 V, as shown in Figure 3. The voltage and current consumed by the turbine were measured using two multimeters: one connected in parallel (for voltage measurement) and the other in series (for current measurement). Power consumption was then calculated as the product of voltage and current. First, the power consumed by the turbine without the rotor (P_{sr}), was recorded, followed by the power consumed with the rotor (P_{cr}), Both power measurements were performed at identical operating speed. The electrical power consumed by the turbine due to the presence of the rotor (P_r), was obtained using the Equation 2.

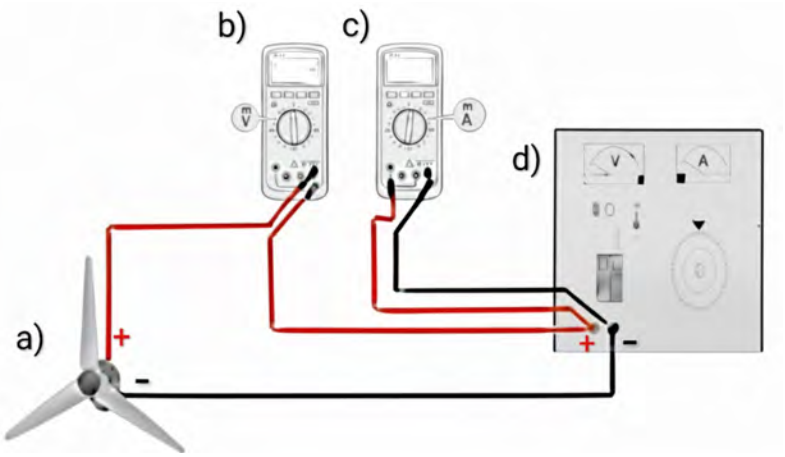

Figure 3. Electrical power measurement system: (a) three-blade turbine (generator DC), (b) multimeter for voltage measurement, (e) multimeter for current measurement, and (f) DC power supply (0–120 V)

$$P_r = P_{cr} - P_{sr} \quad (2)$$

All power values are expressed in watts (W). The experimental torque on the rotor (N·m) derived from electrical power measurements was calculated as follows:

$$\tau_r = \frac{P_r}{2\pi N} \quad (3)$$

where N (s^{-1}) represents the rotor rotational speed.

For the CFD-based simulation, the geometry of the turbine, the motor body, and a section of the wind tunnel were digitally reconstructed. The computational mesh for the wind tunnel–three-blade generator system was generated using ANSYS Fluent Meshing with the Poly-Hexacore method, which produces a polyhedral mesh on the surfaces and hexahedral elements throughout most of the flow domain.

To ensure the numerical reliability of the results, a mesh independence analysis was performed by systematically comparing simulations with different refinement levels until the relative error in the variable of interest (torque) between two consecutive meshes fell below a predefined threshold. The process began with an automatically generated base mesh, followed by successive refinements that approximately doubled the number of elements in each subsequent mesh. The optimal mesh was selected based on the reduction in error between consecutive meshes. Table 1 presents the number of elements used in each case and the corresponding numerical torque values.

Table 1. Mesh independence analysis.

Mesh	Number of Elements	Torque (N·m)
#1	639,139	0.9097
#2	1,080,893	0.6165
#3	2,191,718	0.6500
#4	4,541,751	0.6597

As shown in Table 1, mesh #3, consisting of 2,191,718 elements, provided an appropriate balance between accuracy and computational cost, with an error of only 0.32% compared to mesh #4, even though the latter doubled the number of elements and considerably increased the computational demand. The refined mesh obtained with mesh #3 is shown in Figure 4. Figure 4a illustrates lateral and horizontal cross-sectional views of the elements through the tunnel, while Figure 4b shows the elements on the surface of the rotor blades, generator, and tail.

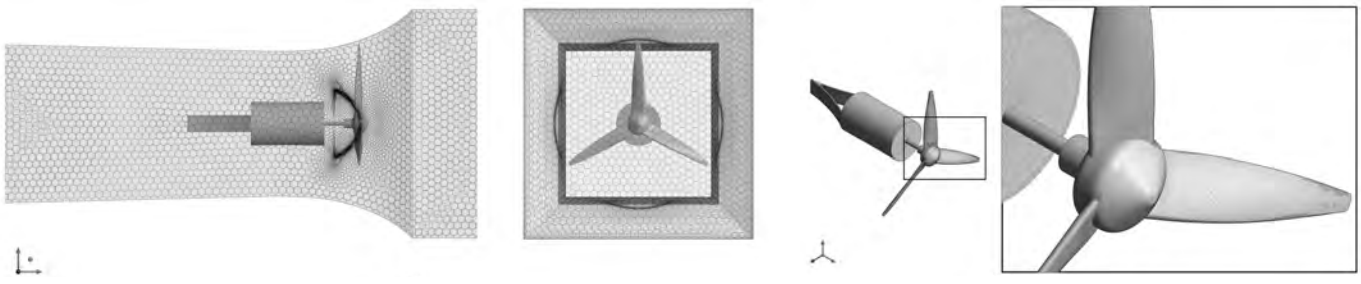

(a) **(b)**

Figure 4. Computational mesh: (a) wind tunnel, (b) three-blade turbine

The turbulent flow within the system was modeled using the k–ω SST turbulence model, which has been widely employed for simulation of wind turbines (Rocha *et al*., 2014; Ji *et al*., 2022, Younoussi & Ettaouil, 2024). The turbine rotation was represented using the Multiple Reference Frame (MRF) approach, based on the experimentally measured rotational speed. As boundary conditions, a no-slip condition was applied to all solid walls, while an inlet velocity of

18.1 m/s matching the experimental conditions was imposed at the front of the wind tunnel. At the outlet, atmospheric pressure was specified. The simulations were performed in ANSYS FLUENT 2025 under steady-state conditions with a convergence criterion of 10^{-5}, using a coupled pressure–velocity scheme. For spatial discretization, the Least Squares Cell-Based method was applied for gradient evaluation, PRESTO! for pressure, and Second-Order Upwind schemes were employed for momentum and turbulence variables.

Results and Discussion

Figure 5 shows the effect of the electrical load (number of light bulbs) on the wind turbine performance in terms of current consumption, voltage, and rotational speed. Regarding current consumption (Figure 5a), a sustained increase is observed up to approximately six light bulbs, reaching a maximum value close to 0.24 A. This is attributed to the decrease in equivalent resistance as the number of parallel loads increases. Beyond this point, the current exhibits a slight decrease and subsequently stabilizes, indicating that the generator can no longer supply more current due to the drastic drop in turbine rotational speed. This behavior is also reflected in Figure 5b, corresponding to voltage, which displays a gradual decrease in the initial load levels, followed by an abrupt drop after six light bulbs, reflecting the loss of rotational speed required to sustain electrical induction. On the other hand, the turbine rotational speed (Figure 5c) presentsa progressive decrease at low loads and a sudden reduction after the same critical point, finally stabilizing below 800 rpm, regardless of the additional load. Overall, the results identify a clear operating threshold around six light bulbs, beyond which the turbine cannot maintain effective energy extraction.

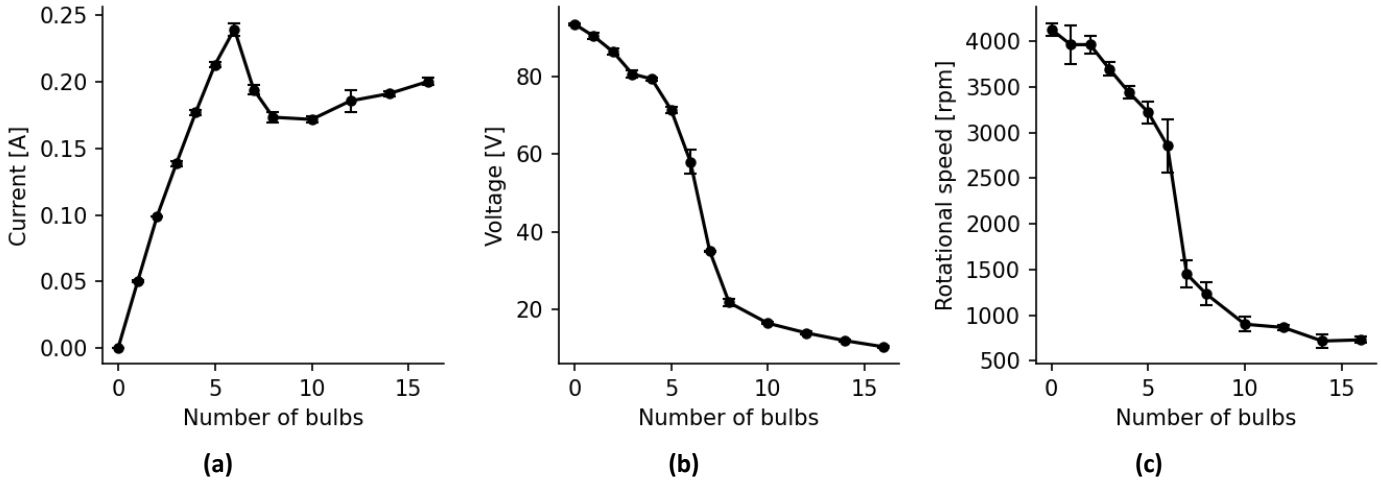

Figure 5. Effect of the electrical load (light bulbs) on (a) current, (b) voltage and (c) turbine rotational speed

The results obtained from Equation 1 are shown in Figure 6, the efficiency increases steadily as the equivalent resistance decreases, reaching a maximum of approximately 0.24 around six lights (Figure 6a), representing the point at which the available aerodynamic torque balances the electrical demand of the load. Beyond this optimal condition, efficiency drops sharply due to the reduction in rotational speed and the consequent decrease in power delivered by the generator. This trend is confirmed in Figure 6b, where efficiency increases almost linearly with current up to approximately 0.20 A, followed by an abrupt drop associated with overload conditions, in which the increased demand does not result in greater energy conversion. The maximum efficiency, corresponding to a generated power of 15.2 W at a wind speed of 18.19 m/s and a rotational speed of 3224 rpm.

Once the maximum efficiency point is exceeded, increasing the load causes a sharp efficiency drop because the rotor speed decreases significantly. When the electrical load increases (i.e., more power is drawn from the generator) at constant wind speed, the resistive torque exerted by the generator on the rotor also increases. If the aerodynamic torque generated by the wind does not increase proportionally, the rotor slows down to balance the extracted energy. Thus, each wind speed has an optimal operating point that maximizes turbine efficiency, known as the optimal tip-speed ratio. Deviating from this point, whether by increasing or decreasing the load, reduces efficiency. A high load slows the rotor speed excessively, while a low load causes the blades to spin too fast, cutting through the air without effectively capturing its energy.

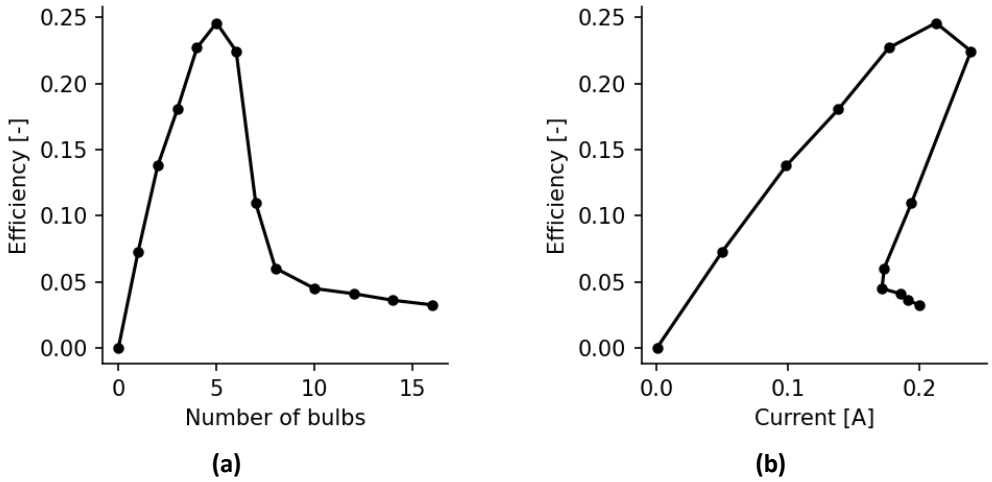

Figure 6. Turbine efficiency, (a) as function of number of resistive loads, and (b) as function of produced current

These results confirm that the wind turbine has a clearly defined operating point to maximize its efficiency, which depends on both the aerodynamic design of the blade and the interaction between the electrical load and the rotor behavior. Identifying this operating point is fundamental for using the system microgeneration applications.

Figure 7 comparesthe experimentally obtained torque values and those obtained through CFD simulation under static conditions. Overall, good agreement is achieved between the two datasets. The relative error between the simulated and experimental values ranged from 4.36% to 12.7%, with an average of 9.27%, confirming the numerical model ability to accurately reproduce the rotor mechanical response. This level of accuracy is consistent with previous studies on small-scale turbines and validates both the use of the k–ω SST turbulence model and the MRF approach for representing the system rotation.

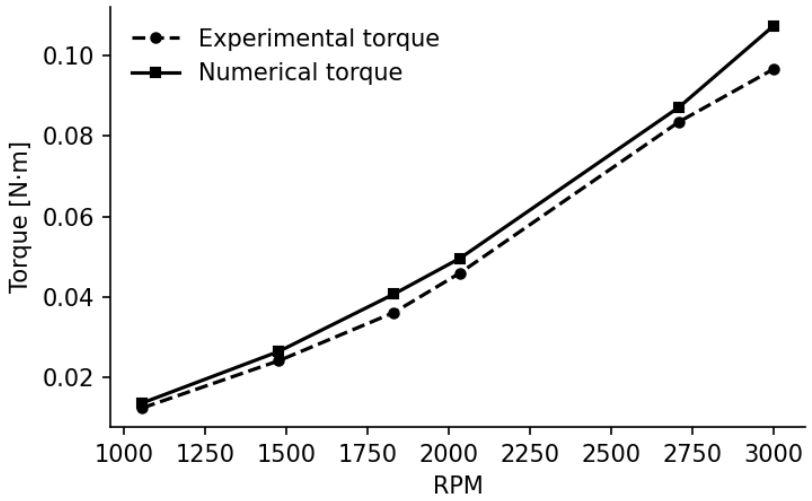

Figure 7. Comparison of simulated and experimental torque values as a function of rotor rotational speed

Figure 8 presents the flow field around and downstream of the turbine, represented by streamlines colored in red and velocity vectors colored with their magnitude show the direction of the flow, close-ups of the wind turbine tail area are also shown. The highest velocity values occur near the rotor blades, especially at the tips. A key observation is the presence of unwanted vortices in the tail region of the wind turbine, whichdisrupts the local velocity field. These structures can induce mechanical instabilities, vibrations, and aerodynamic losses, making them a crucial point to consider in future optimizations of the structural and aerodynamic design.

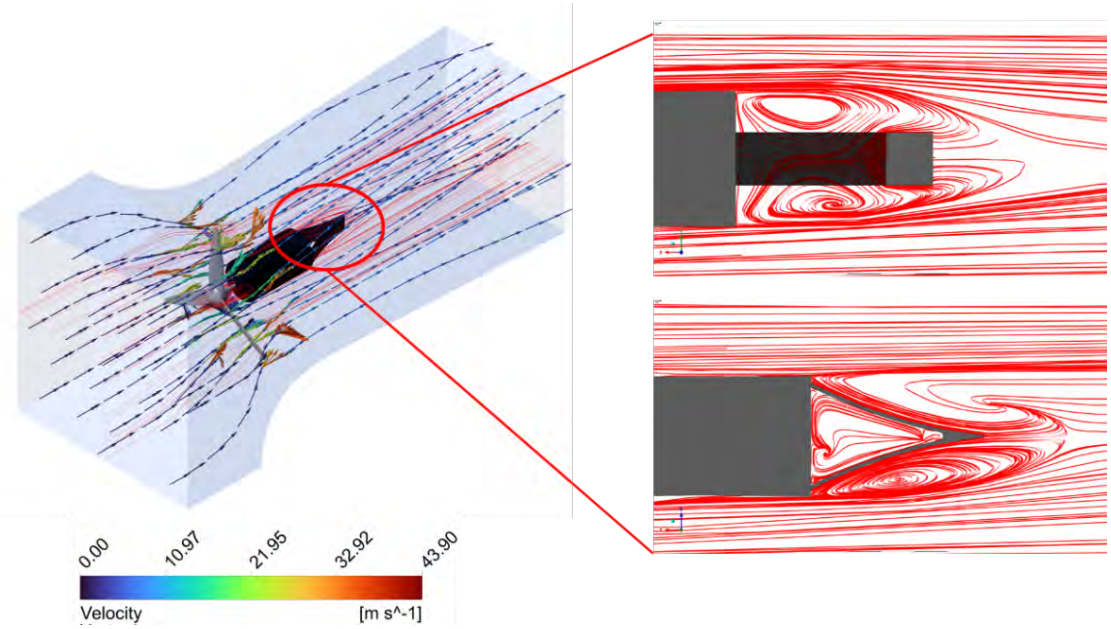

Figure 8. Numerical flow pattern around the wind turbine

On the other hand, the turbulent kinetic energy contours presented in Figure 9 show that the motor body induces a significant region of turbulence, generating a pronounced wake downstream of the wind turbine. This high-energy turbulent zone not only affects the flow pattern around the rotor but can also contribute to load fluctuations and unwanted variations in transmitted torque. These results suggest that it would be necessary to develop a housing with an aerodynamically optimized design for the motor body and tail section in order to minimize turbulence generation, reduce vibrations during operation, and improve the dynamic stability of the system.

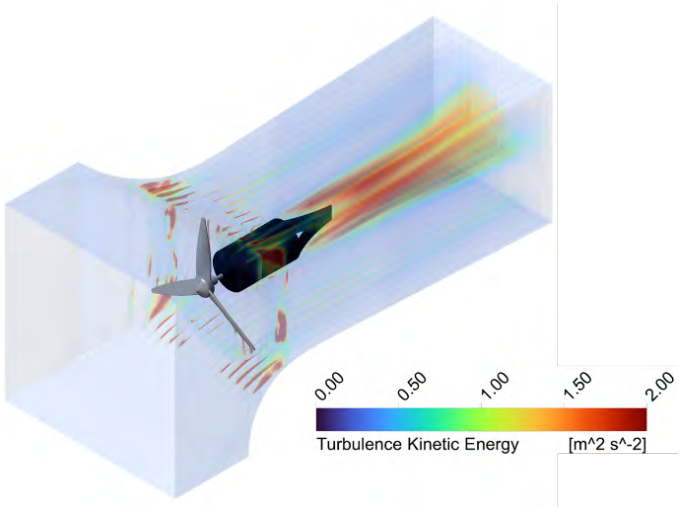

Figure 9. Numerical turbulent kinetic energy contours around the wind turbine

Conclusions

This study evaluated the performance and efficiency of a three-bladed horizontal-axis micro-wind turbine through experimental measurements and numerical simulations. The results demonstrated that the prototype was capable of generation small-scale electrical power efficiently under controlled wind conditions, reaching a maximum output of 15.2 W and a peak efficiency of 24%. Numerical simulations performed with the k-ω SST model and the MRF approach showed strong agreement with the experimental torque values, with a mean deviation of 9.27%, confirming the suitability of CFD as a predictive tool for performance evaluation. The wind tunnel prototype, along with torque and power measurements, provided a solid basis for validating the CFD simulation results.

CFD simulations indicated high turbulence behind the motor casing, suggesting that improvements could reduce wake effects and enhance operational stability. Overall, this study demonstrates that CFD simulations can be effectively used in the development and optimization of low-power wind turbines, contributing to the design of sustainable and accessible renewable energy solutions, especially in rural and off-grid contexts where access to electricity remains limited.

Acknowledgments and Funding: The authors gratefully acknowledge the facilities provided by the thermofluids laboratory of UAM Azcapotzalco and the funding provided by the DPA-UACh to project I-Q-202-25.

Author contributions: L.C.D.-E., A.M.V.-P and J.R.-M: experimental measurements; V.E.M.-B., R. G.-P. and J.V.-L.: design, numerical data collection and analysis and interpretation of data; F.G.-M, V.M.G.-M, A.M.V.-P. and J.R.-M.: conceptualization, supervision and writing.

References

Arpino, F., Cortellessa, G., Dell'Isola, M., Scungio, M., Focanti, V., Profili, M., & Rotondi, M. (2017). CFD simulations of power coefficients for an innovative Darrieus style vertical axis wind turbine with auxiliary straight blades. *Journal of Physics: Conference Series*, *923*(1), 012036. https://doi.org/10.1088/1742-6596/923/1/012036

Betz, A. (1926). *Wind-energie und ihre ausnutzung durch windmühlen* (Vol. 2). Vandenhoeck y Ruprecht.

Escobar-Díaz, A., & Barrero-Páez, L. E. (2009). Modelo matemático de un aerogenerador. *Visión Electrónica*, *3*(2), 48–60. https://doi.org/10.14483/22484728.2835

Espinosa-Dorado, A. L., & Carrillo Núñez, M. P. (2021). Características de la pobreza energética en México: un enfoque desagregado. *Revista Legislativa de Estudios Sociales y de Opinión Pública*, *14*(30), 77–116.

INEGI. (2020). *Información demográfica y social. Censo de Población y Vivienda 2020.*

Ji, B., Zhong, K., Xiong, Q., Qiu, P., Zhang, X., & Wang, L. (2022). CFD simulations of aerodynamic characteristics for the three-blade NREL Phase VI wind turbine model. *Energy*, *249*, 123670. https://doi.org/10.1016/j.energy.2022.123670

Kale, S. A., Gunjal, Y. R., Jadhav, S. P., & Tanksale, A. N. (2013). CFD analysis for optimization of diffuser for a micro wind turbine. *International Conference on Energy Efficient Technologies for Sustainability*, Nagercoil, India, 257–260. https://doi.org/10.1109/ICEETS.2013.6533392

Lanzafame, R., Mauro, S., & Messina, M. (2013). Wind turbine CFD modeling using a correlation-based transitional model. *Renewable Energy*, *52*, 31–39. https://doi.org/10.1016/j.renene.2012.10.007

ONU. (2015b). *Objetivo 7: Garantizar el acceso a una energía asequible, segura, sostenible y moderna*. Recuperado el 16/12/2024 de https://www.un.org/sustainabledevelopment/es/energy/

ONU. (2023). *Informe de los Objetivos de Desarrollo Sostenible. Edición especial* (pp. 26–27).

Ramírez, R. G., Parra, M. S., & González, R. H. (2012). Investigación, desarrollo e innovación tecnológica de sistema del control de aerogeneradores. *Boletín IIE*, abril–junio de 2012.

Rocha, P. C., Rocha, H. B., Carneiro, F. M., Da Silva, M. V., & Bueno, A. V. (2014). k–ω SST (shear stress transport) turbulence model calibration: A case study on a small scale horizontal axis wind turbine. *Energy*, *65*, 412–418. https://doi.org/10.1016/j.energy.2013.11.050

Sánchez-Santillán, O. (2021). *Análisis de la pobreza energética y su impacto en el desarrollo sustentable de México*. Universidad Nacional Autónoma de México, México.

Van der Zwaan, B., & Rabl, A. (2003). Prospects for PV: A learning curve analysis. *Solar Energy*, *74*(1), 19–31.

Wang, Y.-F., & Zhan, M.-S. (2013). 3-dimensional CFD simulation and analysis on performance of a micro-wind turbine resembling lotus in shape. *Energy and Buildings*, *65*, 66–74. https://doi.org/10.1016/j.enbuild.2013.05.045

Younoussi, S., & Ettaouil, A. (2024). Calibration method of the k-ω SST turbulence model for wind turbine performance prediction near stall condition. *Heliyon*, *10*(1). https://doi.org/10.1016/j.heliyon.2024.e24048

Zemamou, M., Aggour, M., & Toumi, A. (2017). Review of Savonius wind turbine design and performance. *Energy Procedia*, *141*, 383–388. https://doi.org/10.1016/j.egypro.2017.11.047

Integral use of prickly pear xoconostle fruits to obtain bioactive compounds using a biorefinery approach

Luis Damián Torres-Gutiérrez, Adrian Batista-Rojas, Eduardo Figueroa-González, Linaloe Lobato-Azuceno, Gabriela González-Chávez y Juan Pascual-Ramírez *

Bioseparations Laboratory, Bioengineering Department, Unidad Profesional Interdisciplinaria de Biotecnología, Instituto Politécnico Nacional, Ciudad de México, México.

* Corresponding author: jpascualr@ipn.mx; Tel.: +52 55 5729 6000 Ext. 56408

Received: April 12, 2025 Accepted: June 28, 2025 Published: January 27, 2026
DOI: https://doi.org/10.56845/rebs.v8i1.667

Abstract: The prickly pear xoconostle (*Opuntia matudae*) currently lacks industrial applications, as its use is mainly focused on traditional products such as beverages, sauces, and confections. To enhance the value of this crop in producing regions, this study evaluated the extraction of bioactive compounds with potential applications in the biotechnology and food industries. The main objective of this study was the extraction of pectin from the fruit peel, through acid hydrolisis. The process comprised the following stages: grinding, ethanol washing, extract recovery, pectin precipitation, and drying, resulting in a yield of 9.95 % of pectin. The washing effluents were analyzed for betalain content, yielding a concentration of 2.021 g/mL as total betalains. This liquid phase was subsequently subjected to distillation; a 70 % yield of ethanol was obtained with 65 % purity. The solid residue obtained from the extraction was further utilized for crude fiber isolation, achieving a yield of 72.3 ± 3.48 %. These findings demonstrate that xoconostle fruits offer a promising raw material for the extraction of pectins, betalains, and crude fiber, and the proposed recyclingrecycle ethanol and water, supports the development of a sustainable process in a biorefinery.

Keywords: xoconostle, pectins, raw fiber, betalains, ethanol

Introduction

Mexico is the country with the highest global diversity and abundance of prickly pear species, with approximately 80 recognized varieties, including green, yellow, criolla, red and xoconostle fruits; the State of Mexico led the national production in 2022 (SECAMPO, 2022). The *Opuntia* genus is widely consumed in the country and includes many species, among which are the nopal vegetable and prickly pear cactus. *Opuntia albicarpa* produces the fruit commonly known as “tuna,” characterized by juicy pulp and a low seed count (Lira-Ortíz *et al*., 2014). In contrast, *Opuntia matudae* produces acidic fruits known as xoconostle, which contain a thick mesocarp and hard seeds located at the center (Gallegos-Vázquez *et al*., 2012). These structural characteristics limit theirindustrial use, restricting xoconostle mostly to traditional culinary applications.

Pectin is a polysaccharide located in the middle lamella of plant cell walls (Muzzarelli *et al*., 2012) that exhibits a variety of bioactive properties derived from its structural composition (Endress, 2011); for example, low-molecular-weight pectins, have been associated with potential anticancer activity in the colon, cardiovascular benefits, and reduced insulin levels (Almeida *et al*., 2015). Previous studies have shown that xoconostle is a viable source of pectin for the food and pharmaceutical industries (Morales-Martínez *et al*., 2018), as well as of betalains (Gengatharan *et al*., 2015; Morales *et al*., 2015) and fiber (Ramírez-Rodríguez *et al*., 2020). However, these compounds have traditionally been obtained through independent processes, and no integrated approach has been implemented to recover multiple bioproducts simultaneously. Consequently, pigment-rich effluents generated during pectin extraction are typically discarded, and solid residues are also eliminated without further valorization.

A biorefinery is defined as a technological platform that enables the production of multiple value-added products (biopolymers, fibers, oils, etc.) from plant, animal, or microbial biomass (Sierra-Ibarra *et al*., 2021). In this study, pectin was extracted from xoconostle, and the resulting by-products were subsequently used to obtain betalains, ethanol, and crude fiber, integrating these steps into a process under a biorefinery approach. In this way, the use of waste from the pectin industry is proposed, while simultaneously diversifying bioproduct generation and enhancing the value of xoconostle cultivation.

Materials and Methods

Pectin was extracted by acid hydrolysis, and the resulting residues were used for the recovery of betalains, ethanol, and crude fiber as described below.

Morphometric characterization

Xoconostle fruits were purchased from a local market in Mexico City. Length, equatorial diameter, and peel thickness were measured for the fruits. Peel, pulp, and seeds were separated to determine the proportion of these fractions relativeto the total fruit.

Pectin extraction

The methodology of Zhang *et al* (2023) was used with minor modifications. The peel was chopped and ground in the presence of ethanol (70 °G.L.). The solids were sieved to remove the colored ethanol and subsequently washed to eliminate soluble compounds. All ethanol effluents were collected for betalain quantification and later distillation. The ground peel was dried to constant weight and designated as alcohol-insoluble residues (AIR). These solids were dispersed in acidified water at a 1:10 ratio (AIR:solvent), using citric acid solution (pH 3) because it is a more environmentally friendly acid compared to HCl, which is the most commonly used for this process. The dispersion was boiled for 30 minutes under constant agitation and centrifuged to obtain an extract rich in pectic substances, while the solid residue was dried and used to obtain raw fiber. Pectin was precipitated by mixing the extract with absolute ethanol (90 °G.L.) at a 1:1 ratio, forming a gel that was subsequently dried at room temperature. Dried pectin was ground and stored in amber containers prior to Fourier Transform Infrared Spectroscopy (FT-IR) analysis using a Bruker Tensor 27 spectrometer (Germany) equipped with attenuated total reflectance.

Total betalains and effluent distillation

Total betalains were quantified as the sum of betacyanins and betaxanthins using the method proposed by Soriano-Santos et al (2007) with slight modifications. Absorbance was measured at 600, 538, and 476 nm, using extinction coefficients of 1120 for betacyanins and 750 for betaxanthins.

Effluents were distilled at atmospheric pressure using a laboratory-scaledistillation unit, and 100 mL distillate fractions were collected periodically. Ethanol concentration was determined using an optical refractometer (PCNRF 080VV, Mettler Toledo, USA) and expressed in Gay-Lussac degrees (°G.L.). Distillation began at 78 °C and ended at 93 °C, when the vapor consisted predominantly of water.

Raw fiber

Raw fiber was obtained following the method described by Guerrero-Colín *et al* (2016). Solid residues were hydrolyzed with 1N HCl for 10 min under boiling conditions and washed with sodium hypochlorite. The remaining solids were dried to constant weight and quantified.

Results and Discussion

Morphometric characterization

Fruits of prickly pear xoconostle were separated into peel, pulp, and seeds. The peel was notably the thickest fraction, whereas the pulp and seeds occupied a minimal space in the central region (Figure 1). The average fruit mass was 74.7 ± 9.7 g, with the peel representing 86.92 % of the total weight (Table 1).

For physical characterization, length (6.05 ± 0.5 cm), equatorial diameter (4.67 ± 0.4 cm) and peel thickness (1.18 ± 0.1 cm) were measured, and their locations within the fruit are illustrated in Figure 1. Due to these morphological characteristics, the peel was the ideal substrate for pectin extraction.

Table 1. Proportion of the fractions of xoconostle fruits

	Peel	Pulp	Seed
g	64.92 ± 7.6	5.02 ± 1.4	4.76 ± 1.1
%	86.92 ± 2.5	6.66 ± 1.8	6.41 ± 1.5

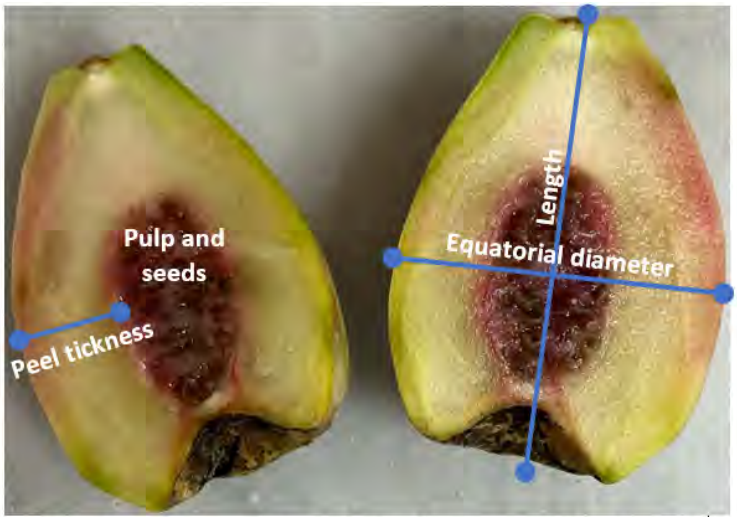

Figure 1. Morphometry of xoconostle fruits

Pectin extraction

Extraction process was carried out in several stages with the objective of obtaining an aqueous extract rich in pectic substances, from which the pectins were separated by insolubilization with ethanol.

It should be noted that an effluent with a high ethanol content was generated, which originated mainly from washing and precipitation, as shown in Figure 2 (b) and 2 (d).

(a) **(b)** **(c)** **(d)** **(e)** **(f)**

Figure 2. Main stages in pectin extraction: (a) Xoconostle peel, (b) Grinding and washing with ethanol to remove pigments, (c) Centrifugation to obtain the extract and solid residue, (d) Gel precipitation by ethanol addition, (e) Pectin gel isolation, and (f) Dried pectin for grinding

A pectin yield of 9.95 % (dry basis) was obtained, which is comparable to 10.46 % reported by Morales-Martínez *et al* (2018). FT-IR spectra (Figure 3) confirmed that the isolated material corresponded to pectin, showing characteristic functional groups and the "fingerprint region" between 1500 and 700 nm, one of the most important characteristics of pectins (Yang *et al*., 2018). A prominent band at 3394 cm^{-1} indicated glucose units of the pectin backbone, while bands in 1737 and 1618 cm^{-1}corresponded to methoxyl groups.

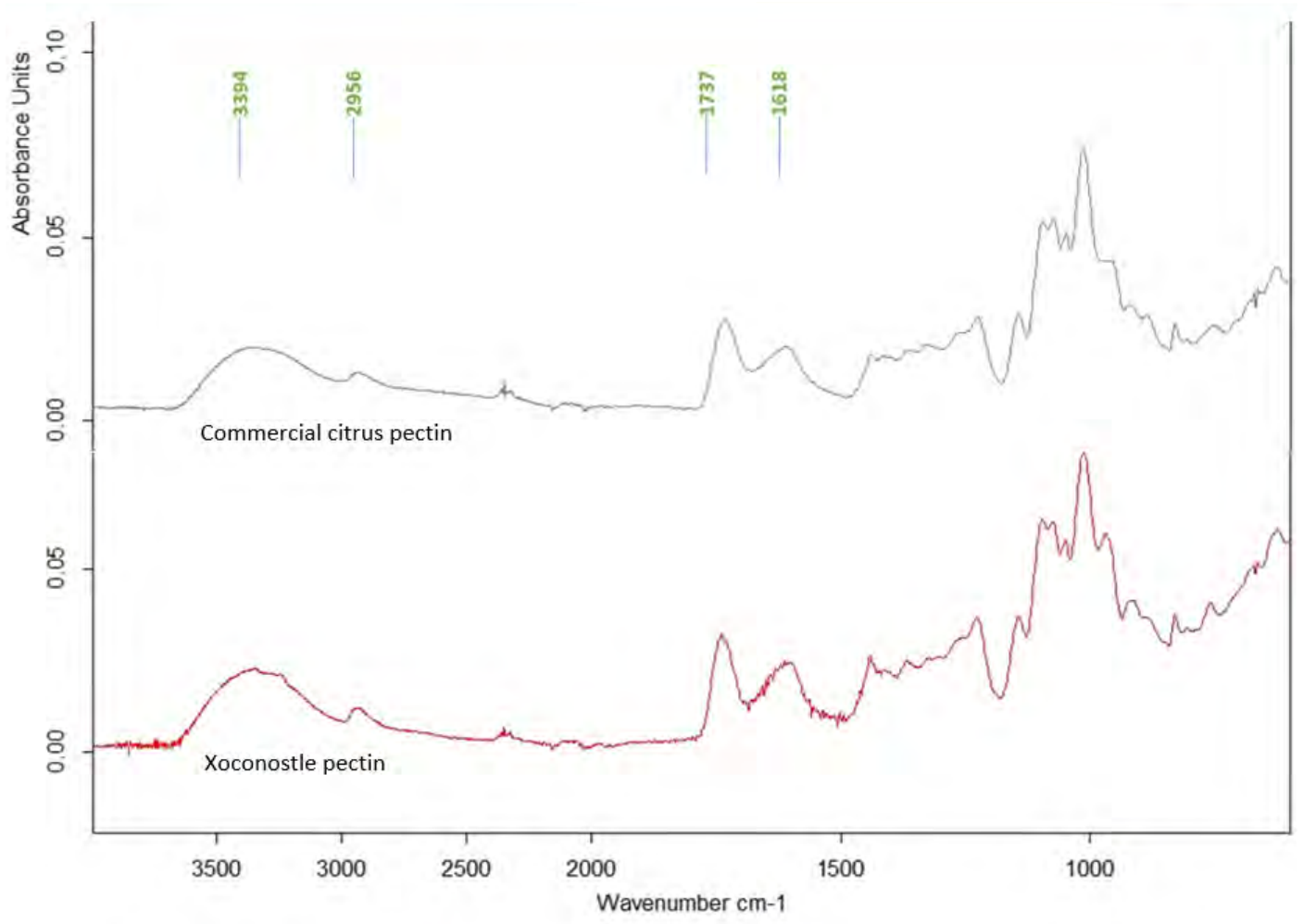

Figure 3. Spectrograms for xoconostle pectin compared with commercial citrus pectin

Total betalains and effluent distillation

Betalain yields were 0.746 g/mL for betacyanins and 1.275 g/mL for betaxanthins, totaling 2.021 g/mL. This demonstrates that process effluents represent a valuable source of natural pigments, thus contributing to the valorization of by-products through the extraction of this bioactive compound.

For effluents distillation, a complete temperature scan was carried out (from 20 °C to 93 °C), with vapor production beginning at 78 °C, approximately 25 min after starting heating as can be seen in Figure 4 (a). As the mixture lost ethanol, temperature increased until it stabilized at 93 °C. During this time mixture allowed ethanol elimination, leaving as a residue an effluent that mostly corresponded to water. This behavior is illustrated in Figure 4(b) where the distillate initially exhibited a concentration of 80 °G.L. which gradually decreased to 2 °G.L. as the vapor becomes predominantly aqueous. The total yield obtained (by mixing all 100 mL fractions) was 70 % with an average ethanol concentration of 65 °G.L. These results demonstrate that it is possible to recover high quality ethanol from peel washing effluents, which can then be reused in the pectin extraction process. It can also be observed that the second-order polynomial equation in Figure 4 (b) allows the prediction of ethanol concentration as a function of temperature.

Ethanol represents one of the major cost factors in pectin production, therefore distilling of effluents can significantly reduce production costs and promote solvent recycling.

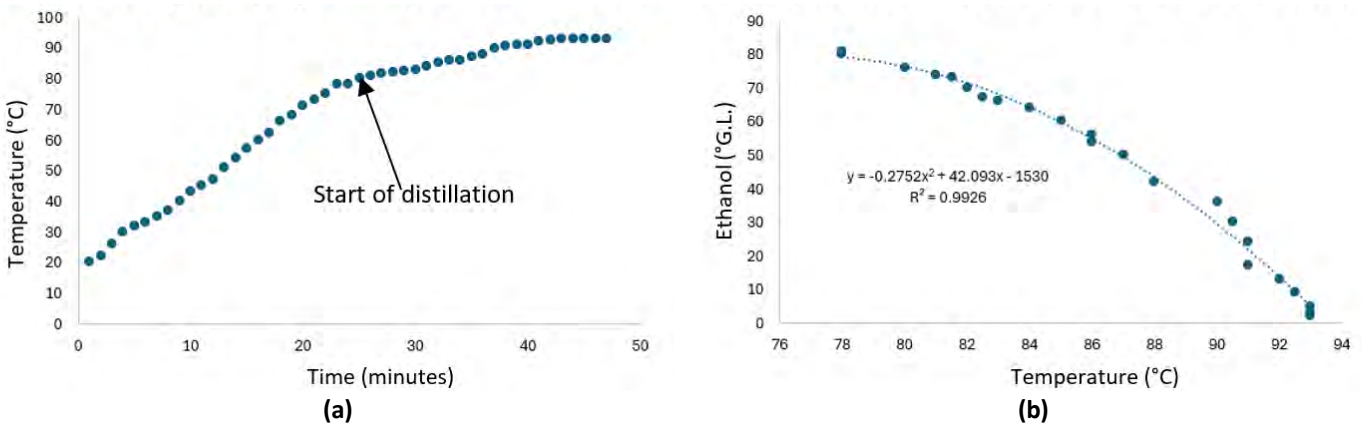

Figure 4.Distillation profiles: (a) temperature versus heating time, and (b) ethanol concentration as a function of temperature

Raw fiber

Raw fiber was isolated from residual solids obtained by centrifugation, as shown in Figure 2 (c). A yield of 72.3 ± 3.48 % of raw fiber was obtained, because starch, protein and part of the lignin were solubilized, leaving mainlynon-digestible components such as cellulose, hemicellulose and residual lignin (AOAC 7.068, 1995). Crude fiber has important applications in food industry (e.g., as a dietary fiber source in cookies and breads) and in biotechnology sector as a fermentation substrate for metabolite production.

Proposal for a biorefinery

Pectin extraction involves several stages that generate by-products with potential value for bioproduct recovery. A proposal for the integrated utilization of products and by-products from this industry is illustrated in Figure 5.

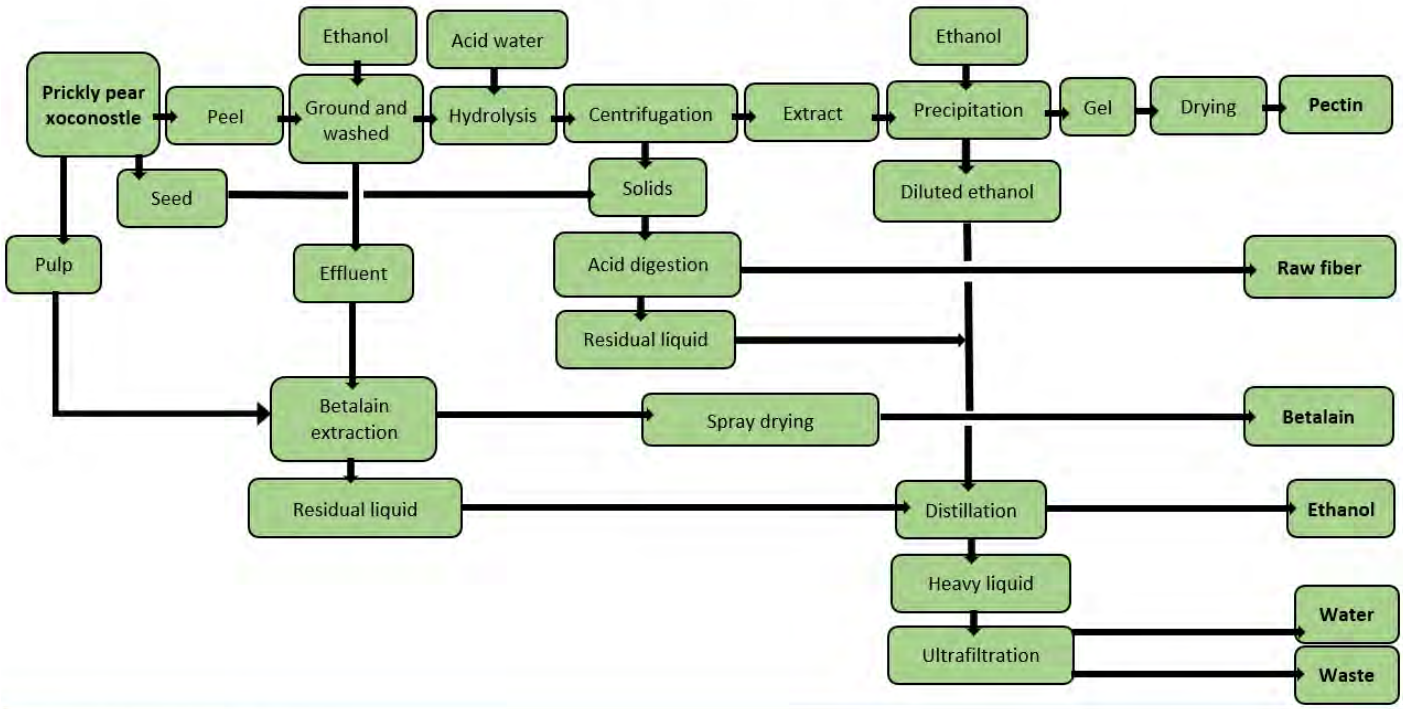

Figure 5. Proposed biorefinery scheme for the extraction of pectin and crude fiber, betalains recovery, and r ethanol and water recycling

As shown in (Figure 5), pectin is the main target product. The washing effluent undergoes betalain recovery and is subsequently sent to distillation together with the ethanol used for gel precipitation. The solids obtained after centrifugation can be combined with seeds for raw fiber production. In addition, it is proposed that the remaining liquid fraction (mainly pigmented water) be treated through membrane ultrafiltration to recover water for reuse in the process. In this way, a single technological unit integrates multiple valorization pathways, allowing pectin extraction to evolve towards a more sustainable and diversified biorefinery approach.

Conclusions

Peels of xoconostle prickly pear fruit were shown to be an important source for the extraction of pectin with properties comparable to those of commercial pectin.

The pectin production process generates several by-products, including water-ethanol mixtures, pigment-rich leachates, and solid shell residues, from which betalains, crude fiber, and recoverable ethanol were obtained.

The valorization of pectin extraction waste within a biorefinery approach contributes to the development of a more sustainable and environmentally friendly industry, promoting the transition of pectin production toward a circular and resource-efficient process.

Acknowledgments and Funding: Authors acknowledge the support of Amelia Romana Jiménez Rodríguez, Bioengineering Department chief, and the funding received for SIP20253973 project.

Author contributions: L.D.T.-G. and A.B.-R: experimental process and data collection; E.F.-G: analysis; L.L.-A: project administration; G.G.-C: provide materials and editing; J.P.-R: supervision and writing.

References

Almeida, E. A. M. S., Facchi, S. P., Martins, A. F., Nocchi, S., Schuquel, I. T. A., Nakamura, C. V., Rubira, A. F., & Muniz, E. C. (2015). Synthesis and characterization of pectin derivative with antitumor property against Caco-2 colon cancer cells. *Carbohydrate Polymers*, *115*, 139–145. https://doi.org/10.1016/j.carbpol.2014.08.085

AOAC. (1995). *Official methods of analysis*. Association of Official Analytical Chemists, Inc., Washington, E. U.

Endress, H. U. (2011). Chapter 8. Pectins: Production, properties and applications. In *Renewable resources for functional polymers and biomaterials: Polysaccharides, proteins and polyesters* (pp. 210–260). The Royal Society of Chemistry.

Gallegos-Vázquez, C., Scheinvar, L., Núñez-Colín, C. A., & Mondragón-Jacobo, C. (2012). Morphological diversity of xoconostles (*Opuntia* spp.) or acidic cactus pears: A Mexican contribution to functional foods. *Fruits*, *67*(2), 109–120. https://doi.org/10.1051/fruits/2012001

Gengatharan, A., Dykes, G. A., & Choo, W. S. (2015). Betalains: Natural plant pigments with potential application in functional foods. *LWT – Food Science and Technology*, *64*, 645–649. http://dx.doi.org/10.1016/j.lwt.2015.06.052

Guerrero-Colín, J. I., Trejo-Márquez, M., Moreno-Lara, J., Lira-Vargas, A. A., & Pascual-Bustamante, S. (2016). Extracción de fibra de los desechos agroindustriales de cacahuate, para su aplicación en el desarrollo de alimentos. *Investigación y Desarrollo en Ciencia y Tecnología de Alimentos*, *1*(2), 806–812.

Kertesz, Z. I. (1951). *The pectic substances*. Interscience Publishers, USA, 628.

Lira-Ortíz, A. L., Reséndiz-Vega, F., Ríos-Leal, E., Contreras-Esquivel, J. C., Chavarría-Hernández, N., Vargas-Torres, A., & Rodríguez-Hernández, A. I. (2014). Pectins from waste of prickly pear fruits (*Opuntia albicarpa* Scheinvar "Reyna"): Chemical and rheological properties. *Food Hydrocolloids*, *37*, 93–99. https://doi.org/10.1016/j.foodhyd.2013.10.018

Morales, P., Barros, L., Ramírez-Moreno, E., Santos-Buelga, C., & Ferreira, I. C. F. R. (2015). Xoconostle fruit (*Opuntia matudae* Scheinvar cv. Rosa) by-products as potential functional ingredients. *Food Chemistry*, *185*, 289–297. http://dx.doi.org/10.1016/j.foodchem.2015.04.012

Morales-Martínez, Y., López-Cuéllar, M. R., Chavarría-Hernández, N., & Rodríguez-Hernández, A. I. (2018). Rheological behaviour of acetylated pectins from cactus pear fruits (*Opuntia albicarpa* and *O. matudae*). *Food Hydrocolloids*, *85*, 110–119. https://doi.org/10.1016/j.foodhyd.2018.07.009

Mussarelli, R. A., Boundrant, J., Meyer, D., Manno, N., DeMarchis, M., & Paoletti, M. G. (2012). Current views on fungal, chitin/chitosan human chitinases, food preservation, glucans, pectins and inulin: A tribute to Henri Braconnot, precursor of the carbohydrate polymer science, on the chitin bicentennial. *Carbohydrate Polymers*, *87*(2), 995–1012. https://doi.org/10.1016/j.carbpol.2011.09.063

Ramírez-Rodríguez, Y., Martínez-Huélamo, M., Pedraza-Chaverri, J., Ramírez, V., Martínez-Tagueña, N., & Trujillo, J. (2020). Ethnobotanical, nutritional and medicinal properties of Mexican drylands Cactaceae fruits: Recent findings and research opportunities. *Food Chemistry*, *312*, 126073. https://doi.org/10.1016/j.foodchem.2019.126073

SECAMPO. (2022). *Secretaría del Campo, Gobierno del Estado de México. Cierra Estado de México año 2022 como líder nacional en producción de tuna*. Consultado en abril de 2025. https://secampo.edomex.gob.mx/eventos-comunicados/

Sierra-Ibarra, E., Gosset-Lagarda, G., & Martínez-Jiménez, A. (2021). Las biorrefinerías son plataformas sustentables y más limpias. *Biotecnología en Movimiento*, *27*, 8–14.

Soriano-Santos, J., Franco-Zavaleta, M. E., Pelayo-Saldívar, C., Armella-Villalpando, M. A., Yáñez-López, M. L., & Guerrero-Legorreta, I. (2007). Caracterización parcial del pigmento rojo del fruto de la "Jiotilla" (*Escontria chiotilla* [Weber] Britton & Rose). *Revista Mexicana de Ingeniería Química*, *6*(1), 19–25.

Yang, X., Nisar, T., Hou, Y., Gou, X., & Guo, Y. (2018). Pomegranate peel pectin as an effective emulsifier. *Food Hydrocolloids*, *85*, 30–38. http://dx.doi.org/10.1016/j.foodhyd.2018.06.042

Zhang, S., Pan, X., Zhao, J., Li, J., Yu, X., Peng, Y., & Wu, J. (2023). Characterization of ionically crosslinked mango peel pectin-based films: Effect of different cations on the improved properties of film. *Food Packaging and Shelf Life*, *38*, 101131. https://doi.org/10.1016/j.fpsl.2023.101131

N/P ratio effect on lipid profiles of native marine microalgae and their potential for sustainable bioproducts

Regina M. Gonzalez-Balderas [1], Julio C. Sacramento Rivero [2], Tanit Toledano-Thompson [1] y Ruby Valdez-Ojeda [1,*]

[1] Laboratorio, Unidad de Energía Renovable, Centro de Investigación Científica de Yucatán, Mérida, Yucatán, México
[2] Facultad de Ingeniería Química, Universidad Autónoma de Yucatán, Periférico Norte km 33.5, Tablaje Catastral 13615, Col. Chuburna de Hidalgo Inn, Mérida, Yucatán 97203, México
* Autor de correspondencia: dubi@cicy.mx; Tel.: (+52 999 981 39 43)

Received: April 2, 2025 Accepted: June 3, 2025 Published: January 30, 2026
DOI: https://doi.org/10.56845/rebs.v8i1.661

Abstract: The increasing demand for energy and growing environmental concerns have accelerated the search for alternative energy sources, with microalgae emerging as a promising candidate. These photosynthetic organisms can produce high-value biomolecules suitable for biofuel production and other industrial applications. However, their utility largely depends on biomass composition, which is influenced by nutrient availability—particularly phosphorus (P) and nitrogen (N). This study investigates the impact of varying N/P ratios (9, 12, and 14) on the lipid content and lipid profiles of marine microalgae strains *Nannochloropsis* (NSRE-1, NSRE-2) and *Nannochloris* (NRRE-2), native to the Yucatán coast of Mexico. The potential use of the extracted lipids in biofuel and value-added product development is also evaluated. Results indicate a significant decline in lipid content across all three strains with increasing N/P ratios ($p < 0.05$). Notably, strain NSRE-1 achieved the highest relative fatty acid content (69.9%) at an N/P ratio of 14, while fatty acid synthesis in NRRE-2 was inhibited at N/P ratios of 12 and 14. These findings underscore the critical role of the N/P ratio in modulating lipid production and composition in microalgae, particularly in endemic strains. Moreover, changes in the N/P ratio stimulated the production of lipophilic compounds with potential applications in bioplasticizer manufacturing. Overall, the useof biofuels and naturally derived plasticizers supports the rising industrial demand for sustainable, renewable alternatives to fossil fuels and conventional plastics.

Keywords: marine microalgae, biofuels, bioplasticizers, N/P ratio, lipid metabolism

Introduction

Over the past several decades, increasing energy demands and escalating environmental challenges have intensified the search for alternative renewable energy sources, including those derived from microalgae (Duarah *et al*., 2022). Microalgae synthesize a wide variety of biomolecules with applications across the pharmaceutical, cosmetic, energy, and aquaculture industries (Borowitzka, 2013). Among microalgae-based biofuels, biodiesel is particularly promising due to its potential to significantly reduce greenhouse gas emissions, including CO_2 and sulfur oxides (SO_x). Microalgal biomass presents several advantages as a biofuel feedstock, such as high photosynthetic efficiency, rapid growth, and high tolerance to environmental contaminants (Li *et al*., 2022). Notably, microalgae can produce lipid yields that exceed those of terrestrial plants by 15- to 300-fold on a dry weight basis (Chisti, 2008).

Microalgal lipid productivity is influenced by numerous physicochemical factors, including light intensity, photoperiod, temperature, and salinity. Nutrient availability—specifically nitrogen (N) and phosphorus (P)—plays a central role in shaping cellular biochemical composition and lipid accumulation (Sharma *et al*., 2012). The nitrogen-to-phosphorus (N/P) ratio is therefore critical for regulating cellular composition, metabolic activity, growth dynamics, and photosynthetic efficiency (Slinksienė *et al*., 2022). For instance, an N/P ratio of 18 maximized chlorophyll content in *Chlorella*, enhancing photosynthetic performance and biomass yields (Beuckels *et al*., 2015). Numerous studies have demonstrated that nutrient stoichiometry directly affects both total lipid content and the distribution of lipid classes. Triacylglycerols (TAGs) are the most relevant lipid fraction for biodiesel production due to their lower degree of unsaturation and higher conversion efficiency compared with saturated fatty acids (D'Alessandro & Antoniosi, 2016). These characteristics translate into favorable physicochemical properties, such as appropriate viscosity, reduced pour point, and overall improved biodiesel quality. Species such as *Chlorella sp.*, *Scenedesmus sp.*, and *Nannochloropsis sp.* have been widely studied for this purpose because of their high lipid content (32–38%) and advantageous fatty acid composition (Chowdhury *et al*., 2019). While many studies have evaluated the effect of environmental factors on microalgal lipid production, limited attention has been given to the potential value-added applications of lipid fractions unsuitable for biodiesel.

This study examines the influence of three N/P ratios (9, 12, and 14) on the lipid content and lipid profile of three native marine microalgae isolated from the Yucatán coast. Furthermore, the potential use of these lipids for biofuel production and other value-added bioproducts is assessed, broadening the scope of their biotechnological applications.

Materials and Methods

Biomass Cultivation

Microalgae strains used in this study were isolated from the coastal area of Puerto Progreso, Yucatán, and identified by López-Rosales *et al*. (2020) as *Nannochloropsis* (NSRE-1 and NSRE-2) and *Nannochloris* (NRRE-1). Cultures were grown in a medium composed of 50% distilled water and 50% seawater, supplemented with 51.02 ± 0.78 mg/L of N-NO_3^-, with an initial pH of 7.06 and a salinity of 22.46 ± 0.85‰ (~20 g/L NaCl).

The N/P ratio was adjusted by adding 100 mg/L of P-PO_4^{3-} in the form of KH_2PO_4 (Sigma Aldrich, St. Louis, MO, USA). Cultures were maintained under continuous illumination at 90 µmol/m^2/s using a 30-W white light source, at 25 ± 2 °C for 22 days. Biomass harvesting was performed following the flocculation method described by Rojo-Cebreros *et al*. (2016), adjusting the pH with 0.5 N NaOH. Samples were centrifuged at 4728 g for 10 min (HERMLE Z 206 A), the supernatant was discarded, and the biomass was washed twice with distilled water to remove residual salts. The resulting pellet was frozen at −20 °C and subsequently lyophilized (Freezone, LABCONCO).

Lipid Extraction

Total lipids were extracted in duplicate using the Folch method (Folch *et al*., 1957). Approximately 38 mg of lyophilized biomass was mixed with chloroform:methanol (2:1, v/v) and processed at 40 °C and 150 rpm for 3 h. The extract was then separated from the residual biomass using a separation funnel. The organic phase was collected and evaporated to obtain the total lipid extract, which was redissolved in chloroform.

Transesterification

Fatty acid methyl esters (FAME) were obtained following the procedure of López-Rosales *et al*. (2019). Total lipids were fractionated by column chromatography using silica gel (Kieselgel, 70–230 mesh). Elution was performed using a solvent gradient consisting of hexane; hexane:ethyl acetate (9:1, 8:2, 7:3); and methanol.

Triacylglycerol-rich fractions (hexane:ethyl acetate, 9:1) were subjected to transesterification using 6% (w/v) sodium methoxide at 60 °C for 90 min in a 25-mL vial. The reaction mixture was passed through silica gel to remove excess catalyst and glycerol.

Data Analysis

All graphs and statistical analyses were carried out using Origin Pro 2018 (OriginLab Corporation). Results are reported as mean ± standard deviation. Total lipid content and relative fatty acid composition were evaluated using two-way ANOVA, considering the N/P ratio and the metabolic response of microalgae (e.g., growth and biomass accumulation) as factors. Statistical significance was defined as $P < 0.05$.

Results and Discussion

Effect of the N/P Ratio on Lipid Content

Figure 1 presents the lipid content (%) of NSRE-1, NSRE-2, and NRRE-1 under N/P ratios of 9, 12, and 14. An increase in the N/P ratio resulted in a consistent decline in lipid accumulation in all strains. Maximum lipid contents were observed at an N/P ratio of 9, reaching 6.21 ± 0.44% for NSRE-1, 7.56 ± 0.28% for NSRE-2, and 8.09 ± 0.10% for NRRE-1. Among the three strains, NRRE-1 exhibited the highest lipid content across all N/P ratios evaluated.

A two-way ANOVA confirmed that the N/P ratio had a significant effect on lipid content in NSRE-1, NSRE-2, and NRRE-1 ($P < 0.05$).

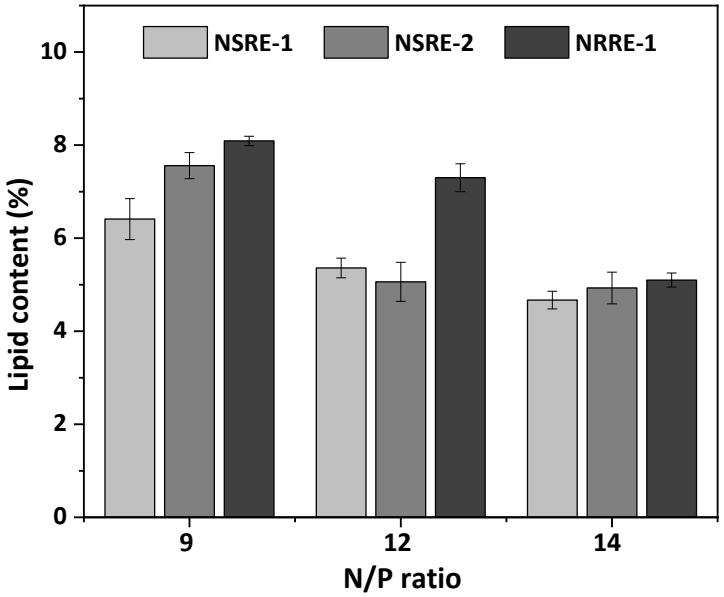

Figure 1. Total lipid content (%, mean ± SD) of the microalgal strains NSRE-1, NSRE-2, and NRRE-1 cultivated under N/P ratios of 9, 12, and 14.

Ding *et al*. (2024) reported comparable trends in *Chlorella* sp. and *Phaeodactylum tricornutum* cultivated in aquaculture wastewater. In their study, lipid content decreased at N/P ratios of 3, 6, and 12, whereas an increase to an N/P ratio of 18 resulted in substantial lipid accumulation—112.34% and 136.92%, respectively. However, lipid content declined again when the N/P ratio increased further to 30 and 36.

Previous studies indicate that under nutrient-rich conditions, microalgal cells predominantly synthesize proteins and nucleic acids, while under nitrogen-sufficient conditions (0.0–0.5 g/L), they tend to accumulate carbohydrates rather than lipids (Tossavainen *et al*., 2019). Accordingly, the reduction in lipid content observed in NSRE-1, NSRE-2, and NRRE-1 at N/P ratios above 9 suggests that higher N/P availability may have favored carbohydrate biosynthesis over lipid accumulation.

Effect of N/P Ratio on the Lipid Profile

Figure 2 presents the relative abundance of saturated (SFA), monounsaturated (MUFA), and polyunsaturated (PUFA) fatty acids in NSRE-1, NSRE-2, and NRRE-1 cultured under N/P ratios of 9, 12, and 14. In NSRE-1, SFA levels increased with increasing N/P ratio, reaching a maximum of 69.9% at N/P = 14. Conversely, MUFA and PUFA fractions decreased as the N/P ratio increased (Figure 2a).

The biomass of NSRE-2 showed a similar trend, as the content of SFA increased with rising N/P ratio. However, in this strain, an increase in N/P ratio also resulted in higher proportions of MUFA and PUFA. Likewise, increasing the N/P ratio reduced the content of organic compounds other than fatty acids. The maximum relative content of SFA in NSRE-2 was 20.2%, a value considerably lower than that observed in NSRE-1 (Figure 2b).

In contrast, NRRE-1 exhibited high sensitivity to changes in the N/P ratio of the culture medium (Figure 2c). Under N/P ratios of 12 and 14, this strain did not promote fatty acid synthesis; instead, it primarily produced other lipophilic compounds, particularly phthalates and adipates.

Rasdi *et al*. (2014) reported similar behavior in *Tisochrysis lutea* and *Nannochloropsis oculata* grown in F/2 medium at six N/P ratios (5, 10, 20, 30, 60, and 120). Their findings indicated that an N/P ratio of 20 enhanced microalgal growth and protein content, whereas an N/P ratio of 120 reduced both parameters but increased lipid accumulation in both

strains. For *N. oculata*, an N/P ratio of 20 favored the production of eicosapentaenoic acid (EPA), while in *T. lutea*, an N/P ratio of 30 promoted the synthesis of docosahexaenoic acid (DHA). Both fatty acids are ideal raw materials for biofuel production. Similarly, Gao *et al*. (2023) reported that an N/P ratio of 18 enhanced optimal growth of *Scenedesmus obliquus* in wastewater, as well as its dry biomass, lipid production, and chlorophyll accumulation (1.70 g/L, 0.49 g/L, and 7.43 mg/L, respectively).

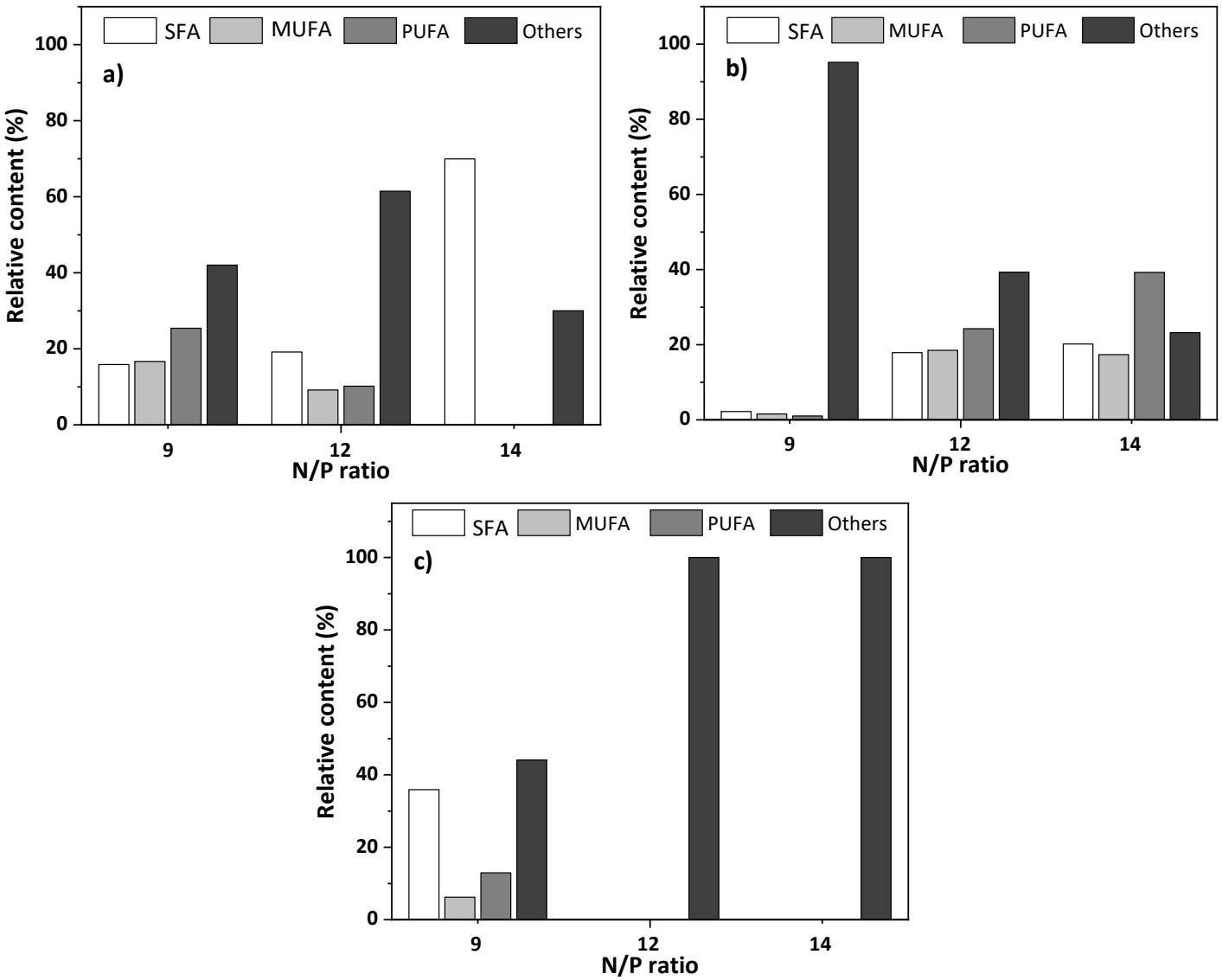

Figure 2. Relative abundance of saturated (SAF), monounsaturated (MUFA), and polyunsaturated (PUFA) fatty acids in the biomass of (a) NSRE-1, (b) NSRE-2, and (c) NRRE-1 cultivated under N/P ratios of 9, 12, and 14

A two-way ANOVA revealed that both the strains and the N/P ratio had significant effects on the relative content of SFA, MUFA, PUFA, and non-fatty-acid lipophilic compounds ($p < 0.05$), mainly phthalates and adipates.

Tables 1, 2, and 3 list the fatty acids identified in the biomass of NSRE-1, NSRE-2, and NRRE-1 grown under N/P ratios of 9, 12, and 14. The fatty acids produced by all strains represent an adequate feedstock for biodiesel production, as they include C16–C18 fatty acids (Chowdhury *et al*., 2019). The relatively low concentrations of saturated and long-chain polyunsaturated fatty acids such as C16:0 (palmitic acid), C18:0 (stearic acid), C18:1 (oleic acid), C18:2 (linoleic acid), and C18:3 (linolenic acid) confer high oxidative stability and favorable thermodynamic properties.

Table 1. Fatty acid profile of NSRE-1 at N/P ratios of 9, 12, and 14.

Fatty acid	Carbon number:saturations	Relative content (%)
N/P 9		
Hexadecanoic Acid	C17:0	13.5
Methyl stearate	C19:0	2.46
Octadecenoic acid	C19:1	16.6
Octadecadienoic acid	C19:2	17.46
Linoleic acid	C20:2	7.98
N/P 12		
Hexadecanoic Acid	C17:0	15.4
Methyl stearate	C19:0	3.71
Octadecenoic acid	C19:1	9.2
Octadecadienoic acid	C19:2	10.17
N/P 14		
Hexadecanoic Acid	C17:0	53.8
Methyl stearate	C19:0	11.3
Methyl butyl hexadecanoate	C21:0	4.9

Table 2. Fatty acid profile of NSRE-2 at N/P ratios of 9, 12, and 14.

Fatty acid	Carbon number:saturations	Relative content (%)
N/P 9		
Hexadecanoic Acid	C17:0	1.7
12-Methyl tetradecanoic acid	C16:0	0.45
Octadecenoic acid	C19:1	1.55
Octadecadienoic acid	C19:2	1.04
N/P 12		
Hexadecanoic Acid	C17:0	13.3
Methyl stearate	C19:0	3.4
2-Methylundecanoic acid	C13:0	1.05
Octadecenoic acid	C19:1	18.5
Octadecadienoic acid	C19:2	16.68
Linoleic acid	C20:2	5.08
Eicosatrienoic acid	C21:3	2.48
N/P 14		
Hexadecanoic Acid	C17:0	15.6
Methyl stearate	C19:0	3.47
Dodecanoic acid	C14:0	1.08
Octadecenoic acid	C19:1	17.5
Octadecadienoic acid	C19:2	23.44
Linoleic acid	C20:2	10.05
Octadecatrienoic acid	C19:3	5.77

Table 3. Fatty acid profile of NRRE-1 at N/P ratios of 9, 12, and 14.

Fatty acid	Carbon number:saturations	Relative content (%)
N/P 9		
Hexadecanoic Acid	C17:0	30.8
Tetradecanoic acid	C17:0	5.2
Dodecanoic acid	C13:1	6.22
Octadecadienoic acid	C19:2	12.9

Effect of the N/P Ratio on the Synthesis of Value-Added Compounds

The lipid extracts of NSRE-1, NSRE-2, and NRRE-1 were found to contain organic compounds suitable for the production of various value-added products, including adipates and phthalates. Adipates are widely used in the cosmetic industry as plasticizers and solvents in formulations such as nail polishes, tanning lotions, liquids, and gels, typically at low concentrations (5–8%) (Chi *et al.*, 2019). They are also found in food packaging materials and films at concentrations of a few thousand micrograms per gram (Vimalkumar *et al.*, 2022). Unlike other plasticizers, adipates exhibit very low toxicity and are readily biodegradable (EPA, 2021).

Because adipates can be synthesized biologically, they represent promising alternatives to synthetic plasticizers. In this study, NSRE-1, NSRE-2, and NRRE-1 were observed to produce two adipates—under specific N/P ratios—that are commonly used in the manufacture of plastics (see Table 4).

Table 4. Adipates synthesized by NSRE-1, NSRE-2, and NRRE-1 at different N/P ratios and their relative content

Name	Structure	Strain	N/P ratio	Relative content (%)
Di(4-octyl) adipate	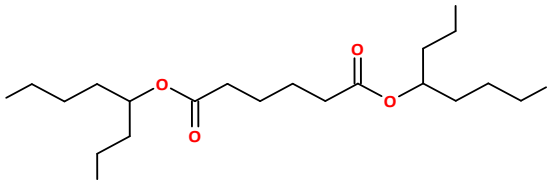	NSRE-1	14	18.5
		NSRE-2	14	10
Bis(2-ethylhexyl) hexanedioate (Di(2-ethylhexyl) adipate)	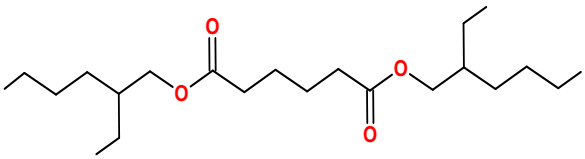	NSRE-2	12	27.8
		NRRE-1	12	34.3
		NRRE-1	14	19

Phthalic acid esters (PAEs), or phthalates (Table 5), were also identified. Phthalates are a class of lipophilic chemical substances widely used as plasticizers and additives to improve the mechanical extensibility and flexibility of various food products. Currently, synthetic PAEs are considered potentially hazardous to ecosystems and to public health. However, PAEs are also naturally produced by microorganisms such as algae, bacteria, fungi, and by higher plants through organic extracts, root exudates, and essential oils.

PAEs are synthesized by several algal species, where they play a role in adaptation to biotic and abiotic stress (Tian *et al.*, 2016). Naturally occurring PAEs include di-n-butyl phthalate, diethyl phthalate, dimethyl phthalate, di(2-ethylhexyl) phthalate, diisobutyl phthalate, and diisooctyl phthalate. Natural PAEs may function as allelochemicals, antibiotics, or insecticides.

Importantly, the natural synthesis of PAEs implies that certain microorganisms are capable of degrading them, which suggests a potential contribution to reducing environmental contamination caused by synthetic PAEs. Numerous studies have investigated microorganisms capable of degrading PAEs, and results demonstrate that several species of bacteria and microalgae possess PAE-degrading capabilities (Hu *et al*., 2021).

PAEs produced by microalgal species hold significant potential for sustainable applications. For instance, they can be incorporated into bioplastic formulations (e.g., PLA, PHB, alginates) to produce materials with improved flexibility and mechanical strength. These bioplastics may have valuable applications in the pharmaceutical, cosmetic, food, and agricultural industries. Moreover, they are considered sustainable compounds, as they can be produced from renewable biomass and tailored according to the microalgal species and cultivation conditions used.

Table 5. Relative content of phthalates synthesized by NSRE-1, NSRE-2, and NRRE-1 under different N/P ratios

Name	Structure	Strain	N/P ratio	Relative content (%)
Bis(6-methylhept-2-yl) phthalate	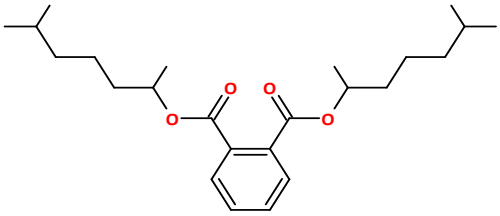	NSRE-1	9	17.4
Bis(2-ethylhexyl) phthalate	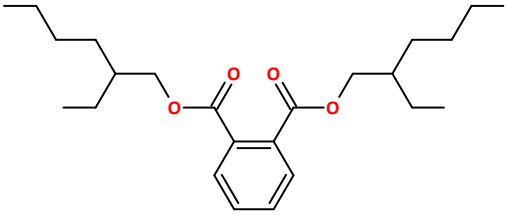	NSRE-1	12	47.7
		NRRE-1	14	80.1
Diisooctyl phthalate	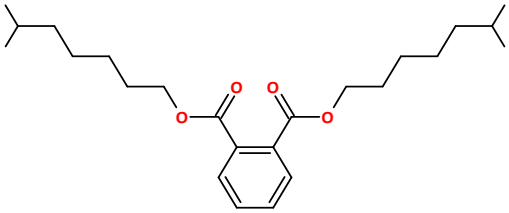	NSRE-2	9	33.9

Conclusions

The results indicate that the N/P ratio influences both the lipid content and the lipid profile of the microalgae. Therefore, it is essential to assess how culture conditions affect the biochemical profile of microalgal strains, particularly when they are endemic.

Furthermore, specific N/P ratios were identified that promote the synthesis of hydrocarbon chains with suitable length and saturation for the production of fatty acid methyl esters. The detection of plasticizer compounds at certain N/P ratios also suggests that their presence can be selectively enhanced under specific cultivation conditions.

Acknowledgments and Funding: We thank the Unidad de Energía Renovable del Centro de Investigación Científica de Yucatán (CICY) for providing all the facilities required to carry out the experimental work. We also acknowledge the Secretaría de Ciencia, Humanidades, Tecnología e Innovación (Secihti) for the scholarship granted to the project titled *"Nutritional study of marine microalgae to enhance their lipid capacity"* (2364085), within the framework of the *Estancias Posdoctorales por México* program.

Author contributions: R.M.G.B: writing, analysis, and interpretation of data; J.C.S.R: analysis and editing; T.T.T: provide materials; R.V.O.: editing, supervision, and funding acquisition.

References

Beuckels, A., Smolders, E., & Muylaert, K. (2015). Nitrogen availability influences phosphorus removal in microalgae-based wastewater treatment. *Water Research*, *77*, 98–106. https://doi.org/10.1016/j.watres.2015.03.018

Borowitzka, M. A. (2013). High-value products from microalgae—their development and commercialisation. *Journal of Applied Phycology*, *25*, 743–756. https://doi.org/10.1007/s10811-013-9983-9

Chi, J., Li, Y., & Gao, J. (2019). Interaction between three marine microalgae and two phthalate acid esters. *Ecotoxicology and Environmental Safety*, *170*, 407–41.

Chisti, Y. (2008). Biodiesel from microalgae beats bioethanol. *Trends in Biotechnology*, *26*(3), 126–131.

Chowdhury, R., Keen, P. L., & Tao, W. (2019). Fatty acid profile and energy efficiency of biodiesel production from an alkaliphilic algae grown in the photobioreactor. *Bioresource Technology Reports*, *6*, 229–236. https://doi.org/10.1016/j.biteb.2019.03.010

D'Alessandro, E. B., & Antoniosi Filho, N. R. (2016). Concepts and studies on lipid and pigments of microalgae: A review. *Renewable and Sustainable Energy Reviews*, *58*, 832–841. https://doi.org/10.1016/j.rser.2015.12.162

Duarah, P., Haldar, D., Patel, A. K., Cheng-Di, D., Singhania, R. R., & Purkait, M. K. (2022). A review on global perspectives of sustainable development in bioenergy generation. *Bioresource Technology*, *348*, 126791. https://doi.org/10.1016/j.biortech.2022.126791

EPA (U.S. Environmental Protection Agency). (2021b). Hexanedioic acid, diisononyl ester. https://comptox.epa.gov/dashboard/dsstoxdb/results?search=dina#invitrodb-bioassays-toxcastdata

Folch, J., Lees, M., & Sloane Stanley, G. H. (1957). A simple method for the isolation and purification of total lipids from animal tissues. *Journal of Biological Chemistry*, *226*(1), 497–509. https://www.jbc.org/article/S0021-9258(18)64849-5/pdf

Gao, L., Ding, W., Xi, J., Gao, S., Zhou, X., Yidi, C., Song, K., Mao, X., Tu, R., & Jiang, G. (2023). Effects of different nitrogen/phosphorus ratios on the growth and metabolism of microalgae *Scenedesmus obliquus* cultured in the mixed wastewater from primary settling tank and sludge thickener. *Process Safety and Environmental Protection*, *170*, 824–833. https://doi.org/10.1016/j.psep.2022.12.059

Hu, R., Zhao, H., Xu, X., Wang, Z., Yu, K., Shu, L., Yan, Q., Wu, B., Mo, C., & He, Z. (2021). Bacteria-driven phthalic acid ester biodegradation: Current status and emerging opportunities. *Environment International*, *154*, 106560. https://doi.org/10.1016/j.envint.2021.106560

Li, S., Li, X., & Ho, S. (2022). Microalgae as a solution of third world energy crisis for biofuels production from wastewater toward carbon neutrality: An updated review. *Chemosphere*, *291*, 1328631. https://doi.org/10.1016/j.chemosphere.2021.132863

López-Rosales, A. R., Ancona-Canché, K., Chavarria-Hernandez, J. C., Barahona-Pérez, F., Toledano-Thompson, T., Garduño-Solórzano, G., López-Adrian, S., Canto-Canché, B., Polanco-Lugo, E., & Valdez-Ojeda, R. (2019). Fatty acids, hydrocarbons and terpenes of *Nannochloropsis* and *Nannochloris* isolates with potential for biofuel production. *Energies*, *12*, 130. https://doi.org/10.3390/en12010130

Rasdi, N. W., & Qin, J. G. (2015). Effect of N:P ratio on growth and chemical composition of *Nannochloropsis oculata* and *Tisochrysis lutea*. *Journal of Applied Phycology*, *27*, 2221–2230. https://doi.org/10.1007/s10811-014-0495-z

Rojo Cebreros, A. H., Morales Plascencia, M. E., Ibarra Castro, L., Martínez Brown, J. M., & Medina Jasso, M. A. (2016). Floculación de *Nannochloropsis* sp. inducida por hidróxido de sodio: eficiencia de floculación, efecto sobre la viabilidad microalgal y su uso como alimento para rotíferos. *Latin American Journal of Aquatic Research*, *44*(4), 662–670. http://dx.doi.org/10.3856/vol44-issue4-fulltext-1

Sharma, K. K., Schuhmann, H., & Schenk, P. M. (2012). High lipid induction in microalgae for biodiesel production. *Energies*, *5*, 1532–1553.

Slinksiene, R., Sendzikiene, E., Mikolaitiene, A., Makareviciene, V., Paleckiene, R., & Ragauskaite, D. (2022). Use of microalgae biomass for production of granular nitrogen biofertilizers. *Green Chemistry Letters and Reviews*, *15*, 416–426. https://doi.org/10.1080/17518253.2022.2071593

Tian, C., Ni, J., Chang, F., Liu, S., Xu, N., Sun, W., Xie, Y., Guo, Y., Ma, Y., & Yang, Z. (2016). Bio-source of di-n-butyl phthalate production by filamentous fungi. *Scientific Reports*, *6*, 19791. https://doi.org/10.1038/srep19791

Tossavainen, M., Ilyass, U., Ollilainen, V., Valkonen, K., Ojala, A., & Romantschuk, M. (2019). Influence of long term nitrogen limitation on lipid, protein and pigment production of *Euglena gracilis* in photoheterotrophic cultures. *PeerJ*, *7*, e6624. https://doi.org/10.7717/peerj.6624

Vimalkumar, K., Zhu, H., & Kannan, K. (2022). Widespread occurrence of phthalate and nonphthalate plasticizers in single-use facemasks collected in the United States. *Environment International*, *158*, 106967. https://doi.org/10.1016/j.envint.2021.106967

Analysis of trends in two climatic variables in the city of Ocotlán, Jalisco

Jessica Rocha-Peña [1], Samuel Cruz-Esteban [2], Ulises Manzanilla-Quiñones [3], Alberto J. Valencia-Botín [4] y Florentina Zurita [1,*]

[1] Environmental Quality Research Center, Centro Universitario de la Ciénega, University of Guadalajara, Ocotlán 47820, Jalisco, Mexico.
[2] Independent researcher, Fraccionamiento Buenos Aires, Tapachula 30798, Chiapas, Mexico.
[3] Forest/Botany Laboratory, Faculty of Agrobiology, Universidad Michoacana de San Nicolás de Hidalgo, Morelia 58030, Michoacán, Mexico.
[4] Plant Health Laboratory, Centro Universitario de la Ciénega, University of Guadalajara, Ocotlán 47820, Jalisco, Mexico.
* Corresponding author: florentina.zurita@academicos.udg.mx

Received: June 13, 2025 Accepted: July 21, 2025 Published: January 31, 2026
DOI: https://doi.org/10.56845/rebs.v8i1.666

Abstract: Global warming affects all inhabited areas of the planet, but its impacts vary significantly across regions. The assessment of local-scale climate trends is fundamental for the development of effective mitigation and adaptation strategies. Currently, there is a lack of studies focused on analyzing climatic behavior and climat-change impacts in the city of Ocotlán, Jalisco. This study analyzes temperature and precipitation trends in Ocotlán, based on data recorded by the "El Fuerte" meteorological station from the National Water Commission. Temperature anomalies were calculated, and the Mann-Kendall test together with Kendall's correlation were applied to detect significant trends. Sen's slope was also estimated to quantify the magnitude of these trends. Additionally, monthly mean plots were generated to visualize the temporal evolution of the variables throughoutthe year. The results indicated an increase in mean temperature and daily thermal range, suggesting signs of climate change. Although precipitation did not exhibit a statistically significant trend, its negative correlation with maximum temperature may indicate a potential future decline in rainfall. These findings contribute to a better understanding of local climatic conditions and provide relevant information for decision-making in key sectors such as agriculture, public health and urban planning.

Keywords: climate change, temperature, precipitation, local climate analysis, trend detection

Introduction

Currently, the planet is facing a global process of climate change, manifested as a sustained increase in the mean atmospheric temperature. This global warming has increased the frequency of extreme weather events and has altered meteorological patterns (Clarke *et al*., 2022). These effects include severe heat waves, intensified precipitation, prolonged drought periods, and an increase in the frequency and intensity of tropical cyclones, among other phenomena, which have significantly affected the water cycle and agricultural production (Pörtner *et al*., 2022). Consequently, they have contributed to a decline in food security and compromised water security (Blunden & Boyer, 2024). The Intergovernmental Panel on Climate Change (IPCC, 2021) has unequivocally stated that greenhouse gases (GHGs), derived from human activities, are the main cause of global warming.

On the other hand, climate change affects all inhabited regions of the planet, although its impacts vary in intensity depending on geographical and environmental conditions. Therefore, a climate assessment at the local scale can provide key information for making more precise decisions regarding mitigation and adaptation to region-specific climate impacts (Doblas-Reyes *et al*., 2021). Among the most relevant climate variables are temperature and precipitation, fundamental physical parameters that determine the environmental conditions of a region (Khavse, Chaudhary, & IMD, 2022). Their analysis relies on statistical methods of climate trend and variability, to identify significant patterns supporting the detection of local climatic changes.

The city of Ocotlán, Jalisco, while having been included in studies on climate change at the regional or state level, has not been evaluated individually. Therefore, this lack of studies represents a significant knowledge gap, that limits the community's capacity to make informed decisions and design adaptation strategies in the face of climate change.

Therefore, the objective of this study is to analyze precipitation and temperature variables (maximum, mean, and minimum) for the period from 1961 to 2024, obtained from the "El Fuerte" meteorological station operated by Nacional Water Commission (CONAGUA) in Ocotlán, Jalisco, in order to detect trends in these variables and identify the warmest months of the year and the months of the rainy season.

Materials and Methods

Study area

The study area corresponds to the municipality of Ocotlán, located in the Ciénega region of the state of Jalisco, Mexico. The municipal seat is situated at 20°21’2.88” N and 102°46’17.76” W, at an elevation of 1,530 m above sea level.

Figure 1. Location map of Ocotlán, Jalisco (IIEGE, 2024)

The municipality of Ocotlán covers an area of 226 km², of which 68.1% is allocated to agricultural use, 8.7% corresponds to urban settlements, 16.8% to tropical forest, 3.1% to temperate forest, 2.2% to grassland, 1.0% to water bodies, and 0.05% shows an apparent absence of vegetation. The predominant climate is semi-warm and sub-humid (IIEG, 2024).

Meteorological data for the analysis of temperature and precipitation were obtained from the CONAGUA climatological station “El Fuerte” (ID 14047), located in Ocotlán, Jalisco (20°19'51" N, 102°45'48" W; 1,540 m a.s.l.). The station provides daily records of precipitation, evaporation, maximum temperature, and minimum temperature. Mean temperature was calculated as the arithmetic average of the daily maximum and minimum values. The dataset spans a 62-year period (1961–2024). However, 1986 was excluded from the analysis due to the complete absence of records for reasons not specified by the data provider.

Calculation of anomalies

One of the methods used to identify warming or cooling trends is the calculation of temperature anomalies. A temperature anomaly denotes the deviation of an observed temperature from a long-term reference mean (NOAA, 2025). It is computed as the difference between the annual mean temperature of a given year and the mean temperature of the reference period. The reference period typically spans at least 30 years. A positive anomaly indicates that the year was warmer compared to the reference period, while a negative anomaly reflects a relative cooling (NOAA, 2025). For the calculation of mean temperature anomalies in this study, anomalies were calculated as the difference between the annual average temperature recorded from 1961 to 2024 and the mean temperature of the reference period (1961 to 1991). Data analysis and graphical representation were performed using Microsoft Excel.

Mean plots and analysis of variance

For this study, mean plots were used as a visual tool to represent the averages of the analyzed variables and to observe their temporal trends. A plot was constructed for each variable with the aim of identifying its monthly behavior (Figure 3). Because the data did not meet the assumptions of normality and homoscedasticity, the analysis of variance (ANOVA) was performed using generalized linear models (GLM) with a Gaussian distribution. Mean comparisons were conducted using Tukey's test (α = 0.05). All statistical analyses were performed in R software, version 4.4.2 (R Core Team, 2025).

Kendall's correlation

Kendall's correlation, also known as Kendall's tau (τ), is a non-parametric measure that assesses the association between two quantitative or ordinal variables. This coefficient makes it possible to identify the presence of a monotonic (increasing or decreasing) relationship between variables, without assuming a normal distribution of the data (El Hashash & Shiekh, 2022).

Mann-Kendall test

The Mann–Kendall test is a widely used non-parametric method for detecting trends in time series data. This test is based on comparing the relative magnitudes between pairs of observations. One of its main advantages is that it does not require the data to conform to any specific distribution (Khavse, Chaudhary, & IMD, 2022). The Mann–Kendall statistic (S) is defined as shown in Equation 1.

$$S = \sum_{k=1}^{n-1} \sum_{j=k+1}^{n} sgn(x_j - x_k) \quad \textbf{(1)}$$

where: n: number of years; xj y xk : annual values in years *j* and *k*, respectively, with *j* < *k*; sgn is the sign function.

A positive value of *S* indicates an increasing trend, whereas a negative value indicates a decreasing trend. After computing *S*, it is necessary to calculate the probability associated with this value and the sample size *n* to statistically assess the significance of the trend. For sample sizes greater than 10, a normal approximation of the Mann–Kendall test can be used (Khavse, Chaudhary, & IMD, 2022). To apply this approximation, the variance of *S* is first computed (Equation 2), and then the standardized test statistic (*Z*) is calculated based on the value of *S*, as shown in Equation 3.

$$VAR(S) = \frac{1}{18}\left[n(n-1)(2n+5) - \sum_{p=1}^{q} t_p(t_p-1)(2t_p+5)\right] \quad \textbf{(2)}$$

where: q: number of tied groups (groups with equal values); t_p: number of data points in group p.

$$Z = \begin{cases} \dfrac{S-1}{\sqrt{VAR(S)}} \; if \; S > 0 \\ 0 \; si \; S = 0 \\ \dfrac{S+1}{\sqrt{VAR(S)}} \; if \; S < 0 \end{cases} \quad \textbf{(2)}$$

Sen's slope

Sen's slope estimator is a non-parametric technique used to estimate the annual rate of change of a variable. It provides a reliable estimate of the trend slope under the assumption of linearity and does not require any specific distributional assumptions for the data being analyzed (Mehmood *et al*., 2024). Kendall's correlation, the Mann–Kendall test, and Sen's slope estimator were computed using R software, version 4.4.2 (R Core Team, 2025).

Results and Discussion

Temperature anomalies

The annual temperature anomalies recorded between 1961 and 2024 reveal alternating periods of warmer and cooler years, but overall they show a clear warming trend (dotted red line, Figure 2). Positive anomalies have increased in magnitude over time, with the highest value occurring in 2024. This finding aligns with global observations: the World Meteorological Organization (WMO, 2025) reported that 2024 was the warmest year on record. Year-to-year temperature variability can be influenced by natural factors such as solar activity and internal climate variability, including El Niño and La Niña events. These processes can modulate, and sometimes temporarily mask, the effects of human-driven global warming at regional and short-term scales (IPCC, 2021).

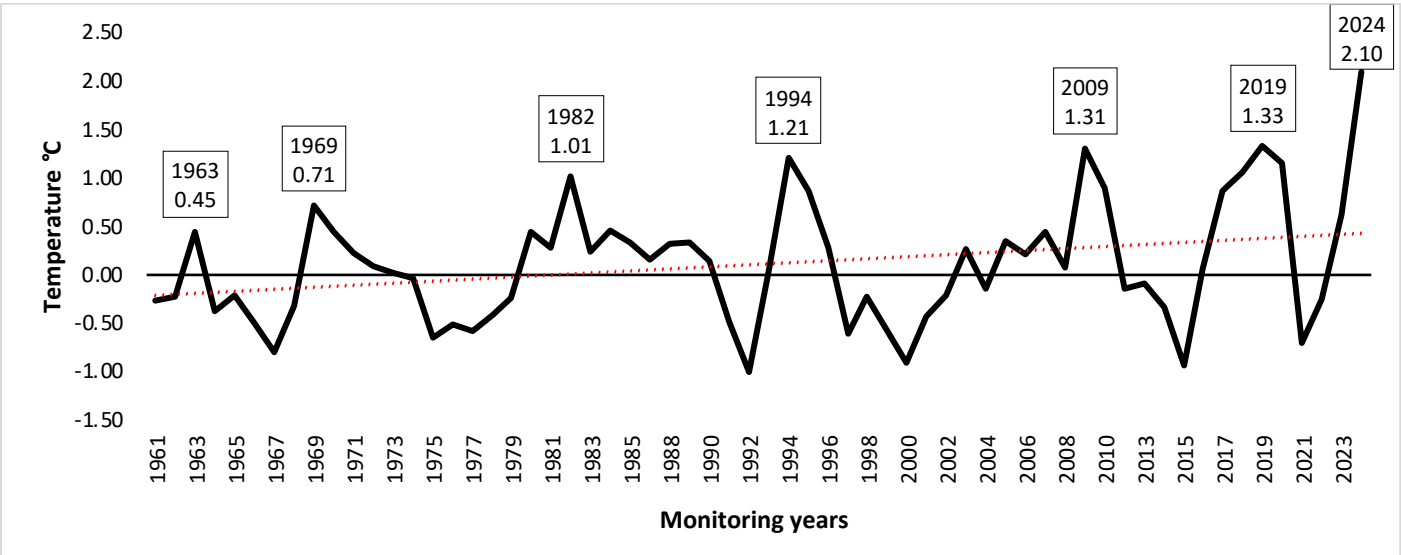

Figure 2. Temperature anomaly plot

It is important to highlight that the results of the temperature anomalies already reflect the manifestation of climate change. Nevertheless, it would be relevant for future studies to further investigate the identification of the natural phenomena and internal climate variability that influence the climate of the city of Ocotlán. This knowledge would be fundamental for improving the capacity for response and planning in short and medium-term decision-making.

Trends of the variables across the months of the year.

The evaluated temperature variables (minimum, mean, and maximum) show similar trends across the 12 months of the year, unlike precipitation, which exhibits a different pattern (Figure 3). Statistical analysis revealed a significant effect of month on maximum temperature ($F = 2221$; $df = 11, 21816$; $P < 0.001$), mean temperature ($F = 5022.8$; $df = 11, 21816$; $P < 0.001$), minimum temperature ($F = 4277.3$; $df = 11, 21816$; $P < 0.001$), and precipitation ($F = 280.14$; $df = 11, 21816$; $P < 0.001$). May was identified as the warmest month of the year, with average values of 31.4 °C for maximum temperature and 23.4 °C for mean temperature, followed by April and June. The lowest temperatures for these variables (mean and maximum) were observed in January and December. Regarding minimum temperature, the highest value occurred in June (16.4 °C), followed by May, July, and August, while the lowest values were recorded in December and January (7.4–8.2 °C) (Figure 3). These colder months are strongly associated with frost events and cold fronts in recent years, which have caused economic losses in agriculture. Therefore, the warmest months in Ocotlán are April, May, and June. Lino (2022) points out that in May, solar rays hit the Earth's surface in Jalisco perpendicularly, which contributes to a significant increase in temperature during that month. Although this phenomenon is repeated later in the year, its thermal effect is attenuated by the presence of rainfall.

Regarding precipitation, although it is present throughout the year, its volume is minimal outside of the rainy season, which begins in May, intensifies between June and August, reaches its peak in July, and ends in November (Figure 3).

This seasonality is consistent with the pattern observed at the state level, which is primarily influenced by the rainy period associated with factors such as the tropical cyclone season (Lino, 2022).

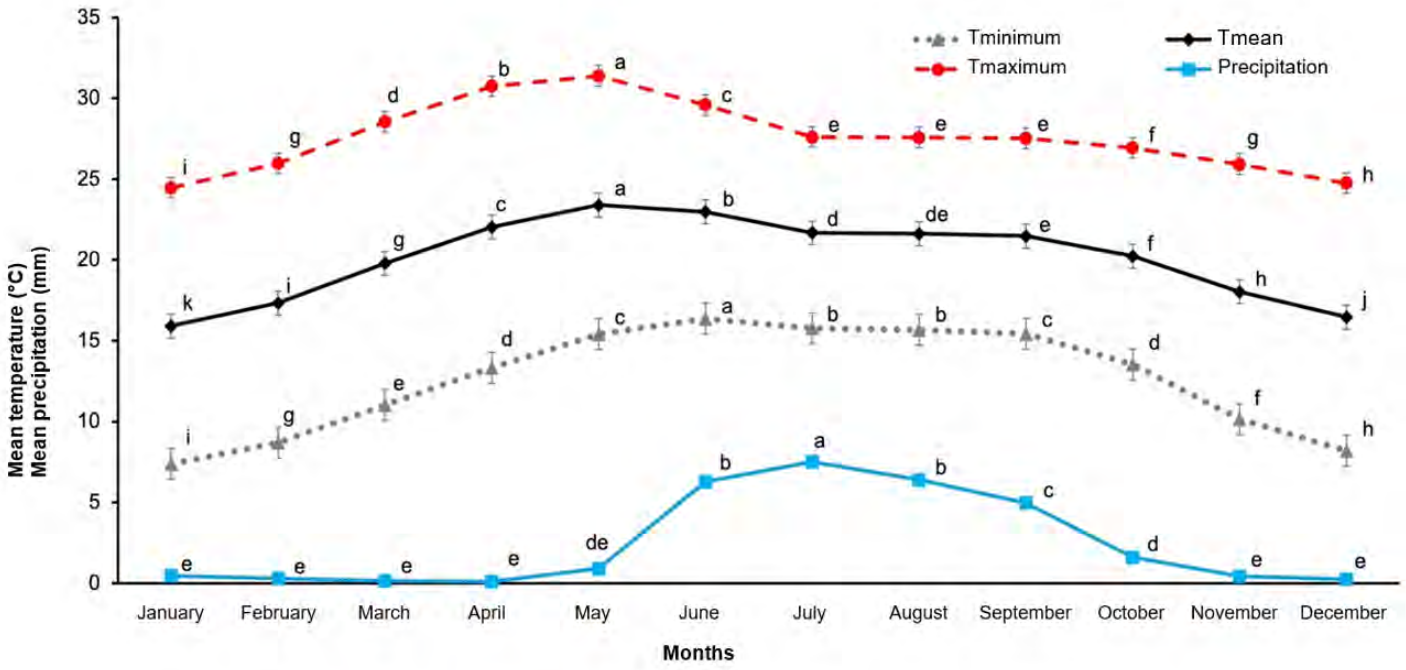

Figure 3. Mean ± SD of the studied variables (maximum, mean, and minimum temperature, and precipitation) corresponding to Ocotlán, Jalisco. Means sharing the same letter are not significantly different (Tukey's test, α = 0.5)

Kendall correlation, Mann–Kendall tests, and Sen's slope estimator

Regarding the Kendall correlation analyses (Figure 4), a significant negative correlation was observed between minimum temperature and time (Figure 4A; Table 1), indicating a progressive decrease in minimum temperature at a rate of −3.2e−05 °C per year. This suggests that Ocotlán is experiencing increasingly colder nights, which may have important implications, particularly for the agricultural sector. In contrast, mean temperature showed a significant positive correlation with time (Figure 4B; Table 1), with an increasing rate of 1.2e−05 °C per year, indicating a sustained rise in overall heat overtime. Similarly, maximum temperature exhibited a significant upward trend at a rate of 8.9e−05 °C per year (Figure 4C; Table 1), confirming an increase in daytime temperatures. The rise in mean temperature—driven primarily by the increase in maximum temperatures—represents a clear indicator of climate warming.

This pattern also reflects an increase in the daily thermal amplitude, a climate-change–related phenomenon that has been documented globally (Simolo & Corti, 2022) and is now evident in Ocotlán. Future studies should examine this variable in more detail, along with the extreme maximum temperature index (TXx) and the extreme minimum temperature index (TNn). At the state level, a significant increase in maximum temperature has been reported, while minimum temperature shows a non-significant decreasing trend (Lino, 2022). It is possible that local factors in Ocotlán, such as surface characteristics and land use, are contributing to this decrease in minimum temperature.

On the other hand, precipitation presents a negative correlation with time, although this is not statistically significant (Figure 4D, Table 1); which suggests high interannual variability or a more complex effect. This reinforces the need to continue monitoring this variable in subsequent years, due to its relevance to water availability and agricultural application.

Other significant correlations were identified between temperature variables (minimum, mean, and maximum) and precipitation (Figure 5), which is relevant for understanding climate interactions in the region. In particular, it was observed that the minimum temperature and the mean temperature show a positive correlation with precipitation (Figure 5A, B), suggesting that, in general, higher minimum and mean temperatures coincided with greater

precipitation records. This pattern can help interpret the apparent negative—though not significant—trend of precipitation observed over the years (Table 1, Figure 4D). In contrast, the maximum temperature showed a significant negative correlation with precipitation (Figure 5C), indicating that as maximum temperatures increase, precipitation tends to decrease.

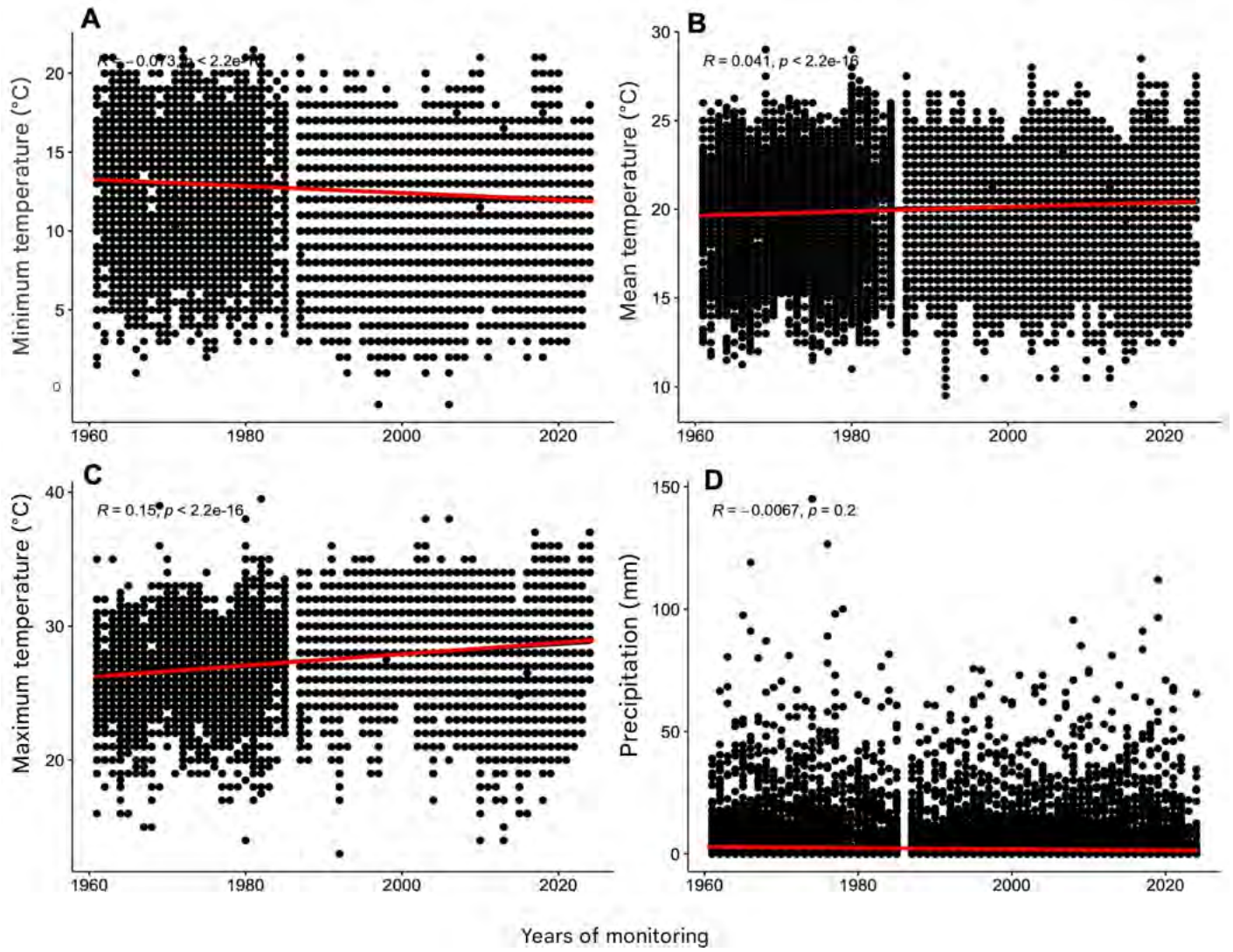

Figure 4. Kendall correlation of variables: A) Minimum temperature vs. time B) Mean temperature vs. time C) Maximum temperature vs. time D) Precipitation vs. time

Table 1. Statistical summary of the Mann–Kendall test for each variable under study with respect to the years

Variable	S	Z	P-value	R and trend	Sen's slope
Minimum temperature	-1.614581e+07	-15.06	p-value < 2.2e-16	R=-0.07 Negative trend	-3.2e-05 °C/year
Mean temperature	9.438886e+06	8.79	p-value < 2.2e-16	R=0.04 Positive trend	1.2e-05 °C/year
Maximum temperature	3.431826e+07	32.07	p-value < 2.2e-16	R=0.15 Positive trend	8.9e-05 °C/year
Precipitation	-7.464290e+05	-0.95	p-value = 0.3434	R=-0.007 Negative trend	0 mm/year

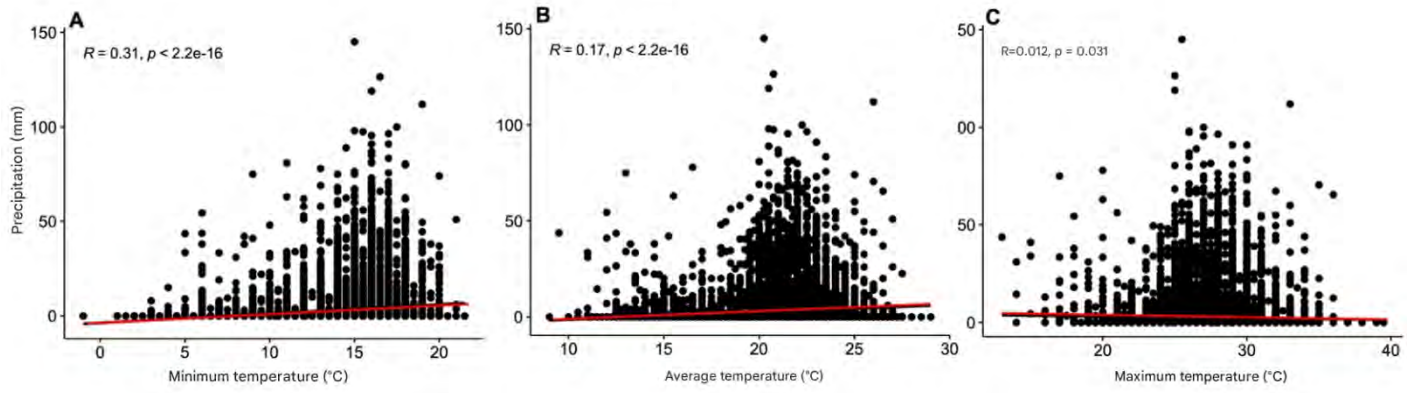

Figure 5. Correlation between the studied variables

The relationship between precipitation and temperature has been the subject of numerous international studies, which show variable results depending on the local conditions of each region. These analyses help improve understanding of climate behavior and support the development of more accurate predictive models. However, in Mexico, comprehensive studies examining the relationship between these variables are still limited, which constrains the ability to adequately interpret the observed climatic patterns (Becerril, Munguía, & del Rivero, 2024).

Conclusions

In the present study, the trends of temperature and precipitation in the city of Ocotlán, Jalisco, were evaluated based on data recorded by the CONAGUA "El Fuerte" meteorological station. The results provide evidence of an increase in mean temperature, as well as an increase in daily thermal amplitude, both considered consistent indicators of climate change. In contrast, precipitation did not exhibit a statistically significant trend; however, due to its negative correlation with maximum temperature, it cannot be ruled out that a significant decrease in precipitation levels may be recorded in the future. Likewise, it was observed that the warmest months of the year and the rainy season in Ocotlán coincide with patterns reported by previous state-level studies, which reinforces the validity of the observed results.

The findings of this research represent a relevant contribution to the urban context of Ocotlán by enhancing the understanding of its climate and the effects of climate change. These aspects should be considered in decision-making processes related to agriculture, urban planning, and public health. Nevertheless, much remains to be investigated regarding local climate dynamics and the potential impacts of climate change in the region.

Acknowledgments and Funding: Jessica Rocha Peña, the first author, gratefully acknowledges the Master's scholarship funding provided by the Secretaría de Innovación, Ciencia y Tecnología del Estado de Jalisco (SECIHTI) in support of this research.

Author contributions: J.R-P. and S.C.-E: writing and analysis and interpretation of data; U. M.-Q: data collection, A.J. V.-B: provide materials, F.Z: conceptualization, design, and editing.

References

Becerril Torres, O. U., Munguía Vázquez, G., & del Rivero Maldonado, G. E. (2024). *Relación dinámica entre temperatura y precipitación pluvial en las regiones de México*. Universidad Autónoma del Estado de México.

Blunden, J., & Boyer, T. (Eds.). (2024). State of the climate in 2023. *Bulletin of the American Meteorological Society*, *105*(8), S1–S484. https://doi.org/10.1175/2024BAMSStateoftheClimate.1

Clarke, B., Otto, F., Stuart-Smith, R., & Harrington, L. (2022). Extreme weather impacts of climate change: An attribution perspective. *Environmental Research: Climate*, *1*(1), 012001. https://doi.org/10.1088/2752-5295/ac6e7d

Doblas-Reyes, F. J., Sörensson, A. A., Almazroui, M., Dosio, A., Gutowski, W. J., Haarsma, R., Hamdi, R., Hewitson, B., Kwon, W.-T., Lamptey, B. L., Maraun, D., Stephenson, T. S., Takayabu, I., Terray, L., Turner, A., & Zuo, Z. (2021). Linking global to regional climate change. En V. Masson-Delmotte, P. Zhai, A. Pirani, S. L. Connors, C. Péan, S. Berger, N. Caud, Y. Chen, L. Goldfarb, M. I. Gomis, M. Huang, K. Leitzell, E. Lonnoy, J. B. R. Matthews, T. K. Maycock, T. Waterfield, O. Yelekçi, R. Yu, & B. Zhou (Eds.), *Climate change 2021: The physical science basis. Contribution of Working Group I to the Sixth Assessment Report of the Intergovernmental Panel on Climate Change* (pp. 1363–1512). Cambridge University Press. https://doi.org/10.1017/9781009157896.012

Instituto de Información Estadística y Geográfica del Estado de Jalisco. (2024). *Ocotlán: Diagnóstico del municipio*. https://iieg.gob.mx/ns/wp-content/uploads/2024/08/Ocotl%C3%A1n.pdf

IPCC. (2021). Summary for policymakers. En V. Masson-Delmotte, P. Zhai, A. Pirani, S. L. Connors, C. Péan, S. Berger, N. Caud, Y. Chen, L. Goldfarb, M. I. Gomis, M. Huang, K. Leitzell, E. Lonnoy, J. B. R. Matthews, T. K. Maycock, T. Waterfield, O. Yelekçi, R. Yu, & B. Zhou (Eds.), *Climate change 2021: The physical science basis. Contribution of Working Group I to the Sixth Assessment Report of the Intergovernmental Panel on Climate Change* (pp. 3–32). Cambridge University Press. https://doi.org/10.1017/9781009157896.001

Khavse, R., Chaudhary, J., & India Meteorological Department (IMD). (2022). Trend assessment in climate variable by Mann–Kendall test of Bastar district of Chhattisgarh. *Mausam*, *73*(1), 79–82. https://doi.org/10.54302/mausam.v73i1.5082

Lino Solano, J. J. (2022). *Tendencias climáticas de los indicadores de temperatura y precipitación en Jalisco, México* [Tesis de maestría, Universidad de Guadalajara]. Biblioteca Digital de la Universidad de Guadalajara.

Mehmood, K., Anees, S. A., Rehman, A., Pan, S., Tariq, A., Zubair, M., Liu, Q., Rabbi, F., Khan, K. A., & Luo, M. (2024). Exploring spatiotemporal dynamics of NDVI and climate-driven responses in ecosystems: Insights for sustainable management and climate resilience. *Ecological Informatics*, *80*, 102532. https://doi.org/10.1016/j.ecoinf.2024.102532

NOAA National Centers for Environmental Information. (2025, 9 de junio). *Global surface temperature anomalies*. Recuperado el 8 de junio de 2025 de https://www.ncei.noaa.gov/access/monitoring/global-temperature-anomalies/

Organización Meteorológica Mundial. (2025, 10 de enero). *La Organización Meteorológica Mundial confirma que 2024 fue el año más cálido jamás registrado al superar en cerca de 1,55 °C los niveles preindustriales*. Organización Meteorológica Mundial. https://wmo.int/es/media/news/la-organizacion-meteorologica-mundial-confirma-que-2024-fue-el-ano-mas-calido-jamas-registrado-al

Pörtner, H.-O., Roberts, D. C., Adams, H., Adelekan, I., Adler, C., Adrian, R., Aldunce, P., Ali, E., Ara Begum, R., Bednar-Friedl, B., Bezner Kerr, R., Biesbroek, R., Birkmann, J., Bowen, K., Caretta, M. A., Carnicer, J., Castellanos, E., Cheong, T. S., Chow, W., & Zaiton Ibrahim, Z. (2022). Technical summary. En H.-O. Pörtner, D. C. Roberts, E. S. Poloczanska, K. Mintenbeck, M. Tignor, A. Alegría, M. Craig, S. Langsdorf, S. Löschke, V. Möller, A. Okem, & B. Rama (Eds.), *Climate change 2022: Impacts, adaptation and vulnerability. Contribution of Working Group II to the Sixth Assessment Report of the Intergovernmental Panel on Climate Change* (pp. 37–118). Cambridge University Press. https://doi.org/10.1017/9781009325844.002

Simolo, C., & Corti, S. (2022). Quantifying the role of variability in future intensification of heat extremes. *Nature Communications*, *13*, 7930. https://doi.org/10.1038/s41467-022-35571-0

Characterization of biogas and effluent produced during the anaerobic digestion of mezcal vinasse

Edgar Israel Hernández-Sosa [1], Jorge Alejandro Santiago-Urbina [1,2], Deneb Peredo-Mancilla [3] y Edwin Alfonso Zelaya-Benavidez [4, *]

[1] Dirección de División de Carrera de Agricultura Sustentable y Protegida, Universidad Tecnológica de los Valles Centrales de Oaxaca, San Pablo Huixtepec, CP 71265, Zimatlán de Álvarez, Oaxaca, México.
[2] Agropecuario y Sector Primario Tonalá SPR DE RL. San Antonio Arrazola, Santa Cruz Xoxocotlán, Oaxaca, México, C.P. 71233
[3] Departamento de Ingeniería en Pesquerías, Universidad Autónoma de Baja California Sur, Boulevard Forjadores S/N, Col. Universitario, C.P. 23080, La Paz, Baja California Sur, México
[4] Universidad Autónoma Comunal de Oaxaca (UACO), Centro Universitario Comunal de San Andrés Solaga, Villa Alta, Oaxaca. C.P. 68844.
* Autor de correspondencia: edwinzelayab@gmail.com; Tel.: (+52 951 3941982)

Received: August 22, 2025 Accepted: October 2, 2025 Published: February 15, 2026
DOI: https://doi.org/10.56845/rebs.v8i1.674

Abstract: The production of mezcal generates vinasse, a liquid waste with high concentrations of organic matter and acidic pH, which represents a potential source of pollution. The use of anaerobic biodigesters has emerged as an alternative for the treatment of this waste stream. This study characterizes the anaerobic digestion (AD) of mezcal vinasse in a 10 m^3 tubular (bag-type) anaerobic biodigester. To this end, daily biogas production was measured and normalized to standard conditions. The methane content in the produced biogas was determined through carbon dioxide (CO_2) removal, and the thermal efficiency of a biogas stove was evaluated. The physicochemical properties of the liquid effluent resulting from the AD process were also assessed. The results demonstrated that the AD treatment of vinasse with an initial Chemical Oxygen Demand (COD) concentration of 44.93 g L^{-1} yielded 15.61 L of biogas per liter of vinasse, with a methane concentration of 68.48%. Furthermore, the thermal efficiency of the biogas stove was 35.45%. The effluent obtained had a pH of 7.5 and a COD concentration of 17.00 g L^{-1}, which represents a 62.16% COD removal relative to the influent. Additionally, its organic carbon content reached 17%, while total nitrogen accounted for 19%. These results indicate a high potential for the proposed approach to be implemented as a strategy for waste valorization method, pollution mitigation, local clean energy production, and agroecological applications.

Keywords: anaerobic digestion, biogas, mezcal vinasses, biofertilizer, renewable energy

Introduction

In recent years, the mezcal industry has experienced rapid growth, reaching a production of 12.239 million liters in 2023. Mezcal is produced in nine Mexican states holding the designation of origin for its commercialization. Oaxaca is the largest producer, accounting for over 90% of the total national production (COMERCAM, 2024). The growth of this industry has brought significant environmental challenges, particularly as the generation of vinasse, a byproduct of the mezcal distillation process. This substance exhibits high concentrations of organic matter (biochemical oxygen demand, BOD_5:22,500–35,000 mg L^{-1} and COD: 35,000–122,000 mg L^{-1}) and high acidity (pH between 3 and 5) (Robles-González *et al*., 2012). Vinasse generation can reach quantities of 10–12 L/L of final distillate, and the majority of this waste is not properly managed or treated; instead, it is dumped directly into drains, soil, rivers, or lakes at high temperatures, posing serious risks to aquatic and terrestrial ecosystems(Crespo-González *et al*., 2018; Jiménez *et al*., 2006). Alternatively, some producers choose to store it; however, due to the lack of adequate treatment systems, they are forced to hire services to empty these containers or tanks without regulatory oversight Which merely relocates the waste management problem rather than resolving it.

Anaerobic digestion (AD) is an alternative method for treating organic waste from various sources, including vinasse (Silva *et al*., 2021; Parsaee *et al*., 2019). This process allows the conversion of organic substrates into a gaseous mixture known as biogas, which has a high methane content, making it suitable for clean energy production (Ullah Khan *et al*., 2017). In addition, the digestate generated during AD comprises partially digested organic matter, micro-and macronutrients, and water. This effluent contains essential nutrients in highly bioavailable forms, making it a valuable biofertilizer and soil conditioner (Nayak & Ranade,2025). Thus, the anaerobic digestion of organic residues is related to important socio-environmental co-benefits, including improved waste management, clean energy generation from local inputs, mitigation of greenhouse gas (GHG) emissions, support for the circular economy, contribution to energy independence, and more sustainable agricultural and livestock practices. In this context, the use of AD has gained popularity in various parts of the world, with more than 20 million systems in China, 4.3 million in India, and

approximately 7,000 in Germany; these three countries are reported to currently have the highest number of anaerobic digestion systems (Zelaya-Benavidez, 2022; Zelaya-Benavidez *et al*., 2023).

A variety of anaerobic digester designs are commercially available; however, some of these systems tend to be more expensive and complex. Nevertheless, the selection of a system should consider the available resources, user characteristics, and specific features of the installation region (Parsaee *et al*., 2019). Zelaya-Benavidez (2022) proposed the use of tubular anaerobic digesters made of polyethylene to treat mezcal vinasse, as they are less expensive and easier to handle than concrete digesters (Zelaya-Benavidez, 2022). In comparison, digesters made of PVC geomembranes, although more expensive, offer longer service life and greater mechanical resistance during installation and operation. In this context, the objective of this study was to evaluate the applicability of PVC tubular anaerobic digesters for the treatment and valorization of mezcal vinasse. To this end, the products resulting from the anaerobic digestion of mezcal vinasse–biogas and liquid effluent (digestate)–were characterized, and the methane content and thermal efficiency of biogas were measured. The results of this study highlight the effectiveness and benefits of treating vinasse using anaerobic biodigesters as an appropriate and sustainable technology for the mezcal industry.

Materials and Methods

Study location

The study was conducted at the "Mezcal Capotlan" palenque located in the Arrazola neighborhood of Santa Cruz Xoxocotlán, Oaxaca, Mexico (17° 2' 27.7" N, 96° 46' 59.8" W). The site was equipped with a functioning tubular biodigester, also known as a bag-type, with a liquid capacity of 10 m^3, manufactured by ARQUEA®, using a PVC geomembrane (Figure 1).

Figure 1. A tubular or bag-type biodigester with a liquid volume of 10 m^3 was used in the present study

Biodigester management

The system was started with fresh bovine manure and mezcal vinasse (VM) at a 1:3 ratio (manure: vinasse, V/V), and the mixture was stabilized with commercial calcium hydroxide ($Ca(OH)_2$) from the brand CALHIDRA®. During the data collection period, the biodigester system was continuously fed 166 L of vinasse per day. The pH of the vinasse was adjusted between 6.3 and 9.9 by adding calcium hydroxide. The vinasse used for the experiment was obtained from an underground cistern on-site, which collected vinasse generated during mezcal distillation in the alembics.

The substrate and effluent were characterized through physicochemical analysis performed by a laboratory accredited by the Mexican Accreditation Entity (EMA). The effluent sample was collected from the outlet of the biodigester on day 21 of operation. The tests performed included microwave digestion/inductively coupled plasma optical emission spectroscopy (ICP-OES) for the determination of phosphorus, K, Ca, Mg, Na, sulfur, Fe, Cu, Mn, Zn, and B; and loss-on-ignition (calcination) for the quantification of organic matter, ash, and organic carbon. The pH levels were measured using a Yieryi® C-600 pH meter in liquid samples collected from both the inlet and outlet streams of the biodigester.

Analytical methods for determining biogas production

Biogas production was measured over a 21-day period, with a 24 h measurement frequency, using a KEUK DONG KI JEON® G-2 model low-pressure analog diaphragm gas meter. The ambient temperature of the site was recorded throughout the experiment, taking readings, every 10 min using an Elitech® RC-5 model temperature sensor.

The daily biogas production was normalized to standard conditions (27.15 K and 1013 hPa) as presented in Equation 1 (Dinuccio *et al*., 2010):

$$V_0^{NPT} = V\frac{(P - P_v)T_0}{P_0 T} \quad \textbf{(1)}$$

where V_0^{NPT} represents the volume (L) of dry biogas normalized to standard pressure and temperature, V is the recorded biogas volume (L), P is the biogas pressure at the time of measurement (hPa), T is the ambient temperature (K), T_0 is the standard temperature (K), and P_v is the water vapor pressure in mmHg as a function of the temperature of the measurement site in hPa, as obtained by Equation 2:

$$P_v = 10(A - \frac{B}{T + C}) \quad \textbf{(2)}$$

where T is ambient temperature (°C). A, B, and C are parameters of the Antoine Equation constants for water. Under the experimental conditions, their values were 8.0713, 1730.6300, and 24.6900, respectively.

Methane content in biogas

The methane content in the produced biogas was determined by CO_2 absorption using a 20% KOH solution combined with the liquid water displacement method (Córdova *et al*., 2022) (Figure 2). The methane percentage was calculated using Equation 3 (Abdel-Hadi, 2008):

$$\%\mathrm{CH_4} = 100\% - \left[\left(\frac{V_1 - V_2}{V_1} * 100\right) + 3\%\right] \quad \textbf{(3)}$$

where $\%\mathrm{CH_4}$represents the methane concentration in the biogas, V_1 is the initial biogas volume(mL), and V_2 is the remaining gas volume after CO_2 removal (mL).

Figure 2. Mechanism of CO_2 removal from biogas

Thermal efficiency

The thermal efficiency of the burner was determined using the "Water Boiling Test" method, which relates the energy transferred to water and the energy released by biogas combustion, as expressed in Equation 4 (Clean Cooking Alliance, 2014):

$$h_c = \frac{\left[\left(\frac{M_a * \Delta T * c}{100}\right) + (M_{av} * H)\right]}{V_{biogas} * \%_{CH4} * PC_{CH4}} \quad \textbf{(4)}$$

where h_c is the thermal efficiency (%), M_a is the initial mass of water (kg), ΔT is the r temperature increase until boiling point (K), c is the specific heat capacity of water (4.2 kJ kg K^{-1}), M_{av} is the mass of evaporated water (kg), H is latent heat of vaporization (2.26 kJ kg^{-1}), V_{biogas} is the volume of biogas consumed (m^3), $\%_{CH4}$is the methane content of the biogas (calculated by Equation 2), and PC_{CH4} is the lower calorific value of methane (34 MJ m^{-3}).

Results and Discussion

Site temperature

Figure 3 shows the site temperature records, with a minimum recorded temperature of 9.2 °C on day 1 and a maximum temperature of 38.0 °C on day 10. The average temperature during the measurement period was 24.78 ±1.16 °C. These

temperature conditions fall within the growth ranges of both psychrophilic (4–20 °C) and mesophilic (20–40 °C) microbial communities, which are commonly involved in anaerobic digestion processes.

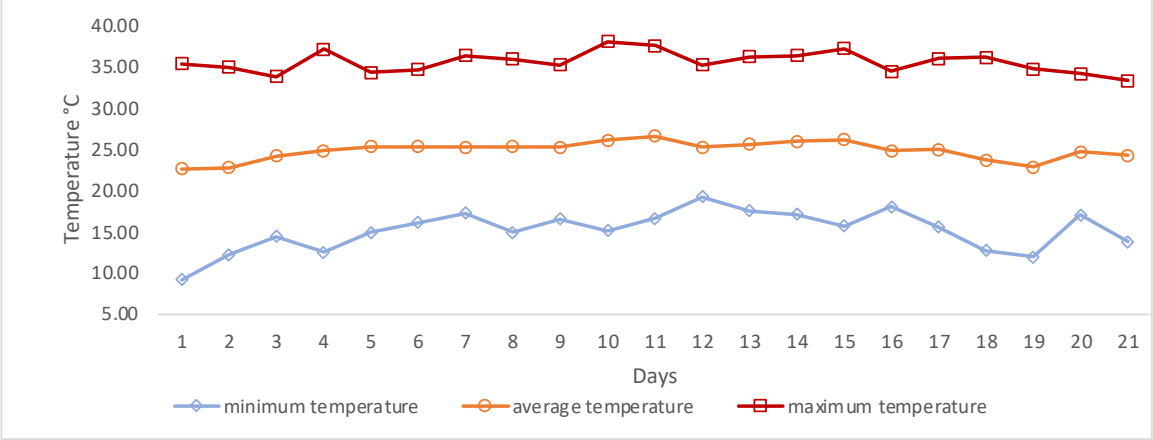

Figure 3. Temperature records of the site where the study was conducted

Physicochemical characterization of substrate and effluent

Table 1 summarizes the physicochemical properties of the mezcal vinasse used as feedstock for the biodigester, as well as those of the digestate (effluent) obtained after anaerobic treatment. The pH of the vinasse indicates a partial degradation of the substrate during storage prior to digestion, as evidenced by a reduction in acidity from fresh vinasse produced at the stills (on average pH=3.5) to a pH of 5.38 at the biodigester inlet.

Table 1. Physicochemical characteristics of vinasse and biodigester effluent (Biol)

Parameter	Units	Vinasse	Effluent
pH		5.38	7.50
Electrical conductivity	dS m^{-1}	5.20	5.01
COD	g L^{-1}	44.930	17.008
BOD_5	g L^{-1}	29.610	3.405
Organic matter	%wt	0.96	0.29
Ashes	%wt	0.41	0.29
Organic carbon	%wt	0.56	0.17
Total nitrogen	%wt	0.80	0.19
Phosphorus	mg L^{-1}	56	400
Potassium	mg L^{-1}	400	5700
Calcium	mg L^{-1}	1300	10200
Magnesium	mg L^{-1}	200	2300
Sodium	mg L^{-1}	81	1000
Sulfur	mg L^{-1}	82	500
Iron	mg L^{-1}	114	294
Copper	mg L^{-1}	6.76	36.30
Manganese	mg L^{-1}	2.56	14.50
Zinc	mg L^{-1}	2.04	20.90
Boro	mg L^{-1}	1.36	11.40

U/M: unit of measurement

Vinasse entered the biodigester with an initial chemical oxygen demand (COD) concentration of 44.930 g/L. After anaerobic digestion, the effluent COD decreased to 17.008 g/L, representing a 62.15% reduction. This reduction

demonstrates the effectiveness of the biodigester in degrading the organic load present in vinasse and confirms its potential as a technically viable alternative for mitigating the environmental impact associated with mezcal production.

The COD removal efficiency obtained in this study (62.15%) fell within the range reported for the anaerobic digestion of vinasse and other distillery effluents. Díaz-Barajas *et al*. (2024) reported COD removal efficiencies close to 81% for mezcal vinasse under high dilution conditions, while removal efficiencies ranging from 49 to 82% have been reported for sugarcane vinasse treated in upflow anaerobic sludge blanket (UASB) reactors (Gomes de Barros *et al*., 2016). In this context, the COD removal achieved in the present study suggests that the implemented tubular biodigester represents a robust and scalable option for the treatment of high strength mezcal vinasse.

Although the pH values of the incoming vinasse were below the optimal range for anaerobic digestion, the substrate was stabilized prior to feeding by the addition of commercial calcium hydroxide adjusting the pH to values between 7.3 and 9.9. This procedure ensured suitable pH operating conditions within the biodigester, where pH values remained between 6.7 and 7.5, which is considered optimal for anaerobic digestion) (Rajendran *et al*., 2012). Furthermore, the COD concentration of the vinasse used in this study (44.930 g L^{-1}) was lower than the values reported by Ibarra-Camacho *et al*. (2019) for vinasse samples produced in Cuban distilleries, where COD concentrations ranged from 51.53 to 54.25 g L^{-1}. Comparison between influent and effluent indicated a 62.14% COD removal and an 88.5% BOD_5 removal after anaerobic digestion, with a hydraulic retention time of 60 days.

Inlet and outlet pH

The pH of the liquid substrate within the biodigester remained within the optimal range for anaerobic digestion (6.7–7.5) throughout the operational period. The average inlet pH was 7.37 ±0.63, while the outlet pH was 7.38 (±0.15). During the initial 24 h of operation, the outlet pH temporally shifted toward alkaline values following substrate feeding, after 48 h of operation, the outlet pH reached a neutral value (Figure 4).

Vinasse load and biogas yield

During the evaluation period, the biodigester was fed with an average of 200 L of mezcal vinasse with an influent COD of 44.93 mg L^{-1}, BOD_5 of 29.62 mg L^{-1}, and pH of 8.2 (± 1.12), which is slightly alkaline for anaerobic digestion. The biogas yield obtained in this study was 15.61 L of biogas per liter of vinasse fed, which is 3.27% higher than values reported in previous studies. However, the average methane content was 2.17% lower than that reported by Lorenzo-Acosta *et al*. (2015). The methane concentration ranged from 63.83 % to 74.25%, with an average of 68.48% (±2.9%), which is lower than those reported in the literature (Ferrer *et al*., 2011; Lorenzo-Acosta *et al*., 2015; Rivera *et al*., 2020) (Figure 4). The biogas yield was 15.61 L/L of vinasse fed to the biodigester.

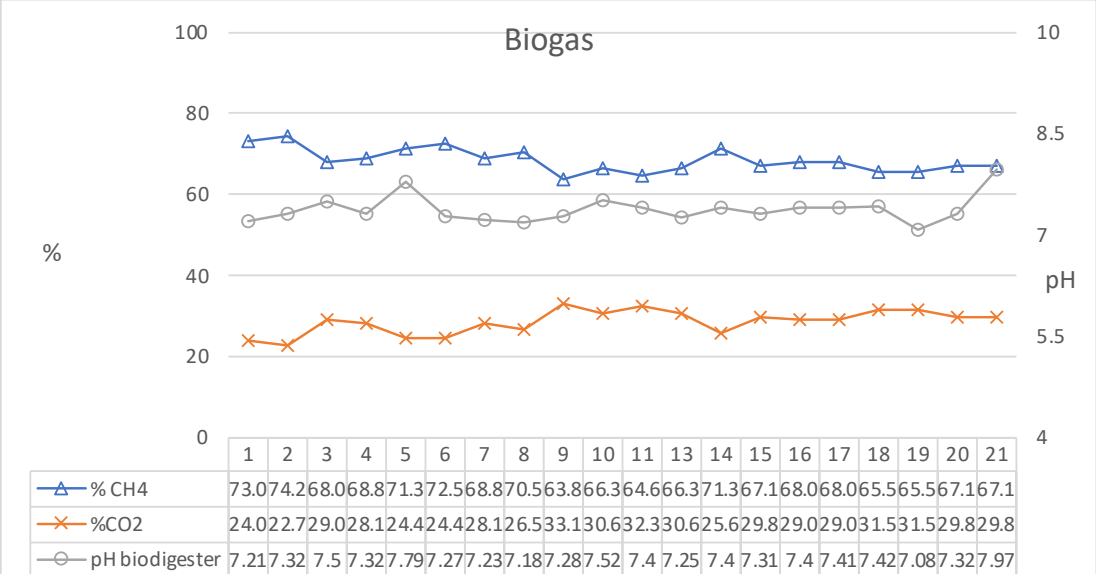

	1	2	3	4	5	6	7	8	9	10	11	13	14	15	16	17	18	19	20	21
% CH4	73.0	74.2	68.0	68.8	71.3	72.5	68.8	70.5	63.8	66.3	64.6	66.3	71.3	67.1	68.0	68.0	65.5	65.5	67.1	67.1
%CO2	24.0	22.7	29.0	28.1	24.4	24.4	28.1	26.5	33.1	30.6	32.3	30.6	25.6	29.8	29.0	29.0	31.5	31.5	29.8	29.8
pH biodigester	7.21	7.32	7.5	7.32	7.79	7.27	7.23	7.18	7.28	7.52	7.4	7.25	7.4	7.31	7.4	7.41	7.42	7.08	7.32	7.97

Figure 4. Amount of methane, carbon dioxide in the biogas and operating pH of the biodigester

To evaluate the potential social impact of biogas adoption, the biogas produced during the study was used for food preparation at the site and the volume of biogas consumed was recorded for each activity (Table2). The results indicate that the daily biogas production is sufficient to meet the cooking energy requirements of approximately 15 people, using common food preparations such as beans, eggs, tortillas, and coffee.

Table 2. Food cooked with biogas and the amount of biofuel used

Food	Amount of biogas needed (m^3)
1 kg beans	2.350
30 eggs, 2.5 kg sausage	0.505
19 L of fish stock (10 kg fish)	2.460
2.5 kg stewed meat 1 kg rice	1.581
5 L of coffee brewed in a pot 2.5 kg of fried tortillas	0.918
5 L of coffee	0.257

Thermal efficiency of the biogas burner

The thermal efficiency of the biogas burner is a key parameter affecting overall energy conversion efficiency. In this study, thermal efficiency decreased with increasing valve opening and unfavorable wind conditions. The maximum thermal efficiency achieved was 35.45% corresponding to a 25% valve opening, while the minimum efficiency was 17.9% at a 100% valve opening, which is similar to the values reported by Zelaya-Benavidez (2023). These results emphasize the need for improved biogas stove designs to enhance energy utilization efficiency, particularly when compared with liquefied petroleum gas (LP) stoves, which can reach thermal efficiencies of up to 53% (Víquez-Arias *et al*., 2018).

Conclusions

The rapid growth of mezcal production in Mexico has been accompanied by significant environmental challenges, particularly related to the inadequate management of organic residues such as vinasse. The results of this study demonstrate that anaerobic digestion is a technically and environmentally viable alternative for the treatment and valorization of mezcal vinasse enabling the simultaneous generation of renewable energy and nutrient-rich effluent with potential applications in soil improvement.

Specifically, the anaerobic treatment of 200 liters per day of mezcal vinasse in a 10 m^3 tubular biodigester operating under psychrophilic-mesophilic conditions produced 15.61 L of biogas per liter of mezcal vinasse, with an average methane content of 68%. The biodigester a 62.16% COD removal efficiency while maintaining stable pH conditions near 7.38. The resulting effluent exhibited a high nutrient content, indicating its potential use as a biofertilizer or soil amendment. Biogas utilization in a conventional burner resulted in a maximum thermal efficiency of 35.45% highlighting both the feasibility of local energy recovery and the opportunity for further improvements in burner design.

Acknowledgments and Funding: To Mezcal Capotlán and its collaborators for all the support and facilities provided to carry out this study.

Author contributions: E. H.-S.: drafted the first version of the manuscript; J. S.-U.: study supervision; D. P.-M.: critical review of the manuscript, contributed to the final draft; E. Z.-B.: data analysis and interpretation.

References

Abdel-Hadi, M. (2008). A simple apparatus for biogas quality determination. *Misr Journal of Agricultural Engineering*, *25*, 1055–1066.

Clean Cooking Alliance. (2014). *The water boiling test version 4.2.3: Cookstove emissions and efficiency in a controlled laboratory setting*. https://cleancooking.org/binary-data/DOCUMENT/file/000/000/399-1.pdf

COMERCAM (Consejo Mexicano Regulador de la Calidad del Mezcal). (2024). *Informe estadístico 2024*. https://comercam-dom.org.mx/wp-content/uploads/2024/04/PUBLICO_INFORME_2024.pdf

Córdova, V., Ibarlucía, D., & Santalla, E. (2022). Desarrollo y validación de un mecanismo para remover CO_2 y cuantificar la producción de CH_4 en sistemas de digestión anaerobia. *RedBioLAC*, *6*(1).

Crespo-González, M. R., González-Eguiarte, D. R., Rodríguez-Macías, R., Corral, J. A. R., & Durán-Puga, N. (2018). Caracterización química y física del bagazo de agave tequilero compostado con biosólidos de vinaza como componente de sustratos para cultivos en contenedor. *Revista Internacional de Contaminación Ambiental*, *34*(3), 373–382. https://doi.org/10.20937/rica.2018.34.03.01

Dinuccio, E., Balsari, P., Gioelli, F., & Menardo, S. (2010). Evaluation of the biogas productivity potential of some Italian agro-industrial biomasses. *Bioresource Technology*, *101*(10), 3780–3783. https://doi.org/10.1016/j.biortech.2009.12.113

Ferrer, I., Garfí, M., Uggetti, E., Ferrer-Martí, L., Calderon, A., & Velo, E. (2011). Biogas production in low-cost household digesters at the Peruvian Andes. *Biomass and Bioenergy*, *35*(5), 1668–1674. https://doi.org/10.1016/j.biombioe.2010.12.036

Ibarra-Camacho, R., Leon-Duharte, L., & Osoria-Leyva, A. (2019). Caracterización fisico-química de vinazas de destilerías. *Revista Cubana de Química*, *31*(2), 246–257. http://scielo.sld.cu/scielo.php?script=sci_arttext&pid=S2224-54212019000200246&lng=es&nrm=iso

Jiménez, A. M., Borja, R., Martín, A., & Raposo, F. (2006). Kinetic analysis of the anaerobic digestion of untreated vinasses and vinasses previously treated with *Penicillium decumbens*. *Journal of Environmental Management*, *80*(4), 303–310. https://doi.org/10.1016/j.jenvman.2005.09.011

Lorenzo-Acosta, Y., Doménech-López, C. F., Eng-Sánchez, C. F., Almeida-Del Olmo, C. O., & Chanfón-Curbelo, J. M. (2015). Tratamiento industrial de vinazas de destilerías en reactores UASB. *Tecnología Química*, *35*(1), 108–123. http://www.redalyc.org/pdf/4455/445543784001.pdf

Nayak, J. K., & Ranade, V. V. (2025). Valorisation of digestate: Characteristics, products, processes and potential. *Chemical Engineering Journal Advances*, *24*, 100887. https://doi.org/10.1016/j.ceja.2025.100887

Parsaee, M., Kiani, M. K., & Karimi, K. (2019). A review of biogas production from sugarcane vinasse. *Biomass and Bioenergy*, *122*, 117–125. https://doi.org/10.1016/j.biombioe.2019.01.034

Rajendran, K., Aslanzadeh, S., & Taherzadeh, M. J. (2012). Household biogas digesters—A review. *Energies*, *5*(8), 2911–2942. https://doi.org/10.3390/en5082911

Rivera, R. C., Solís-Oba, M. M., Gasperin, V. C., & Oba, A. S. (2020). Producción de biogás mediante codigestión de estiércol bovino y residuos de cosecha de tomate (*Solanum lycopersicum* L.). *Revista Internacional de Contaminación Ambiental*. https://doi.org/10.20937/rica.53545

Robles-González, V., Galíndez-Mayer, J., Rinderknecht-Seijas, N., & Poggi-Varaldo, H. M. (2012). Treatment of mezcal vinasses: A review. *Journal of Biotechnology*, *157*(4), 524–546. https://doi.org/10.1016/j.jbiotec.2011.09.006

Silva, A. F., Brasil, Y. L., Koch, K., & Amaral, M. C. (2021). Resource recovery from sugarcane vinasse by anaerobic digestion – A review. *Journal of Environmental Management*, *295*, 113137. https://doi.org/10.1016/j.jenvman.2021.113137

Ullah Khan, I., Hafiz Dzarfan Othman, M., Hashim, H., Matsuura, T., Ismail, A. F., Rezaei-DashtArzhandi, M., & Wan Azelee, I. (2017). Biogas as a renewable energy fuel – A review of biogas upgrading, utilisation and storage. *Energy Conversion and Management*, *150*, 277–294. https://doi.org/10.1016/j.enconman.2017.08.035

Vázquez-Lira, J. C. (2018). *Constantes-de-antonio*. CETA – UNAM. Recuperado el 12 de abril de 2024 de https://ceta.zaragoza.unam.mx/w-content/recursosi/calculadoras/constantes-de-antonio/constantes-de-antonio.htm

Víquez-Arias, J., Caydiid, M., & Omondi, P. A. (2018). Evaluación de la eficiencia térmica en estufas fabricadas y modificadas a biogás. *RedBioLAC*, *2*.

Zelaya-Benavidez, E. A. (2022). *Evaluación de biodigestores para la obtención de biogás y biofertilizante a partir de vinazas de mezcal* [Tesis de doctorado, Instituto Politécnico Nacional].

Zelaya-Benavidez, E. A., Hernández-Teyssier, E. L., & Peredo-Mancilla, D. (2023). Codigestión anaeróbica psicrofílica de desechos de alimentos y heces de perro en un biodigestor casero: Producción de biogás y eficiencia térmica. *RedBioLAC*, *7*, 35–43.

Valorization of pistachio shells as green composite material: an approach that contributes to sustainable development

Natalia Gutiérrez-Aldana [1], Israel Arzate-Vázquez [2,*], Juan Vicente Méndez-Méndez [2], Hugo Martínez-Gutiérrez [2] y José Jorge Chanona-Pérez [3]

[1] Facultad de Estudios Superiores Aragón (FES Aragón), Universidad Nacional Autónoma de México, Ciudad de México, Mexico
[2] Laboratorio de Microscopia de Fuerza Atómica y Nanoindentación, Centro de Nanociencias y Micro y Nanotecnologías, Instituto Politécnico Nacional, Ciudad de México, Mexico
[3] Departamento de Ingeniería Bioquímica, Escuela Nacional de Ciencias Biológicas, Instituto Politécnico Nacional, Ciudad de México, Mexico
* Autor de correspondencia: iarzate@ipn.mx

Received: June 10, 2025 Accepted: July 21, 2025 Published: February 17, 2026
DOI: https://doi.org/10.56845/rebs.v8i1.672

Abstract: The increase in the production of conventional plastics has generated an environmental crisis that is difficult to reverse. In response to this problem, this study proposes the development of a green composite material (GCM) from pistachio shells and a matrix based on potato starch, calcium chloride ($CaCl_2$) and polyvinyl alcohol (PVA). A series of steps were followed to prepare the GCM, including cleaning, drying, milling, sieving, mixing, compression molding and drying. Once the GCM was obtained, a perceptual analysis was performed and its microstructure and hardness were characterized by optical microscopy and Vickers tests, respectively. The granulometric analysis revealed that the milled sample had a high proportion of coarse particles with sizes ranging from 0.71 to 1.70 mm, which accounted for 74.98%. These particles exhibited a slightly elongated complex morphology (circularity = 0.73 ± 0.04 and aspect ratio = 1.27 ± 0.16). The GCM exhibited a compact structure with a low degree of porosity and a visual finish similar to that of wood chipboard. The perceptual analysis carried out with experts and non-experts, showed a good acceptance of the material, highlighting its innovation, stiffness. and sustainability as the most outstanding attributes. In the microstructural analysis, a heterogeneous distribution of the particles was observed, as well as the presence of irregular pores. Finally, Vickers hardness tests showed that the GCM exhibited a hardness value of 33.63 ± 16.49 HV, which is comparable to that of other biocomposite materials. In conclusion, it was possible to produce a GCM from pistachio shell waste with adequate physical characteristics, which represents an attractive and viable sustainable alternative to replace conventional plastics and offers potential multiple applications in various industrial sectors.

Keywords: biocomposite material, pistachio shells, agro-industrial waste, sustainable material

Introduction

Human progress depends on the transformation of natural resources; however, this has led to the use of materials that do not return to natural cycles, causing serious damage to ecosystems. In particular, dependence on petroleum-based materials, such as plastics, has created an environmental crisis that is difficult to reverse. To satisfy growing demand, plastic production has increased significantly in recent decades and is estimated to reach 1.8 billion tons by 2050 (Taib *et al*., 2023). Against this scenario, green composite materials (GCM) have emerged as an innovative and sustainable alternative. These are materials that incorporate a matrix and a filler, at least one of which comes from biological and sustainable sources (Rafiee *et al*., 2021). Their development seeks to improve mechanical properties while reducing environmental impact, positioning them as a viable option compared to conventional materials, particularly petroleum-based plastics. On the other hand, the generation of agro-industrial waste is a global environmental problem, with approximately 140 billion tons per year (Balasundar *et al*., 2019). This waste can be valorized instead of being discarded or incinerated, which would reduce the demand for natural resources. In this context, nut waste (shells) represents an interesting option for the development of green composite materials, with pistachios (*Pistacia vera L.*) being particularly important due to their abundance. Globally, 1,026,802 tons of pistachios are produced annually, of which 35-40% corresponds to shells, equivalent to approximately 389,180 metric tons (McNeill *et al*., 2024).

The pistachio fruit is an almost oval-shaped drupe. It consists of a single seed (kernel), covered by a thin edible layer (testa or skin), enclosed by a hard, smooth, inedible shell (endocarp) (Kashaninejad & Tabil, 2011). Figure 1a shows an image of a pistachio with its main parts. An important aspect of pistachio shells is their chemical composition, which consists of 47.08% cellulose, 26.56% hemicellulose, 13.74% lignin, 7.52% moisture, 0.92% waxes, and 4.18% ash (Balasundar *et al*., 2019). The high cellulose content in pistachio shells is higher than that reported for other nut shells, such as hazelnuts, almonds, and pecans, among others (Queirós *et al*., 2020). This suggests that the mechanical and thermal properties of a composite material made from pistachio shells may be superior to those made from other shells (Arzumanova, 2021). Recent research has identified that pistachio shells are mainly composed of cells called puzzle-shaped polylobular sclereids, which have a three-dimensional (3D) structure, as shown in Figures 1b-c (Huss *et al*.,

2020; Xiao *et al*., 2021). Figure 1b shows an optical microscopy image of pistachio shell tissue, highlighting the very compact arrangement of the sclereids. Similarly, Figure 1c shows a confocal laser scanning microscopy (CLSM) image where the polylobular sclereids with a puzzle-like morphologycan be clearly seen, exhibiting a high topological cross-linking. Additionally, it can be observed that cellulose (green coloration) is abundantly distributed throughout all cells, and that lignin (red coloration) is mainly concentrated in the composite middle lamella. Thanks to these properties, pistachio shells are a viable and attractive alternative for use as a component in the manufacture of GCM**.** Therefore, this study aims to develop a green composite material from pistachio shells and an ecological binder, such as potato starch, in order to create a material suitable for the manufacture of objects that reduce or replace the use of conventional plastics.

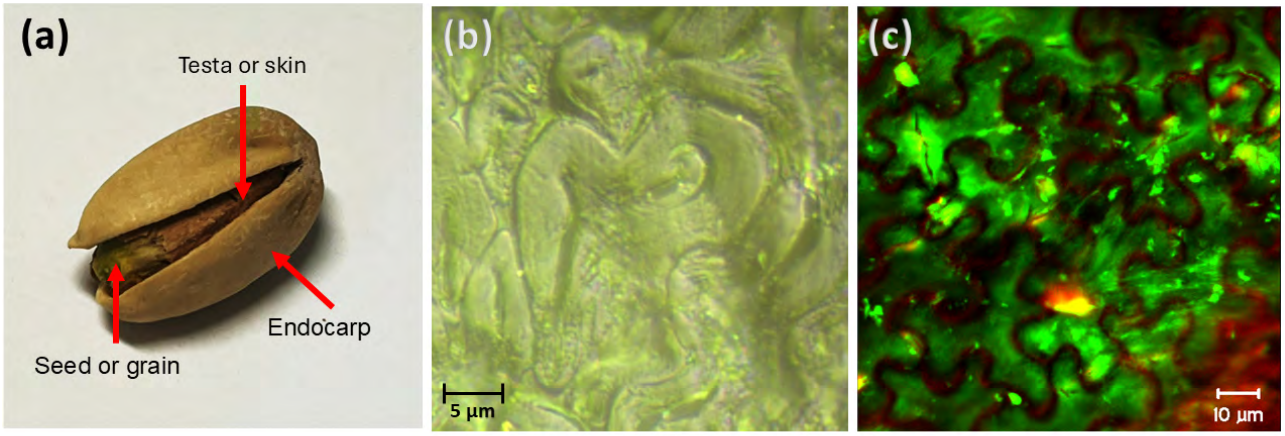

Figure 1. Morphology and microstructure of the pistachio shell: (a) image of a complete pistachio nut showing its main parts, (b) optical microscopy image showing the compact structure of the shell, and (c) MCBL image showing the topological cross-linking of 3D polylobular cells and their chemical composition (green corresponds to cellulose and red to lignin)

Materials and Methods

Raw materials and reagents

Whole pistachios (*Pistacia vera* L.) from the Woonderful brand (USA) were purchased at a supermarket in Mexico City. Potato starch (03967-500G), calcium chloride (C1016-500G), and polyvinyl alcohol (341584-1KG) were supplied by Sigma-Aldrich (USA).

Harvesting, conditioning, and milling of pistachio shells

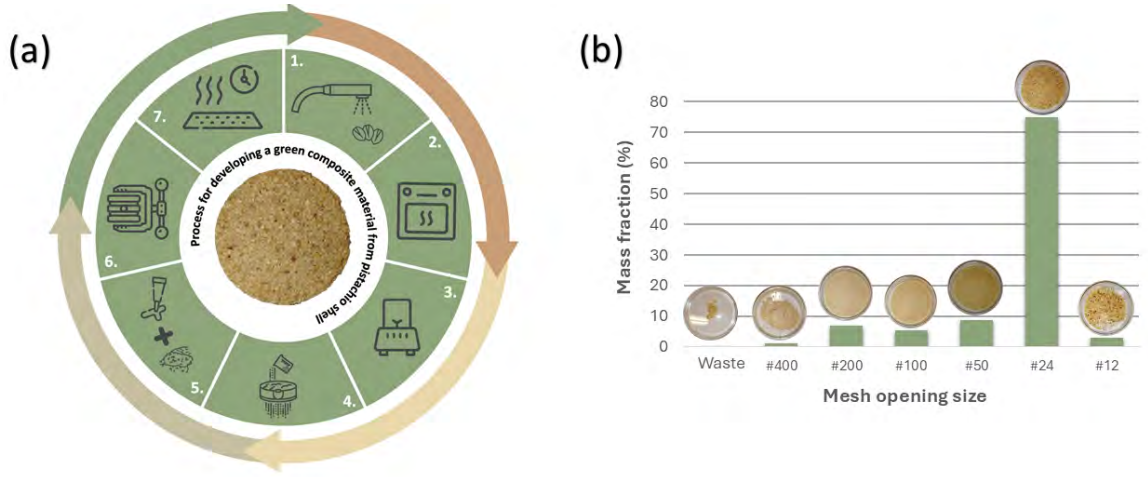

Figure 2. (a) Diagram of the process for producing a GCM from pistachio shells: (1) cleaning, (2) drying, (3) grinding, (4) sieving, (5) mixing, (6) compression molding, and (7) demolding and drying. (b) Histogram of the particle size distribution of the pistachio shell sample milled for 2 minutes

Figure 2a shows a general diagram of the steps carried out to elaborate the GCM. First, the whole fruits were shelled manually to separate the shells from the seeds. The pistachio shells were washed with tap water and dried in an oven at 40°C for 12 hours. They were then milled in a blade mill (GC-300, CGOLDENWALL, China) operating at a rotational speed of 28,000 rpm for a period of 2 minutes.

Particle size analysis

The particle size distribution of the milled pistachio shell sample was analyzed using a series of 8-inch diameter stainless steel sieves with different mesh sizes: #12, #24, #50, #100, #200, and #400 (WS Tyler, USA). The sample was shaken for 20 minutes in a vibrating sieve shaker. Subsequently, the fraction of retained mass (%) was calculated for each sieve, and a particle size distribution (PSD) histogram was generated. The average particle size (D_{mean}) and standard deviation (σ) were determined using Equations 1 and 2, respectively, where n_i and D_i correspond to the percentage of retained mass (%) and the average particle size retained in the sieve (µm), in that order.

$$D_{mean} = \frac{\sum n_i \, D_i}{\sum n_i} \quad \textbf{(1)}$$

$$\sigma = \left(\frac{\sum n_i (D_i - D_{mean})^2}{\sum n_i} \right)^{1/2} \quad \textbf{(2)}$$

Morphological analysis

The morphology of the particles in the most abundant mass fraction (sieve #24) was analyzed using image analysis techniques. Digital images of the particles were captured using an optical microscope (BX51, Olympus, Japan) with a magnification of 5x. The images were then processed with ImageJ v. 1.45s software (https://ij.imjoy.io/) to determine some morphological parameters such as circularity, Feret diameter, and aspect ratio (AR), following the methodology proposed by Nicolás-Bermúdez *et al*. (2018). The parameter values were expressed as mean ± standard deviation.

Preparation of the matrix (binder)

After several experimental trials, the optimal proportions of the polymer matrix were determined: 20% (w/w) potato starch, 16.5% (w/w) calcium chloride ($CaCl_2$), and 2% (w/w) polyvinyl alcohol. Initially, the calcium chloride was dissolved in water using a magnetic stirrer for 2 minutes. Subsequently, the potato starch and PVA were added, and the solution was heated to 75°C for 50 minutes under constant stirring until the starch gelatinization was achieved.

Elaboration of the GCM (mixing, pressing, and drying)

To elaborate the composite material, the milled sample of the shells was added to the binder in a ratio of 60% (w) shells / 40% (w) polymer matrix. The components were mixed manually until all the pistachio particles were incorporated into the matrix, forming a homogeneous mass. The resulting mass was poured into molds of different geometries: a 5 cm diameter cylinder, a silicone unicorn mold, and a 12 x 12 cm^2 rectangular mold with abstract shapes printed in 3D. The counterpart of each mold was placed in position, and the samples were compacted with a manual press for 15 minutes. Finally, the counterpart was removed, and the samples were demolded and dried at room temperature for approximately 36 hours.

Physical characterization of GCM

Perceptual analysis

Once the GCM was obtained, a comprehensive description of the composite material was made in order to analyze its general appearance, homogeneity, and possible surface irregularities. To evaluate its potential application, a perceptual analysis was carried out with a sample of 30 people: 15 with experience in materials and 15 without experience in the area. The material was presented to the panelists in different shapes (cylinder, unicorn, and

rectangular panel). Participants rated various attributes on a scale from -3 to 3, where 3 represents the most desirable characteristic and -3 the least desirable.

Microstructural analysis of the GCM

The microstructure of the GCM was analyzed using optical microscopy and confocal laser scanning microscopy (CLSM). Cylindrical samples were used for both analyses. Several images at different magnifications were taken of different areas of the sample surface using an optical microscope (BX51, Olympus, Japan). The samples were also examined using a CLSM (LSM 710 NLO, Carl Zeiss, Germany), where the samples were excited with a 488 nm wavelength laser for lignin detection (detection range: 470-630 nm). Images at different magnifications were captured on the coarse particles and in the polymer matrix.

Vickers hardness test (HV)

Finally, the mechanical strength of the material was evaluated using the Vickers hardness test. The test was performed by applying a load of 1 kgf to the surface of the GCM (cylindrical samples) with a controlled descent of 0.1 kgf over 30 seconds. A total of 30 measurements were taken at different areas of the samples. After the tests were performed, the diagonals of the indentation marks were measured with an optical microscope, and the Vickers hardness HV was calculated using Equation 3.

$$HV = 1.854\ x\ \frac{F}{(d)^2} \quad \textbf{(3)}$$

Where HV is the Vickers hardness, F is the applied force (kgf), d is the average diagonal of the indentation mark (mm), and 1.854 is a conversion factor based on the geometry of the indenter. Hardness values were expressed as average ± standard deviation.

Results and Discussion

Particle size analysis of the milled pistachio shell sample

Milling is an important pretreatment stage in the GCM manufacturing process. The main objective of milling is to reduce the initial size of the shells so that the particles can be properly mixed with the polymer matrix (binder). Figure 2b shows a histogram of the PSD of pistachio shells, which were milled with a blade mill for 2 minutes. As can be observed in the figure, most of the particles were retained in the 24-mesh sieve (74.98%), which corresponds to particle sizes of 0.71 to 1.7 mm. It was also observed that fine particles (≤ 710 µm) with a wide size dispersion were generated, which exhibited mass fraction values of less than 10%. The D_{mean} and σ values were 1038.75 µm and 462.94 µm, respectively. The high σ value is associated with the wide dispersion of fine particle sizes generated during milling. This fragmentation behavior, where mostly coarse particles are generated, has also been observed in pecan, almond, and pine nut shells (Queirós *et al*., 2020). In particular, the mass fraction retained in sieve 24 reported in our study was significantly higher compared to the mass fraction retained (particle sizes of 1-2 mm) in pecan (36.5%), almond (42.4%), and pine nut (37.4%) shells. These results reveal that it is more difficult to reduce the initial size of pistachio shells due to their good mechanical properties. However, the fragmentation behavior of any material depends on multiple factors such as the type of mill used, operating conditions (e.g., grinding time), moisture and chemical composition of the material, microstructure of the material, etc. Likewise, the particle size of a milled sample of agro-industrial waste is a very important factor because it can strongly influence the process of manufacturing a GCM and its functional properties. In a study conducted by Nunes *et al*. (2024), the authors demonstrated that the properties of a rice-based biocomposite vary according to the particle size used, highlighting the importance of this variable in the development of sustainable materials.

Morphological analysis of particles retained in sieve 24

The morphology of the most abundant particles retained in sieve 24 was analyzed using image analysis techniques. The results showed that these particles exhibit complex morphologies with circularity and aspect ratio (AR) values of 0.73

± 0.04 and 1.27 ± 0.16, respectively. Circularity is a parameter that measures the similarity of a particle to a circle, where a particle with a value of 1 has a perfect circle shape. Therefore, the pistachio particles analyzed do not approximate circular shapes. Conversely, the AR parameter is a measure of the degree of elongation of a particle. Based on the AR value obtained, the pistachio particles have slightly elongated shapes. Likewise, the Feret diameter value was 1146.66 ± 127.42 µm, which is very similar to the D_{mean} value (1038.75 µm). In addition to particle size, particle shape is another key factor that can influence the manufacturing process and mechanical properties of GCM. Specifically, the interaction between the polymer matrix and the particles, which is influenced by the size and shape of the particles, may exhibit regions or anchor points where there is greater affinity between the two elements. Both variables can also influence the compaction stage of the GCM and, consequently, its functional properties. The AR and the level of order (orientation) of the particles (fillers) in a composite material can drastically influence the properties and control the transfer of stresses throughout the material. Mariano *et al*. (2017) reported that composite materials that have fillers with high AR values and exhibit a high level of organization display excellent mechanical properties (e.g., high elastic modulus values).

Macroscopic evaluation of the GCM

Figure 3 shows images from different perspectives of a tablet of the GCM produced in this study. The macroscopic evaluation of the GCM made from pistachio shells was based on the expressive-sensory scale proposed by Sauerwein *et al*. (2017), which considers key tactile and visual attributes to describe the material experience. According to this scale, the GCM can be characterized as a matte-finish material with gradual coloring and a light beige tone (Figure 3). To the touch, it has a predominantly rough, dry, and hard texture with a slightly irregular surface, reflecting the nature of the reinforcement (pistachio shells) used. In terms of perceived temperature, the material was classified as neutral to slightly cold, which coincides with its low porosity and compact structure. No moisture was detected, so it was also considered non-sticky and non-damp. In addition, the surface showed no deformation or displacement when handled, so it was perceived as non-flexible. The material also showed excellent cohesion between its components and no shell particles detached when handled. Finally, the material is perceived as lightweight.

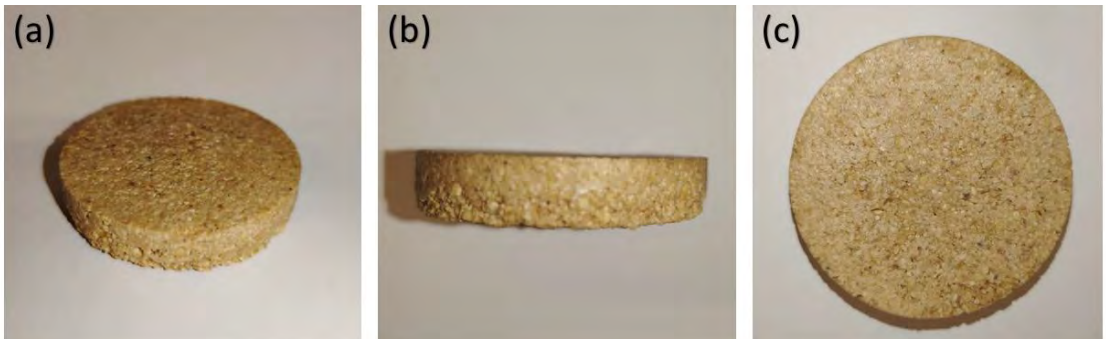

Figure 3. Images of a GCM tablet made from pistachio shell waste: (a) isometric perspective, (b) side view, and (c) top view

Perceptual analysis of GCM based on pistachio shells

The results of the perceptual analysis are displayed in Figure 4, which demonstrates that the material was perceived as natural, organic, and innovative. At the same time, it was considered opaque, rough, complex, and expensive. Among the main comments made by the participants, the following were highlighted: its lightness, resistance, and appearance similar to marble or MDF (chipboard). This type of response coincides with the materials classified within group 4 (Bimodal) of the study conducted by Thundathil *et al*. (2023), which stand out for evoking both visual and tactile sensations. However, the material was also perceived as coarse or rough, suggesting an affinity with the materials in group 3 (Dominantly Tactile, Rough/Natural), characterized by pronounced textures and a less refined appearance. Although this work does not formally address the machinability of GCM, it has been found that when the material is subjected to sanding processes, its surface roughness decreases. In this condition, the material could be associated with group 1 (Tactile dominant, smooth/textile), which includes materials perceived as smooth. In addition to these attributes, the perception of the material's complexity was reflected in a value of -1 on the bipolar scale between simple and complex, indicating a tendency toward complexity. According to Thundathil *et al*. (2022), complexity correlates positively with attributes such as interesting and unusual and negatively with boring, ordinary, and smooth. It has been

documented that greater complexity favors the perception of novelty, so this assessment may contribute positively to the acceptance of the material. On the other hand, GCM was also perceived as moderately expensive, with a score of 0.5. This assessment may be related to the general public's perception of sustainable materials. As Carus *et al*. (2014) point out, biopolymer-based products can cost up to three times more than conventional plastics due to factors such as economies of scale and technical limitations for mass production. Although this perception of higher cost is not always based on technical knowledge of the process, participants are likely to associate the natural aesthetics and novelty of the material with a more exclusive or limited-edition product, which may influence their judgment of economic value (Manu *et al*., 2022).

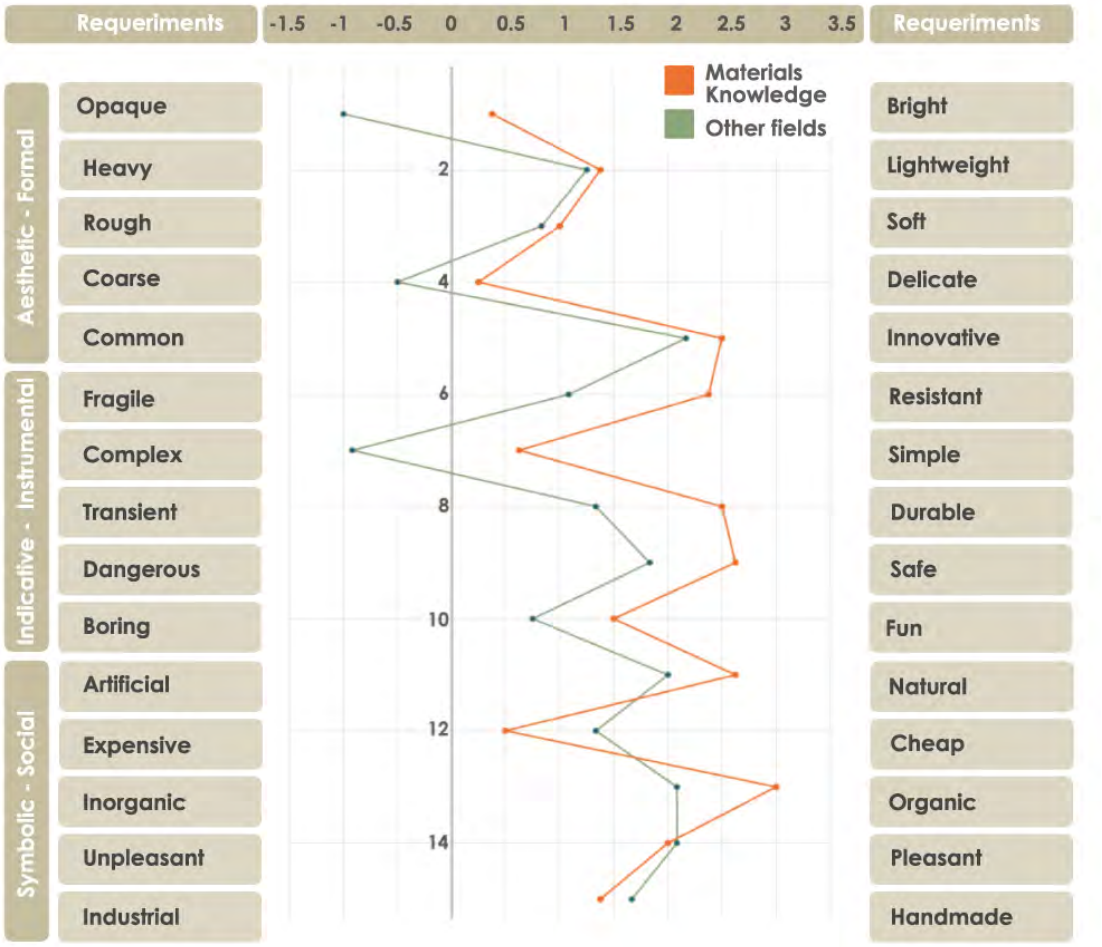

Figure 4. Results of perceptual analysis performed on the GCM, where different attributes were evaluated

Microstructural analysis

The surface microstructure of the GCM was analyzed using optical microscopy and CLSM (Figure 5). Both techniques revealed that the material consists of coarse particles (sieve 24), binder with fine particles, and interfacial regions between the particles and the binder (Figure 5 a-b). CLSM clearly showed the fine particles distributed over the binder (Figure 5b). The analyses also revealed the presence of some irregularly shaped pores smaller than 1 mm (Figure 5c). These pores were randomly distributed over the surface of the material. The presence of pores could be associated with the poor distribution of the polymer matrix over the particles and the compaction stage. This coincides with observations made in composites with a high walnut shell filler content (20% w/w), where rough surfaces, voids, and cracks have been reported due to heterogeneous distribution of the reinforcement (filler) (Lala *et al*., 2018). These irregularities may also influence the biodegradability of the material, as it has been observed that fibers larger than 500 µm generate rougher surfaces, which favors water absorption and microbial attack, accelerating the degradation of the material (Nunes *et al*., 2024).

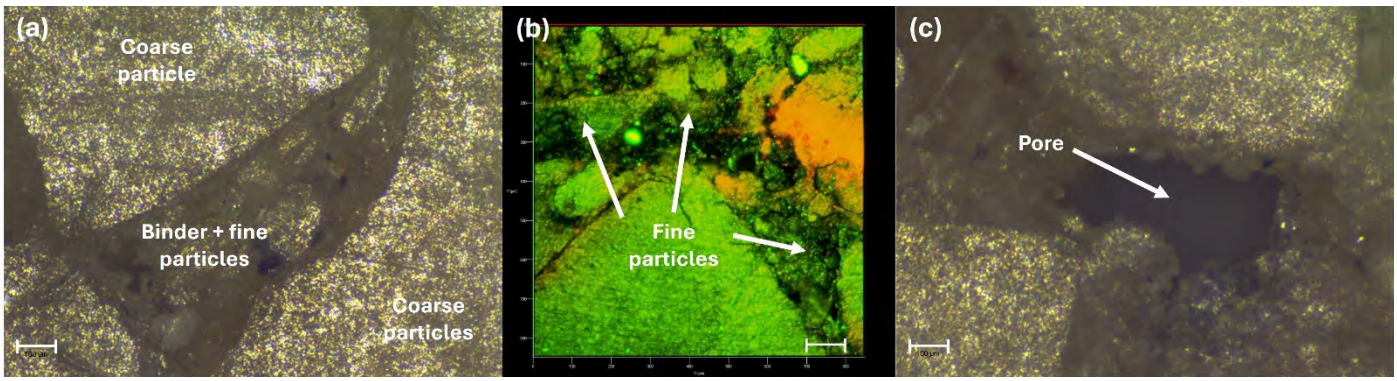

Figure 5. Images of the surface microstructure of GCM obtained using optical microscopy (a and c) and CLSM (b). For the MCBL images, the autofluorescence of the lignin present in the pistachio shell particles was used. For all images, the scale bar represents 100 µm

Vickers hardness test (HV)

The GCM obtained from pistachio shells had an average Vickers hardness value of 33.63 ± 16.49 HV. The standard deviation showed a high value, which can be attributed to the heterogeneity of the sample, which, as mentioned above, has different phases: coarse particles, binder plus fine particles, and interphase (particle-binder). In a recently published study, Yu *et al*. (2025) developed materials reinforced with bamboo and copper. The authors mechanically characterized their material and reported that oven-dried material had higher hardness (38.4 HV) compared to air-dried material (29.1 HV). This is attributed to the removal of moisture, which negatively affects the formation of the material. These results are very similar to those reported for our pistachio shell-based material.

Conclusions

Using the methodology proposed in this study, a green composite material was successfully developed from pistachio shell waste and a binder based on potato starch, calcium chloride, and PVA. The GCM exhibited good cohesion between its components and a compact, homogeneous structure. In general, the material was well received by participants in the perceptual analysis, who highlighted its innovation and perceived mechanical robustness. Microstructural analysis showed that the material consists of different phases: coarse particles, binder with fine particles, and interfacial regions (pistachio particles/binder). Mechanical testing revealed that the GCM has a Vickers hardness value comparable to that of other composite materials. In addition, possible applications of the material were explored through the design and manufacture of ornamental and functional prototypes. Figure 6 shows two representative examples: (a) a piece with a decorative unicorn design and (b) a panel with abstract shapes. The results obtained in this study suggest that this GCM represents a sustainable and viable alternative for the development of products that reduce the use of conventional plastics, while promoting the valorization of agro-industrial waste such as pistachio shells.

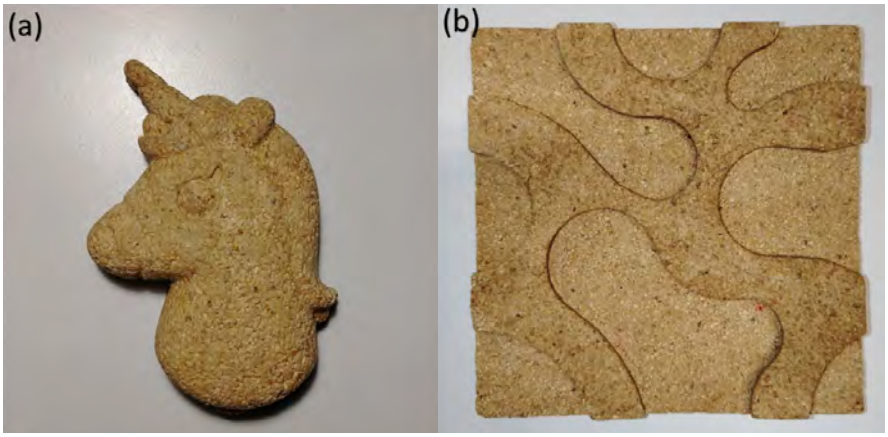

Figure 6. Examples of applications of GCM based on pistachio shells: (a) a piece with an ornamental design in the shape of a unicorn and (b) a panel with abstract shapes inspired by the cellular structure of pistachio shells

Acknowledgments and funding: Authors would like to thank the Center for Nanoscience and Micro and Nanotechnology at the IPN for providing the resources and infrastructure necessary for this research. This work was carried out with financial support from the National Polytechnic Institute-Mexico (Project Nos. 20240509, 20251050, 20251011, 20251166).

Author Contributions N.G.-A.: conceptualization, writing, analysis and interpretation of data, design and editing; I.A.-V.: conceptualization, writing, analysis and interpretation of data, editing, supervision, project administration and funding acquisition; J.V.M.-M.: materials provision, data collection, writing, analysis and interpretation of data; H.M.-G.: writing, analysis and interpretation of data; J.J.C.-P.: writing, analysis and interpretation of data.

References

Arzumanova, N. B. (2021). Polymer biocomposites based on agro waste: Part III. Shells of various nuts as natural filler for polymer composites. *New Materials, Compounds and Applications*, *5*(1), 19–44.

Balasundar, P., Narayanasamy, P., Senthil, S., Al-Dhabi, N. A., Prithivirajan, R., Kumar, R. S., Ramkumar, T., & Bhat, K. S. (2019). Physico-chemical study of pistachio (*Pistacia vera*) nutshell particles as a bio-filler for eco-friendly composites. *Materials Research Express*, *6*(10), 105339. https://doi.org/10.1088/2053-1591/ab3b9b

Carus, M., Eder, A., & Beckmann, J. (2014). GreenPremium prices along the value chain of biobased products. *Industrial Biotechnology*, *10*(2), 83–88. https://doi.org/10.1089/ind.2014.1512

Huss, J. C., Antreich, S. J., Bachmayr, J., Xiao, N., Eder, M., Konnerth, J., & Gierlinger, N. (2020). Topological interlocking and geometric stiffening as complementary strategies for strong plant shells. *Advanced Materials*, *32*(48), 2004519. https://doi.org/10.1002/adma.202004519

Kashaninejad, M., & Tabil, L. G. (2011). Pistachio (*Pistacia vera* L.). En E. M. Yahia (Ed.), *Postharvest biology and technology of tropical and subtropical fruits* (pp. 218–247e). Woodhead Publishing. https://doi.org/10.1533/9780857092618.218

Lala, S. D., Deoghare, A. B., & Chatterjee, S. (2018). Mechanical and morphological characterization of walnut shell reinforced epoxy composite. *IOP Conference Series: Materials Science and Engineering*, *377*(1), 012011. https://doi.org/10.1088/1757-899X/377/1/012011

Manu, T., Nazmi, A. R., Shahri, B., Emerson, N., & Huber, T. (2022). Biocomposites: A review of materials and perception. *Materials Today Communications*, *31*, 103308. https://doi.org/10.1016/j.mtcomm.2022.103308

Mariano, M., Zornio, C. F., Fakhouri, F. M., & Martelli, S. M. (2017). Influence of natural fillers size and shape into mechanical and barrier properties of biocomposites. En V. K. Thakur, M. K. Thakur, & M. R. Kessler (Eds.), *Handbook of composites from renewable materials* (1ª ed., pp. 459–487). Wiley. https://doi.org/10.1002/9781119441632.ch56

McNeill, D. C., Pal, A. K., Nath, D., Rodriguez-Uribe, A., Mohanty, A. K., Pilla, S., Gregori, S., Dick, P., & Misra, M. (2024). Upcycling of ligno-cellulosic nutshells waste biomass in biodegradable plastic-based biocomposites uses—A comprehensive review. *Composites Part C: Open Access*, *14*, 100478. https://doi.org/10.1016/j.jcomc.2024.100478

Nicolás-Bermúdez, J., Arzate-Vázquez, I., Chanona-Pérez, J. J., Méndez-Méndez, J. V., Rodríguez-Castro, G. A., & Martínez-Gutiérrez, H. (2018). Morphological and micromechanical characterization of calcium oxalate (CaOx) crystals embedded in the pecan nutshell (*Carya illinoinensis*). *Plant Physiology and Biochemistry*, *132*, 566–570. https://doi.org/10.1016/j.plaphy.2018.10.008

Nunes, F. M., Moraes, J. A. R., Machado, Ê. L., Lutterbeck, C. A., Rizzetti, T. M., & Santana, R. M. C. (2024). Rice-based biocomposites: The influence of the rice husk granulometry on physical and biodegradation properties of rice bran matrix biocomposites. *Journal of Material Cycles and Waste Management*, *26*(5), 2935–2946. https://doi.org/10.1007/s10163-024-02009-2

Queirós, C. S. G. P., Cardoso, S., Lourenço, A., Ferreira, J., Miranda, I., Lourenço, M. J. V., & Pereira, H. (2020). Characterization of walnut, almond, and pine nut shells regarding chemical composition and extract composition. *Biomass Conversion and Biorefinery*, *10*(1), 175–188. https://doi.org/10.1007/s13399-019-00424-2

Rafiee, K., Schritt, H., Pleissner, D., Kaur, G., & Brar, S. K. (2021). Biodegradable green composites: It's never too late to mend. *Current Opinion in Green and Sustainable Chemistry*, *30*, 100482. https://doi.org/10.1016/j.cogsc.2021.100482

Sauerwein, M., Karana, E., & Rognoli, V. (2017). Revived beauty: Research into aesthetic appreciation of materials to valorise materials from waste. *Sustainability*, *9*(4), 529. https://doi.org/10.3390/su9040529

Taib, N.-A. A. B., Rahman, M. R., Huda, D., Kuok, K. K., Hamdan, S., Bakri, M. K. B., Julaihi, M. R. M. B., & Khan, A. (2023). A review on poly lactic acid (PLA) as a biodegradable polymer. *Polymer Bulletin*, *80*(2), 1179–1213. https://doi.org/10.1007/s00289-022-04160-y

Thundathil, M., Nazmi, A. R., Shahri, B., Emerson, N., Müssig, J., & Huber, T. (2023). Visual–tactile perception of biobased composites. *Materials*, *16*(5), 1844. https://doi.org/10.3390/ma16051844

Xiao, N., Felhofer, M., Antreich, S. J., Huss, J. C., Mayer, K., Singh, A., Bock, P., & Gierlinger, N. (2021). Twist and lock: Nutshell structures for high strength and energy absorption. *Royal Society Open Science*, *8*(8), 210399. https://doi.org/10.1098/rsos.210399

Yu, Z., Wu, Y., Mou, Q., Li, X., Li, T., Cai, Z., He, L., & Li, X. (2025). Green and sustainable metal-reinforced bamboo composites with high self-bonding performances. *Industrial Crops and Products*, *223*, 120053. https://doi.org/10.1016/j.indcrop.2024.120053

Full-scale ornamental constructed wetlands for caffeine removal from rural wastewater and coffee-processing effluents

Brenda Lizeth Monzón-Reyes [1], María Cristina López Méndez [2], Ismael Vera-Puerto [3], Mayerlin Sandoval-Herazo [1,4,5] and Luis Carlos Sandoval Herazo [1,4,*]

[1] Wetlands and Environmental Sustainability Laboratory, Division of Graduate Studies and Research, Tecnológico Nacional de México/Instituto Tecnológico Superior de Misantla, Km 1.8 Carretera a Loma Del Cojolite, Misantla 93821, Veracruz, México
[2] Division of Postgraduate Studies and Research, Tecnológico Nacional de México/Instituto Tecnológico Superior de Misantla, Misantla, Veracruz, 93821, México
[3] Centro de Innovación en Ingeniería Aplicada (CIIA), Departamento de Obras Civiles, Facultad de Ciencias de la Ingeniería, Universidad Católica del Maule, Av. San Miguel 3605, Talca, Chile
[4] Facultad de Ingeniería, Universidad de Sucre, Sincelejo 700001, Colombia
[5] Instituto Tecnológico de Úrsulo Galván, Tecnológico Nacional de México, Carretera Cd Cardel-Chachalacas km 4.5, Úrsulo Galván 91667, Veracruz, México
* Corresponding author: lcsandovalh@gmail.com

Received: August 30, 2025 Accepted: October 7, 2025 Published: February 19, 2026
DOI: https://doi.org/10.56845/rebs.v8i1.668

Abstract: The coffee agroindustry is one of the main economic activities in rural communities of developing countries. However, its processing generates wastewater with high organic loads and emerging contaminants such as caffeine. In the absence of proper sanitation infrastructure, these discharges are often combined with municipal wastewater, increasing the risk of water pollution and threatening both environmental and community health. In this context, sustainable and low cost treatment alternatives are requerid to mitigate these impacts, particularly in rural settings. This study evaluated the performance of a full-scale hybrid system consisting of a settler tank followed by constructed wetland cells (SF-CW and SSF-CW) planted with ornamental species (*Eichhornia crassipes, Alocasia odora, Hedychium coronarium, Heliconia psittacorum* and *Zantedeschia aethiopica*). Monitoring was carried out from February to July 2024, including caffeine analysis by UV-Vis spectrophotometry during both the coffee harvesting and processing season and periods when only rural domestic wastewater was treated. The system achieved an average caffeine removal efficiency of over 99% during the coffee processing season. The ornamental plants adapted well to the operational conditions, showing high resilience and stable growth, as well as potential ornamental and commercial value. This work provides full-scale operational evidence of the potential of ornamental constructed wetlands as a practical and replicable solution for treating rural wastewater mixed with coffee-processing effluents, while simultaneously delivering environmental protection, social benefits, and local economic opportunities for rural communities.

Keywords: caffeine, coffee processing, rural economy, sustainable treatments, constructed wetlands

Introduction

Rural communities rely heavily on local agro-industries, which serve not only as sources of employment and income but also as essential pillars of their cultural and social identity. These activities also have the potential to invigorate rural economies, create meaningful job opportunities, and help curb migration to urban areas (Mazloum Yar, 2024).

Among these agro-industries, coffee cultivation and processing stand out for their economic and social relevance across many tropical countries in Latin America, Asia, and Africa, while also contributing to biodiversity conservation and sustainable development (Utrilla-Catalan *et al*., 2022). In Latin America, coffee production, harvesting, processing, and retail activities contribute between 0.3% and 3.7% of national gross domestic product. In Mexico, as of 2017, 48% of all coffee producers were classified as smallholders. Nearly half of the country's coffee production takes place on small plots (Harvey *et al*., 2021), and globally, farmers with less than 5 ha supply about 60% of the world's coffee market (Siles *et al*., 2022).

This agricultural activity, while sustaining thousands of families, requires intensive water use and produces large volumes of wastewater with high organic loads, which are often discharged without adequate treatment (Alemayehu *et al*., 2020; Campos *et al*., 2021). In rural communities, this wastewater commonly mixes with municipal effluents, increasing the complexity of its management and heightening the risk of pollution in nearby rivers, streams, and soils (Dadi *et al*., 2018). Coffee-processing wastewater (CPWW) may contain high concentrations of organic matter, nutrients, and elevated acidity (Amare *et al*., 2023). Previous research has largely focused on conventional water quality

parameters (BOD, COD, TDS, pH, TN, among others), often neglecting emerging contaminants present in coffee-processing wastewater, such as caffeine.

Caffeine is an alkaloid widely consumed and valued for its stimulating effects on humans. It is present in a broad range of everyday foods and products, including coffee, tea, chocolate, soft drinks, energy beverages, and pharmaceutical formulations (Quadra *et al*., 2020). Daily caffeine intake per person is estimated to range from 400 to 800 mg (Ebrahimzadeh *et al*., 2021).

The presence of caffeine in water bodies is directly associated with human-derived pollution and is considered an emerging risk in aquatic systems. Studies have shown that caffeine can alter the physiology of aquatic organisms and affect the reproduction and growth of fish and plants, owing to its ability to easily cross biological membranes and accumulate within cells and tissues (de Cravalho *et al*., 2024). Evidence also shows that, in several vertebrates, caffeine can inhibit phosphodiesterases, modulate adenosine receptors, and induce oxidative stress mechanisms that help explain its effects on aquatic species (Rodrigues *et al*., 2025). Furthermore, caffeine can persist in aquatic environments for periods ranging fromseveral months to multiple years, and it shows high stability under various environmental conditions, including changes in salinity, temperature, and light (Rodrigues *et al*., 2025).

Caffeine has been detected in municipal and rural wastewater at concentrations ranging from 22.29 to 64 µg/L (de Oliveira *et al*., 2019; Vymazal *et al*., 2017), while values between 13.6 and 388 mg/L have been reported in wastewater from coffee processing (Figueroa Campos *et al*., 2020). These differences demonstrate the wide range of caffeine concentrations that can occur in wastewater, reflecting both the diversity of consumption patterns and the types of activities carried out within communities. Moreover, caffeine has been identified as a persistent compound in the environment, further increasing its environmental relevance (Korekar *et al*., 2020). This variability represents a significant environmental challenge, particularly in rural settings where the lack of adequate sanitation infrastructure allows these compounds to reach surface and groundwater bodies directly.

The inadequate management of these combined discharges compromises not only environmental health but also the well-being of rural communities that depend on water for drinking, irrigation, and productive activities (Liang & Yue, 2021). Consequently, there is a pressing need to implement sustainable, accessible, and low-cost alternatives that align with the real conditions of these localities while generating sufficient scientific evidence to allow their replication in areas with similar characteristics.

One promising solution is the use of constructed wetlands systems that mimic the functioning of natural wetlands through the interaction of plants, microorganisms, and substrates (Mihret *et al*., 2024). Their treatment efficiency relies on a combination of physical, chemical, and biological processes that act synergistically (Brix, 2020). Among the key physicochemical mechanisms are contaminant adsorption onto substrates and organic matter, as well as the filtration and sedimentation of suspended particles (Vispo *et al*., 2023). Biologically, plants play a central role by absorbing and accumulating contaminants in their tissues, releasing oxygen into the rhizosphere, and stimulating the microbial activity associated with their root systems, thereby enhancing both aerobic and anaerobic biodegradation processes (Sandoval *et al*., 2019). These removal mechanisms can eliminate emerging organic contaminants such as caffeine (Ilyas & van Hullebusch, 2019).

Constructed wetlands provide multiple benefits: they diversify rural economies by incorporating commercially valuable ornamental plants, enhance the visual quality of community spaces, promote biodiversity, and foster social engagement in water management and stewardship (Monzón-Reyes *et al*., 2025; Zitácuaro-Contreras *et al*., 2021). However, most studies to date have been conducted at the laboratory scale, and only a small proportion involve full-scale systems (C. Chen *et al*., 2022; Nocetti *et al*., 2024; Sandoval Herazo *et al*., 2023). This limitation hinders the broader implementation of real-scale wetland technologies implemented under actual operating conditions.

In this context, the objective of this study is to evaluate caffeine removal from rural and coffee-processing wastewater using full-scale ornamental constructed wetlands, highlighting their role as an innovative and sustainable strategy to address both environmental and social challenges faced by rural communities.

Materials and Methods

Study site

This study was conducted in the rural community of Salvador Díaz Mirón, located in the municipality of Misantla, Veracruz, Mexico, located at coordinates 19°47'20" N and 96°52'20" W (Figure 1). Data were collected from February to July 2024. Due to its mountainous location at 917 m above sea level. Community is primarily dedicated to agricultural activities such as coffee cultivation and livestock production (Rodríguez-Macedo *et al*., 2014). The climate is classified as temperate tropical, semi-warm, and humid, with an average annual temperature of 20.1 °C and annual precipitation of 1,900 mm (INEGI, 2024).

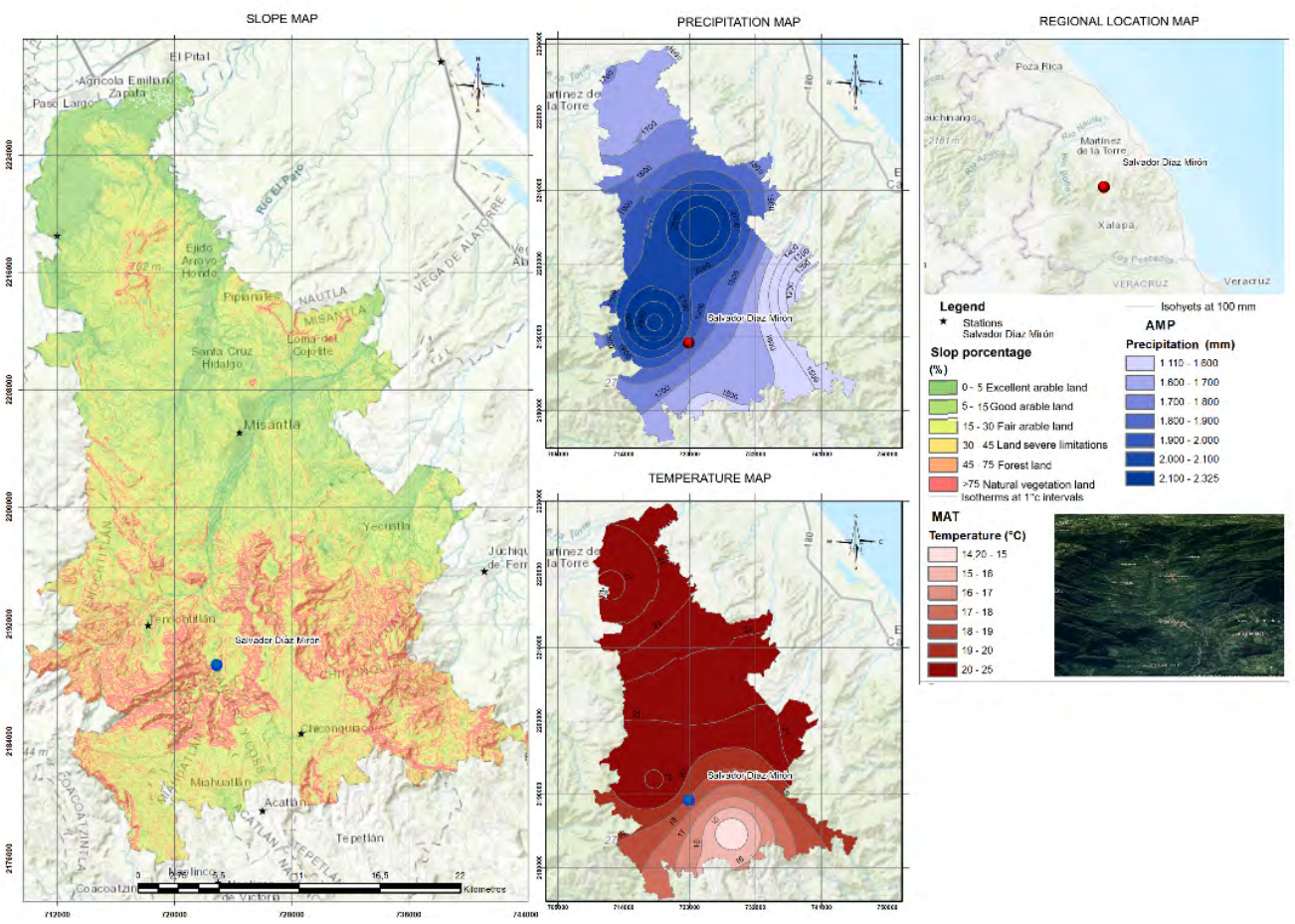

Figure 1. Location map of Salvador Díaz Mirón, Misantla, Veracruz, México

Experimental desing

The full-scale treatment system was constructed in 2022 with funding from the "Proyectos para el Fomento Ambiental 2022" program issued by the Secretaría de Medio Ambiente del Estado (SEDEMA). The system consists of a sedimentation tank followed by a hybrid constructed wetland: one free-surface flow cell (SF-CW) and three subsurface flow cells (SSF-CWs), as shown in Figure 2. The cells were filled with red volcanic gravel with a particle size of 3–5 cm, with coarser material placed at the bottom to reduce clogging risk. The system operated continuously with a hydraulic retention time (HRT) of 4 days. Ornamental plants were arranged in monoculture and polyculture, including the following species: *Eichhornia crassipes* (SSF-CW), *Alocasia odora* + *Hedychium coronarium* (SSF-CW), *Heliconia psittacorum* (SSF-CW), and *Zantedeschia aethiopica* (SSF-CW). Plants in the SSF-CW cells were planted at a density of 4 units/m² (Calheiros *et al*., 2015), except for *Eichhornia crassipes*, which was established at a density of 40 units/m². Six sampling points were selected within the system (Figure 2), in addition to the direct discharge from coffee-processing activities.

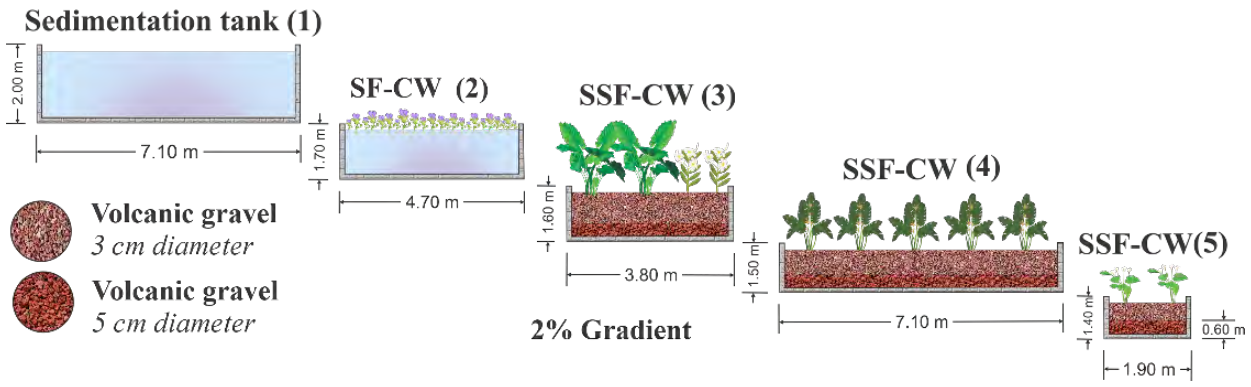

Figure 2. Layout of the constructed wetland cells (Monzón-Reyes *et al*., 2026)

Data collection and analysis

Caffeine was analyzed monthly during the coffee-processing season (February–April 2024), as well as during the three subsequent months (May–July 2024). Samples were collected every 15 days,at three different times of the day. Caffeine quantification was performed using UV–Vis spectrophotometry with a Genesys 10S Vis instrument, previously calibrated with the C0750 caffeine standard (Sigma-Aldrich). The methodology adopted was taken from García Martínez *et al*. (2018).

Removal efficiency was determined using the equation 1 (M. Sandoval-Herazo *et al*., 2021):

$$Removal\ efficiency\ = \frac{Ci\ -\ Ce}{Ci} \times\ 100 \quad \textbf{(1)}$$

where Ci represents the influent contaminant concentration (mg/L) and Ce corresponds to the effluent concentration (mg/L).

Data normality was examined using the Kolmogorov–Smirnov test, with a significance threshold of α = 0.05. As the data did not meet normality assumptions, a non-parametric Kruskal-Wallis test was applied, and multiple comparisons among groups were conducted using Dunn's post-hoc procedure. All statistical analyses were performed in Minitab® v.16 (Minitab Inc., State College, Pennsylvania). This analytical approach is similar to that described by Vera-Puerto *et al*. (2021).

To assess the growth of the plant species implemented in the system, their height was measured using a measuring tape.

Results and Discussion

Caffeine removal

The characterization of the community's wastewater, including caffeine concentrations at the washing point, at the point without CPWW influence, and at the system inlet, is presented in Table 1.

Table 1. Caffeine concentrations at different sampling points during and outside the coffee-processing season

Sampling point	Harvest season (mg/L)	Outside harvest season (mg/L)
Washing point CPWW	335.03 ± 45.30	NR*
Point without CPWW discharge	0.08 ± 0.03	0.15 ± 0.08
Influent	38.85 ± 10.40	0.84 ± 0.57

* NR= No reported

Figure 3 shows the point where the coffee-processing wastewater mixes with the community's municipal wastewater.

Figure 3. Discharge of community's municipal wastewater and coffee-processing wastewater

Caffeine concentrations found in this study were markedly higher than those typically observed in municipal wastewater. Li *et al*. (2013), Vymazal *et al*. (2017), and Herrera-Melián *et al*. (2023) documented values of 0.057 mg/L, 0.083 mg/L, and 0.124 mg/L, respectively. The elevated levels reported here are attributed to the combined discharge of municipal effluents with CPWW, where caffeine concentrations during the fermentation stage can reach up to 388.6 ± 85.9 mg/L (Figueroa Campos *et al*., 2020). On average, the system achieved removal efficiencies above 99%, aligning with findings reported by de Oliveira *et al*. (2019) and Teoh *et al*. (2022) for tropical environments, as well as with full-scale observations reported by Chen *et al*. (2016) for rural wastewater treatment.

Caffeine reduction in constructed wetlands is commonly associated with photodegradation and aerobic biodegradation, both facilitated by oxygen availability and atmospheric exposure (M. Sánchez *et al*., 2022; Vymazal *et al*., 2017). Nonetheless, Chen *et al*. (2016) noted that anaerobic biodegradation may also play an important role.This pathway may contribute significantly in the present system, as illustrated in Figure 4, where the highest removal contributions were observed in zones characterized by low oxygen availability: sedimentation tank and the SSF-CW cells.

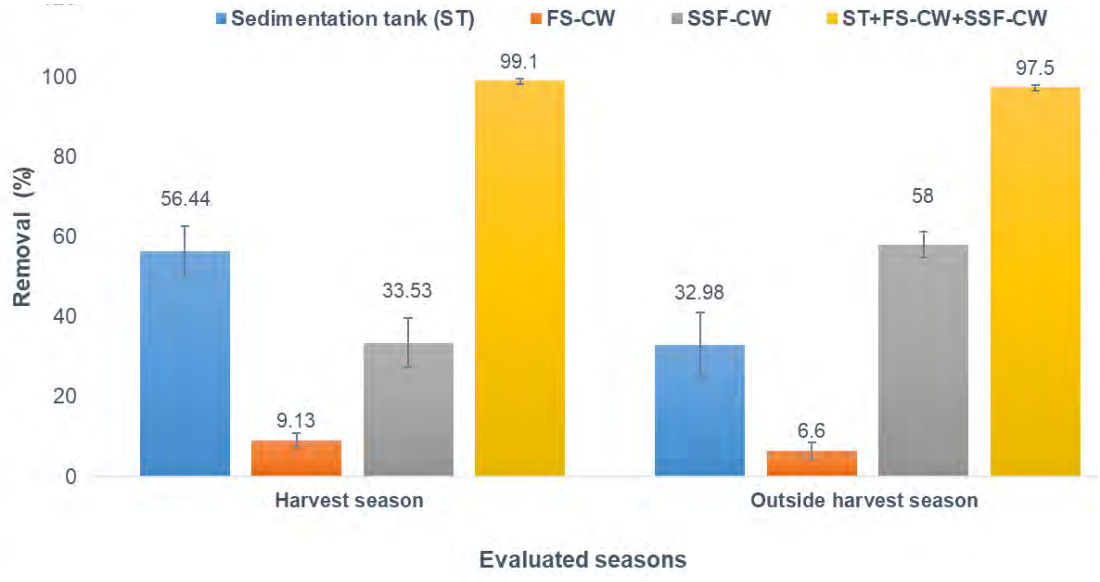

Figure 4. Caffeine removal efficiencies of the wetland system

Vegetation has additionally been identified as a significant contributor to caffeine attenuation (Ilyas and van Hullebusch, 2020; Zhang *et al*., 2013). This effect appears more pronounced in cells that host a larger number and greater diversity of plant species under both monoculture and mixed-species configurations.

Removal performance across the integrated wetland system (Figure 4) revealed that the SSF-CW contributed 33.53% and 58% of the total removal during the two evaluated periods. However, maximum removal were observed when the treatment system was evaluated as an integrated treatment train. No significant seasonal differences were detected across treatment stages ($p > 0.05$), suggesting that the proposed configuration is capable of buffering the seasonal rise in caffeine concentrations during the harvest period. This indicates that the combined operation of the SF-CW and SSF-CW represents an effective treatment strategy.

Plant growth and adaptation

Figure 5 illustrates plant height throughout the monitoring period, with measurements taken every two and three months. In the case of *Eichhornia crassipes*, which is not included in the graph, the population increased from 120 to 920 individuals within a 15 m² area, reaching its peak flowering in July. In this system, *Heliconia psittacorum* and *Hedychium coronarium* exhibited flowering levels that exceeded those reported in previous studies (Carrera-Alvarado *et al*., 2023), demonstrating strong performance under real operating conditions. However, no significant differences were detected for *Zantedeschia aethiopica* by the end of the study ($p > 0.05$). This limited response may be associated with the high temperatures recorded at the site, which ranged from 28 to 35 °C, given that this species reaches optimal growth between 15 and 28 °C (Casierra *et al*., 2012).

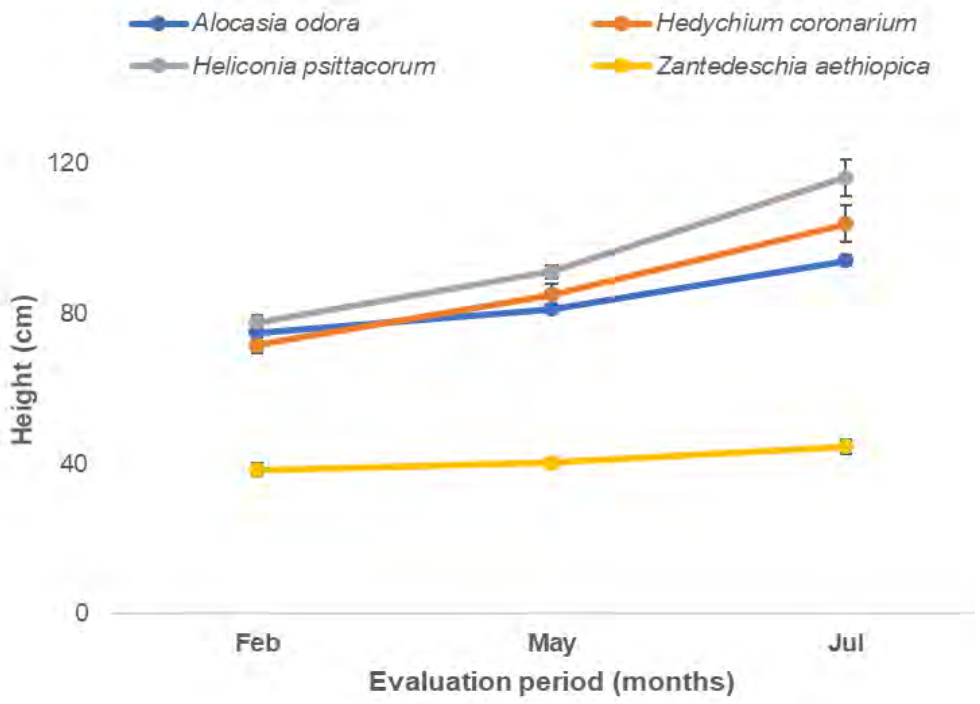

Figure 5. Growth of the evaluated species during the study period

Overall, the plant species exhibited healthy development despite the elevated caffeine concentrations present in the system (Figure 6). *Heliconia psittacorum* and *Hedychium coronarium* are highly resilient to toxic conditions and are recognized for their effectiveness in removing pharmaceutical compounds, including caffeine (Arredondo *et al*., 2022). This resilience not only supports the continuity of treatment processes but also helps maintain the ornamental quality of the plants, which sustained vigorous growth, flowering, and visually attractive foliage.

Their tolerance to elevated contaminant concentrations, combined with sustained ornamental quality, suppor their suitability for use in constructd wetlands in tropical regions. In addition to contributing to contaminant removal, they help preserve the visual appeal of the system, which enhances social acceptance, and they also provide meaningful commercial value through the sale of flowers and foliage. Their incorporation therefore serves environmental, social, and economic functions.

Figure 6. Vegetative development of the evaluated species in the hybrid wetland system

Perspectives and future challenges

This study provides valuable evidence on the effectiveness of full-scale constructed wetlands in removing caffeine from rural wastewater, where effluents from coffee processing are mixed with municipal discharges. However, several limitations should be acknowledged. The results are based on a single coffee harvest and processing season, highlighting the need for longer-term monitoring to assess system performance over time. Additional research is also required to better understand caffeine accumulation in plant biomass, sludge, and the filter media, as well as to identify potential intermediate metabolites formed during degradation processes.

Future work should aim to validate these results in rural communities with varying climatic, topographic, and sociocultural conditions to strengthen model reproducibility and regional applicability. Long-term assessments are likewise recommended to capture seasonal dynamics, regeneration cycles of ornamental species, and a comprehensive evaluation of the ultimate fate of caffeine within the system.

Conclusions

The ornamental constructed wetlands achieved average caffeine removal efficiencies exceeding 99% when treating rural wastewater mixed with coffee-processing discharges, demonstrating their effectiveness as a treatment option under real operating conditions. Furthermore, ornamental species such as *Heliconia psittacorum* and *Hedychium coronarium* showed good adaptation to the system conditions, maintaining their ornamental quality and suggesting potential added value through their commercial use. This multifunctionality supports the role of ornamental constructed wetlands as an integrated solution with environmental and socio-economic benefits for rural communities.

Acknowledgments and Funding: We gratefully acknowledge the Gobierno del Estado de Veracruz and the Secretaría de Medio Ambiente del Estado for providing the funding that made this project possible. We also thank the Secretaría de Ciencia, Humanidades, Tecnología e Innovación (SECIHTI) for the support provided through the scholarship awarded to CVU: 1088095. Additional partial funding was provided by TecNM through the Convocatoria 2024: Proyectos de Investigación Científica, Desarrollo Tecnológico e Innovación, under project No. 21030, which is also sincerely appreciated.

Author contributions: B.L.M-R: Writing, analysis and interpretation of data; M.C.L-M: Analysis and interpretation of data; I.V-P: Design, Conceptualization and editing; L.C.S-H: Editing, supervision, funding acquisition and provide materials.

References

Alemayehu, Y. A., Asfaw, S. L., & Tirfie, T. A. (2020). Management options for coffee processing wastewater. A review. *Journal of Material Cycles and Waste Management*, *22*(2), 454–469. https://doi.org/10.1007/s10163-019-00953-y

Amare, G., Dobo, B., & Haile, E. (2023). The Effect of Wet Coffee Processing Plant Effluent on Physicochemical and Bacteriological Quality of Receiving Rivers Used by Local Community: Case of Aroresa District, Sidama, Ethiopia. *Environmental Health Insights*, *17*. https://doi.org/10.1177/11786302231165186

Calheiros, C. S. C., Bessa, V. S., Mesquita, R. B. R., Brix, H., Rangel, A. O. S. S., & Castro, P. M. L. (2015). Constructed wetland with a polyculture of ornamental plants for wastewater treatment at a rural tourism facility. *Ecological Engineering*, *79*, 1–7. https://doi.org/10.1016/j.ecoleng.2015.03.001

Campos, R. C., Pinto, V. R. A., Melo, L. F., Rocha, S. J. S. S. da, & Coimbra, J. S. (2021). New sustainable perspectives for "Coffee Wastewater" and other by-products: A critical review. *Future Foods*, *4*, 100058. https://doi.org/10.1016/j.fufo.2021.100058

Chen, Y., Vymazal, J., Březinová, T., Koželuh, M., Kule, L., Huang, J., & Chen, Z. (2016). Occurrence, removal and environmental risk assessment of pharmaceuticals and personal care products in rural wastewater treatment wetlands. Science of The Total Environment, 566–567, 1660–1669. https://doi.org/10.1016/j.scitotenv.2016.06.069

Chen, C., Luo, J., Bu, C., Zhang, W., & Ma, L. (2022). Efficacy of a large-scale integrated constructed wetland for pesticide removal in tail water from a sewage treatment plant. *Science of The Total Environment*, *838*, 156568. https://doi.org/10.1016/j.scitotenv.2022.156568

Carrera-AlvaradoGisela, G., Velasco-Velasco, J., García Osorio, C., Salinas-Ruíz, J., & Baltazar-Bernal, O. (2023). Producción de heliconias en municipios de Veracruz. Agro-Divulgación, 3(1). https://doi.org/10.54767/ad.v3i1.143

Dadi, D., Mengistie, E., Terefe, G., Getahun, T., Haddis, A., Birke, W., Beyene, A., Luis, P., & Van der Bruggen, B. (2018). Assessment of the effluent quality of wet coffee processing wastewater and its influence on downstream water quality. *Ecohydrology & Hydrobiology*, *18*(2), 201–211. https://doi.org/10.1016/j.ecohyd.2017.10.007

de Cravalho, A. C. C., da Silva Paganini, W., de Almeida Piai, K., & Bocchiglieri, M. M. (2024). The presence of pharmaceuticals and caffeine in water, as well as the methods used to eliminate them. Current Opinion in Environmental Science & Health, 39, 100550. https://doi.org/10.1016/j.coesh.2024.100550

de Oliveira, M., Atalla, A. A., Frihling, B. E. F., Cavalheri, P. S., Migliolo, L., & Filho, F. J. C. M. (2019). Ibuprofen and caffeine removal in vertical flow and free-floating macrophyte constructed wetlands with Heliconia rostrata and Eichornia crassipes. *Chemical Engineering Journal*, *373*, 458–467. https://doi.org/10.1016/j.cej.2019.05.064

Ebrahimzadeh, G., Nodehi, R. N., Alimohammadi, M., Rezaei Kahkah, M. R., & Mahvi, A. H. (2021). Monitoring of caffeine concentration in infused tea, human urine, domestic wastewater and different water resources in southeast of Iran- caffeine an alternative indicator for contamination of human origin. Journal of Environmental Management, 283, 111971. https://doi.org/10.1016/j.jenvman.2021.111971

Figueroa Campos, G. A., Sagu, S. T., Saravia Celis, P., & Rawel, H. M. (2020). Comparison of Batch and Continuous Wet-Processing of Coffee: Changes in the Main Compounds in Beans, By-Products and Wastewater. *Foods*, *9*(8), 1135. https://doi.org/10.3390/foods9081135

García Martínez, E., Fuentes López, A., & Fernández Segovia, I. (2018). Extracción y cuantificación de cafeína mediante espectroscopía UV-Visible en café, té y cacao. ETSIAMN. Universitat Politècnica de València, 1–9. https://riunet.upv.es/handle/10251/104055

Harvey, C. A., Pritts, A. A., Zwetsloot, M. J., Jansen, K., Pulleman, M. M., Armbrecht, I., Avelino, J., Barrera, J. F., Bunn, C., García, J. H., Isaza, C., Munoz-Ucros, J., Pérez-Alemán, C. J., Rahn, E., Robiglio, V., Somarriba, E., & Valencia, V. (2021). Transformation of coffee-growing landscapes across Latin America. A review. Agronomy for Sustainable Development, 41(5), 62. https://doi.org/10.1007/s13593-021-00712-0

Hernández, S. S., Partida-Sedas, J. G., Cruz-Castillo, J. G., Cadena Chamorro, E., Escamilla Prado, E., & Valdez Velarde, E. (2024). TECNOLOGÍAS DEL BENEFICIADO DE CAFÉ Y TRATAMIENTO DE EFLUENTES LÍQUIDOS. Tropical and Subtropical Agroecosystems, 27(2). https://doi.org/10.56369/tsaes.5099

Herrera-Melián, J. A., Guedes-Alonso, R., Tite-Lescano, J. C., Sosa-Ferrera, Z., & Santana-Rodríguez, J. J. (2023). Enhancing pharmaceutical removal in a full-scale constructed wetland with effluent recirculation. Journal of Environmental Chemical Engineering, 11(6), 111167. https://doi.org/10.1016/j.jece.2023.111167

Ilyas, H., & van Hullebusch, E. (2019). Role of Design and Operational Factors in the Removal of Pharmaceuticals by Constructed Wetlands. *Water*, *11*(11), 2356. https://doi.org/10.3390/w11112356

INEGI, I. N. de E. y G. (2024). Climatología-INEGI.

Korekar, G., Kumar, A., & Ugale, C. (2020). Occurrence, fate, persistence and remediation of caffeine: a review. Environmental Science and Pollution Research, 27(28), 34715–34733. https://doi.org/10.1007/s11356-019-06998-8

Li, X., Zheng, W., & Kelly, W. R. (2013). Occurrence and removal of pharmaceutical and hormone contaminants in rural wastewater treatment lagoons. Science of The Total Environment, 445–446, 22–28. https://doi.org/10.1016/j.scitotenv.2012.12.035

Liang, X., & Yue, X. (2021). Challenges facing the management of wastewater treatment systems in Chinese rural areas. *Water Science and Technology*, *84*(6), 1518–1526. https://doi.org/10.2166/wst.2021.332

Mazloum Yar, F. G. (2024). Rural Industries and Their Role in the Development of Rural Areas and Afghanistan's National Economy. *Jurnal Indonesia Sosial Teknologi*, *5*(10), 4706–4723. https://doi.org/10.59141/jist.v5i10.7035

Mihret, D., Gonse, A., Lamisso, S., & Kannan, N. (2024). Constructed wetland-based wastewater treatment of a coffee-washing plant and its impacts: a case study of Kege processing plant, Ethiopia. *AQUA — Water Infrastructure, Ecosystems and Society*, *73*(4), 804–817. https://doi.org/10.2166/aqua.2024.008

Monzón-Reyes, B. L., González-Moreno, H. R., Month, A. E. Á., Peralta Vega, A. J., Ballut-Dajud, G., & Sandoval Herazo, L. C. (2025). Wastewater Management Strategies in Rural Communities Using Constructed Wetlands: The Role of Community Participation. *Earth*, *6*(2), 18. https://doi.org/10.3390/earth6020018

Monzón-Reyes, B. L., Vera-Puerto, I., Florez, V. V., Méndez, M. C. L., Month, A. E. Á., Meléndez-Armenta, R. Á., & Herazo, L. C. S. (2026). Municipal and coffee wastewater treated by a full-scale Constructed Wetlands using ornamental plants under tropical climate. Ecological Engineering, 222(September 2025). https://doi.org/10.1016/j.ecoleng.2025.107809

Nocetti, E., Hadad, H. R., Di Luca, G. A., Mufarrege, M. de las M., & Maine, M. A. (2024). Performance of a multi-stage hybrid wetland system for the treatment of a dairy effluent. *Journal of Water Process Engineering*, *58*, 104797. https://doi.org/10.1016/j.jwpe.2024.104797

Quadra, G. R., Paranaíba, J. R., Vilas-Boas, J., Roland, F., Amado, A. M., Barros, N., Dias, R. J. P., & Cardoso, S. J. (2020). A global trend of caffeine consumption over time and related-environmental impacts. Environmental Pollution, 256, 113343. https://doi.org/10.1016/j.envpol.2019.113343

Rodrigues, S., Alves, R. S., & Antunes, S. C. (2025). Impact of Caffeine on Aquatic Ecosystems: Assessing Trophic-Level Biological Responses. Journal of Xenobiotics, 15(3), 86. https://doi.org/10.3390/jox15030086

Rodríguez-Macedo, M., González-Christen, A., & León-Paniagua, L. S. (2014). Diversidad de los mamíferos silvestres de Misantla, Veracruz, México. Revista Mexicana de Biodiversidad, 85(1), 262–275. https://doi.org/10.7550/rmb.36143

Sandoval-Herazo, M., Martínez-Reséndiz, G., Fernández Echeverria, E., Fernández-Lambert, G., & Sandoval Herazo, L. C. (2021). Plant Biomass Production in Constructed Wetlands Treating Swine Wastewater in Tropical Climates. Fermentation, 7(4), 296. https://doi.org/10.3390/fermentation7040296

Sandoval, L., Zamora-Castro, S., Vidal-Álvarez, M., & Marín-Muñiz, J. (2019). Role of Wetland Plants and Use of Ornamental Flowering Plants in Constructed Wetlands for Wastewater Treatment: A Review. Applied Sciences, 9(4), 685. https://doi.org/10.3390/app9040685

Sandoval Herazo, L., Marín-Muñiz, J., Alvarado-Lassman, A., Zurita, F., Marín-Peña, O., & Sandoval-Herazo, M. (2023). Full-Scale Constructed Wetlands Planted with Ornamental Species and PET as a Substitute for Filter Media for Municipal Wastewater Treatment: An Experience in a Mexican Rural Community. *Water*, *15*(12), 2280. https://doi.org/10.3390/w15122280

Siles, P., Cerdán, C. R., & Staver, C. (2022). Smallholder Coffee in the Global Economy—A Framework to Explore Transformation Alternatives of Traditional Agroforestry for Greater Economic, Ecological, and Livelihood Viability. Frontiers in Sustainable Food Systems, 6. https://doi.org/10.3389/fsufs.2022.808207

Utrilla-Catalan, R., Rodríguez-Rivero, R., Narvaez, V., Díaz-Barcos, V., Blanco, M., & Galeano, J. (2022). Growing Inequality in the Coffee Global Value Chain: A Complex Network Assessment. *Sustainability*, *14*(2), 672. https://doi.org/10.3390/su14020672

Vera-Puerto, I., Escobar, J., Rebolledo, F., Valenzuela, V., Olave, J., Tíjaro-Rojas, R., Correa, C., & Arias, C. (2021). Performance Comparison of Vertical Flow Treatment Wetlands Planted with the Ornamental Plant Zantedeschia aethiopica Operated under Arid and Mediterranean Climate Conditions. Water, 13(11), 1478. https://doi.org/10.3390/w13111478

Vispo, C., Geronimo, F. K., Jeon, M., & Kim, L.-H. (2023). Performance Evaluation of Various Filter Media for Multi-Functional Purposes to Urban Constructed Wetlands. Sustainability, 16(1), 287. https://doi.org/10.3390/su16010287

Vymazal, J., Dvořáková Březinová, T., Koželuh, M., & Kule, L. (2017). Occurrence and removal of pharmaceuticals in four full-scale constructed wetlands in the Czech Republic – the first year of monitoring. *Ecological Engineering*, *98*, 354–364. https://doi.org/10.1016/j.ecoleng.2016.08.010

Zhang, D. Q., Hua, T., Gersberg, R. M., Zhu, J., Ng, W. J., & Tan, S. K. (2013). Fate of caffeine in mesocosms wetland planted with Scirpus validus. Chemosphere, 90(4), 1568–1572. https://doi.org/10.1016/j.chemosphere.2012.09.059

Zitácuaro-Contreras, I., Vidal-Álvarez, M., Hernández y Orduña, M. G., Zamora-Castro, S. A., Betanzo-Torres, E. A., Marín-Muñíz, J. L., & Sandoval-Herazo, L. C. (2021). Environmental, Economic, and Social Potentialities of Ornamental Vegetation Cultivated in Constructed Wetlands of Mexico. *Sustainability*, *13*(11), 6267. https://doi.org/10.3390/su13116267

Bioremediation of slaughterhouse wastewater: Evaluation of nitrogen pollutant removal using constructed wetlands

Jesús Castellanos-Rivera [1], Graciela Elizabeth Nani-González [1], Oscar Marín-Peña [1], Jacel Adame-García [2], Mayerlin Sandoval Herazo [1,2,3] y Luis Carlos Sandoval-Herazo [1,3,*]

[1] Wetlands and Environmental Sustainability Laboratory, Division of Graduate Studies and Research, Tecnológico Nacional de México/Instituto Tecnológico Superior de Misantla, Km 1.8 Carretera a Loma Del Cojolite, Misantla 93821, Veracruz, Mexico.
[2] Tecnológico Nacional de México/Instituto Tecnológico de Úrsulo Galván, Carretera Cd Cardel-Chachalacas km 4.5, Úrsulo Galván 91667, Veracruz, Mexico.
[3] Facultad de Ingeniería, Universidad de Sucre, Sincelejo 700001, Colombia.
* Corresponding author: lcsandovalh@gmail.com; Tel.: +522351104181

Received: June 13, 2025 Accepted: July 21, 2025 Published: March 2, 2026
DOI: https://doi.org/10.56845/rebs.v8i1.665

Abstract: The increasing generation of slaughterhouses wastewater is posing a serious threat to ecosystems and human health due to high levels of contaminants such as total nitrogen (TN), NH_4^+, NO_3^- and NO_2^-, which, if not properly treated, can cause environmental problems such as eutrophication. Constructed wetlands (CWs) have emerged as an effective and cost-efficient alternative to conventional wastewater treatment technologies, including slaughterhouse wastewater. This study evaluated the efficiency of CWs in the removal of nitrogenous compounds in slaughterhouse wastewater using the plant species *Typha latifolia* and *Heliconia latispatha*. Eight horizontal subsurface flow constructed wetlands (HSF-CWs) units were implemented with different species combinations, and nitrogen pollutant concentrations were monitored over a one-year period. Results showed that the polyculture of *T. latifolia* and *H. latispatha* achieved the highest TN (64-65%) and NH_4^+ (89%) removal efficiency, while systems with individual *T. latifolia* and *H. latispatha* showed intermediate efficiencies of 57% and 48%, respectively. For nitrate (NO_3-), the polyculture achieved an efficiency of 91%, while *T. latifolia* reached 78% and *H. latispatha* 68%. Finally, in nitrite removal (NO_2^-), the polycultures showed a removal efficiency of 92%, while *T. latifolia* and *H. latispatha* achieved efficiencies of 82% and 73%, respectively. In comparison, the control presented the lowest efficiencies in all parameters (33-65%). This study concludes that HCs, planted with *T. latifolia* + *H. latispatha*, are a viable and economical alternative for the treatment of slaughterhouse wastewater, offering a more sustainable option compared to more complex and expensive technologies, such as electrocoagulation or nanofiltration systems. The use of polycultures and the combination of technologies is recommended to maximize treatment efficiency.

Keywords: slaughterhouse wastewater, nitrogenous contaminants; constructed wetlands, ornamental plants, bioremediation

Introduction

The rapid generation of industrial wastewater, especially in meat production, is placing increasing pressure on communities and ecosystems, threatening not only environmental balance but also the health and future of entire generations (Boukouvalas *et al*., 2024). Wastewater from slaughterhouses contains high concentrations of pollutants, including total nitrogen (TN), ammonium (NH_4^+), nitrates (NO_3^-), and nitrites (NO_2^-). If these compounds are not properly treated, they can have significant environmental impacts, such as eutrophication and contamination of surface and groundwater bodies (Brennan *et al*., 2021; Silveira *et al*., 2021). In addition, nitrogen compounds have been identified as one of the main causes of water quality degradation in various regions of the world (Wang *et al*., 2024).

Proper treatment of effluents from slaughterhouses is crucial to mitigate their environmental impact. Nature-based solutions (NBS), such as constructed wetlands (CWs), have emerged as an effective and sustainable alternative to conventional wastewater treatment methods (Agaton & Guila, 2023). These systems are attractive not only because of their operational simplicity and low cost, but also because of their high effectiveness in removing pollutants such as nitrogen, which is one of the main causes of eutrophication in water bodies (Waly *et al*., 2022).

CWs have been widely used to treat various types of wastewaters, demonstrating their versatility and effectiveness in a range of contexts. They have proven effective in treating domestic and industrial wastewater (Herazo *et al*., 2021), as well as in removing contaminants from specific industries, such as heavy metals (Yu *et al*., 2022) and textile dyes (Patil *et al*., 2022). They have also been applied in the treatment of agricultural runoff and pesticides (McCalla *et al*., 2022), petroleum hydrocarbons (Taha *et al*., 2023), and pharmaceuticals (Hu *et al*., 2021), obtaining favorable results in reducing nitrogen compounds present in the effluents studied.

However, although CW shave proven to be efficient in treating various types of wastewater, their ability to treat slaughterhouse effluents, which have a higher organic load and nitrogen concentration, has not yet been fully explored, particularly regarding nitrogen removal performance (Fang *et al*., 2022).

This study focused on evaluating the efficiency of a CW system for treating slaughterhouse wastewater, with special attention to the removal of nitrogenous contaminants such as TN, NH_4^+, NO_3^-, and NO_2^-. To this end, macrophytes such as *Typha latifolia* and *Heliconia latispatha* were used, species that have demonstrated a great capacity to improve filtration and nutrient removal in wetland systems (Aguilar-Cortés *et al*., 2025; Sandoval-Herazo *et al*., 2021). In addition, the results obtained were compared with other conventional treatment methods to position constructed wetlands as a viable and economical solution for treating effluents from slaughterhouses.

Bioremediation using CWs is an innovative and environmentally friendly option for treating slaughterhouse wastewater. This study highlights the significant potential of this nature-based solution (NBS) within the agro-industrial sector, addressing one of today's greatest environmental challenges. By focusing on the efficiency of constructed wetlands in removing nitrogen from slaughterhouse effluents, this research not only expands knowledge about their applicability but also provides key guidelines for their implementation, positioning them as a sustainable, economical, and high-impact alternative for the meat industry.

Materials and Methods

Study site

This study was conducted at the facilities of the National Technological Institute of Mexico (TecNM), Misantla Campus, Veracruz, Mexico. The research was carried out during 2023, from January to December. The area where the work was carried out is characterized by a warm and humid climate, with an average annual temperature of approximately 22.7 °C. In addition, the region receives an average annual rainfall of 2036.4 mm, which influences the environmental conditions of the site. The campus is located 300 meters above sea level (Figure 1), which provides a relevant geographical context for the study of constructed wetlands and their capacity to treat slaughterhouse wastewater.

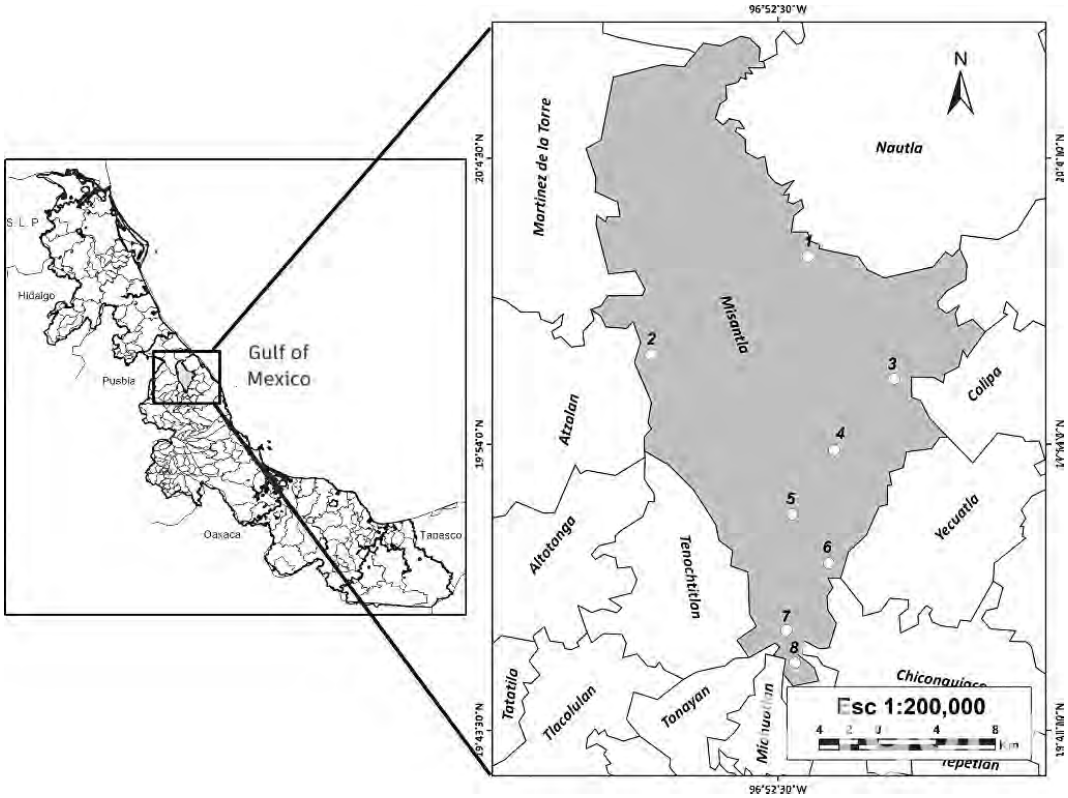

Figure 1. Geographical location of the study area

Description of the experimental units

The wastewater used in this study was obtained from wastewater from a slaughterhouse located 1.2 km from the experimental area. This water was collected in a 1,200-liter sedimentation tank, which was placed 50 cm above the level of the experimental units to ensure gravity flow to the constructed wetlands.

The treatment system consisted of eight subsurface horizontal flow wetland units (HSF-CWs), constructed on a mesocosm scale using reinforced concrete. The dimensions of each experimental unit were 150 cm long, 40 cm wide, and 100 cm deep, with a water saturation depth set at 65 cm. The units were arranged in a linear alignment, with each contiguous cell being a direct replica of the previous one.

The units were assigned according to the type of experimental treatment: a control cell (without vegetation, but with the same filter medium as the others), a cell with polyculture of the species *Typha latifolia* and *Heliconia latispatha*, a cell with monoculture of *Typha latifolia*, and a cell with monoculture of *Heliconia latispatha*. This experimental design allowed for a detailed and replicated assessment of the impact of different plant configurations on the performance of wetlands for contaminant removal.

The filter medium used in all units was red tezontle, with a particle diameter between 5 and 8 mm and a porosity of 0.5, which facilitated adequate interaction between the water and plant roots. All experimental units were operated with a hydraulic retention time (HRT) of 5 days, which allowed the simulation of adequate conditions for the bioremediation process of wastewater in the constructed wetland system.

Vegetation development

Monitoring plant development was essential to understanding the functional role of plants in removing nitrogen compounds within the constructed wetland system. To this end, periodic assessments of the growth of the plant species used were carried out from the initial establishment of the plants until the end of the experimental period.

The variables considered included plant height and plant density. The first parameter was determined using standardized measurements with an UltraTech® digital caliper, while the number of flowers was recorded manually through direct inspection in the field. Measurements were taken every two months, allowing growth to be recorded over time and correlated with nitrogen removal efficiency parameters.

This continuous monitoring provided key data on the vigor and phenological status of the plants, which are fundamental elements in the efficiency of the bioremediation process, since greater biomass and plant activity are usually associated with a greater capacity to assimilate and transform nitrogen compounds present in wastewater.

Monitoring of water quality parameters

For a complete characterization of the quality of the collected wastewater, physicochemical analyses were performed to determine the levels of various key parameters, such as total nitrogen (TN), ammonium (NH_4^+), nitrate (NO_3^-), and nitrite (NO_2^-). The analyses were performed using an HI801 IRIS™ visible spectrophotometer (Hanna Instruments, USA) following the procedures established in standard water analysis methods (APHA/AWWA/WEF, 2012) to ensure the accuracy and reliability of the results obtained.

In addition, water environmental conditions, including temperature and pH, were monitored using a Hanna HI9811-51 portable multiparameter meter (HANNA® Instruments, Woonsocket, RI, USA). These parameters are essential for evaluating the environment in which bioremediation reactions take place and the behavior of contaminants. Likewise, dissolved oxygen (DO) was quantified using a specific Hanna HI9146-04 meter (HANNA® Instruments), which is crucial for understanding the dynamics of biodegradation and redox processes in the wetland. Environmental parameters were recorded daily using a DAVIS™ 6152 Vantage Pro2 automatic weather station.

These analyses provided essential data for interpreting the system's efficiency in removing nitrogenous contaminants, allowing correlations to be established between physicochemical conditions and the plants' ability to assimilate and transform the compounds present in wastewater.

Statistical analysis

To evaluate the system's effectiveness in removing nitrogenous contaminants, a randomized experimental design was used, which allowed for control of the variability of the experimental conditions and ensured the validity of the results obtained. The data collected during the study were analyzed using analysis of variance (ANOVA) to identify significant differences between the treatments and conditions evaluated. Subsequently, a comparison of means test was performed using Tukey's method, with a significance level of $p \leq 0.05$. This analysis provided detailed information on the differences in nitrogen removal efficiency between the different experimental groups, allowing the authors to determine which treatments were statistically superior in terms of their performance in the bioremediation of slaughterhouse wastewater. Statistical analysis was performed using IBM® SPSS® Statistics software, which ensured robustness and accuracy in the handling and processing of data obtained throughout the experimental period.

Results and Discussion

Characterization of the effluent

The results obtained in this study provide valuable information on the quality of the influent and the concentrations of nitrogenous pollutants present in slaughterhouse wastewater. Table 2 shows the physicochemical characterization of the influent. The differences between the average concentrations observed during the study period were significant for NH_4^+-N and NO_2^--N, but not significant for the other parameters analyzed ($p < 0.001$).

Regarding TN concentrations (250.3 ± 8.7 mg/L), the values found were within the ranges reported by other authors who used different conventional treatments in various countries (Bazrafshan *et al*., 2022; Fatima *et al*., 2021; Teo *et al*., 2023). For NH_4^+–N, the values obtained were similar to those reported by Phan *et al*. (2020), while for NO_3^-–N and NO_2^-–N, considerably higher values were recorded compared to those reported by the same author.

Table 1**.** Average concentrations of nitrogen contaminants in influent and effluent

Parameter	Units	Influent	*Typha latifolia*	*Heliconia latispatha*	Polyculture	Control
TN	mg/L	250.299 ± 8.669	106.502 ± 2.374	127.487 ± 5.085	88.494 ± 2.342	165.728 ± 6.212
NH_4^+–N	mg/L	172.801 ± 10.275	38.474 ± 1.915	58.239 ± 2.994	18.127 ± 1.056	92.315 ± 4.175
NO_3^-–N	mg/L	22.553 ± 1.240	4.790 ± 0.199	7.036 ± 0.436	2.077 ± 0.111	9.047 ± 0.385
NO_2^-–N	mg/L	7.721 ± 0.263	1.401 ± 0.034	2.032 ± 0.076	0.573 ± 0.024	3.280 ± 0.205

All values are expressed as mean ± standard error (n=12).

Environmental conditions and plant growth

The study was conducted in a tropical climate, which was reflected in the values of the environmental parameters recorded during the experimental period (Table 2). The climatic conditions observed indicate that both species were able to develop favorably, suggesting that environmental variability within these parameters did not represent a significant constraint on their growth.

On the one hand, *Heliconia latispatha* found a favorable environment for its growth, as the average temperature during the study period was within its optimal development range, which varies between 18 and 34 °C. Likewise, the relative humidity recorded exceeded the minimum threshold of 50% necessary for its proper development. In addition, high solar radiation, together with intense lighting, favored its growth, given that this species requires high levels of light for optimal physiological performance (Jagtap *et al*., 2024; Malakar & Biswas, 2022).

Table 2. Environmental parameters measured throughout the study

Parameter	Average ± SD*
Ambient temperature (°C)	28.6 ± 5.6
Precipitation (mm)	120.0 ± 3.2
Solar radiation (W/m^2)	99.0 ± 11.1
Relative humidity (%)	95.1 ± 6.8
Light intensity (lux)	54748.7 ± 5937.5

*Standard Deviation, these values correspond to the entire study period (n=365).

On the other hand, *Typha latifolia*, known for its ability to adapt to different climates, also found suitable conditions for its development (Sesin *et al*., 2021). However, its growth is favored in tropical areas, as this species tolerates temperatures of up to 30 °C; therefore, the values recorded during the study remained within its upper tolerance limit. In addition, its ability to adapt to different levels of relative humidity allowed it to thrive in the environmental conditions recorded. Similarly, although it can develop under different levels of solar radiation, the values obtained coincide with those reported in other tropical regions where its successful growth has been documented (Wasko *et al*., 2022).

It is important to note that the recorded precipitation may have contributed to maintaining favorable water conditions for both species, especially for *Typha latifolia*, which thrives in aquatic ecosystems (Haldan *et al*., 2022). Taken together, these environmental factors suggest that the climatic conditions during the study were suitable for the development of both species, with environmental variability not representing a limiting factor. However, it is important to note that no specific analysis was conducted on the possible effect of precipitation on effluent dilution. Although daily monitoring of environmental parameters was carried out to ensure relatively stable conditions, it is recommended that future research include more detailed monitoring of the impact of factors such as precipitation, evapotranspiration, and other environmental parameters on treatment efficiency, especially in systems exposed to tropical climatic conditions.

However, in terms of plant development, *Typha latifolia* had the highest average height, reaching a maximum of 200 cm in monoculture and 210 cm in polyculture (Figure 2a).

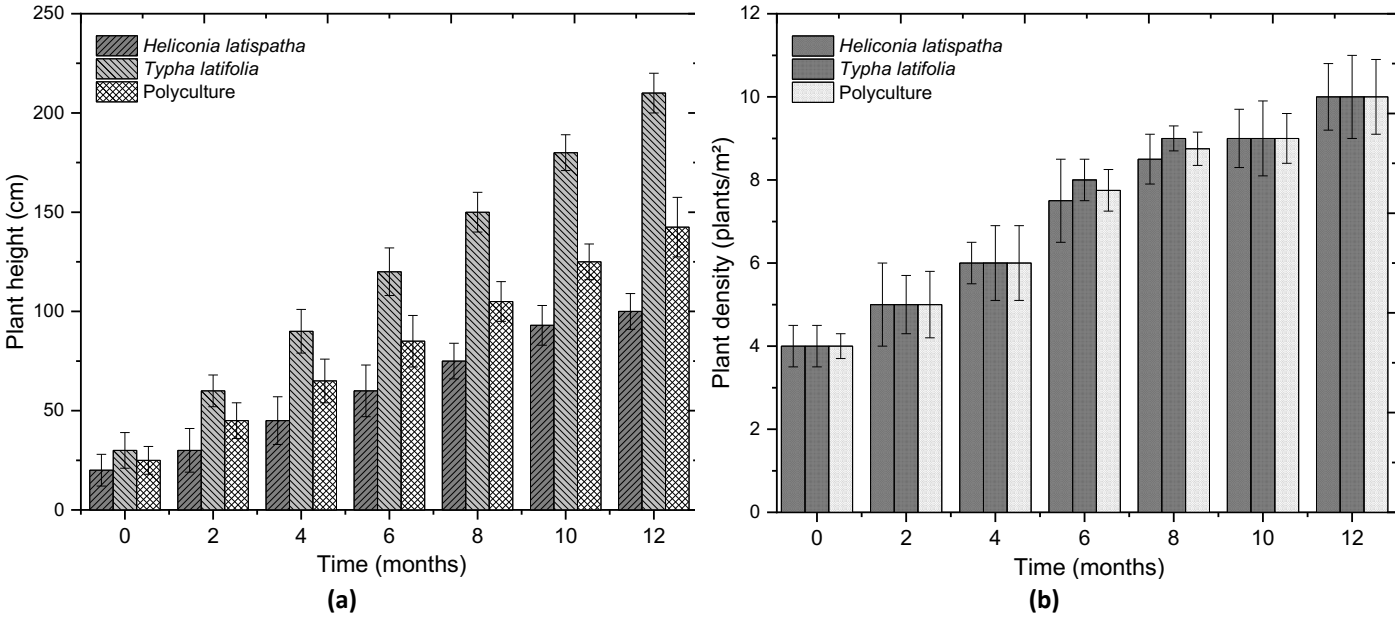

Figure 2. Vegetative development of plant species in monoculture and polyculture, (a) Height (b) Plant density

The maximum height values for *H. latispatha* ranged from 90 cm in polyculture to 124 cm in monoculture, which is characteristic of this species. However, in terms of plant density, *T. latifolia* showed the greatest increase in

monoculture (Figure 2b); nevertheless, *H. latispatha* showed very similar results. Likewise, in polyculture, *H. latispatha* showed overall growth and plant density comparable to those of *T. latifolia*.

Monitoring of control parameters (pH, water temperature (T), and dissolved oxygen (DO))

Figures 3–5 illustrate the behavior of the control parameters (pH, T, and DO) monitored during the study period. In this study, the pH values recorded in the influent throughout the experiment ranged from 7.9 to 8.1, with an average of 8.01 ± 0.6. The outlets of the HSF-CWs systems recorded an average value of 7.42 ± 0.45. Likewise, values of 8.13 ± 0.58 in the influent and 7.15 ± 0.24 in the effluent was also observed.

The pH analysis showed significant differences between the influent and the systems with vegetation (Figure 3). However, no significant differences were observed between the systems with vegetation or between these and the control. The results in the planted systems were similar, although *H. latispatha* differed significantly from the control. The pH values recorded in the influent (7.9–8.1) and effluent (7.15–7.42) are within the ranges reported in similar studies for HSF-CWs systems. For example, previous research has documented pH values between 6.1 and 7.9 in wetlands planted with ornamental and common vegetation, such as *Canna indica* and *Typha domingensis* (Faisal *et al*., 2023), as well as *Juncus effusus* (Meng *et al*., 2024). The pH analysis showed that the CWs managed to reduce the pH of the influent to more neutral values in the effluent, which is beneficial for its discharge into receiving bodies or for its possible reuse (Sánchez *et al*., 2021). The significant differences observed between the influent and the systems with vegetation highlight the contribution of the biological and physicochemical processes inherent in these systems, such as microbial activity, plant absorption, and chemical precipitation processes (Banc *et al*., 2021).

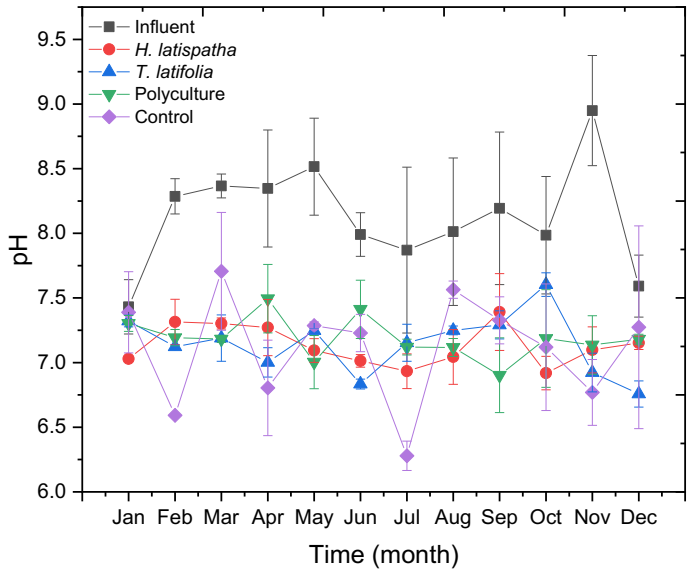

Figure 3. pH behavior throughout the experiment

In the case of temperature, no significant differences were observed between the different treatments used (Figure 4). *H. latispatha* and *T. latifolia* showed homogeneous behavior in thermal regulation, with temperatures within a similar range.

The observed temperature range (20–30 °C) is optimal for microbial activity and processes such as nitrification and denitrification. Amiri *et al*. (2022) observed that CWs planted with typical wetland species, such as *Phragmites australis* and *Typha latifolia*, showed a greater capacity to regulate temperature. On the other hand, studies such as that by Stefanatou *et al*. (2023) have shown that the use of ornamental plants in CWs not only improves aesthetics but also contributes to the regulation of parameters such as temperature and dissolved oxygen.

Regarding DO, when comparing the results of the study period, all systems with vegetation showed significant differences with respect to the influent and the system without vegetation, as well as among themselves (Figure 5). The planted systems showed significant differences compared to the influent and the control. The influent had an

average DO of 0.7 ± 0.09 mg/L, with values between 0.50 and 0.85 mg/L, indicating initial conditions of low oxygenation, typical of slaughterhouse wastewater due to its high organic load. In contrast, the systems with vegetation showed a significant increase in DO values, ranging between 1.51 and 2.08 mg/L. On the other hand, systems without vegetation (control) presented lower values (0.52 to 1.15 mg/L), confirming that vegetation plays a key role in improving DO through mechanisms such as oxygen transfer through plant tissues and the generation of aerobic microzones in the rhizome. When comparing systems planted with *Typha latifolia* (a typical wetland species) and ornamental species such as *H. latispatha*, as well as a combination of both in polyculture, the results showed significant differences in oxygenation capacity. This behavior may be related to differences in the ability of plants to transfer oxygen through their rhizosphere. Previous studies have shown that ornamental species such as *Zantedeschia aethiopica* and *Canna indica* can also play an important role in oxygen transfer, although their efficiency may be lower compared to typical plants such as *T. latifolia* and *Cyperus papyrus* (Singh & Chakraborty, 2021).

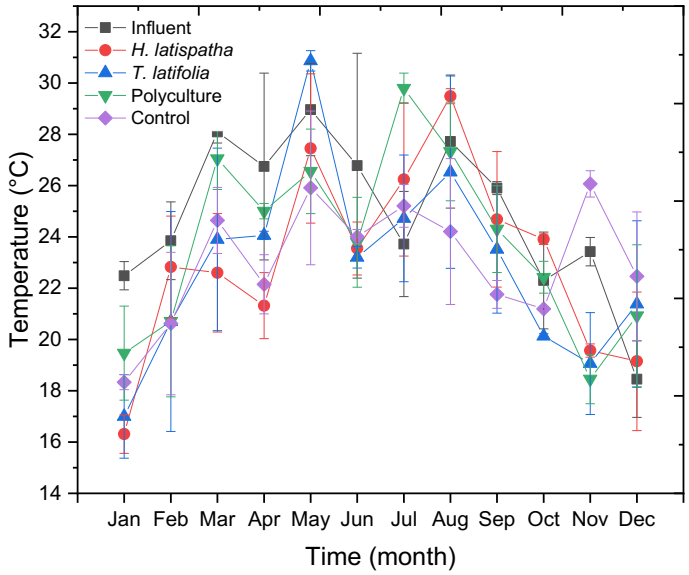

Figure 4. Temperature behavior throughout the experiment

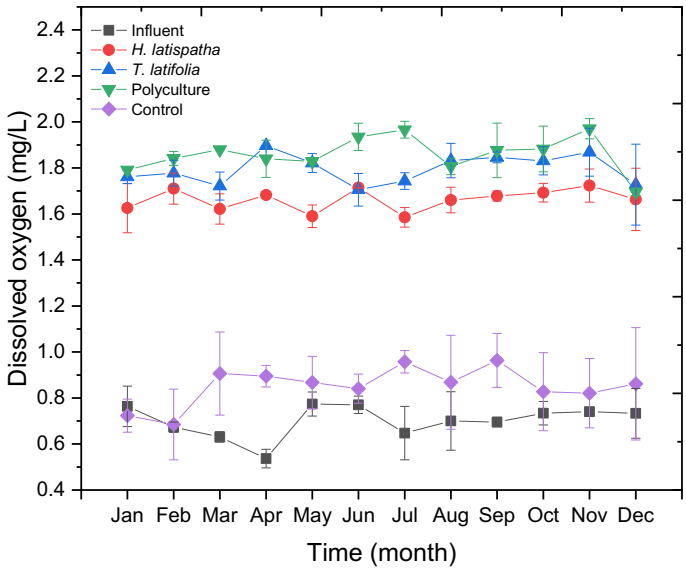

Figure 5. DO behavior throughout the experiment

Removal efficiencies of TN, NH_4^+, NO_3^-, and NO_2^-

Figures 6-9 show the inlet and outlet concentrations, as well as the removal efficiencies for the nitrogen compounds analyzed in this study (TN, NH_4^+, NO_2^-, and NO_3^--N).

For TN, the polyculture of *H. latispatha* and *T. latifolia* showed the highest removal efficiency, with average values of 64–65% (Figure 6). Effluent concentrations were also the lowest, reaching 88 ± 2.342 mg/L. This superior performance can be attributed to the synergy between the two species, which combine their different capacities for absorption, tolerance, and promotion of microbiological processes in the rhizosphere.

Individual systems showed intermediate efficiencies, with *T. latifolia* outperforming *H. latispatha* throughout the monitoring period (57% vs. 48%). This result may be due to the fact that *T. latifolia* is a typical wetland plant with a greater capacity to promote nitrification and denitrification, processes that are essential for TN removal.

The control system, without plants, showed the lowest removal efficiencies (33%) and the highest effluent concentrations (166 ± 6.212 mg/L). This highlights the crucial role of plants in TN removal, as they not only act as passive filters, but also facilitate key biological processes through oxygenation of the root zone.

No significant differences were observed whitin each treatment across the study period, suggesting stability in the performance of the systems studied. However, between different treatments, all comparisons showed significant differences, highlighting the differential effectiveness of each system. Polyculture was significantly more efficient than individual systems with *H. latispatha* or *T. latifolia*, which in turn were more effective than the control system. This

pattern suggests that species diversification in constructed wetlands may be an optimal strategy for maximizing TN removal in wastewater treatment systems.

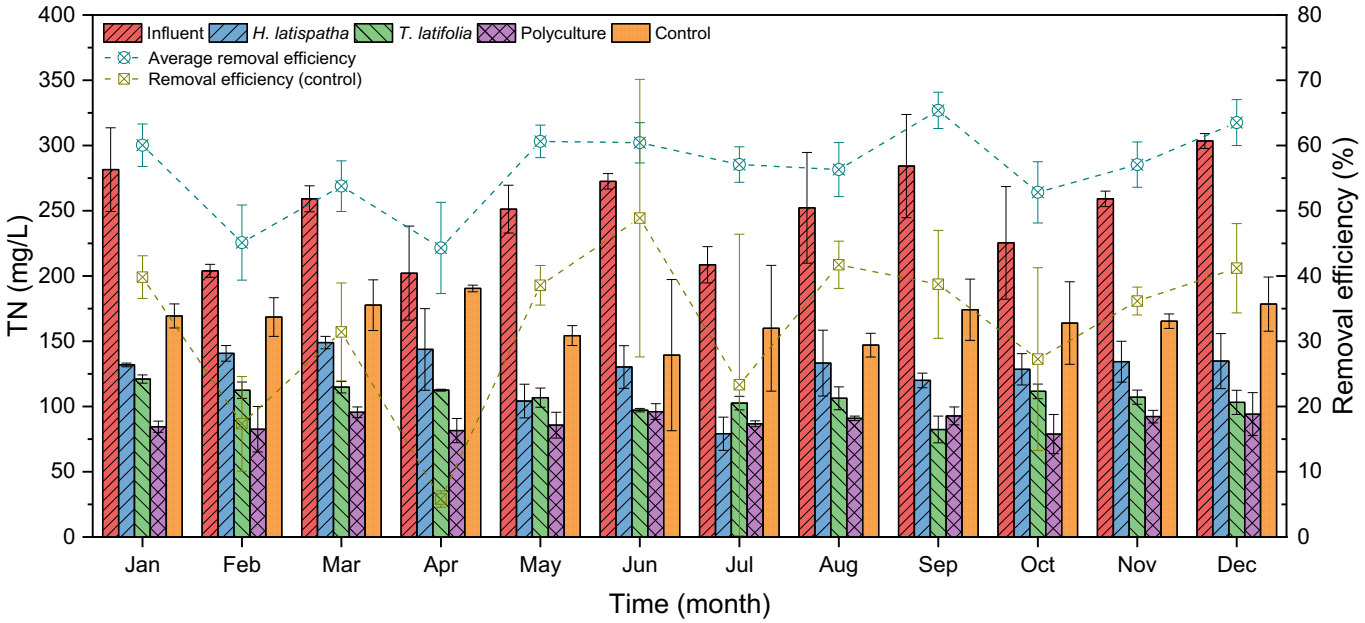

Figure 6. Concentrations at inlet, outlet, and removal efficiencies of TN in CWs

The results of this study highlight the effectiveness of CWs systems in eliminating TN, with superior performance in polyculture. The ability of *T. latifolia* to promote denitrification and its positive interaction with *H. latispatha* appear to be key factors in this effectiveness. In contrast, systems without plants (control) were significantly less efficient, highlighting the importance of plants as active components in constructed wetlands. These findings reinforce the importance of designing systems that optimize the combination of plant species to maximize the removal of pollutants in wastewater with high nitrogen content, such as that from slaughterhouses. The stability observed between years suggests that these systems can offer sustainable and reliable solutions for wastewater treatment.

In the current study, *T. latifolia* consistently showed higher TN removal efficiencies than *H. latispatha* during the evaluation period. *T. latifolia* achieved an efficiency of 57%, compared to 48% for *H. latispatha*, with effluent concentrations of 107 ± 2.374 mg/L and 127 ± 5.085 mg/L, respectively. These differences can be attributed to the ability of typical wetland plants such as *T. latifolia* to promote nitrification and denitrification processes in the rhizosphere, due to greater oxygenation and associated microbial activity. In contrast, ornamental plants, although contributing to TN removal, appear to be less efficient in promoting these key processes.

In reference studies, wetland plants such as *Typha latifolia*, *Cyperus papyrus*, and *Canna indica* have demonstrated greater TN removal capacity compared to systems using ornamental plants. For example, Michael *et al*. (2020), in a horizontal subsurface flow system with *Cyperus papyrus*, reported efficiencies of 97.6% for TN in slaughterhouse effluents, while Mohammed & Ismail (2021) achieved an efficiency of 90.2% using *Canna indica* in dairy wastewater. These values far exceed those achieved by *H. latispatha* in the present study.

In systems that use ornamental plants, such as those reported by Almeida-Naranjo *et al*. (2020) with *Heliconia stricta* in hybrid wetlands, TN removal was significantly lower, with values not exceeding 56%. This performance is comparable to that observed in the present study for *H. latispatha* (46–48%).

The difference in TN removal efficiency may be related to the functional characteristics of the plants. Wetland species, such as *T. latifolia*, are adapted to high humidity conditions and have extensive root systems that promote substrate oxygenation and stimulate bacterial activity, facilitating nitrification and denitrification processes. On the other hand, ornamental plants such as *H. latispatha*, although aesthetically attractive and useful in certain applications, have a lower capacity to contribute to these biological processes.

The results of this study, together with data reported in the literature, highlight the superiority of wetland plants over ornamental plants in TN removal. While *H. latispatha* may be useful in specific applications, wetland plants such as *T. latifolia* represent a more efficient option for wastewater treatment systems that require high nitrogen removal rates. These findings underscore the importance of selecting appropriate species based on treatment objectives and wastewater characteristics.

When comparing the results of this study with other technologies that do not use constructed wetlands, it is noteworthy that Tabelini *et al*. (2023) reported TN removal efficiencies of 75–80% when using activated sludge systems and anaerobic lagoons to treat wastewater from the dairy industry. Although these technologies exceed the efficiencies obtained in the present study, it is important to consider that wastewater from slaughterhouses tends to have higher concentrations of nitrogen and organic compounds, which could explain the lower efficiency of constructed wetland-based systems. In addition, activated sludge systems require more infrastructure and energy consumption, while constructed wetlands represent low-cost technologies.

Akarsu *et al*. (2021) achieved 78% efficiency in removing TN from slaughterhouse wastewater using electrocoagulation and electro flotation, resulting in significantly lower effluent concentrations. However, these technologies have limitations related to high operating costs and advanced technical requirements, which can make them unfeasible in rural or resource-constrained regions, where constructed wetlands represent a more sustainable alternative.

Studies such as those by Mkilima *et al*. (2022) and Meiramkulova *et al*. (2020) reported TN removal efficiencies of 98–99% in poultry slaughterhouse wastewater using nanofiltration membranes. Although these technologies produce high-quality effluents, their application in slaughterhouse wastewater faces challenges related to the pretreatment required to prevent membrane clogging, as well as the management of the concentrates generated. In contrast, constructed wetlands offer a simpler and more economical option, albeit with lower removal efficiencies.

Lopes *et al*. (2022) reported a 65% efficiency in TN removal in wastewater from poultry slaughterhouses using combined anaerobic–anoxic–aerobic reactors, an efficiency comparable to that obtained in the polyculture system in this study. However, combined reactors require greater monitoring and technical control, while constructed wetlands are more robust to variations in wastewater quality.

Although advanced technologies offer greater efficiencies in TN removal, constructed wetlands represent a more sustainable, economical, and adaptable alternative for treating slaughterhouse wastewater. The results of this study highlight the importance of polycultures as a strategy for optimizing TN removal, positioning constructed wetlands as a viable option for resource-constrained environments.

With regard to NH_4^+, NO_3^-, and NO_2^-, the results highlight significant differences in performance between the treatments and the control, underscoring the importance of plant species and their combinations in the removal of nitrogen compounds from slaughterhouse wastewater.

According to Figure 7, in the case of NH_4^+, polyculture systems showed the highest removal efficiency (89%), achieving the lowest effluent concentrations (18 mg/L). Systems with *T. latifolia* also demonstrated a high capacity for NH_4^+ removal (77%), significantly outperforming systems with *H. latispatha*, which achieved efficiencies of 65%.

The removal of NO_3^--N (Figure 8) followed a similar trend to that observed for NH_4^+, with polyculture being the most effective treatment, with efficiencies of 91% and effluent concentrations of 2 mg/L. Systems with *T. latifolia* (78%) outperformed systems with *H. latispatha* (68%), highlighting the superiority of typical wetland plants in nitrate treatment.

As shown in Figure 9, in the case of NO_2^-, polycultures also showed the highest removal capacity (92%), with effluent concentrations of 0.57 mg/L.

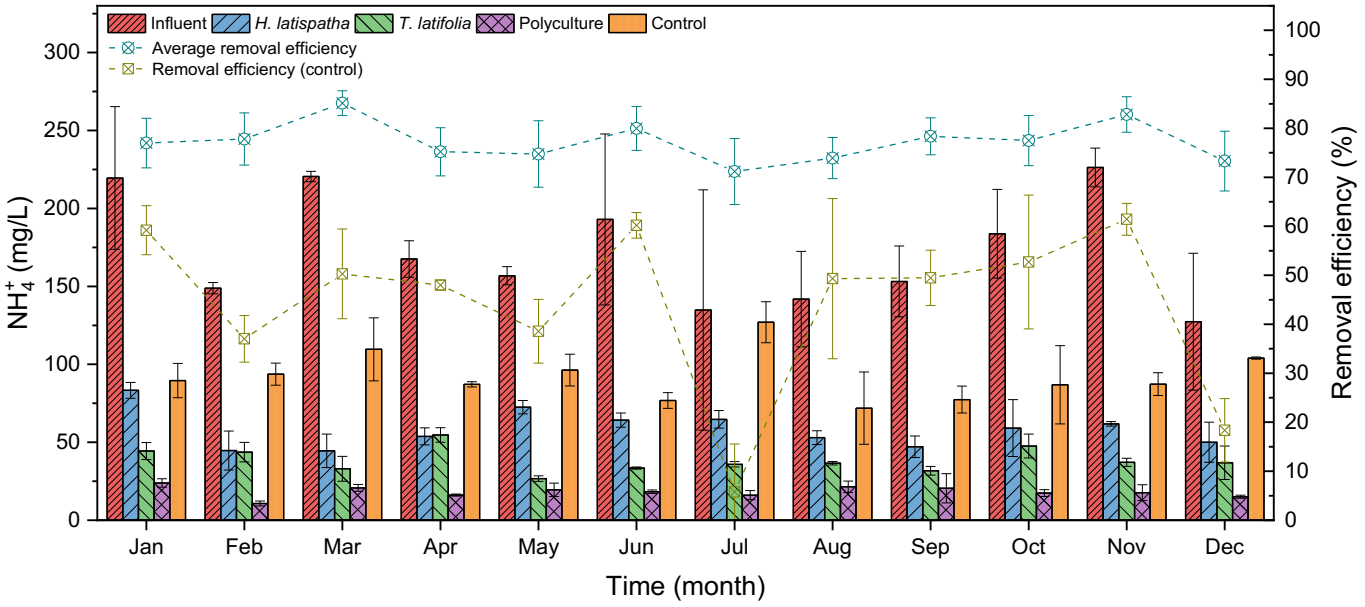

Figure 7. Inlet and outlet concentrations and removal efficiencies of NH_4^+ in CWs.

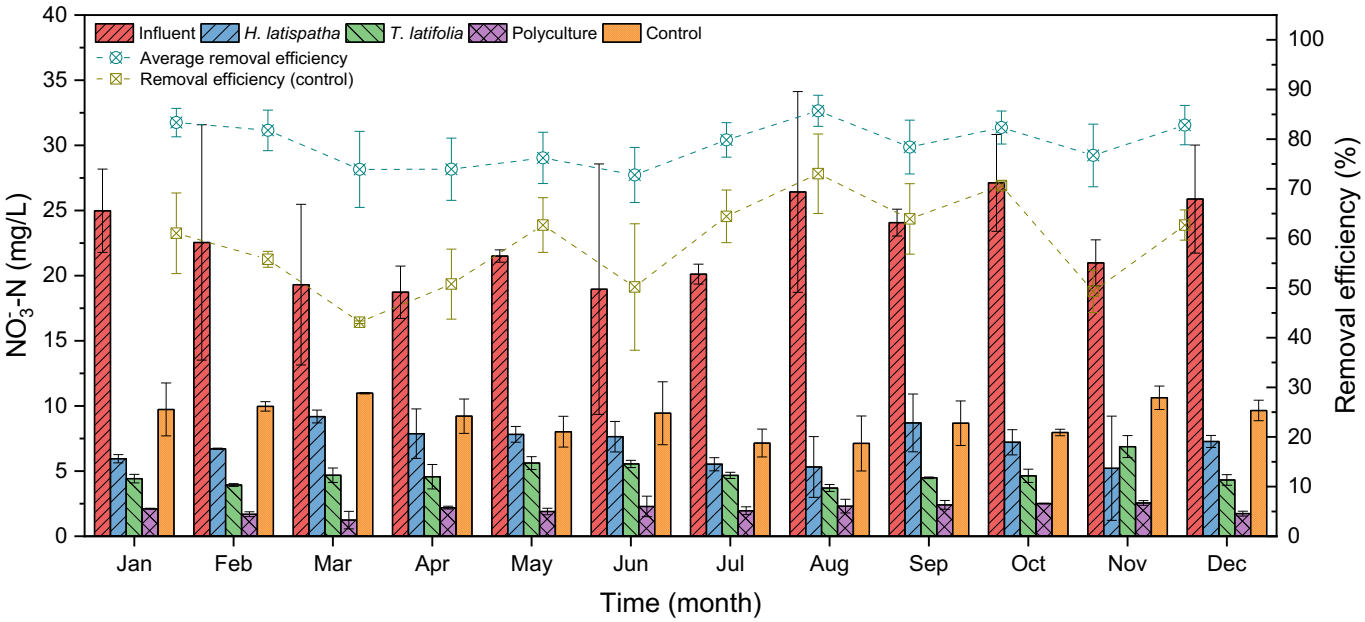

Figure 8. Inlet and outlet concentrations and removal efficiencies of NO_3^--N in CWs.

Systems with *T. latifolia* showed high removal efficiencies (82%), with effluent concentrations of 1.4 mg/L. Systems with *H. latispatha*, on the other hand, showed lower efficiencies (73%). No significant differences were observed across the study period for systems with the same treatment, indicating stability in the efficiency of constructed wetlands over time. However, significant differences were found between the different treatments in all cases, highlighting that polycultures were consistently superior in the removal of NH_4^+, NO_3^-–N, and NO_2^-–N.

The above results show that polycultures of *H. latispatha* + *T. latifolia* maximize the removal of nitrogen compounds in slaughterhouse wastewater, which could be attributed to the combination of plant absorption mechanisms and microbial activity facilitated by the roots. The superior capacity of *T. latifolia* compared to *H. latispatha* could be explained by its greater tolerance and adaptation to flooded and nutrient-rich environments.

When comparing the values in this study with those reported in other research on ornamental plants, it can be seen that the removal efficiencies of *H. latispatha* are lower than those of other ornamental species evaluated in effluent

treatment systems. For example, in the study by Madeira *et al*. (2022) in Portugal, an NH_4^+ removal efficiency of 72% was reported, which is higher than that obtained in this study. Additionally, Michael *et al*. (2020) reported an NH_4^+ removal efficiency of 97.4% in a system that used *Cyperus papyrus*, demonstrating significantly higher efficiency in wetland plants compared to ornamental plants.

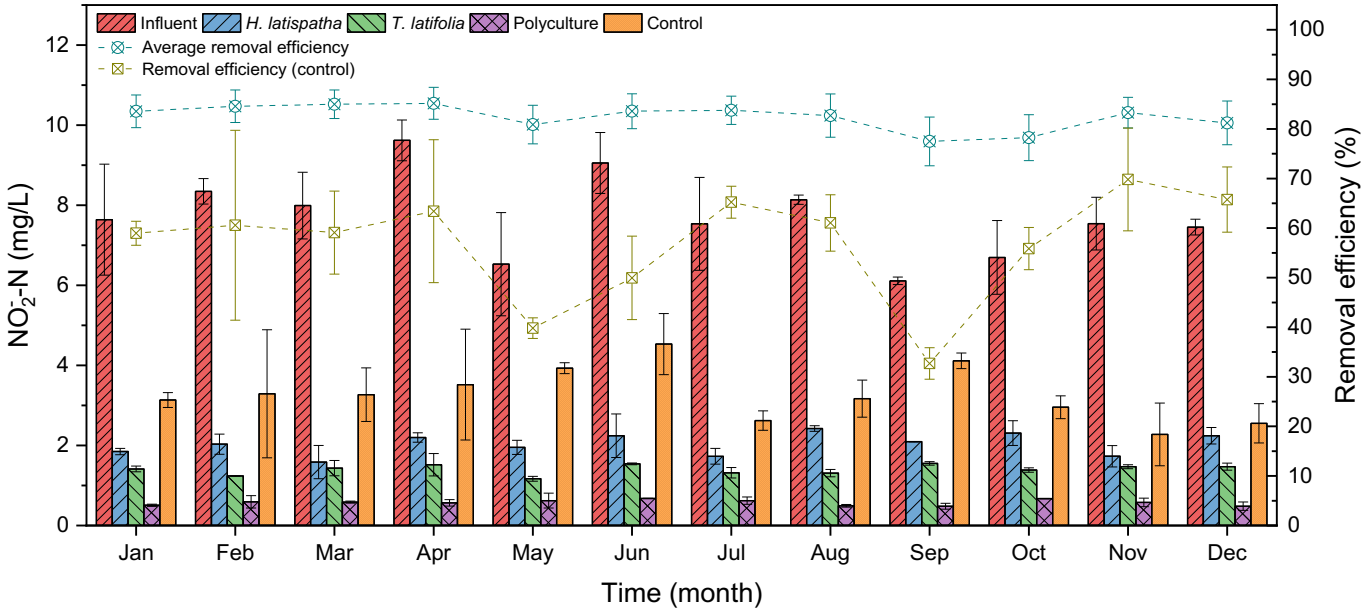

Figure 9. Concentrations at inlet, outlet, and removal efficiencies of NO_2^--N in CWs.

Regarding wetland plants, the removal efficiencies of *T. latifolia* in this study are close to the values reported by Galindo Montero *et al*. (2024) in Colombia, who documented NH_4^+ removal efficiencies of 89% in a horizontal subsurface wetland system with *Typha domingensis*. This suggests that wetland plants, such as *T. latifolia*, are more effective than ornamental plants in treating effluents. However, other studies, such as those by Suwerda *et al*. (2022), reported NH_4^+ removal efficiencies of 97.4%, indicating that some wetland species may be even more effective at removing these compounds.

Badejo *et al*. (2020) in Nigeria and Michael *et al*. (2020) in Tanzania also reported NO_3^--N removal efficiencies higher than those observed in this study. In particular, Michael *et al*. (2020) documented a NO_3^--N removal efficiency of 97.6%, higher than the values obtained for T. latifolia in this study (78%). This suggests that certain wetland species, such as *Cyperus papyrus*, perform better at removing NO_3^--N than *T. latifolia*.

The results obtained were compared with those reported in the literature for technologies that do not use constructed wetlands, with the aim of highlighting the advantages and limitations of wetlands in the treatment of this type of effluent. When comparing these results with those reported for technologies that do not use constructed wetlands, significant differences in pollutant removal capacity can be observed, although the efficiency of slaughterhouse wastewater treatment tends to be lower in systems without wetlands.

For example, Tabelini *et al*. (2023) in Brazil, using activated sludge systems and anaerobic lagoons, reported removal efficiencies of 70% for NH_4^+ and 64% for NO_3^-–N, values that are lower than those obtained in this study for *T. latifolia* (81% for NH_4^+ and 77% for NO_3^-–N). This indicates that the use of constructed wetlands may be more efficient than traditional biological systems, such as activated sludge systems, in the treatment of NH_4^+ and NO_3^-–N in slaughterhouse wastewater.

In addition, Michael *et al*. (2020) in Tanzania used a biodigester combined with a constructed wetland, reporting removal efficiencies of 97.4% for NH_4^+, 97.6% for NO_3^-–N, and 99.1% for NO_2^-–N. Although this combined system is highly efficient, the reported values are considerably higher than those obtained in this study. However, it is important to consider that the system evaluated by Michael *et al*. (2020) includes a biodigestion stage, which improves the

removal of NH_4^+ and other pollutants, which may explain the differences in the reported efficiencies. In the case of slaughterhouse wastewater, a system based solely on constructed wetlands, such as the one evaluated in this study, has a considerably lower efficiency but still offers advantages compared to technologies that do not incorporate this component.

On the other hand, in the study by Madeira *et al*. (2022) in Portugal, which used phytoremediation through vertical flow wetlands, an NH_4^+ removal efficiency of 72% was reported. This value is higher than that obtained in this study for *H. latispatha* (67%) and closer to that of *T. latifolia* (81%), suggesting that the type of wetland and the species used play a significant role in NH_4^+ removal efficiency. Furthermore, as this is a vertical flow wetland system, differences in performance may occur depending on the configuration and operating conditions of the systems.

Another key aspect to consider is the type of wastewater being treated. In this study, slaughterhouse wastewater is particularly complex, as it contains high concentrations of organic matter, suspended solids, and nutrients such as NH_4^+, which makes its treatment more challenging. Wetland plants such as *T. latifolia* are more effective in this type of water due to their ability to tolerate aquatic environments with high organic loads and their specialized nutrient absorption mechanisms. In contrast, technologies such as electrocoagulation and electro flotation, used by Akarsu *et al*. (2021) in Turkey, are effective for removing suspended solids and certain pollutants, but do not have the same capacity to efficiently remove nutrients such as NH_4^+ and NO_3^-–N, especially in slaughterhouse effluents. Electrocoagulation, for example, can remove up to 94% of COD; however, its performance in nutrient removal is limited, demonstrating a clear advantage of constructed wetland-based systems.

The results obtained in this study for the removal of NH_4^+, NO_3^--N, and NO_2^- using constructed wetlands with *H. latispatha* and *T. latifolia* are competitive with those reported for other technologies, especially in the treatment of slaughterhouse wastewater. Although activated sludge systems or combined biodigesters can achieve higher efficiencies in certain circumstances, constructed wetlands, as observed in this study, remain a viable and efficient option for the treatment of slaughterhouse effluents, with the added advantage of being natural and sustainable systems. Furthermore, the use of ornamental plants in combination with wetland plants in polyculture shows optimized performance in contaminant removal, which could be a key strategy for improving the efficiency of slaughterhouse wastewater treatment systems.

Conclusions

This study provides robust evidence on the effectiveness of constructed wetlands (CWs) as a sustainable and economical solution for treating slaughterhouse wastewater, with a special focus on the removal of nitrogenous pollutants such as TN, NH_4^+, NO_3^-, and NO_2^-. Through a rigorous experimental design, it was demonstrated that CWs, particularly those planted with *Typha latifolia* and *Heliconia latispatha*, are capable of achieving competitive removal efficiencies comparable to those of more expensive conventional technologies, such as activated sludge and electrocoagulation systems.

The research revealed that polyculture of *T. latifolia* and *H. latispatha* offered the highest efficiency in removing TN (64–65%) and NH_4^+ (89%), highlighting the synergy between the two species, which not only favored nutrient absorption but also supported key microbiological processes in the rhizosphere. Furthermore, comparative analysis with other studies and technologies showed that, although CWs do not achieve the removal levels of other advanced treatment technologies, such as nanofiltration membranes or combined biodigesters, their low cost, operational simplicity, and sustainability make CWsa viable option, especially in regions with limited resources.

The superior performance of *T. latifolia* in nitrogen removal, together with the good results obtained with *H. latispatha* in combination, underscores the importance of selecting plant species based on effluent characteristics and treatment objectives. These findings suggest that constructed wetlands can be an effective solution for the bioremediation of slaughterhouse wastewater, helping to mitigate the environmental impact of these effluents in an ecological and economical manner.

Finally, the results also highlight the importance of considering local climatic and environmental conditions in the design of CW systems, as factors such as temperature, solar radiation, and relative humidity significantly influence the

growth and performance of plant species. This study provides a useful foundation for future research that can further optimize CWsystems, expand their applicability to other industries and regions, and promote the use of nature-based solutions for wastewater treatment globally.

Hybrid constructed wetlands (horizontal and vertical flow) are recommended for treating slaughterhouse wastewater due to their greater capacity to promote nitrification and denitrification processes. It is also suggested to combine CWs with complementary technologies, such as biodigesters or anaerobic bioreactors, especially when dealing with wastewater with high organic load and high nitrogen concentrations, such as effluents from slaughterhouses. This combination can improve the overall efficiency of the system by addressing different types of pollutants and offering solutions for situations where CWs alone are not sufficient to comply with environmental regulations and standards.

Acknowledgments and Funding: We would like to thank the National Technological Institute of Mexico/Higher Technological Institute of Misantla, specifically the Wetlands and Environmental Sustainability Laboratory, for granting us permission to carry out the study, and the Secretariat of Science, Humanities, Technology, and Innovation (SECIHTI) for the scholarship awarded to carry out the doctoral studies. The Secretariat of Science, Humanities, Technology and Innovation (SECIHTI) granted financial support for the development of the project with code: CF-2023-I-2318: "EVALUATION OF THE USE OF NATURE-BASED TECHNOLOGIES FOR THE TREATMENT OF WASTEWATER PRODUCED IN MUNICIPAL SLAUGHTERHOUSES IN TROPICAL AREAS", in the 2023 Frontier Science Call, a project from which this research is derived.

Author contributions: J.C.-R.: writing, analysis and interpretation of data, conceptualization, design, data collection, supervision; G.E.N.-G.: funding acquisition; O.M.-P.: editing; J.A.-G.: conceptualization, supervision; M.S.H.: project administration; L.C.S.-H.: writing, provide materials, design, project administration, funding acquisition.

References

Agaton, C. B., & Guila, P. M. C. (2023). Ecosystem services valuation of constructed wetland as a nature-based solution to wastewater treatment. *Earth*, *4*(1), 78–92. https://doi.org/10.3390/earth4010006

Aguilar-Cortés, G., Martínez-Castellanos, G., Martínez-Reséndiz, G., Zamora-Castro, S. A., Monroy-Pineda, M. C., & Sandoval Herazo, L. C. (2025). Removal of glyphosate in agricultural runoff using subsurface constructed wetlands in monocultures and polycultures of tropical plants. *Processes*, *13*(3), 860. https://doi.org/10.3390/pr13030860

Akarsu, C., Deveci, E. Ü., Gönen, Ç., & Madenli, Ö. (2021). Treatment of slaughterhouse wastewater by electrocoagulation and electroflotation as a combined process: process optimization through response surface methodology. *Environmental Science and Pollution Research*, *28*(26), 34473–34488. https://doi.org/10.1007/s11356-021-12855-4

Almeida-Naranjo, C. E., Guachamín, G., Guerrero, V. H., & Villamar, C.-A. (2020). Heliconia stricta Huber behavior on hybrid constructed wetlands fed with synthetic domestic wastewater. *Water*, *12*(5), 1373. https://doi.org/10.3390/w12051373

Amiri, K., Bekkari, N. eddine, Debbakh, A. E., Chaib, W., & Kherifi, W. (2022). Urban wastewater treatment by pilot-scale vertical subsurface flow constructed wetland planted with *Typha latifolia* and *Phragmite australis* under arid climate. *Water, Air, & Soil Pollution*, *233*(8), 345. https://doi.org/10.1007/s11270-022-05802-7

APHA/AWWA/WEF. (2012). *Standard methods for the examination of water and wastewater*. https://doi.org/https://doi.org/ISBN9780875532356

Badejo, A. A., Ndambuki, J. M., Kupolati, W. K., & Adeyemo, S. (2020). EVALUATION OF TWO-STAGE SUBSURFACE FLOW CONSTRUCTED WETLANDS FOR ABATTOIR. 101–111.

Banc, C., Gautier, M., Blanc, D., Lupsea-Toader, M., Marsac, R., & Gourdon, R. (2021). Influence of pH on the release of colloidal and dissolved organic matter from vertical flow constructed wetland surface sludge deposits. *Chemical Engineering Journal*, *418*, 129353. https://doi.org/10.1016/j.cej.2021.129353

Bazrafshan, E., Zakeri, H. R., Vieira, M. G. A., Derakhshan, Z., Mohammadi, L., Mohammadpour, A., & Mousavi Khaneghah, A. (2022). Slaughterhouse wastewater treatment by integrated chemical coagulation and electro-Fenton processes. *Sustainability*, *14*(18), 11407. https://doi.org/10.3390/su141811407

Boukouvalas, C., Kekes, T., Oikonomopoulou, V., & Krokida, M. (2024). Life cycle assessment of energy production from solid waste valorization and wastewater purification: A case study of meat processing industry. *Energies*, *17*(2), 487. https://doi.org/10.3390/en17020487

Brennan, B., Lawler, J., & Regan, F. (2021). Recovery of viable ammonia–nitrogen products from agricultural slaughterhouse wastewater by membrane contactors: a review. *Environmental Science: Water Research & Technology*, *7*(2), 259–273. https://doi.org/10.1039/D0EW00960A

Faisal, A. A. H., Taha, D. S., Hassan, W. H., Lakhera, S. K., Ansar, S., & Pradhan, S. (2023). Subsurface flow constructed wetlands for treating of simulated cadmium ions-wastewater with presence of *Canna indica* and *Typha domingensis*. *Chemosphere*, *338*, 139469. https://doi.org/10.1016/j.chemosphere.2023.139469

Fang, Y., Wang, H., Han, J., Li, Z., & Wang, A. (2022). Enhanced nitrogen removal of constructed wetlands by coupling with the bioelectrochemical system under low temperature: Performance and mechanism. *Journal of Cleaner Production*, *350*, 131365. https://doi.org/10.1016/j.jclepro.2022.131365

Fatima, F., Du, H., & Kommalapati, R. R. (2021). Treatment of poultry slaughterhouse wastewater with membrane technologies: A review. *Water*, *13*(14), 1905. https://doi.org/10.3390/w13141905

Galindo Montero, A. A., Berrio Arrieta, Y. M., & Pimienta Serrano, E. V. (2024). Treatment of slaughterhouse wastewater through a series system: Upflow anaerobic reactor and artificial wetland. *Water*, *16*(5), 700. https://doi.org/10.3390/w16050700

Haldan, K., Köhn, N., Hornig, A., Wichmann, S., & Kreyling, J. (2022). Typha for paludiculture—Suitable water table and nutrient conditions for potential biomass utilization explored in mesocosm gradient experiments. *Ecology and Evolution*, *12*(8). https://doi.org/10.1002/ece3.9191

Herazo, L. C. S., Zurita, F., Nani, G., Del Ángel-Coronel, O. A., & Aguilar, F. A. A. (2021). Treatment of swine effluent mixed with domestic wastewater and vegetation development in monoculture and polyculture horizontal subsurface flow wetlands. *Ecological Engineering*, *173*, 106432. https://doi.org/10.1016/j.ecoleng.2021.106432

Hu, X., Xie, H., Zhuang, L., Zhang, J., Hu, Z., Liang, S., & Feng, K. (2021). A review on the role of plant in pharmaceuticals and personal care products (PPCPs) removal in constructed wetlands. *Science of The Total Environment*, *780*, 146637. https://doi.org/10.1016/j.scitotenv.2021.146637

Jagtap, A. Y., Jadhav, P. R., Safeena, S. A., Solanke, A. U., Pagariya, M. C., Prasad, K. V., & Kawar, P. G. (2024). Integrating molecular and phenotypic approaches to assess genetic diversity in Heliconia genotypes. *Genetic Resources and Crop Evolution*. https://doi.org/10.1007/s10722-024-02264-0

Lopes, C. L., de Assis, T. M., Passig, F. H., Lima Model, A. N. de, Mees, J. B. R., Cervantes, F. J., Gotardo, J. T., & Gomes, S. D. (2022). Nitrogen removal from poultry slaughterhouse wastewater in anaerobic-anoxic-aerobic combined reactor: Integrated effect of recirculation rate and hydraulic retention time. *Journal of Environmental Management*, *303*, 114162. https://doi.org/10.1016/j.jenvman.2021.114162

Madeira, L., Carvalho, F., Ribau Teixeira, M., & Almeida, A. (2022). Phytoremediation as a sustainable alternative for organic matter removal from slaughterhouse wastewater pretreated by immediate one-step lime precipitation. *KnE Materials Science*. https://doi.org/10.18502/kms.v7i1.11621

Malakar, M., & Biswas, S. (2022). Heliconias: dramatic flowers of the tropics and subtropics. En *Floriculture and Ornamental Plants* (pp. 729–776). Springer Nature Singapore. https://doi.org/10.1007/978-981-15-3518-5_26

McCalla, L. B., Phillips, B. M., Anderson, B. S., Voorhees, J. P., Siegler, K., Faulkenberry, K. R., Goodman, M. C., Deng, X., & Tjeerdema, R. S. (2022). Effectiveness of a constructed wetland with carbon filtration in reducing pesticides associated with agricultural runoff. *Archives of Environmental Contamination and Toxicology*, *82*(3), 317–329. https://doi.org/10.1007/s00244-021-00909-0

Meiramkulova, K., Devrishov, D., Zhumagulov, M., Arystanova, S., Karagoishin, Z., Marzanova, S., Kydyrbekova, A., Mkilima, T., & Li, J. (2020). Performance of an integrated membrane process with electrochemical pre-treatment on poultry slaughterhouse wastewater purification. *Membranes*, *10*(10), 256. https://doi.org/10.3390/membranes10100256

Meng, T., Cheng, W., & Li, D. (2024). Effects of ammonium/nitrate ratios on plant growth and nitrogen and phosphorus removal in an ecological floating bed system. *Chemistry and Ecology*, 1–15. https://doi.org/10.1080/02757540.2024.2432910

Michael, S., Paschal, C., Kivevele, T., Rwiza, M. J., & Njau, K. N. (2020). Performance investigation of the slaughterhouse wastewater treatment facility: a case of Mwanza City Slaughterhouse, Tanzania. *Water Practice and Technology*, *15*(4), 1096–1110. https://doi.org/10.2166/wpt.2020.085

Mkilima, T., Bazarbayeva, T., Assel, K., Nurmukhanbetova, N., Ostretsova, I., Khamitova, A., Makhanova, S., & Sergazina, S. (2022). Pore size in the removal of phosphorus and nitrogen from poultry slaughterhouse wastewater using polymeric nanofiltration membranes. *Water*, *14*(18), 2929. https://doi.org/10.3390/w14182929

Mohammed, N. A., & Ismail, Z. Z. (2021). Green sustainable technology for biotreatment of actual dairy wastewater in constructed wetland. *Journal of Chemical Technology & Biotechnology*, *96*(5), 1197–1204. https://doi.org/10.1002/jctb.6631

Patil, R., Zahid, M., Govindwar, S., Khandare, R., Vyavahare, G., Gurav, R., Desai, N., Pandit, S., & Jadhav, J. (2022). Constructed wetland: a promising technology for the treatment of hazardous textile dyes and effluent. En *Development in Wastewater Treatment Research and Processes* (pp. 173–198). Elsevier. https://doi.org/10.1016/B978-0-323-85583-9.00016-8

Phan, M. N., Nhi Tran, N. Van, Yu, J., & Nguyen, T. P. (2020). Treatment of ammonium in slaughterhouse wastewater by UASB technology combined with EGSB using anammox and PVA gel. *Vietnam Journal of Science, Technology and Engineering*, *62*(1), 85–89. https://doi.org/10.31276/VJSTE.62(1).85-89

Sánchez, M., Gonzalo, O. G., Yáñez, S., Ruiz, I., & Soto, M. (2021). Influence of nutrients and pH on the efficiency of vertical flow constructed wetlands treating winery wastewater. *Journal of Water Process Engineering*, *42*, 102103. https://doi.org/10.1016/j.jwpe.2021.102103

Sandoval-Herazo, M., Martínez-Reséndiz, G., Fernández Echeverria, E., Fernández-Lambert, G., & Sandoval Herazo, L. C. (2021). Plant biomass production in constructed wetlands treating swine wastewater in tropical climates. *Fermentation*, *7*(4), 296. https://doi.org/10.3390/fermentation7040296

Sesin, V., Davy, C. M., & Freeland, J. R. (2021). Review of *Typha* spp. (cattails) as toxicity test species for the risk assessment of environmental contaminants on emergent macrophytes. *Environmental Pollution*, *284*, 117105. https://doi.org/10.1016/j.envpol.2021.117105

Silveira, N. C., Oliveira, G. H. D., Damianovic, M. H. R. Z., & Foresti, E. (2021). Two-stage partial nitrification-Anammox process for nitrogen removal from slaughterhouse wastewater: Evaluation of the nitrogen loading rate and microbial community analysis. *Journal of Environmental Management*, *296*, 113214. https://doi.org/10.1016/j.jenvman.2021.113214

Singh, S., & Chakraborty, S. (2021). Bioremediation of acid mine drainage in constructed wetlands: Aspect of vegetation (*Typha latifolia*), loading rate and metal recovery. *Minerals Engineering*, *171*, 107083. https://doi.org/10.1016/j.mineng.2021.107083

Stefanatou, A., Schiza, S., Petousi, I., Rizzo, A., Masi, F., Stasinakis, A. S., Fyllas, N., & Fountoulakis, M. S. (2023). Use of climbing and ornamental plants in vertical flow constructed wetlands treating greywater. *Journal of Water Process Engineering*, *53*, 103832. https://doi.org/10.1016/j.jwpe.2023.103832

Suwerda, B., Kasjono, H., Haryanti, S., & Yushananta, P. (2022). Poultry slaughterhouse wastewater treatment using combine anaerobic filter with constructed wetland methods. *Open Access Macedonian Journal of Medical Sciences*, *10*(E), 611–617. https://doi.org/10.3889/oamjms.2022.8741

Tabelini, D. B., Lima, J. P. P., Borges, A. C., & Aguiar, A. (2023). A review on the characteristics and methods of dairy industry wastewater treatment in the state of Minas Gerais, Brazil. *Journal of Water Process Engineering*, *53*, 103779. https://doi.org/10.1016/j.jwpe.2023.103779

Taha, S. Y., Almansoory, A. F., Al-Baldawi, I. A., Abdullah, S. R. S., Ismail, N. 'Izzati, Hazaimeh, M., & Sharuddin, S. S. N. (2023). Hybrid constructed wetland for treatment of power plant effluent polluted with hydrocarbons. *Journal of Water Process Engineering*, *56*, 104372. https://doi.org/10.1016/j.jwpe.2023.104372

Teo, C. J., Karkou, E., Vlad, O., Vyrkou, A., Savvakis, N., Arampatzis, G., & Angelis-Dimakis, A. (2023). Life cycle environmental impact assessment of slaughterhouse wastewater treatment. *Chemical Engineering Research and Design*, *200*, 550–565. https://doi.org/10.1016/j.cherd.2023.11.016

Waly, M. M., Ahmed, T., Abunada, Z., Mickovski, S. B., & Thomson, C. (2022). Constructed wetland for sustainable and low-cost wastewater treatment: Review article. *Land*, *11*(9), 1388. https://doi.org/10.3390/land11091388

Wang, Y., Wang, F., Fang, Y., Fu, Y., & Chen, N. (2024). Storm-induced nitrogen transport via surface runoff, interflow and groundwater in a pomelo agricultural watershed, southeast China. *Environmental Pollution*, *346*, 123629. https://doi.org/10.1016/j.envpol.2024.123629

Wasko, J. D., McGonigle, T. P., Goldsborough, L. G., Wrubleski, D. A., Badiou, P. H., & Armstrong, L. M. (2022). Use of shoot dimensions and microscopic analysis of leaves to distinguish *Typha latifolia*, *Typha angustifolia*, and their invasive hybrid *Typha xglauca*. *Wetlands Ecology and Management*, *30*(1), 19–33. https://doi.org/10.1007/s11273-021-09836-2

Yu, G., Wang, G., Chi, T., Du, C., Wang, J., Li, P., Zhang, Y., Wang, S., Yang, K., Long, Y., & Chen, H. (2022). Enhanced removal of heavy metals and metalloids by constructed wetlands: A review of approaches and mechanisms. *Science of The Total Environment*, *821*, 153516. https://doi.org/10.1016/j.scitotenv.2022.153516

Optimization of mixing in agitated reactors: A CFD-based approach for energy efficiency and dispersion in biphasic systems

José Alfredo Parra-Reyes [*], Isaac Salvador Cuevas Sosa, Adrián López Yáñez, Rafael Alejandro Ángel Cuapio, and Gastón Martínez-de-Jesús

[1] División de Ingeniería Química y Bioquímica, Tecnológico Nacional de México/ TES de Ecatepec, Av. Tecnológico S/N, Colonia. Valle de Anáhuac, Ecatepec de Morelos, C. P. 55210, Estado de México. México.
* Corresponding author: jalfred.parra.r.1@gmail.com; Tel.: +525567576919

Received: August 23, 2025 Accepted: October 2, 2025 Published: March 19, 2026
DOI: https://doi.org/10.56845/rebs.v8i1.675

Abstract: A Computational Fluid Dynamics (CFD) study was conducted to simulate the hydrodynamic behavior of a Norstone-type high-shear impeller operating in a stirred unbaffled tank containing a biphasic system (glycerin-hexane). A transient, multiphase Eulerian-Eulerian approach was implemented in ANSYS Fluent under laminar flow conditions. The model captured the formation of four distinct recirculation loops and identified zones of high-energy dissipation at the impeller blades, which are critical for the dispersion of the secondary phase. Experimental validation was conducted using temperature sensors (Max6675 thermocouples) connected to an Arduino Uno; good agreement between simulated and measured temperatures was observed. This work provides a validated CFD framework and fundamental insight into the flow dynamics, establishing a solid foundation for optimizing impeller geometry and operating conditions to achieve greater mixing homogeneity and energy efficiency in industrial biphasic systems**.**

Keywords: CFD, high-shear impeller, mixing efficiency, laminar flow, Euler–Euler model

Introduction

Optimizing industrial processes is a key strategy for enhancing operational efficiency and reducing environmental impact by rationalizing energy and resource use. In this context, stirred reactors, widely used in the pharmaceutical, chemical, and biotechnological industries, require a thorough analysis of their geometry, operating conditions, and governing hydrodynamics. Key hydrodynamic variables such as turbulent kinetic energy (TKE), velocity fields, circulation patterns, energy dissipation rates, and mixing times are essential for evaluating their performance and are necessary for assessing dispersion quality and system homogenization (Oshinowo L. & Marshall E., 2001).

Computational Fluid Dynamics (CFD) facilitates the analysis and optimization of these parameters through numerical simulations, reducing the need for extensive experimental studies. This approach provides a robust quantitative basis for improving mixing performance, optimizing energy consumption, and establishing reliable scale-up strategies (Stuparu *et al*., 2021). Moreover, its implementation can support the development of technologies aligned with circular economy principles, such as the valorization of agro-industrial residues to obtain high-value products (Obando-Galicia Y., 2024).

The thorough analysis of hydrodynamic variables using CFD has become a high-impact engineering tool, indispensable for the design and operation of efficient and sustainable mixing systems. This methodology is rooted in solving a model based on the conservation equations of mass and momentum, which form a coupled system of nonlinear partial differential equations. Since analytical solutions are possible only for highly simplified cases, CFD provides reliable approximations for complex engineering problems through specialized software, enabling the detailed analysis of hydrodynamic variables. The CFD approach applies the finite volume method to discretize the differential equations and transform them into a system of algebraic equations that can be solved using iterative methods (Andersson, 2012). The equations that describe the behavior of a multiphase system are the continuity equation (Eq. 1) and the momentum transfer equation (Eq. 2).

$$\frac{\partial}{\partial t}\left(\alpha_q \rho_q\right) + \nabla \cdot \left(\alpha_q \rho_q \vec{v}_q\right) = \sum_{p=1}^{n}\left(\dot{m}_{pq} - \dot{m}_{qp}\right) + S_q \quad \textbf{(1)}$$

$$\frac{\partial}{\partial t}\left(\alpha_q \rho_q \vec{v}_q\right) + \nabla \cdot \left(\alpha_q \rho_q \vec{v}_q \vec{v}_q\right) = -\alpha_q \nabla \mathrm{p} + \nabla \cdot \bar{\bar{\tau}}_q + \alpha_q \rho_q \vec{g} + \sum_{p=1}^{n}\left(\vec{R}_{pq} + \dot{m}_{pq}\vec{v}_{pq} - \dot{m}_{qp}\vec{v}_{qp}\right) + \left(\vec{F_q} + \vec{F}_{lift,q} + \vec{F}_{vm,q}\right) \quad \textbf{(2)}$$

where the stress tensor of each phase, $\bar{\bar{\tau}}_q$, is expressed by

$$\overline{\overline{\tau_q}} = \alpha_q \mu_q \left(\nabla \vec{v}_q + \nabla \vec{v}_q^T\right) + \alpha_q \left(\lambda_q - \frac{3}{2}\mu_q\right) \nabla \cdot \vec{v}_q \bar{\bar{\mathrm{I}}} \quad \textbf{(3)}$$

Here, α_q is thephase volume fraction, $\vec{v}_q$represents the velocity, ρ_q is the density of phase q; $\dot{m}_{pq}$and $\dot{m}_{qp}$denote the mass transfer terms between phases p and q. The coefficients $\mu_q$and $\lambda_q$correspond to the shear viscosity and the apparent viscosity of each phase, respectively. The q^{th} phase is subjected to several forces, including the external force $\vec{F}_q$, the lift force $\vec{F}_{lift,q}$, and the virtual mass force $\vec{F}_{vm,q}$. In addition, interphase interactions are governed by the interfacial force $\vec{R}_{pq}$, which depends on effects such as friction, pressure, and cohesion, and satisfies the symmetrical conditions $\vec{R}_{pq} = -\vec{R}_{qp}$and $\vec{R}_{qq} = 0$. All phases share the same pressure p, and the interfacial velocity between phases is denoted by $\vec{v}_{pq}$.

The energy conservation equation is incorporated, as given by Eq. 4.

$$\frac{\partial}{\partial \partial}(\rho E) + \nabla \cdot \left(\vec{v}(\rho E + p)\right) = \nabla \cdot \left(k_{eff} \nabla \mathrm{T} - \sum_q \sum_j h_{j,q} \vec{J}_{j,q} + \left(\bar{\bar{\tau}}_{eff} \cdot \vec{v}\right) \right) + s_h \quad \textbf{(4)}$$

where k_{eff} is the effective thermal conductivity $(k + k_t$, where k_t is the turbulent thermal conductivity defined according to the selected turbulence model), and $\vec{J}_j$ is the diffusion flux of species j. The first three terms on the right-hand side of Eq. (4) correspond to energy transfer by conduction, species diffusion, and viscous dissipation, respectively. S_h includes the volumetric heat source previously defined in the model.

In Eq. 5,

$$E = h - \frac{p}{\rho} + \frac{v^2}{2} \quad \textbf{(5)}$$

where sensible enthalpy h is defined for incompressible flows as

$$h = \sum_j Y_j h_j + \frac{p}{\rho} \quad \textbf{(6)}$$

Y_j is the mass fraction of species *j* and

$$h_j = \int_{T_{ref}}^{T} C_{p,j}\, dT \quad \textbf{(7)}$$

(ANSYS, 2016).

In this study, CFD approach was used to characterize the hydrodynamics of biphasic mixing systems, evaluating key parameters to guide the optimization of industrial reactor design and operation.

Materials and Methods

*T*he mixing system consisted of a high a shear impeller (Norstone® model, Norstone Inc., PA), based on the patent by Steinmetz (1993) and an unbaffled flat-bottomed glass tank. The dimensions of the impeller were diameter (D) of 49 mm, height (h) of 6 mm, and groove diameter of 3 mm, as shown in Figure 1a. The mixing tank had a diameter (T) of

142 mm. The impeller was set at a C/T ratio of 0.73, where C is the distance from the bottom of the tank to the impeller center (Figure 1b).

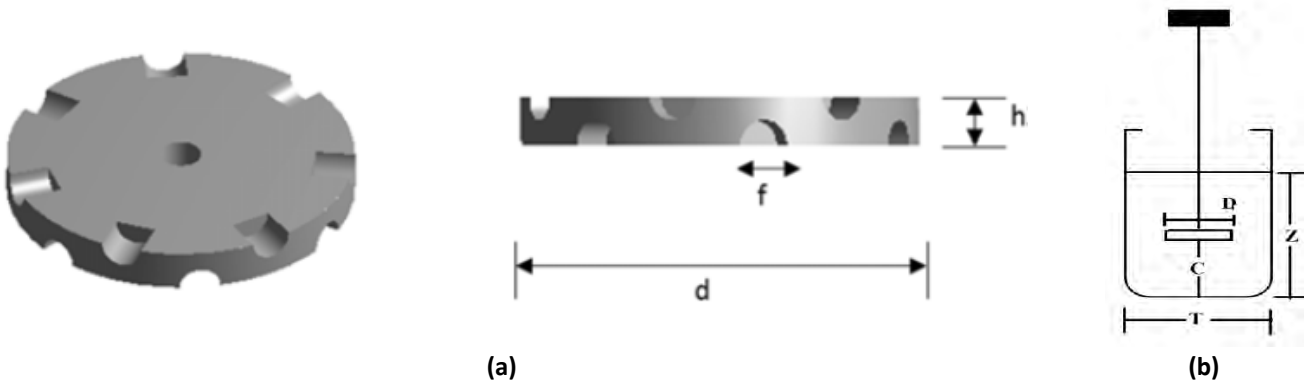

Figure 1. (a) Geometry impeller, (b) Geometry reactor

The stirred tank was modeled using ANSYS Fluent v. 2024 R1 (Student) (ANSYS, Inc., 2024). The geometry was generated in the DesignModeler module, and the computational mesh was built in the Meshing module, both in ANSYS Workbench. The model solved the governing conservation equations for mass and momentum. The simulations were performed on a laptop with an Intel Core i5-13420H processor running at 2.10 GHz, 16 GB of RAM, and an NVIDIA GeForce RTX 4050 graphics card.

The simulation was performed under transient conditions with a time step of 0.001 s. To represent the multiphase nature of the system, the Eulerian–Eulerian model was employed under a laminar flow formulation. The impeller rotation was simulated using the Multiple Reference Frame (MRF) approach. In this approach, the rotating region is approximated as a quasi-steady state to obtain the mean rotational field at a lower computational cost (Deglon & Meyer, 2006). It should be noted that, due to its inherent limitations, the MRF approach does not reproduce transient rotor–stator interactions; therefore, the reported quantities must be interpreted as averages or approximations of the rotational field in a pseudo-steady regime. The region surrounding the impeller (RRF), a cylinder of radius 35 mm and height of 16 mm, was assumed to rotate at 280 RPM. A standard pressure–velocity coupling scheme was used, together with the QUICK discretization scheme. The shaft and the impeller were considered rotating walls at the same velocity as RRF. The no-slip condition was applied to the tank wall.

For experimental validation, two temperature sensors (Max6675 thermocouples) were connected to an Arduino Uno microcontroller. The sensors were installed on the inner tank walls at two different heights: Sensor 1 at 45 mm and Sensor 2 at 115 mm from the bottom. Validation was performed by comparing simulation results with experimental data using temperature-versus-time graphs. The working fluid was glycerin at 23 °C; its viscosity (1.2 Pa·s) was determined using an MCR 72 Anton Paar rheometer, and its density (1260 kg m^{-3}) was determined by using a graduated cylinder and an analytical balance. Hexane at 50 °C was used as the second phase at a mass fraction of 20%.

Results and Discussion

The temperature evolution during the initial seconds of the process was analyzed experimentally, as this stage exhibits the highest rate of heat transfer. This behavior was then compared with the results obtained from the CFD simulations, as shown in Figure 2. The differences between the curves obtained from the simulations and those measured experimentally were minimal, suggesting that the CFD model accurately reproduces the observed thermal behavior. Jadhav and Barigou (2022) studied a 3D Eulerian-Lagrangian CFD model to simulate the turbulent flow and mixing of coarse dense particles in a standard batch vessel, mechanically agitated by a down-pumping pitched-blade turbine. Their numerical results were experimentally validated using positron emission particle tracking. Both datasets show very good agreement. Our results suggest that it is possible to validate CFD results with simple techniques.

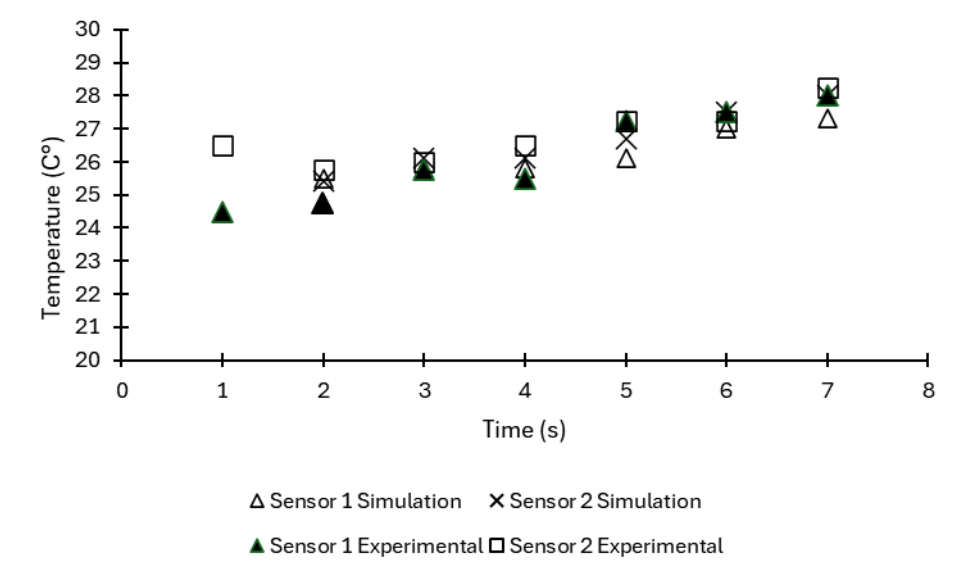

Figure 2. Comparison of experimental and simulated temperature profiles

In Figure 3a, the normalized velocity field $\boldsymbol{u}/\boldsymbol{u}_{\text{tip}}$ is shown in the mid-plane of the tank for the continuous phase (glycerin). The highest velocity magnitudes are concentrated in the immediate vicinity of the impeller, reflecting the transfer of mechanical energy from the impeller to the fluid. It is important to note that high-speed regions also coincide with high shear stress and viscous dissipation, which together produce intense local mixing (Martínez-de Jesús *et al*., 2018).

Figure 3b shows the flow pattern, where four main recirculation loops generated by the radial discharge of the impeller are clearly distinguished: two located in the upper region and two in the lower region. These patterns are characteristic of an impeller operating in the laminar flow regime. Identifying these vortices and recirculation zones not only provides insight into the internal hydrodynamics of the reactor but also establishes a solid foundation for optimizing operating conditions and guiding the design of more efficient stirred reactors.

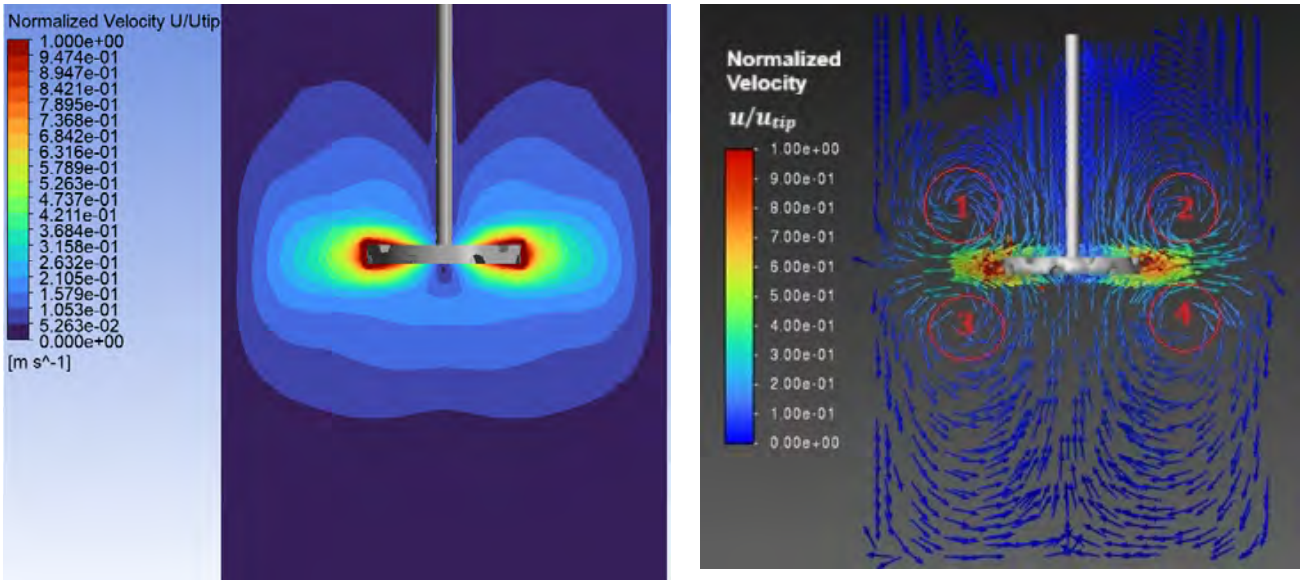

(a) **(b)**

Figure 3. (a) Normalized velocity field of the entire reactor for the continuous phase (glycerin), (b) Normalized velocity vectors of the entire reactor for the continuous phase (glycerin)

Figure 4 depicts the evolution of the dispersed phase over time. The impeller surface is shown to be the primary site for hexane dispersion. Figure 5 shows the contour of the laminar viscous dissipation. The highest values (in red) are

concentrated around the impeller blades, particularly along the leading edges and in regions of greater curvature. This indicates that, in these areas, the mechanical energy supplied by the impeller is primarily converted into heat through shear stresses. In contrast, the regions between the blades and toward the central axis exhibit minimal dissipation (blue tones), demonstrating that the laminar contribution outside the impeller boundary layer is negligible. This information helps assess mixing efficiency, identify potential recirculation zones, and understand the initial generation of hydrodynamic instabilities. It also provides a basis for guiding improvements to the impeller and agitation system, promoting a more uniform distribution of energy throughout the reactor.

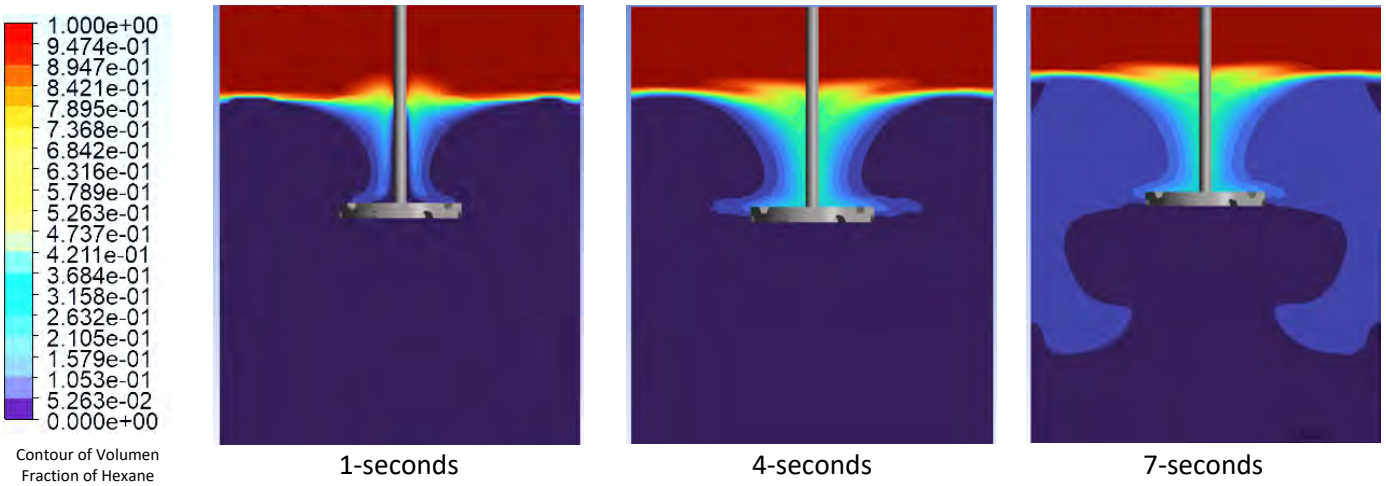

Figure 4. Phase contours corresponding to the dispersed phase (hexane)

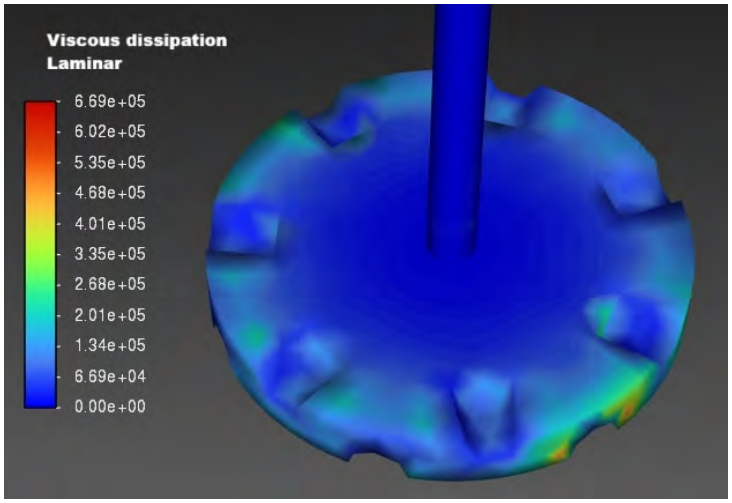

Figure5. Contours of laminar viscous dissipation

Conclusions

Computational Fluid Dynamics (CFD) simulations were utilized to characterize the hydrodynamic behavior of a Norstone-type high-shear impeller operating in a biphasic system. The analysis provided valuable insights into velocity fields, phase contours, and viscous dissipation contours, which are essential for understanding the dispersion of the secondary phase. The highest values for these parameters were observed in regions located near the impeller. To validate the numerical model, experimental temperature data were collected from strategically placed sensors. The strong agreement between the simulation results and the experimental data not only confirms the flow patterns predicted by the simulations but also validates the observed thermal variations. This combined approach of simulation and experimental analysis serves as a solid foundation for optimizing operating parameters in industrial processes. Consequently, these findings provide valuable insights for enhancing mixing efficiency in agitated tank systems handling biphasic flows, enabling more effective energy utilization and reduced processing times.

Acknowledgments and Funding: Gastón Martínez de Jesús and Adrián López Yáñez thank the support of COMECYT (Apoyo para estancias de investigación 2025)

Author contributions: J.A.P.-R.: writing – original draft, validation, investigation, formal analysis, conceptualization; A.L.Y.: writing – review & editing, investigation; R.A.A.C., M.I.N.-G. and A.M.-G.: writing – review & editing. G.M.-d.J.: writing – validation, investigation, formal analysis, conceptualization.

References

Andersson, B. (2012). *Computational fluid dynamics for engineers*. Cambridge University Press.

ANSYS, Inc. (2016). *ANSYS Fluent theory guide (Release 2016 R2)*.

ANSYS, Inc. (2024). *Ansys for students*. Ansys. https://www.ansys.com/academic/students

Deglon, D. A., & Meyer, C. J. (2006). CFD modelling of stirred tanks: Numerical considerations. *Minerals Engineering*, *19*(10), 1059–1068. https://doi.org/10.1016/j.mineng.2006.04.001

Jadhav, A. J., & Barigou, M. (2022). Eulerian–Lagrangian modelling of turbulent two-phase particle–liquid flow in a stirred vessel: CFD and experiments compared. *International Journal of Multiphase Flow*, *155*, 104191. https://doi.org/10.1016/j.ijmultiphaseflow.2022.104191

Martínez-de Jesús, G., Ramírez-Muñoz, J., García-Cortés, D., & Cota, L. G. (2018). Computational fluid dynamics study of flow induced by a grooved high-shear impeller in an unbaffled tank. *Chemical Engineering & Technology*, *41*(3), 580–589. https://doi.org/10.1002/ceat.201700091

Obando-Galicia, Y., Martínez-de Jesús, G., & Totosaus, A. (2024). Assisted (ultrasound or high shear impeller) soybean oil/lecithin extraction of polyphenolic compounds from red cactus pear peel: Extracts effects on oleogels properties. *Revista Mexicana de Ingeniería Química*, *23*(2), 1–11. https://doi.org/10.24275/rmiq/Alim24237

Oshinowo, L. M., Bakker, A., & Marshall, E. M. (2001). Virtual efficiency: Simulating mixing impellers using computational fluid dynamics. *Flow Control*, *7*(7), 28–33.

Steinmetz, M. (1993). *U.S. Patent No. 5,201,635*. U.S. Patent and Trademark Office. https://patents.google.com/patent/US5201635A/en

Stuparu, A., Susan-Resiga, R., & Bosioc, A. (2021). CFD simulation of solid suspension for a liquid–solid industrial stirred reactor. *Applied Sciences*, *11*(12), 5705. https://doi.org/10.3390/app11125705

Transformation of construction and demolition waste into high value zeolitic materials

Daniel Sánchez Bravo [1], Gleysi Estefanía Morales Martínez [1], J. Andrés Tavizón Pozos [2], Luis Eduardo Trujillo Villanueva [3], Felipe Legorreta García [3], Gabriela A. Vázquez Rodriguez [1,*]

[1] Chemistry Department, Universidad Autónoma del Estado de Hidalgo, Pachuca de Soto, Hidalgo, Mexico
[2] Researchers for Mexico, Department of Basic Sciences, Universidad Autónoma Metropolitana – Azcapotzalco, Mexico City, Mexico
[3] Earth and Materials Sciences Department, Universidad Autónoma del Estado de Hidalgo, Pachuca de Soto, Hidalgo, Mexico
* Corresponding author: gvazquez@uaeh.edu.mx

Received: May 23, 2025 Accepted: July 26, 2025 Published: April 7, 2026
DOI: https://doi.org/10.56845/rebs.v8i1.670

Abstract: Zeolites, microporous crystalline materials composed mainly of silicon and aluminum, possess physicochemical properties that make them valuable in water treatment and catalysis applications. Using construction and demolition waste (CDW) as raw material for producing zeolites represents a sustainable strategy to reduce its environmental impact. Thus, the present work addresses the synthesis of zeolites from CDW within the framework of the circular economy. Crushed brick waste was used and subjected to a hydrothermal process in a stainless-steel reactor with 2 M KOH, at 160 °C, for 6, 8, 10, and 12 hours. After treatment, the products were characterized by powder X-ray diffraction to evaluate their crystallinity. The results showed a progressive evolution in the formation of crystalline phases: at 6 hours an amorphous material was obtained; at 8 hours the first signs of nucleation of ordered phases were identified; at 10 hours zeolitic structures were consolidated, including aluminosilicates typical of zeolites, such as phillipsite; and finally, at 12 hours secondary phases were observed. It is concluded that it is feasible to transform CDW into functional zeolites by hydrothermal synthesis, with an optimum reaction time of about 10 hours. This approach allows the valorization of solid waste and contributes to the production of high-value materials, promoting sustainable practices in the materials science field.

Keywords: circular economy, phillipsite, bricks, hydrothermal synthesis, zeolites

Introduction

Zeolites are microporous materials composed of crystalline structures consisting of three-dimensional tetrahedral arrangements of silicon (Si^{4+}) and aluminum (Al^{3+}) cations surrounded by oxygen anions (O^{2-}), which form channels and cavities of molecular size. According to their origin, zeolites can be classified into three main categories: natural, synthetic, and modified (Gallo-González & Vázquez-Rodríguez, 2021). Naturally occurring zeolites are generated when there is an abrupt drop in temperature in basaltic magmas with high silica content, or when these magmas interact with saline or alkaline solutions. As a result of these specific geological conditions, natural zeolite deposits are commonly found near active or inactive volcanoes (Schifter & Bosch, 1988). As for synthetic zeolites, these are obtained from non-zeolitic precursors, commonly through a process known as hydrothermal synthesis. This method uses materials with a high silica content as starting materials, such as aluminosilicates, volcanic glass, diatomite, ashes, glass or ceramic waste, among others. Finally, modified zeolites are natural zeolites whose surface or internal structure has been altered or modified to improve their properties and applications (Yuna, 2016).

Physicochemical properties of zeolites, such as their high specific surface area, pore size, thermal stability, and ion exchange capacity, in combination with their structural properties, explain their numerous applications in water treatment processes and the capture of atmospheric pollutants, as well as in catalysis in the petrochemical industry and for biodiesel production, to name a few (Rhodes, 2010).

An important aspect that has emerged in recent years is the possibility of using waste as raw material for new products, which represents a key strategy to reduce the environmental impact of waste and promote the circular economy (Malladi *et al*., 2024). As mentioned above, several studies have demonstrated that it is possible to synthesize zeolites from solid waste. A particular case is construction and demolition waste (CDW), which includes all waste generated by construction, renovation, and demolition activities of buildings, works, and structures; CDW includes concrete, ceramics, bricks, gypsum, and other mineral-based materials (Hasibuan *et al*., 2025). This waste, which has traditionally been considered an environmental problem due to its high volume of generation and limited reuse, has gained relevance as a potential source of aluminosilicates, essential compounds for zeolite synthesis.

For example, Wang and Chen (2017) developed a method to produce analcime-type zeolites from CDW using a combined sintering and alkaline hydrolysis process, obtaining a granular material with a multiscale porous structure and high heavy metal adsorption capacity. Similarly, Wang and Zhang (2013) developed a zeolite-loaded ceramsite from CDW, whose porous structure showed favorable properties for water treatment. More recently, Hernández-Palomares and Espejel-Ayala (2022) successfully synthesized precipitated silica, alkali silicates, and zeolites from thermally and chemically treated CDW, confirming their potential as precursors of high value-materials.

These precedents support the technical feasibility of recycling CDW as a raw material for zeolite production. However, challenges remain regarding the optimization of synthesis conditions, the characterization of the resulting phases, and their functional application in real-world environments. Therefore, the main objective of this work is the synthesis of zeolites using a hydrothermal process and CDW as the starting material.

Materials and Methods

CDW used in this study was provided by the Engineering and Architecture Department of the university. Representative brick samples were selected and subjected to a multi-stage pretreatment to obtain the starting material. First, the bricks were processed using a jaw crusher (Allis Mineral Systems, Oak Creek, USA), yielding fragments approximately 2–3 cm in diameter. Subsequently, a roller mill (Quinn Co., Whittier, USA) was used to reduce the size to particles smaller than 1 cm. The resulting material was homogenized using a sample divider (HGG-I, CGOLDENWALL, Germany) to ensure the representativeness of the final subsample. This subsample was then pulverized using a Bico E mill (Burbank, USA), and finally, an agate mill (Pulverisette 2, Fritsch, Germany) produced a fine powder. This powder was sieved with a No. 200 mesh to obtain particles smaller than 0.074 mm.

With the prepared starting material, hydrothermal synthesis was carried out. A laboratory-scale, high-pressure stainless-steel reactor (TGYF-C, 50 mL) was used. The reactor was loaded with 2.5 g of the starting material and 30 mL of a KOH 2 M solution. The reactor was maintained at 160°C for the following synthesis periods: 6, 8, 10, and 12 hours.

Once the process was complete, the reactor was allowed to cool to room temperature. The resulting material was washed with distilled water, centrifuged to separate the product, and then dried in an oven at 100°C for 16 hours. Finally, the dried product was crushed and sieved again with a No. 200 mesh. Product characterization was performed by powder X-ray diffraction (PXRD) on an Inel instrument (Equinox 2000, USA) with a cobalt source and an analysis time of 15 minutes per sample.

Results and Discussion

PXRD characterization was performed on the four samples corresponding to the products obtained after hydrothermal treatments of 6, 8, 10, and 12 hours. Figure 1 shows the characterization results, which reveal a progressive development of crystallinity as a function of the reaction time.

In the sample resulting from the 6-hour treatment, a diffraction pattern characterized by low counts in most peaks (< 250) was observed, indicating a predominantly amorphous phase. Despite the partial dissolution of the precursor (powdered brick), crystalline remnants were identified with signals located at 25.60°, 32.45°, 32.80°, and 35.45° (2θ), associated with silicon dioxide, as can be seen in Figure 2.

These remnant peaks indicate that, although the dissolution of the original brick structure has begun, the reorganization process toward new phases is not yet significant. This behavior is characteristic of the initial stage of hydrothermal synthesis, in which the precursor components begin to deconstruct, generating an amorphous matrix rich in silicates but lacking long-range order.

After 8 hours of treatment, a moderate improvement in the diffraction pattern was observed. New peaks appeared at 32.29°, 32.78°, 35.30°, 38.30°, and a distinctive peak at 41.30° (2θ). Although the intensities of these peaks remain relatively low (less than 500 counts), an increase in the structural organization of the material is evident, as shown in Figure 3.

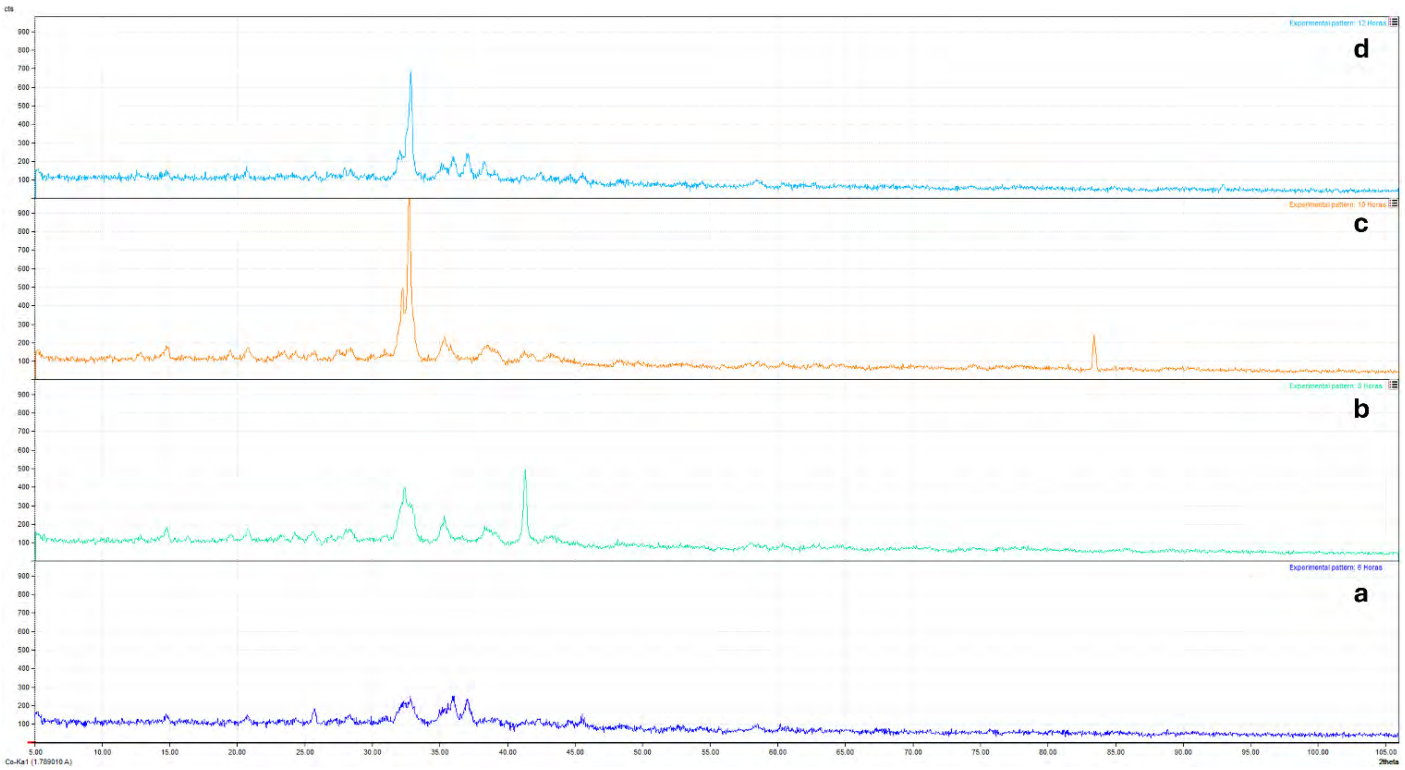

Figure 1. Diffraction patterns of the samples synthesized after (a) 6; (b) 8; (c) 10; and (d) 12 hours.

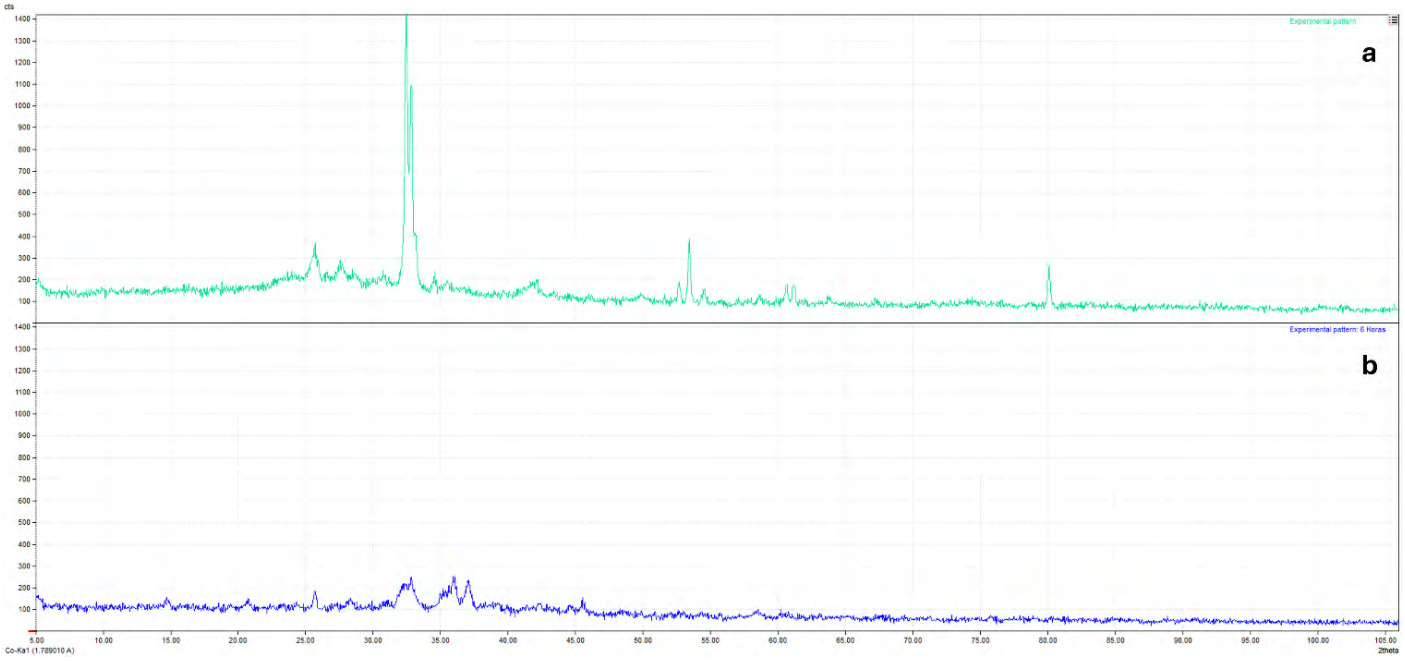

Figure 2. Diffractograms of (a) silicon dioxide and (b) the sample synthesized after 6 hours.

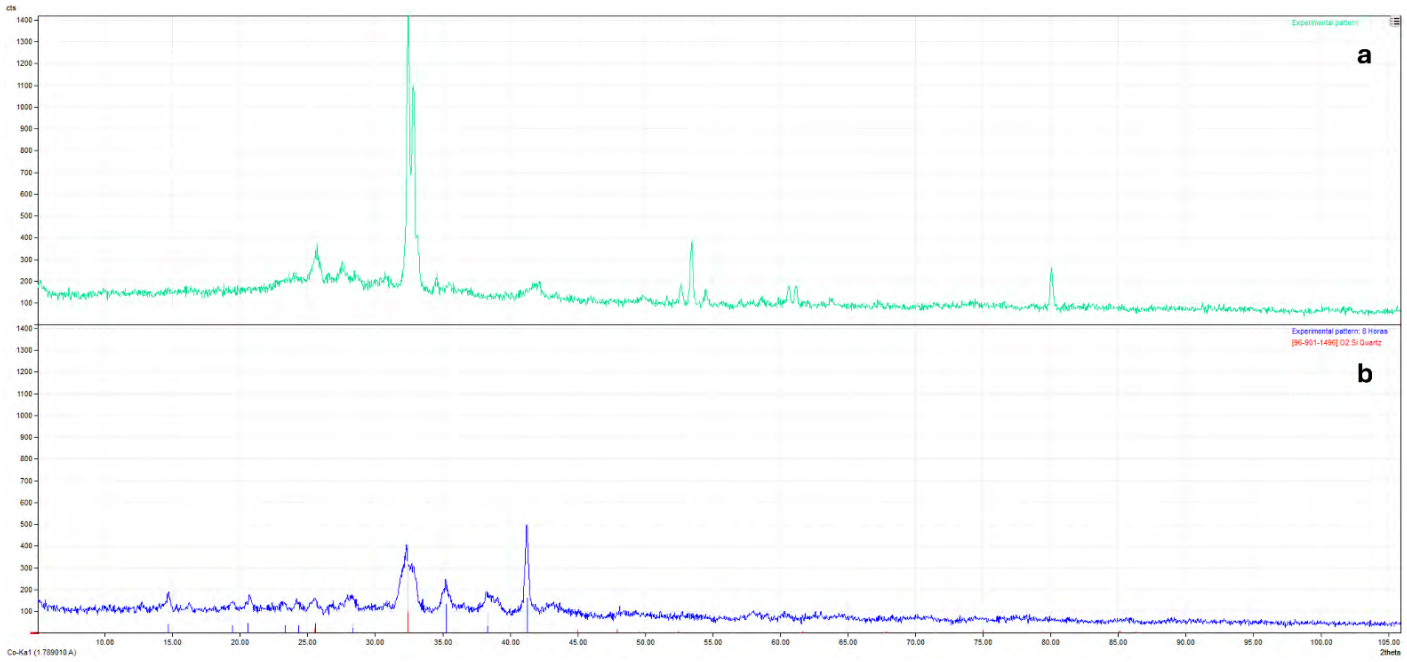

Figure 3. Diffractograms of (a) silicon dioxide and (b) the sample synthesized after 8 hours.

These new peaks suggest the onset of crystalline growth, likely associated with early stage zeolitic phases. Despite the difficulty in precisely identifying all signals due to their low intensity, the presence of silicon dioxide was again confirmed, along with indications of emerging phases that are still not well defined. This stage represents a transition between the initial disorganization and the beginning of the reconstruction of ordered structures typical of zeolites.

After 10 hours of treatment, the XRD pattern of the sample showed a notable change compared to the samples obtained at shorter synthesis times (Figure 4). The peaks became more defined, with higher intensity and a lower baseline, which indicates a considerable increase in the crystallinity of the product. Several phases were identified with greater confidence:

- Silicon dioxide (SiO_2) as the main phase
- A potassium-rich phase
- Mixed potassium–sodium aluminosilicate, compatible with zeolitic structures

The development of these phases reveals a significant transformation of the precursor into crystalline structures with characteristics of zeolitic materials. The identification of the potassium–sodium aluminosilicate is particularly relevant, since these compounds are typical in the synthesis of phillipsite-type zeolites, which are characterized by well-defined intracrystalline channels and high cation-exchange capacity (Pansini *et al*., 1996). Furthermore, the increase in the intensity of the peak located at 32.78° (2θ) stands out as a predominant signal of the growth of a specific crystalline phase, possibly corresponding to the zeolitic phase of interest.

The sample treated for 12 hours showed an XRD pattern similar to that of the sample synthesized in 10 hours, although with slight modifications in the relative intensity of some peaks and the appearance of new signals at 35.98°, 37.08°, and 38.33° (2θ) (Figure 5). These signals may indicate the formation of secondary phases, possibly due to structural reorganization reactions or the depletion of key reactants in the hydrothermal medium.

These new phases were tentatively associated with compounds containing aluminum, potassium, and silicon. However, due to the complexity of the pattern and the possible overlap of peaks, complementary analysis using other techniques (for example, infrared spectroscopy or scanning electron microscopy) is required to confirm the composition and morphology of these phases.

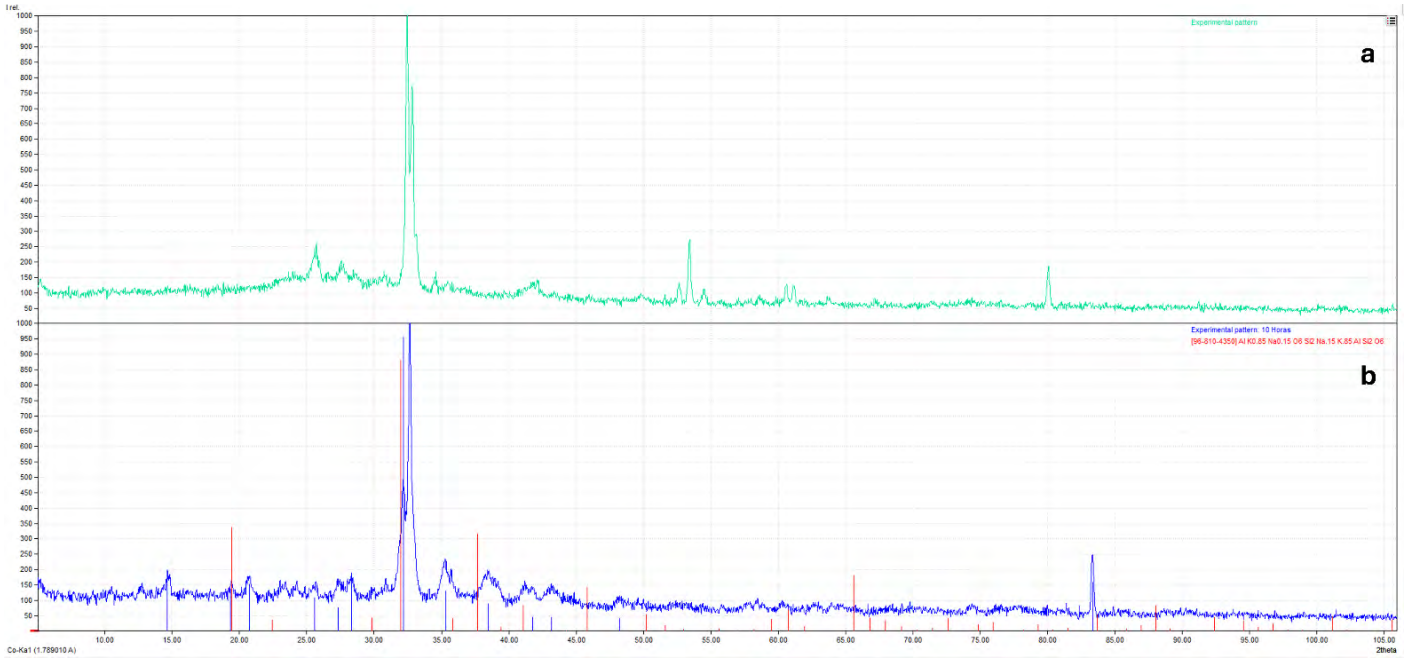

Figure 4. Diffractograms of (a) silicon dioxide and (b) the sample synthesized after 10 hours

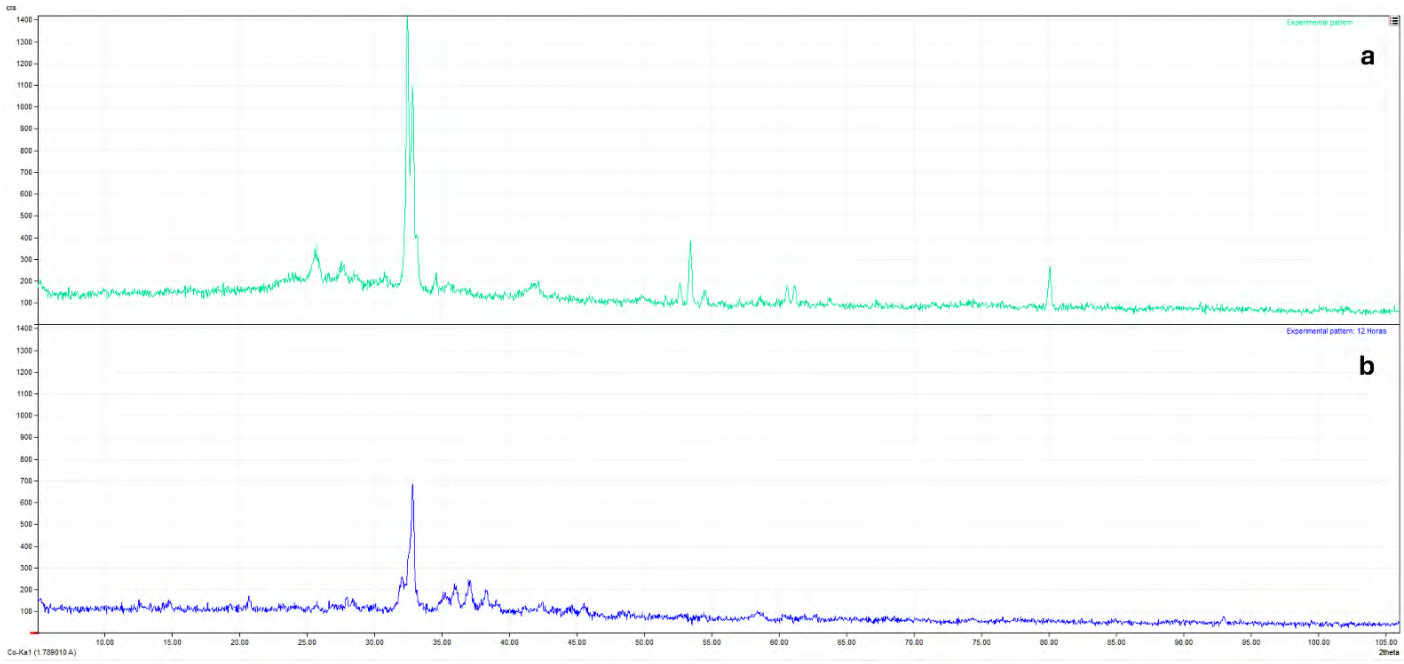

Figure 5. Diffractograms of (a) silicon dioxide and (b) the sample synthesized after 12 hours

It is worth noting that, although a good level of crystallinity is maintained in this sample, the slight decrease in the intensity of the peak at 32.78° suggests that undesired or less-ordered phases may be forming, because of recrystallization-related processes or the development of competing structures.

The mineralogical evolution observed throughout the synthesis process indicates a progressive transformation of the precursor material toward more ordered structures. The XRD analysis shows that reaction time is a critical factor in the development of zeolitic phases, as summarized in Figure 6.

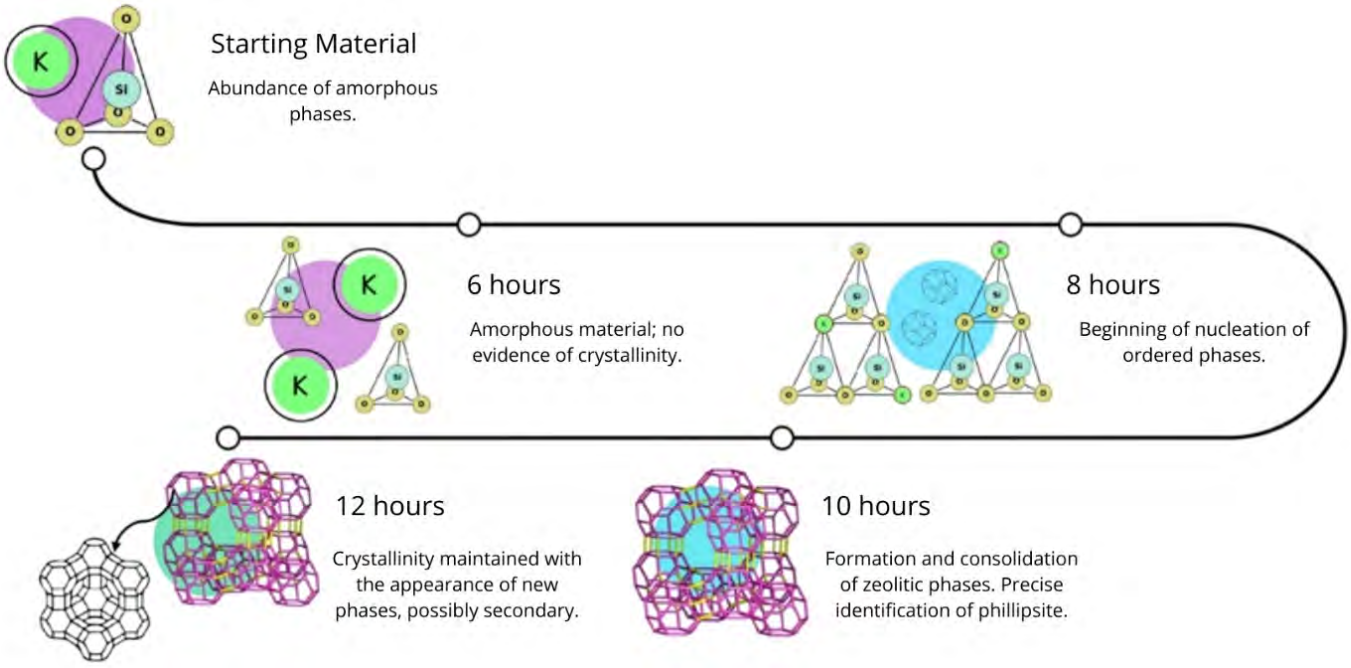

Figure 6. Synthesis of phillipsite by the hydrothermal method

These results support the feasibility of using construction and demolition waste (CDW) as a raw material for zeolite synthesis via hydrothermal processes, contributing to the valorization of this waste within the circular economy framework. However, they also highlight the need to optimize synthesis parameters to prevent the formation of secondary undesired phases over extended periods.

Conclusions

The present study demonstrates the technical feasibility of transforming construction and demolition waste, specifically bricks, into zeolites through a hydrothermal synthesis process. Through different treatment times (6, 8, 10, and 12 hours), a progressive evolution in the material's crystallinity was observed, and optimal formation of zeolitic phases was found after approximately 10 hours. This reaction period led to the identification of compounds characteristic of phillipsite-type structures in the product. These findings not only validate the use of construction and demolition waste as viable precursors for obtaining high value zeolitic materials but also align with the principles of the circular economy by converting an abundant solid waste into a functional resource. However, it was observed that excessive reaction times may induce the formation of undesired secondary phases, highlighting the need for careful optimization of process parameters. Overall, this work offers a sustainable strategy for waste management and the development of materials with applications in water treatment and catalysis, among other fields.

Author contributions: D.S.-B. Writing, analysis and interpretation of data, conceptualization, design, data collection, editing; G.E.M.-M. Supervision, data collection, investigation; J.A.T.-P. Supervision, analysis, project coadministration; L.E.T.-V. Analysis and interpretation of data; F.L.-G. Supervision, revision; G.A.V.-R. Conceptualization, writing, editing, supervision, project administration.

References

Gallo-González, A. K., & Vázquez-Rodríguez, G. A. (2021). Uso de zeolitas para el control de fuentes no puntuales de contaminación del agua: revisión. *Ingeniería del Agua*, *25*(4), 241–255. https://doi.org/10.4995/Ia.2021.15897

Hasibuan, G. C. R., Al Fath, M. T., Yusof, N., Dewi, R. A., Syafridon, G. G. A., Jaya, I., & Anas, M. R. (2025). Integrating circular economy into construction and demolition waste management: A bibliometric review of sustainable engineering practices in the built environment. *Case Studies in Chemical and Environmental Engineering*, 101159. https://doi.org/10.1016/j.cscee.2025.101159

Hernández-Palomares, A., & Espejel-Ayala, F. (2022). Precipitated silica, alkali silicates and zeolites from construction and demolition waste materials. *Journal of Cleaner Production*, *348*, 131346. https://doi.org/10.1016/j.jclepro.2022.131346

Malladi, R. C., S, Ajayan, A. S., Chandran, G., & Selvaraj, T. (2024). Upcycling of construction and demolition waste: Recovery and reuse of binder and fine aggregate in cement applications to achieve circular economy. *Cleaner Engineering and Technology*, 100864. https://doi.org/10.1016/j.clet.2024.100864

Pansini, M., Colella, C., Caputo, D., De'Gennaro, M., & Langella, A. (1996). Evaluation of phillipsite as cation exchanger in lead removal from water. *Microporous Materials*, *5*(6), 357–364. https://doi.org/10.1016/0927-6513(95)00071-2

Rhodes, C. J. (2010). Properties and applications of zeolites. *Science Progress*, *93*(3), 223–284. https://doi.org/10.3184/003685010x12800828155007

Schifter, I., & Bosch, P. (1988). *La zeolita: Una piedra que hierve*. Fondo de Cultura Económica.

Wang, C., & Chen, X. (2017). Preparation and characterization of granular zeolite material from construction and demolition waste for lead removal. *Desalination and Water Treatment*, *72*, 354–359. https://doi.org/10.5004/dwt.2017.20695

Wang, C., & Zhang, F. (2013). Zeolite loaded ceramsite developed from construction and demolition waste. *Materials Letters*, *93*, 380–382. https://doi.org/10.1016/j.matlet.2012.08.139

Yuna, Z. (2016). Review of the natural, modified, and synthetic zeolites for heavy metals removal from wastewater. *Environmental Engineering Science*, *33*(7), 443–454. https://doi.org/10.1089/ees.2015.0166

Hydrothermal carbonization of rice husk for the production of hydrochar as a biofuel

Erik Samuel Rosas-Mendoza *, Alejandro Alvarado-Lassman, Juan Manuel Méndez-Contreras, Norma Alejandra Vallejo-Cantú and Ofelia Landeta-Escamilla

División de Estudios de Posgrado e Investigación, Tecnológico Nacional de México/Instituto Tecnológico de Orizaba, Av. Oriente 9, 852. Col. Emiliano Zapata, Orizaba, Veracruz C.P. 94320, México
* Corresponding author: erik.rm@orizaba.tecnm.mx

Received: January 12, 2026 Accepted: April 23, 2026 Published: April 25, 2026
DOI: https://doi.org/10.56845/rebs.v8i1.683

Abstract: Rice is a widely consumed food product worldwide, and it generates an agro-industrial waste product called rice husk, which currently lacks economic value and is poorly managed due to its difficult handling. Therefore, the objective of this work was to carry out the hydrothermal carbonization of rice husk to produce hydrochar as a biofuel using different reaction conditions. The hydrothermal carbonization of the rice husk was performed in a 1 L stainless steel reactor, model CF-1, using temperatures of 180, 190, and 200 °C and reaction times of 1, 2, and 3 h, respectively. The rice husk and the hydrochars were analyzed for pH, moisture content, total solids, volatile solids, ash content, electrical conductivity, elemental analysis, and higher heating value (HHV). The main results showed that the hydrochars had acidic pH values, moisture content below 10%, TS and VS values above 90% and 74%, respectively, high ash content and electrical conductivity, and HHV values greater than 15 MJ/kg. The thermochemical conversion of rice husks helps reduce the volume of a difficult-to-manage agro-industrial waste product and, in turn, provides a biofuel with a higher HHV than the initial biomass (14.34 MJ/kg). At the end of the study, it was observed that one hour was sufficient to improve the HHV compared to uncarbonized rice husks, due to the increase in C (> 38%) and low moisture (< 8%).

Keywords: rice husk, hydrothermal carbonization, hydrochar, biofuel

Introduction

One of the most consumed agricultural products is rice, a cereal considered a staple food for approximately half the world's population (Nzereogu *et al*., 2023). In Mexico, rice production during the 2022–2023 period was approximately 157,000 metric tons (SIAP, 2023a). Rice consumption yields two types of residues: straw and rice husk (RH). The husk is the outer layer of the rice grain (Bushra and Remya, 2020) and comprises 20% of the total grain weight (Naranjo *et al*., 2023). It has a low bulk density, ranging from 96 to 140 kg/m^3 (Nzereogu *et al*., 2023). RH is a type of lignocellulosic biomass composed primarily of cellulose (35%), hemicellulose (30%), and lignin (18%) (Nizamuddin *et al*., 2018). Its physicochemical properties include moisture (4.5–10.8%), volatile matter (70.2–78.5%), ash (3.4–17%), and fixed carbon (3.4–19.8%) (Bushra and Remya, 2020). However, RH also has a high silica content (18–25%) of its total weight (Kordi *et al*., 2023), which makes this residue difficult to manage and utilize in the same way as other agricultural residues.

As one of the alternatives for utilizing RH, hydrothermal carbonization (HTC) can be employed. This is a thermochemical process carried out in the presence of compressed water at temperatures ranging from 180 to 250 °C (Higgins *et al*., 2020) and under autogenous pressures of around 4 MPa (Ighalo *et al*., 2025). HTC is considered a sustainable process due to the operational energy savings and the elimination of sample pretreatment steps (Pauline and Joseph, 2020; Orzama-Hugo *et al*., 2024; Selvaraj *et al*., 2025). The main products resulting from the HTC are: 1) A carbon-rich solid phase known as hydrochar, 2) A liquid phase abundant in organic compounds referred to as process water (Ischia *et al*., 2024), and 3) Synthesis gas, composed mainly of CO_2 and CO (Higgins *et al*., 2020). Hydrochar has characteristics that make it attractive as a biofuel due to its higher heating value (HHV) and it has an HHV between 13 and 30 MJ/kg, depending on the initial energy content of the raw material (Romano *et al*., 2023).

Recently, several applications of HCT using RH have been carried out under different operating conditions, among which the following stand out: 1) Nizamuddin *et al*. (2018) performed the HTC process with microwaves at 220 °C for 30 min. The hydrochar yield was 35.9% with a HHV of 16.10 MJ/kg, used as an adsorbent, carbon sequestrant, and soil remediator for agriculture. 2) Danso-Boateng *et al*. (2020), evaluated the adsorption capacity of the hydrochar obtained at 200 °C for 20 h, observing that after the process there is an increase in C and a decrease in O, going from 53.7% to 74.1% C. 3) Hossain *et al*. (2020) evaluated the properties of hydrochar as a fuel and adsorbent, obtaining hydrochar at 180 °C for 20 min of reaction with a HHV between 20.27 and 19.02 MJ/kg. 4) Yang *et al*. (2021) carried out a co-HTC with RH and coal from the Zhundong region at 200 °C for 2 h and the hydrochar had a composition of 98.9% SiO_2 in the

ash. 5) Li *et al*. (2021) added metal chlorides to the HTC feed water to evaluate the improvement of carbonization, and this addition directly affected the hydrochar yields from 28.97% to 47.10%.

Based on the previous analysis, it was identified that there is a need to evaluate the hydrothermal carbonization of rice husk at low and intermediate operational temperatures during moderate times. In this regard, the novelty of this work lies in performing the HCT at 180, 190, and 200 °C for 1, 2, and 3 hours, seeking a cost-effective process for obtaining hydrochar as a biofuel. Therefore, the objective of this work is to carry out the hydrothermal carbonization of rice husks for the production of hydrochar as a biofuel.

Materials and Methods

The materials and methods used during this investigation are described below.

Collection and characterization of rice husk

Rice husk (RH), provided by a food processing plant in Orizaba, Veracruz, Mexico, were used as raw material and this plant generates approximately 10,000 metric tons per month of rice husk. Usually, the processed RH consists of domestic rice plus rice imported from countries such as India, Thailand, Vietnam, and Pakistan (SIAP, 2023b). The RH were transported and stored in the Environmental Engineering Laboratory I of the Technological Institute of Orizaba for its analysis. As part of the study, a physicochemical characterization was performed in triplicate using the following methods: pH was determined by TAPPI T252 om-90; moisture and total solids content were determined by gravimetric method 2540 B; and volatile solids and ashes content were determined by gravimetric method 2540 E. Additionally, electrical conductivity (EC) was determined using a conductivity meter (HANNA® Instruments, HI98130, USA). Elemental analysis was also performed using an analyzer (Perkin Elmer, PE2400, USA) to determine carbon, hydrogen, nitrogen, and sulfur content. Oxygen content was determined by difference using CHNS and ashes.

Application of the hydrothermal carbonization of the rice husk

Because the rice husk had a low moisture content, it was ground and hydrated at a mass ratio of 1:3 rice husk:water. After hydration, the moisture content of the rice husk was 75.58 ± 2.40%., that represents the minimum moisture content (70%) for the hydrothermal carbonization process according to Pagés-Díaz and Huiliñir (2020). The hydrothermal carbonization was carried out in a 1 L high-pressure stainless steel reactor (Toption Instruments, CF-1, China), as shown in Figure 1. The reactor were operated at 180, 190 and 200 °C, with different reaction times 1, 2, and 3 hours, respectively.

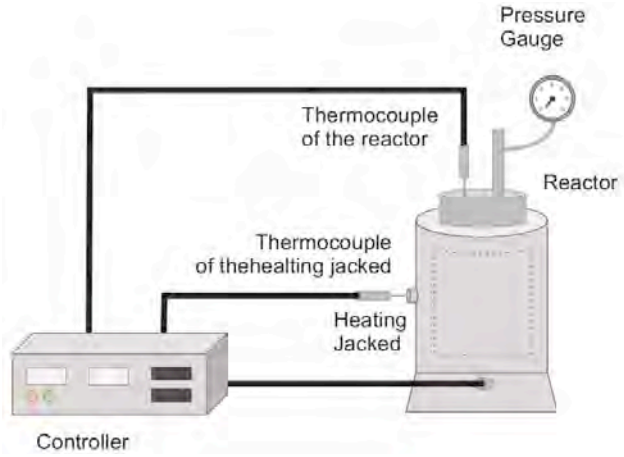

Figure 1. Hydrothermal carbonization reactor for obtaining hydrochar from rice husk

Determination of the higher heating value

From the elemental analysis and the ashes content, the higher heating value (HHV) was determined using the Equation 1, employed by Parikh and Chinniwala (2002):

$$HHV = 0.3491 * \mathrm{C} + 1.1783 * \mathrm{H} + 0.1005 * S - 0.1034 * O - 0.015 * N - 0.0211 * Ash \quad \textbf{(1)}$$

where: C = Carbon (%), H = Hydrogen (%), S = Sulfur (%), O = Oxygen (%), N = Nitrogen (%) and Ash = (%). All percentages were expressed by weight. HHV values are expressed in MJ/kg.

Results and Discussion

Characterization of the rice husk and the hydrochars

The following are presented the results of the physicochemical characterization of the RH and the hydrochars in the Table 1. Based on the pH measurement, the rice husk showed a value close to neutral, similar to 6.5 reported by Nwajiaku *et al.* (2018), which is a typical pH value for RH. However, when comparing the moisture content of the RH, a higher value was obtained in contrast to 7.5 of Hossain *et al*. (2020) and 9.3 of Steven *et al*. (2021). Although the moisture percentage of the RH analyzed in this study was 10.30 ± 0.09%, it was found to be insufficient for the biomass to undergo the hydrothermal carbonization process, as this process requires at least 70% moisture according to Pagés-Díaz and Huiliñir (2020). Therefore, it was necessary to hydrate the RH as explained in the previous section. Furthermore, the 78.71 ± 0.19% of VS content indicates the availability of organic matter present in the sample for carbonization. Regarding ash content, the value of 21.29 ± 0.19% is higher than that reported by Nwajiaku *et al*. (2018) with 11.5% and Steven *et al*. (2021) with 17.6%. It is important to mention that, according to Steven *et al*. (2021), between 83.6 and 93.5% of the ash content corresponds to silica present in the RH. The presence of silica in the animal feed makes this type of waste difficult to manage. The limitations due to its high silica concentration are: 1) animals cannot digest it, and 2) it is highly resistant to burning (Ojeda-Rodríguez *et al*., 2024). On the other hand, the electrical conductivity was 373.67 ± 8.08 µS/cm, a value close to 330 µS/cm reported by Nwajiaku *et al*. (2018).

Regarding the behavior of the hydrochars, their pH values are below 4, as shown in Table 1, indicating acidic behavior due to the increased temperature and the reaction time of the HCT process. These values are consistent with Masoumi *et al*. (2021) findings that hydrochars have an acidic pH. It is noteworthy that the moisture content of the hydrochars is lower than that of the RH, because after the hydrothermal carbonization process, the process water was removed from the hydrocarbons by evaporation over two to three hours at 105 °C. A moisture content of less than 10% is a key criterion for evaluating the HHV of a biofuel. The moisture content (%) of the hydrochars ranged from 5.43 ± 0.04 to 8.28 ± 0.19, as shown in Table 1. The percentages of TS, VS and ash are proportional to the moisture content. It can be observed in the Table 1 that all hydrochars presented values above 90% for TS, obtaining ranges of 74.44 ± 0.16 to 75.36 ± 0.05 for VS (%) and 24.64 ± 0.05 to 25.56 ± 0.16 for ash (%). By comparing with the literature, Yang *et al*. (2021), carbonized RH at 200 °C and 2, obtaining an ash content of 21.99%; while Nakason *et al*. (2017), obtained hydrochar at 200 °C during 1, 2 and 3 h, reporting 20.9, 21.2 and 21.6% ash, respectively. Electrical conductivity shows an increasing trend with increasing temperature and time. This increase is due to the structural arrangement of the carbon atoms conferred by the HTC; at higher temperatures, the hydrochar structure becomes even more defined, allowing for improved electron flow (Selvaraj *et al*., 2025). This is further supported by the amount of carbon obtained in the elemental analysis, as well as the conversion to a solid through the production of primary carbon (Ischia *et al*., 2024).

Table 1. Physicochemical characterization of the rice husk and the hydrochars obtained under different operational conditions

		pH	Moisture (%)	TS (%)	VS (%)	Ash (%)	EC (µS/cm)
Rice husk		6.79 ± 0.01	10.30 ± 0.09	89.70 ± 0.09	78.71 ± 0.19	21.29 ± 0.19	373.67 ± 8.08
180 °C	1 h	3.88 ± 0.01	7.49 ± 0.20	92.51 ± 0.20	75.04 ± 0.38	24.96 ± 0.38	559.67 ± 7.02
	2 h	3.69 ± 0.00	7.89 ± 0.54	92.11 ± 0.54	75.03 ± 0.22	24.97 ± 0.22	729.67 ± 2.52
	3 h	3.85 ± 0.04	6.91 ± 0.22	93.09 ± 0.22	75.36 ± 0.05	24.64 ± 0.05	781.00 ± 6.56
190 °C	1 h	3.69 ± 0.03	6.17 ± 0.01	93.83 ± 0.01	75.06 ± 0.07	24.94 ± 0.07	678.33 ± 16.01
	2 h	3.73 ± 0.10	5.43 ± 0.04	94.57 ± 0.04	74.94 ± 0.09	25.06 ± 0.09	703.00 ± 6.93
	3 h	3.68 ± 0.01	6.55 ± 0.12	93.45 ± 0.12	75.08 ± 0.16	24.92 ± 0.16	789.33 ± 41.86
200 °C	1 h	3.86 ± 0.02	6.05 ± 0.05	93.95 ± 0.05	74.82 ± 0.12	25.18 ± 0.12	792.67 ± 6.81
	2 h	3.84 ± 0.02	5.78 ± 0.05	94.22 ± 0.05	74.44 ± 0.16	25.56 ± 0.16	766.67 ± 12.90
	3 h	3.65 ± 0.02	8.28 ± 0.19	91.72 ± 0.19	74.74 ± 0.20	25.26 ± 0.20	663.67 ± 8.33

Elemental analysis and HHV evaluation

Regarding the elemental analysis of the RH, the C content was 36.70 ± 0.42%, which contrasts with the value reported by Hossain *et al*. (2020), which was 25.9%. The percentages of HNS are similar to those found by Hossain *et al*. (2020), that were 4.7, 0.6 and 0.3%, respectively. However, Steven *et al*. (2021) mention a similar C content of 36.60%, but higher percentages of H (5.83%) and N (3.31%). The presence of CHON in the RH, especially C, is highly favorable for hydrochar, as it is a solid residue rich in C. The reason why the properties of the RH evaluated in this research differ from those reported in the literature can be attributed to the fact that the processed rice in this case study, and therefore its waste, consists of domestic rice plus rice imported from countries such as India, Thailand, Vietnam, and Pakistan (SIAP, 2023b); these are cultivated under different environmental conditions, including soil type, climate of each growing region, and planting and harvesting seasons.

Table 2. Results of the elemental analysis and the higher heating value of the rice husk and the hydrochar obtained under different operational conditions

		C (%)	H (%)	N (%)	S (%)	O (%)	HHV (MJ/kg)
Rice husk		6.79 ± 0.01	10.30 ± 0.09	89.70 ± 0.09	78.71 ± 0.19	21.29 ± 0.19	373.67 ± 8.08
180 °C	1 h	39.14 ± 0.94	5.25 ± 0.05	0.57 ± 0.02	0	30.08 ± 0.97	16.21 ± 0.50
	2 h	38.59 ± 0.04	5.09 ± 0.04	0.59 ± 0.03	0	30.75 ± 0.04	15.76 ± 0.04
	3 h	39.39 ± 0.46	4.69 ± 0.06	0.58 ± 0.00	0	28.69 ± 0.52	15.75 ± 0.29
190 °C	1 h	40.53 ± 0.63	4.77 ± 0.46	0.45 ± 0.26	0	29.31 ± 0.84	16.21 ± 0.86
	2 h	39.71 ± 0.57	4.92 ± 0.09	0.25 ± 0.01	0	30.05 ± 0.65	16.03 ± 0.38
	3 h	39.50 ± 0.65	4.71± 0.07	0.30± 0.02	0	30.56 ± 0.71	15.65 ± 0.39
200 °C	1 h	39.41 ± 0.24	4.77 ± 0.03	0.30 ± 0.00	0	30.33 ± 0.28	15.71 ± 0.15
	2 h	40.67 ± 0.29	4.79 ± 0.02	0.23 ± 0.00	0	28.75 ± 0.28	16.33 ± 0.10
	3 h	41.00 ± 0.41	4.71 ± 0.03	0.26 ± 0.02	0	28.77 ± 0.40	16.36 ± 0.14

For the elemental analysis of the hydrochars, the carbon content ranged from 39.14 ± 0.94 to 41.00 ± 0.41% under the different operating conditions, as shown in Table 2. Yang *et al*. (2021) reported a very similar value of 41.56%, while Nizamuddin *et al*. (2018) and Hossain *et al*. (2020) found 47.2% carbon. Table 2 also shows a trend of decreasing H_2O and O_2 concentrations as temperature and reaction time increase, due to the dehydration and decarboxylation reactions responsible for these decreases (Masoumi *et al*., 2021; Yang *et al*., 2021). The increase in C percentages and the decrease in H and O percentages, as a result of the HTC, are due to the decomposition of the RH; that is, as H and O are eliminated as H_2O and CO_2, C concentrates in the hydrochar. Finally, the N concentration was very low compared to CHO, while S was absent.

Evaluating the HHV, Table 2 shows that the RH was 14.34 ± 0.09 MJ/kg, which is the reference value for analyzing the trend of using higher HTC severities to obtain hydrochar with HHV values higher than the initial biomass. The highest HHV value was 16.36 ± 0.14 MJ/kg for hydrochar obtained at 200 °C for 3 h. Comparing these results with other authors, Nizamuddin *et al*. (2018) reported 16.10 MJ/kg for hydrochar obtained at 220 °C for 30 minutes, while Hossain *et al*. (2020) found a value of 20.27 MJ/kg at 180 °C for 20 minutes, but with a very low ash content, equivalent to 9.4%. The similarities or differences in the results of this research compared to other authors can also be attributed to the region where the rice was cultivated, the agricultural practices used for rice cultivation, and the physicochemical composition of the RH as a component of the hydrochars. Finally, the hydrochars processed by HTC from the RH can be used for heat and electricity generation through combustion, replacing fuels such as charcoal.

Conclusions

The purpose of this work was to perform the hydrothermal carbonization of rice husk from a food processing plant to produce hydrochars as a biofuel using different operating conditions for hydrothermal carbonization. It is important to

highlight that rice husk is a residue with low moisture content, which had to be hydrated for the HCT, but possess valuable characteristics, including their carbon content, thus allowing for the utilization of a biomass that currently lacks an adequate management plan. Characterization of the hydrochar revealed that it is an acidic product with a high ash content, attributed to the amount of silica inherent in rice husks. HHV of the hydrochars values ranged from 15.71 to 16.36 MJ/kg, indicating that it is possible to improve the HHV of rice husk through HTC. The hydrothermal carbonization process proved to reduce the volume of rice husks and yield a biofuel such as hydrochar.

Acknowledgments and Funding: Authors acknowledge the support provided by the Tecnológico Nacional de México (TecNM) Project number 22524.25-P.

Author contributions: E.S.R.-M.: Writing – original draft, Conceptualization, Project administration, Funding acquisition, Methodology, Investigation, Supervision, Formal analysis, Writing – review & editing, Resources; A.A.-L.: Methodology, Investigation, Supervision; J.M.M.-C.: Methodology, Investigation, Supervision; N.A.V.-C.: Formal analysis, Writing – review & editing, Resources; O.L.-E.: Formal analysis, Writing – review & editing, Resources.

References

Bushra, B., & Remya, N. (2020). Biochar from pyrolysis of rice husk biomass: Characteristics modification and environmental application. *Biomass Conversion and Biorefinery, 14*, 5759–5770. https://doi.org/10.1007/s13399-020-01092-3

Chen, Z., Gou, Y., & Lou, L. (2024). A critical review of hydrochar-based photocatalysts by hydrothermal carbonization: Synthesis, mechanisms, and applications. *Biochar, 6*, 74. https://doi.org/10.1007/s42773-024-00364-9

Danso-Boateng, E., Mohammed, A. S., Sander, G., Wheatley, A. D., Nyktari, E., & Usen, I. C. (2021). Production and characterisation of adsorbents synthesised by hydrothermal carbonisation of biomass wastes. *SN Applied Sciences, 3*, 257. https://doi.org/10.1007/s42452-021-04273-5

Higgins, L. J. R., Brown, A. P., Harrington, J. P., Ross, A. B., Kaulich, B., & Mishra, B. (2020). Evidence for a core-shell structure of hydrothermal carbon. *Carbon, 161*, 423–431. https://doi.org/10.1016/j.carbon.2020.01.060

Hossain, N., Nizahuddin, S., Griffin, G., Selvakannan, P., Mubarak, N. M., & Indra Mahlia, T. M. (2020). Synthesis and characterization of rice husk biochar via hydrothermal carbonization for wastewater treatment and biofuel production. *Scientific Reports, 10*, 18851. https://doi.org/10.1038/s41598-020-75936-3

Ighalo, J. O., Akaeme, F. C., Georgin, J., De Oliveira, J. S., & Franco, D. S. P. (2025). Biomass hydrochar: A critical review of process chemistry, synthesis methodology, and applications. *Sustainability, 17*(4), 1660. https://doi.org/10.3390/su17041660

Ischia, G., Berge, N. D., Bae, S., Marzban, N., Román, S., Farru, G., Wilk, M., Kulli, B., & Fiori, L. (2024). Advances in research and technology of hydrothermal carbonization: Achievements and future directions. *Agronomy, 14*(5), 955. https://doi.org/10.3390/agronomy14050955

Kordi, M., Farrokhi, N., Pech-Canul, M. I., & Ahmadikhah, A. (2023). Rice husk at a glance: From agro-industrial to modern applications. *Rice Science, 31*(1), 14–32. https://doi.org/10.1016/j.rsci.2023.08.005

Li, Y., Hagos, F. M., Chen, R., Qian, H., Mo, C., Di, J., Gai, X., Yang, R., Pan, G., & Shan, S. (2021). Rice husk hydrochars from metal chloride-assisted hydrothermal carbonization as biosorbents of organics from aqueous solution. *Bioresources and Bioprocessing, 8*. https://doi.org/10.1186/s40643-021-00451-w

Masoumi, S., Borugadda, V. B., Nanda, S., & Dalai, A. K. (2021). Hydrochar: A review on its production technologies and applications. *Catalysts, 11*, 939. https://doi.org/10.3390/catal11080939

Nakason, K., Panyapintopol, B., Kanokkantapong, V., Viriya-Empikul, N., Kraithong, W., & Pavasant, P. (2017). Hydrothermal carbonization of unwanted biomass materials: Effect of process temperature and retention time on hydrochar and liquid fraction. *Journal of the Energy Institute, 91*(5), 786–796. https://doi.org/10.1016/j.joei.2017.05.002

Naranjo, J., Juiña, E., Loyo, C., Romero, M., Vizuete, K., Debut, A., Ponce, S., & Murillo, H. A. (2023). Preparation of adsorbent materials from rice husk via hydrothermal carbonization: Optimization of operating conditions and alkali activation. *Resources, 12*(12), 145. https://doi.org/10.3390/resources12120145

Nizamuddin, S., Hussain-Siddiqui, M. T., Ahmed-Baloch, H., Mujawar-Mubarak, N., Griffin, G., Madapusi, S., & Tanksale, A. (2018). Upgradation of chemical, fuel, thermal, and structural properties of rice husk through microwave-assisted hydrothermal carbonization. *Environmental Science and Pollution Research, 25*, 17529–17539. https://doi.org/10.1007/s11356-018-1876-7

Nwajiaku, I. M., Olanrewaju, J. S., Sato, K., Tokunari, T., Kitano, S., & Masunaga, T. (2018). Change in nutriment composition of biochar from rice husk and sugarcane bagasse at varying pyrolytic temperatures. *International Journal of Recycling of Organic Waste in Agriculture, 7*, 269–276. https://doi.org/10.1007/s40093-018-0213-y

Nzereogu, P. U., Omah, A. D., Ezema, F. I., Iwuoha, E. I., & Nwanya, A. C. (2023). Silica extraction from rice husk: Comprehensive review and applications. *Hybrid Advances, 4*, 100111. https://doi.org/10.1016/j.hybadv.2023.100111

Ojeda-Rodriguez, V. E., Escobar-Morales, B., Méndez-Contreras, J. M., Vallejo-Cantú, N. A., Alvarado-Lassman, A., & Rosas-Mendoza, E. S. (2024). Cascarilla de arroz, un residuo agrícola sin ser aprovechado en México. *Tendencias en Energías Renovables y Sustentabilidad, 3*(1), 105–110. https://doi.org/10.56845/terys.v3i1.319

Orzama-Hugo, R., Naranjo, J., Gavilanez-Alvarez, I., Cando, V. M., Tixi-Gallegos, K., Sánchez-Moreno, H., Londo, F., Danilo-Gavilanez, O., & Coello-Cabezas, J. (2024). Production of hydrochar by low-temperature hydrothermal carbonization of residual biomass from cocoa production for mercury adsorption in acidic aqueous solutions. *Case Studies in Chemical and Environmental Engineering, 10*, 100938. https://doi.org/10.1016/j.cscee.2024.100938

Pagés-Díaz, J., & Huiliñir, C. (2020). Valorization of the liquid fraction of co-hydrothermal carbonization of mixed biomass by anaerobic digestion: Effect of the substrate to inoculum ratio and hydrochar addition. *Bioresource Technology, 317*, 123989. https://doi.org/10.1016/j.biortech.2020.123989

Parikh, P. P., & Channiwala, S. A. (2002). A unified correlation for estimating HHV for solid, liquid and gaseous fuel. *Fuel, 81*, 1051–1063. https://doi.org/10.1016/S0016-2361(01)00131-4

Pauline, A. L., & Joseph, K. (2020). Hydrothermal carbonization of organic wastes to carbonaceous solid fuel: A review of mechanisms and process parameters. *Fuel, 279*, 118472. https://doi.org/10.1016/j.fuel.2020.118472

Romano, P., Stampone, N., & Giacomo, G. D. (2023). Evolution and prospects of hydrothermal carbonization. *Energies, 16*(7), 3125. https://doi.org/10.3390/en16073125

Selvaraj, P. S., Ettiyagounder, P., Sabarish, K., Periasamy, K., Rengasamy, B., Veeraswamy, D., Karchiyappan, T., & Kathirvel, S. (2025). Hydrothermal carbonization approach for transforming biomass waste to value-added hydrochar and its applications in water remediation. *Desalination and Water Treatment, 322*, 101199. https://doi.org/10.1016/j.dwt.2025.101199

Servicio de Información Agroalimentaria y Pesquera. (2023a). *Expectativas agroalimentarias 2023*.

Servicio de Información Agroalimentaria y Pesquera. (2023b). *Panorama agroalimentario: Agricultura regenerativa, la vía para un futuro sustentable*.

Steven, S., Restiawaty, E., & Bindar, Y. (2021). Routes for energy and bio-silica production from rice husk: A comprehensive review and emerging prospect. *Renewable and Sustainable Energy Reviews, 149*, 111329. https://doi.org/10.1016/j.rser.2021.111329

Yang, L., Wang, H., Zhu, J., Sun, W., Xu, Y., & Wu, S. (2021). Co-combustion and ash characteristics of Zhungong coal with rice husk hydrochar prepared by the hydrothermal carbonization technology for co-combustion. *IET Renewable Power Generation, 16*(2), 329–338. https://doi.org/10.1049/rpg2.12324